A Three-Dimensional Variably-Saturated Subsurface Modelling System for River Basins

Geoff Parkin

Department of Civil Engineering
University of Newcastle upon Tyne

March 1996

A dissertation submitted in fulfillment of the requirements for the doctoral degree.

" ... many books,
Wise men have said, are wearisome; who reads
Incessantly, and to his reading brings not
A spirit and judgement equal or superior
(And what he brings what needs he elsewhere seek?),
Uncertain and unsettled still remains ... "

John Milton.
Paradise Regained, Book IV.

A Three-Dimensional Variably-Saturated Subsurface Modelling System for River Basins

ABSTRACT

There are many circumstances where lateral flows in the upper soil layers above the regional groundwater table are important for hillslope and catchment hydrology, and in particular for the transport of contaminants. Perched water tables frequently occur in Quaternary drift sequences, reducing rates of recharge to the underlying aquifers and altering contaminant migration pathways; recent experimental and modelling studies have demonstrated the potential importance of lateral flows in the unsaturated zone, even in homogeneous soils; and lateral interflow at the hillslope scale, and its role in generating storm runoff, is the subject of intense current debate amongst hydrologists.

A numerical model for simulating transient three-dimensional variably-saturated flow in complex aquifer systems (the Variably-Saturated Subsurface flow, or VSS, model), capable of representing these conditions, is presented in this thesis. The VSS model is based on the extended Richards equation for saturated as well as unsaturated conditions, and also includes capabilities for modelling surface-subsurface interactions, stream-aquifer interactions, prescribed head and flow boundary conditions, plant and well abstractions, and spring discharges. A simple but novel approach is taken to solving the three-dimensional non-linear Richards equation on a flexible-geometry finite-difference mesh, using Newton-Raphson iteration and an adaptive convergence algorithm.

The VSS model is implemented as a module of the catchment flow and transport modelling system, SHETRAN. The reliability of the full SHETRAN modelling system is demonstrated using verification and validation tests, including comparisons against analytical solutions for simple cases, and simulations of storm runoff in a small Mediterranean catchment. Simulations of flow and contaminant transport in complex sequences of Quaternary drift deposits demonstrate the full capabilities of the modelling system under real-world conditions.

CONTENTS

APPENDICES

LIST OF TABLES

LIST OF FIGURES

LIST OF SYMBOLS

The following list includes all variables in this thesis used in the VSS model (Chapters 4 and 5); it does not include variables used only in the literature review (Chapter 3) or in the verification tests (Chapter 6).

Name	Description
A_0	plan area of an element [L^2]
A_i	coefficient of $\Delta\psi_{i-1}^{n+1,m+1}$ in column tri-diagonal solver [$L^2\ T^{-1}$]
$A_{i,j}$	cross-sectional area of face *j* of cell *i* perpendicular to the direction of flow [L^2]
$A_{i,j}'$	effective cross-sectional area of face *j* of cell *i* perpendicular to the direction of flow [L^2]
$A_{k,j}$	cross-sectional area for cell *k* in the adjacent column, connected to cell *i* on face *j*, perpendicular to the direction of flow [L^2]
B_i	coefficient of $\Delta\psi_i^{n+1,m+1}$ in column tri-diagonal solver [$L^2\ T^{-1}$]
C_i	coefficient of $\Delta\psi_{i+1}^{n+1,m+1}$ in column tri-diagonal solver [$L^2\ T^{-1}$]
C_s	spring discharge coefficient [$L^{-1}\ T^{-1}$]
d_w	depth of ponded or stream water [L]
d_x	distance from the stream channel side to the adjacent computational node [L]
d_B	thickness of stream bed sediments [L]
e	base for natural logarithms (constant) [-]
e_s	evaporation rate at the ground surface [$L\ T^{-1}$]
e_w	evaporation rate from surface water (including precipitation) [$L\ T^{-1}$]
f(.)	function (of ψ) [$L^3\ T^{-1}$]
F_i	interim coefficient in column solver [$L^2\ T^{-1}$]
G_i	interim coefficient in column solver [$L^2\ T^{-1}$]

h hydraulic head [L]

h_0 initial hydraulic head [L]

h_b prescribed head at the model bottom boundary [L]

h_i hydraulic head for cell *i* [L]

h_l prescribed head at the model boundary [L]

I infiltration rate (-ve for infiltration, +ve for exfiltration) [L T^{-1}]

k_r relative hydraulic conductivity [-]

$\underline{K}=(K_x,K_y,K_z)$ principal components of saturated hydraulic conductivity [L T^{-1}]

$K_a=(K_x \text{ or } K_y)$ saturated lateral hydraulic conductivity in the aquifer in the x or the y direction [L T^{-1}]

K_{ex} effective hydraulic conductivity for flow through the channel sides [L T^{-1}]

$\overline{K_i}$ mean saturated lateral hydraulic conductivity for cell *i* at an abstraction well [L T^{-1}]

$K_{i,j}$ hydraulic conductivity (a function of ψ) in the *j*th direction for cell *i* [L T^{-1}]

$K_{k,j}$ hydraulic conductivity (a function of ψ) in the *j*th direction for cell *k* in the adjacent column, connected to cell *i* on face *j* [L T^{-1}]

$k_{r,i}$ relative hydraulic conductivity for cell *i* [-]

K_x saturated hydraulic conductivity in the x direction [L T^{-1}]

K_y saturated hydraulic conductivity in the y direction [L T^{-1}]

K_z saturated hydraulic conductivity in the z direction [L T^{-1}]

$K_{z,i}$ vertical hydraulic conductivity for cell *i* [L T^{-1}]

$K_{z,i}^{S}$ vertical saturated hydraulic conductivity for cell *i* [L T^{-1}]

K_B saturated hydraulic conductivity of stream bed sediments [L T^{-1}]

m parameter for the soil characteristic and unsaturated hydraulic conductivity functions [-]

n	parameter for the soil characteristic and unsaturated hydraulic conductivity functions [-]
n	porosity [-]
$\mathbf{n}$	unit outward normal to the model boundary [-]
n_c	number of cells intersected by the screened part of an abstraction well [-]
q	specific volumetric flow rate out of the porous medium (general source/sink term) [T^{-1}]
q_b	rate of upflow from the deeper regional aquifer [$L\ T^{-1}$]
q_i	specific volumetric flow rate into cell i from sources and sinks [T^{-1}]
$q_{inf}(=I)$	infiltration rate (-ve for infiltration, +ve for exfiltration) [$L\ T^{-1}$]
q_l	prescribed lateral flux at the model boundary [$L\ T^{-1}$]
q_p	net precipitation at the ground surface [$L\ T^{-1}$]
q_{sp}	specific volumetric sink term for spring discharge [T^{-1}]
q_t	specific volumetric sink term for plant extraction [T^{-1}]
q_w	specific volumetric flow rate out of an abstraction well [T^{-1}]
$q_{w,i}$	specific volumetric flow rate out of each cell intersected by the screened part of an abstraction well [T^{-1}]
$Q_{i,j}$	lateral flow rate into cell i through face j [$L^3\ T^{-1}$]
$Q_{i,j}^{sai}$	lateral flow rate into cell i through face j at a stream channel face [$L^3\ T^{-1}$]
$Q_{i,+}$	vertical flow rate into cell i through the top of the cell [$L^3\ T^{-1}$]
$Q_{i,-}$	vertical flow rate into cell i through the bottom of the cell [$L^3\ T^{-1}$]
R_i	right-hand side term for cell i in column solver [$L^2\ T^{-1}$]
S_s	specific storage [L^{-1}]
t	time [T]
V_i	volume of cell i [L^3]

w	exponent in *w*-order mean for hydraulic conductivities [-]
W_j	width of face *j* of an element (equal to either Δx_i or Δy_i) [L]
x	lateral ordinate [L]
$\underline{x}=(x,y,z)$	position vector [L]
y	lateral ordinate [L]
z	vertical ordinate [L]
z_b	elevation above datum of the model lower boundary [L]
z_c	elevation above datum of the cell from which spring discharge takes place [L]
z_g	elevation above datum of the ground surface [L]
z_{gs}	elevation above datum of the (effective) stream channel bed [L]
z_i	elevation above datum of the computational node for cell *i* [L]
$z_{k,j}$	elevation above datum of the computational node for cell *k* in an adjacent column which is connected to cell *i* on face *j* [L]
z_p	elevation above datum of the top of the stream channel seepage face [L]
z_r	elevation above datum of the bottom of the root zone [L]
z_s	elevation above datum of stream water surface [L]
z_{sp}	elevation above datum of spring discharge point [L]
α	parameter for the soil characteristic and unsaturated hydraulic conductivity functions [-]
$\beta_{z+,j}$	interim coefficient in column solver [$L^2\ T^{-1}$]
$\beta_{z-,j}$	interim coefficient in column solver [$L^2\ T^{-1}$]
ε_I	criterion for convergence of the inner iteration calculations [L]
ε_O	criterion for convergence of the outer iteration calculations [L]
$\gamma^1_{i,j}$	interim coefficient in column solver [$L^2\ T^{-1}$]
$\gamma^2_{i,j}$	interim coefficient in column solver [$L^2\ T^{-1}$]

$\delta_{i,j}$ flag for secondary cells in current column [-]

$\delta_{ij}(=\delta_{i,j})$ form of $\delta_{i,j}$ used for convenience in subscripts [-]

$\delta_{k,j}$ flag for secondary cells in adjacent column [-]

$\delta_{kj}(=\delta_{k,j})$ form of $\delta_{k,j}$ used for convenience in subscripts [-]

ΔL_j distance between a computational node and the *j*th edge of an element for the current column [L]

ΔL_j^1 distance between a computational node and the *j*th edge of an element for the adjacent column [L]

Δt computational timestep [T]

Δx_i , Δy_i , Δz_i dimensions of cell *i* [L]

$\Delta z'$ distance representative of a typical cell depth [L]

$\Delta \Psi^{n+1,m+1}$ solution vector for column solver (difference in values of ψ over a column iteration) [L]

$\Delta \psi_I$ difference in values of ψ between two inner iterations [L]

$\Delta \psi_O$ difference in values of ψ between two outer iterations [L]

$\Delta \psi_i^{n+1,m+1}$ difference in values of ψ for cell *i* over a column iteration [L]

η_i storage coefficient for cell *i* [L^{-1}]

$\bar{\eta}_i$ effective storage coefficient in the capillary fringe for cell *i* [L^{-1}]

θ volumetric soil water content [-]

θ_r residual volumetric soil water content [-]

$\theta_s(=n)$ saturated volumetric soil water content (equivalent to porosity, n) [-]

Θ relative saturation [-]

σ time-weighting factor [-]

ϕ angle between the line joining the nodes of adjacent cells and the horizontal [-]

ψ pressure potential [L]

$\underline{\Psi}^{n+1,m}$ vector of pressure potentials for all cells in a column at time level $n+1$, column iteration m [L]

$\underline{\Psi}^{n+1,m+1}$ vector of pressure potentials for all cells in a column at time level $n+1$, column iteration $m+1$ [L]

ψ_c pressure potential for the cell from which spring discharge takes place [L]

ψ_i pressure potential for cell i [L]

ψ_i^n pressure potential for cell i at time level n [L]

ψ_i^{n+1} pressure potential for cell i at time level $n+1$ [L]

$\psi_i^{n+1,m}$ pressure potential for cell i at time level $n+1$, column iteration m [L]

$\psi_i^{n+1,m+1}$ pressure potential for cell i at time level $n+1$, column iteration $m+1$ [L]

$\psi_{k_j}^{\ n}$ pressure potential for cell k in the adjacent column, connected to cell i on face j, at time level n [L]

$\psi_{k_j}^{\ n+1}$ pressure potential for cell k in the adjacent column, connected to cell i on face j, at time level $n+1$ [L]

$<.>_a$ arithmetic mean (conductivity) [L T^{-1}]

$<.>_g$ geometric mean (conductivity) [L T^{-1}]

$<.>_h$ harmonic mean (conductivity) [L T^{-1}]

$<.>_w$ w-order mean or power-averaging formula (conductivity) [L T^{-1}]

$<.>_{wh}$ weighted harmonic mean (conductance) [L^2 T^{-1}]

CHAPTER 1 INTRODUCTION

1.1 Background

Lateral flows above the regional groundwater table can occur under several different circumstances, and can be important for hillslope and catchment hydrology, and in particular for the transport of contaminants. For example, lateral flows may occur in perched water tables, in highly permeable near-surface soil horizons, or in some circumstances within the unsaturated zone. These flows are often neglected in numerical modelling studies.

One particular case where near-surface lateral flows may need to be modelled is for predictions of the migration of radionuclides from a subsurface source, as part of safety assessment studies for a potential radioactive waste repository in west Cumbria, UK. Studies of the migration of radionuclides in shallow aquifers and surface waters are currently being undertaken in support of such assessment studies within the Water Resource Systems Research Unit (WRSRU), University of Newcastle-upon-Tyne.

SHETRAN is a physically-based, distributed catchment flow, sediment transport, and contaminant migration modelling system which is being used in the radionuclide migration studies at WRSRU. SHETRAN is based upon the Système Hydrologique Européen (SHE) flow modelling system, which was originally conceived with the intention that it could be applied to "studies of land-use changes and their impacts, irrigation schemes, point and non-point source pollution, conjunctive uses of water and sediment yield" (**Abbott et al., 1986a**). Since the original conception of the development of such a modelling system, SHE and SHETRAN have begun to be extensively applied in all of these areas. However, development of the modelling system is continuing in the light of new research into physical processes and numerical methods, and methods of validation and application are continuing to evolve.

For this particular application of simulating the migration of radionuclides in the near-surface environment it has been concluded that the capabilities of the existing subsurface flow components of SHETRAN are not adequate in all circumstances of interest. The development of a new subsurface flow component for SHETRAN has been undertaken, therefore, to provide an improved subsurface flow capability.

1.2 Aims of the study

The aims of the work described in this thesis are:

- to review the characteristics of the west Cumbrian coastal plain aquifers;

- to review techniques for modelling three-dimensional complex aquifer systems; the reviews are primarily concerned with flow, but also necessarily need to consider contaminant transport;

- to identify modelling techniques relevant to the west Cumbrian coastal plain aquifers, and appropriate to the scale and complexity required for general catchment scale modelling;

- to specify a conceptual model;

- to develop a mathematical model based on the conceptual model;

- to develop appropriate numerical techniques to solve the equations specified in the mathematical model;

- to implement the mathematical model and numerical techniques as a component of the SHETRAN modelling system;

- to extend the contaminant transport components of SHETRAN to be compatible with the new subsurface flow model; and

- to test the new model, and to run first applications of the model.

During the development of the new subsurface flow model (hereafter referred to as the Variably-Saturated Subsurface flow, or VSS, model), several specialised areas of research have been reviewed. These include: three-dimensional groundwater and variably-saturated flow and transport modelling; unsaturated zone modelling; well hydraulics; and stream-aquifer interactions. Each of these areas has its own particular focus, and detailed models have been presented in the literature to investigate the fundamental processes governing flow and transport. For the development of a general-purpose subsurface flow model, which will be applied as a component of SHETRAN primarily at the catchment scale, equations have been

chosen or developed, based on well-proven methods, which can represent these processes at an appropriate level of detail and sophistication. The initial literature reviews upon which the development of the VSS model has been based were completed by the Summer of 1992.

1.3 Outline of the thesis

Chapter 1 includes the aims of the thesis (development and implementation of a new model for variably-saturated porous media), the types of environments and modelling scales for which the new model is designed, and descriptions of the SHETRAN modelling system.

Chapter 2 is a review of literature on the geology and hydrogeology of the coastal plain of west Cumbria, which is the focus area for development of the new VSS model (although the model is more generally applicable).

Chapter 3 is a review of literature on processes and modelling techniques for the types of conditions for which the VSS model may be applied, with particular reference to the conditions in west Cumbria; the chapter includes development of basic process equations, and equations describing boundary conditions and source/sink terms.

Chapter 4 is a concise statement of the conceptual and mathematical model, based on the equations developed in Chapter 3.

Chapter 5 includes a brief discussion of numerical methods that can be used to solve the equations in Chapter 4, and a detailed account of the methods used in the new VSS model.

Chapter 6 contains results from a series of verification tests, demonstrating the performance and capabilities of the new VSS model under idealised and hypothetical conditions.

Chapter 7 contains results from two applications of the new VSS model to real world case studies: the first involves comparison of simulated streamflow in a Mediterranean catchment with observed data; the second involves demonstrating the effects of geological structure in Quaternary drift deposits on subsurface conditions.

Chapter 8 contains a summary of the thesis, and a brief statement of areas in which further research work could be pursued.

Appendix A contains a report on the implementation of SHETRAN V3 (the version before the inclusion of the new VSS model) on a parallel processing system.

Appendix B contains mathematical details of one of the numerical methods used in the model.

1.4 The west Cumbrian coastal plain

Investigations are in progress into the feasibility of siting a potential deep disposal repository for intermediate, and some low, level radioactive waste near the Sellafield industrial complex in west Cumbria (Fig. 1.1). The repository would be at a depth of several hundreds of metres below ground, within the hard rock environment. The near-surface deposits overlying, and in the vicinity of, the site (both onshore and offshore) comprise interbedded and glacio-tectonically modified layers of Quaternary material (clays, sands, gravels, peat) overlying fissured sandstone. The VSS model development is focused on this environment, but the model will be sufficiently general to allow other environments to be simulated.

1.5 Modelling environments

SHETRAN is designed to be a very general modelling system; applications of the SHE and SHETRAN have been made at spatial scales ranging from 30 m^2 to 5000 km^2 for a variety of environments (**Bathurst and O'Connell, 1992**). Distinctions can be made between several basic types of environment (in terms of relief or lithology), which both the existing SHETRAN and the new VSS model may be expected to be capable of simulating:

a) *upland catchments*: characterised by steep topography, shallow poorly developed soils, and fast surface or near-surface (interflow) runoff;

b) *deep regional aquifers*: generally characterised by shallow topography, and slow response times;

c) *unconsolidated sediments*: these can usually be treated as a porous medium;

d) *fissured/fractured/faulted rocks*: only rocks which can be characterised as a single anisotropic heterogeneous porous medium at the modelling scale will be considered in the first instance;

e) *surface soils*: flow characteristics can be greatly modified by the presence of organic matter, and by the development of preferential flow pathways (macropores).

Simplifications are often made in catchment models to represent the processes acting in each of these environments at an appropriate level of detail. The appropriate level of detail depends upon the type of application; for example, the use of a two-dimensional vertically-averaged aquifer model may be adequate for simulations of total catchment runoff, whereas a simulation of contaminant migration from a point source may require a three-dimensional representation of aquifer flows.

1.6 Modelling scales

1.6.1 Timescales

The usual simulation timestep will be one or two hours, reduced during storm events. The maximum timestep used will normally be controlled by conditions near the ground surface (surface runoff, evaporation and infiltration). Simulations of up to approximately 30 years are expected to be achievable on currently available workstations, taking a reasonable amount of computer time (several hours). (A macroscale model for flow and contaminant transport is currently being developed within WRSRU which is intended to be capable of giving results of the type produced by SHETRAN over periods of hundreds of years.)

1.6.2 Vertical scales

The vertical dimension will be determined either by the depth to the base of a clearly defined aquifer, or by the degree of mixing of deep groundwater and meteoric water over the simulation timescale. A maximum vertical dimension of 50 metres is thought likely to be sufficient for most applications; however, the only theoretical limit on the thickness of aquifers which can be modelled is due to the available computer resources. The minimum vertical dimension will be less than 1 metre for shallow upland soils overlying impermeable bedrock.

1.6.3 Lateral scales

Lateral scales for SHETRAN applications (past, present, and future) vary widely. The underlying physics and numerical methods can be applied at different scales, although care has to be taken in selecting parameter values and representations of catchments (such as

vegetation distributions and topography) which are appropriate for use at a given scale. This is a continuing area of research, with much of the recent effort being devoted to stochastic descriptions of aquifer properties to represent heterogeneities at either the local or the regional scale (eg. **Dagan, 1987**). The impetus for these theoretical studies arises particularly from the observation that the magnitude of effective dispersivities derived from large-scale field experiments (macrodispersivities) increases with the size of the experiment (**Gelhar, 1986**). The approach taken for the development of the VSS model is consistent with that of the existing SHETRAN: the model is deterministic, and the effects of sub-grid scale heterogeneities are accounted for by using an effective dispersivity approach; therefore, a full review of stochastic models is not included in this thesis.

The scales associated with typical SHETRAN applications are:

a) *small plot* - a few square metres (eg. a single grid element);
b) *large plot* - 10's to 100's of square metres (eg. 100 elements of 1 square metre);
c) *research catchment* - 1 to 10 square km (eg. 500 elements of 50 x 50 metres);
d) *catchment* - 10 to 100 square km (eg. 200 elements of 0.5 x 0.5 km.);
e) *large catchment / region* - >100 square km (eg. 500 elements of 1 square km).

1.7 The existing SHETRAN V3 modelling system

1.7.1 Subdivision of a catchment

Three types of elements are used to define the finite difference representation of a catchment: basic elements (usually called grid elements), bank elements, and stream channel links. A typical part of a catchment is shown in Fig. 1.2. The catchment is divided into a basic grid of rectangular elements, with stream channel links running along the edge of the grid elements. Bank elements (which are optional for any simulation) are narrow elements along each side of the stream channel links. Grid and bank elements have a vertical extent, and form a column which is divided into a number of cells.

1.7.2 Structure of SHETRAN V3

The SHETRAN modelling system is written in a hierarchical, modular form. SHETRAN V3 has five components:

- Frame (FR, overall control);
- Library (SHE, general purpose routines);
- Water flow (WAT);
- Sediment transport (SY);
- Contaminant transport (CM).

Each component is made up of a number of modules.

1.7.3 Flow component

The water flow component of SHETRAN V3 consists of the following modules:

- Evapotranspiration/interception (ET);
- Overland/channel (OC);
- Unsaturated zone (UZ);
- Saturated zone (SZ);
- Exchange (aquifer channel) (EX);
- Snowmelt (SM);
- Stream bank (BK).

Subsurface flow calculations are currently carried out within SHETRAN V3 by three modules: the saturated zone module uses the vertically-averaged Boussinesq equation to simulate two-dimensional flow in unconfined aquifers only; the unsaturated zone module uses the Richards equation to simulate vertical flow in the unsaturated zone above the water table, and is coupled to the saturated zone solution by a mass balance procedure; and the aquifer-channel exchange module handles flows within a connected stream-aquifer system.

1.7.4 Contaminant transport component

A component for modelling contaminant transport in catchments has been developed, which includes transport in the saturated and unsaturated zones, in surface water, and adsorbed to sediment particles, as well as uptake by plants. Full details of the subsurface modules of the contaminant transport component can be found in **Ewen (1990)** and **Ewen (1991)**; an overview of the component is given in **Ewen (1995)**.

The contaminant transport module for the saturated zone simulates three-dimensional transport, using a three-dimensional flow field calculated from the two-dimensional Boussinesq head distribution. This approach, with its obvious limited capabilities, was designed to be used in the interim period, until the new three-dimensional subsurface flow module had been completed.

1.8 The SHETRAN V4 modelling system, including the new VSS model, developed in this study

SHETRAN V4 is based upon the same finite difference representation of a catchment as SHETRAN V3. The VSS model is integrated into the system, and entirely replaces the unsaturated zone, the saturated zone, and the aquifer-channel exchange modules of SHETRAN V3. The three-dimensional capabilities of the VSS model provide flow fields for use in the contaminant migration component, replacing the interim approximations to three-dimensional saturated zone flows used in SHETRAN V3.

1.9 Use of the new model

It is becoming increasingly clear that one of the most important uses of a model as complex as SHETRAN is for supplying detailed supporting evidence, based on theoretically justifiable physical principles, for simpler models. The new VSS model has been designed in this spirit, therefore, and is intended for use as a simulation tool for investigating subsurface flow and transport in complex aquifer systems in some detail. Given the complex and detailed nature of the model applications, it is likely that most simulations will be computationally intensive (the model has been developed on powerful Unix workstations).

1.10 Some notes on nomenclature

The term *variably-saturated* is used in this report to describe environments or models which involve both saturated and unsaturated regions (the most commonly used alternative description is saturated-unsaturated).

The term *groundwater* is used to describe water stored in (saturated) aquifers (not including water stored in the unsaturated zone). Note that the unsaturated zone is defined to include regions that are temporarily saturated, near the ground surface or in perched water tables for example.

Several concepts that are commonly used in either groundwater hydrology or in studies involving the unsaturated zone are made redundant by the development of a three-dimensional model which uses more fundamental soil and rock properties (this was recognised by **Freeze (1971)**). The concepts of *transmissivity* and *specific yield*, which relate to two-dimensional aquifer models, are therefore not used. In the unsaturated zone, terms relating to the soil characteristic function (pressure potential versus moisture content) such as *wilting point*, *field capacity*, and *residual moisture content* are not directly used, although they can be useful for general descriptive purposes. The underlying physical basis for other terms such as *infiltration capacity* is also contained in the more fundamental parameters.

1.11 Parallel processing

During the development of the VSS model described in this thesis there have been very rapid improvements in the computer hardware available for scientific processing. The processing power of the Unix workstations available in the WRSRU on which all development work has taken place has increased by at least an order of magnitude during this period.

An early aim of the thesis was to investigate the use of parallel processing technology and algorithms to improve the computational performance of numerical modelling systems, as it was thought that work in this area would be essential for the development of a useful catchment scale three-dimensional model. Some preliminary work on parallel processing was completed, in which version 3 of the SHETRAN modelling system (the version prior to the integration of the VSS model) was parallelised successfully. Some feasibility studies on different parallel processing systems were also completed. Given the improvements in computer hardware, however, the need to develop the VSS model specifically for a parallel computer architecture became less, and further work was not undertaken.

Descriptions of the successful parallelisation of SHETRAN V3, and of the feasibility studies, are given in full in Appendix A.

1.12 Contributions of this thesis

There are several features of the VSS model developed in this thesis which form notable contributions to catchment scale hydrological modelling, and which distinguish VSS from other variably-saturated models reported in the literature.

• The implementation of VSS as a component of the catchment flow and transport modelling system, SHETRAN, provides a comprehensive general-purpose tool for integrated surface-subsurface modelling. The inclusion of the VSS model is a significant enhancement of the capabilities of SHETRAN.

• The flexible-geometry finite-difference mesh used in VSS has been designed to be particularly suitable for simulating flow and transport in the complex layered structures which occur in some Quaternary drift deposits. The VSS model provides an appropriate tool for detailed investigation of the effects of the structure and properties of drift deposits on the movement of contaminants, and in controlling recharge.

• There is a comprehensive treatment of boundary conditions for VSS; in particular, the near-channel mesh refinement within a catchment scale modelling system, allowing for most types of stream-aquifer interactions including the development of unsaturated regions below the stream channel, is a substantial improvement over existing catchment scale models.

• The column-based solution algorithm together with the adaptive convergence algorithm has proved to be a computationally feasible method of solving the three-dimensional variably-saturated flow equations. Simulations of flow and transport in a catchment over a 30 year period using timesteps of approximately one hour have been run successfully using SHETRAN V4 (these were not run as part of this thesis). Simulations of integrated surface and fully three-dimensional variably-saturated subsurface flow and transport using timesteps of about one hour and run over periods of several decades represents the state-of-the-art in physically-based catchment modelling.

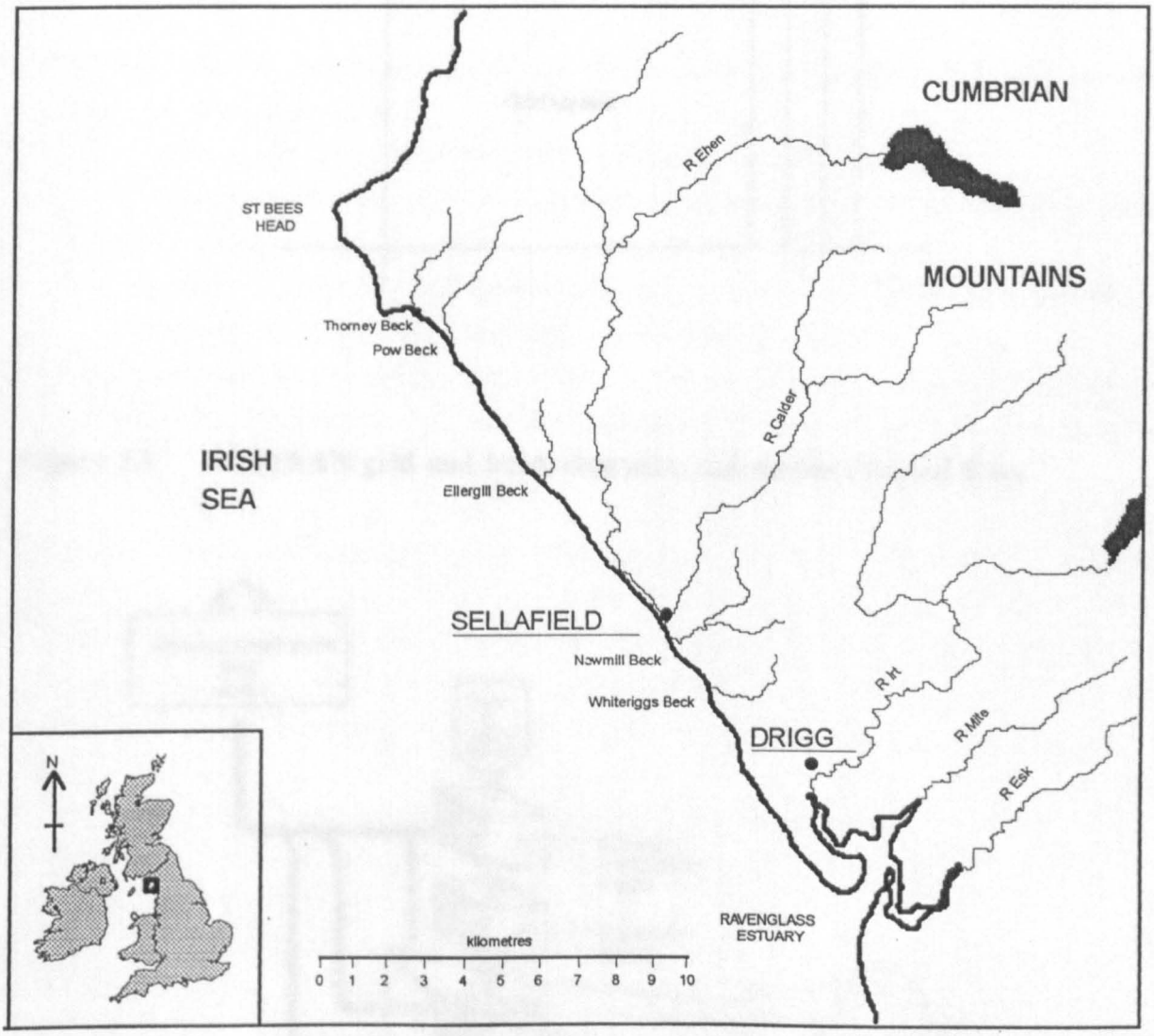

Figure 1.1 The study area: west Cumbrian coastal plain

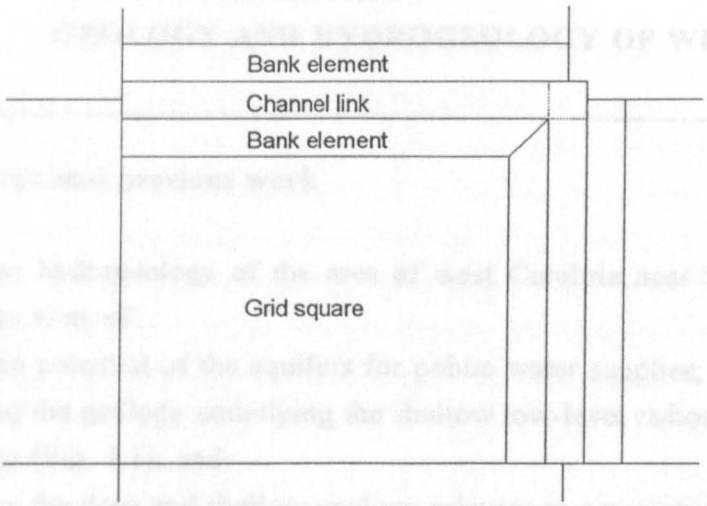

Figure 1.2 SHETRAN grid and bank elements, and stream channel links

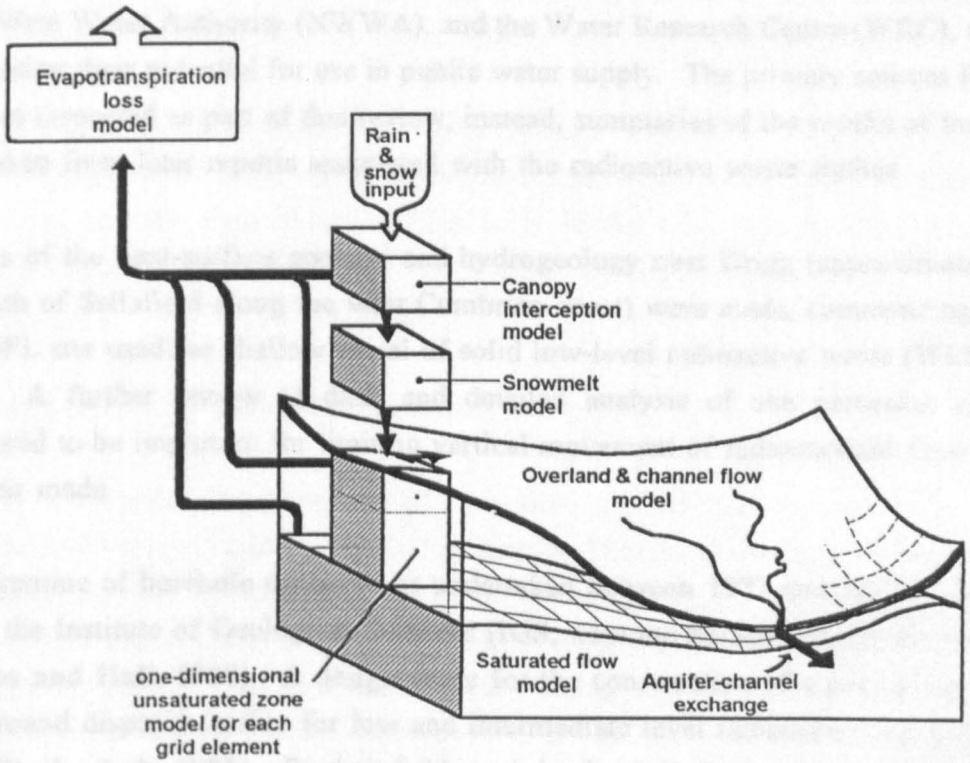

Figure 1.3 SHETRAN V3.4 modelling system flow component

CHAPTER 2 LITERATURE REVIEW: GEOLOGY AND HYDROGEOLOGY OF WEST CUMBRIA

2.1 Field surveys and previous work

Field studies of the hydrogeology of the area of west Cumbria near Sellafield have been carried out with the aims of:

1) assessing the potential of the aquifers for public water supplies;
2) investigating the geology underlying the shallow low-level radioactive waste disposal site at Drigg (Fig. 1.1); and
3) investigating the deep and shallow geology relevant to a potential deep repository for intermediate level radioactive waste near Sellafield (Fig. 1.1).

Further information is available from mines in the Carboniferous sequences north-east of Sellafield. This chapter is a review of the published information generated from the various surveys. No original field data have been examined as part of this work.

Surveys of the west Cumbrian coastal plain aquifers have been carried out by the former North West Water Authority (NWWA), and the Water Research Centre (WRC), with the aim of assessing their potential for use in public water supply. The primary sources for this work were not inspected as part of this review; instead, summaries of the results of the work have been taken from later reports associated with the radioactive waste studies.

Surveys of the near-surface geology and hydrogeology near Drigg (approximately 20km to the south of Sellafield along the west Cumbrian coast) were made, commencing in 1977, at the BNFL site used for shallow burial of solid low-level radioactive waste (**Williams et al., 1985**). A further review of data, and detailed analysis of one particular clay horizon considered to be important for limiting vertical movement of radionuclides from the wastes, was later made.

A programme of borehole drilling was undertaken between 1977 and 1979 at the Sellafield site by the Institute of Geological Sciences (IGS; now the British Geological Survey, BGS) (**Holmes and Hall, 1980**). A design study for the construction of a possible offshore deep underground disposal facility for low and intermediate level radioactive waste was made in 1981 (**Black et al., 1981**). Further field work in the Sellafield area has since taken place, focused particularly on an onshore location for the potential radioactive waste repository. The interpretation of this work current at the time of this review is summarised in **Nirex (1992a)**,

with a detailed analysis of the hydrogeology given in **Nirex (1992b)**. The field programme connected with the potential onshore deep disposal facility is continuing, with several deep boreholes already drilled, and further deep boreholes planned. Of more direct significance to the present work, a programme of shallow boreholes and associated work is in progress, with the primary aim of characterising the nature of the Quaternary deposits. This will provide information on the three-dimensional geometry of the deposits, on their hydraulic characteristics, and on the flow and transport pathways within the deposits. Unfortunately, data from this programme were not available in time for this review.

2.2 Regional geological setting

The study area lies on the western side of the Lake District massif, a glaciated region with a central zone of Lower Palaeozoic metasediments and igneous rocks, surrounded by younger Permo-Triassic and Carboniferous strata (**Moseley, 1978**). Rocks of these types in the central upland area are mostly well exposed, but only limited outcrops are seen in the surrounding areas. The central Lower Palaeozoic rocks have generally very low permeabilities and underlie the surrounding rocks which contain several major aquifers (**Patrick, 1978**).

The study area for this thesis lies along the western flank of the central upland area. The general dome structure of the massif is evident in the westward-dipping strata underlying the coastal plain and the offshore region (Fig. 2.1). In the study area the Sherwood Sandstone Group hosts the principal aquifer, and is overlain by Quaternary deposits.

2.3 The Sherwood Sandstone Group

The Sherwood Sandstone Group (SSG) has been divided into two formations, an upper sandstone and a lower St. Bees Sandstone. The St. Bees Sandstone has recently been further sub-divided into two formations (**Nirex, 1992a**), an upper Calder Sandstone and the lower retaining the name St. Bees Sandstone. The sandstones are generally described as dull red or orange in colour, with low-angle cross-bedding (of thickness varying from a few centimetres to over two metres) dipping at 10-15° to the west or south-west. They are composed of rounded quartz grains (a result of sub-aerial deposition), relatively well cemented with a calcareous cement. Certain well cemented horizons have been used as a building stone throughout west Cumbria, but the sandstone can be locally friable. Argillaceous content

decreases towards the upper layers of the formation. Numerous shale partings are evident.

Black et al. (1981) reported that there were no detailed data available on the orientation and frequency of jointing in the SSG of west Cumbria. They suggest, however, some joint spacings based on observations from outcrops near St. Bees Head of around 6 metres for subvertical joints, and 'several metres' for subhorizontal joints, with the likelihood that further secondary jointing would be expected within these intervals. Further information on jointing in the SSG in the eastern Lake District is given in **Moseley and Ahmed (1967)**. They describe high frequencies of jointing in fine-grained sandstone, with localised zones of up to 10 parallel joints in less than 10 cm, separated by a metre of unjointed rock.

Patrick (1978) considered that the fissures in the SSG "are well developed and contribute 98% of the total transmissivity in West Cumbria". Evidence from field surveys to assess the potential of the SSG as an aquifer suggests that fracture zones are generally associated with fault zones (**Black et al., 1981**) - only boreholes located in fault zones were productive.

2.4 Quaternary deposits

The Quaternary deposits overlying the sandstone aquifer consist of complex interbedded units of boulder clays, sands and gravels. In places they have been glacio-tectonically modified and/or covered with more recent deposits of alluvium, wind-blown sand, and peat. The significant feature of the lithological and stratigraphic descriptions of these deposits upon which all authors agree is that they are highly complex and variable, and are not yet well understood.

The deposits have been interpreted to be the result of one or more phases of the Devensian glaciation. **Williams et al. (1985)** refer to two major phases of glaciation: the Main and Scottish Re-advance. Three separate advances were recognised by **Trotter et al. (1937)** based on lithological evidence and characteristics of glacial erratics. Multi-layered till sequences can, however, be caused by a single glacial period, being due to oscillation in the advance and retreat of an ice sheet.

The coarse-grained sands and gravels which form a significant part of the deposits have a glacio-fluvial origin. **Holmes and Hall (1980)** described them as follows:

"Coarse-grained sediments predominate, suggesting a glacial outwash mode of deposition, in which a braided river, fed by glacial outwash material, meandered across a flood plain. In swift currents, only coarse material was deposited while finer material was washed away. The finer material was deposited in only sluggishly flowing or stagnant water. As the river moved laterally across its flood plain, the nature of the sediments deposited varied from coarse to fine as in the cross-sections."

Within the gravel deposits, large boulders have been reported both at Sellafield (**Holmes and Hall, 1980**) and at Drigg (**Williams et al., 1985**).

Peat layers can be found within the deposits, especially towards the higher ground inland. In addition, deposits of alluvium, scree, and lake materials are evident (**Nirex, 1992a**). Post-glacial deposits of blown sand, peat, and alluvium at Drigg are reported to be typically 2 to 3 metres thick, reaching a maximum of 6 metres (**Williams et al., 1985**).

The total thickness of the onshore Quaternary deposits varies from zero to around 100 metres (**Nirex, 1992a**). Offshore, the total thickness can be more than 200 metres (**Pantin, 1977**). **Nirex (1992a)** notes that "In some important aspects of Quaternary history, the commonly accepted interpretation of offshore data differs significantly from that onshore". Both onshore and offshore there is evidence of buried channels cut into the sandstone bedrock, where the thickness of the glacial deposits is greatest.

The thickness of each of the lithologies is highly variable. **Holmes and Hall (1980)** describe clay layers up to 12 metres thick, and silty sands up to 15 metres thick, at the Sellafield site. **Williams et al. (1985)** describe an 'idealised' glacial sequence at the Drigg site further south along the coast, but note the frequent variations from this conceptualisation, both in the thicknesses and number of horizons. In general, the deposits at Sellafield are less stratified and more complex than those at Drigg.

The lateral correlation of the horizons can be extremely difficult to interpret, especially at Sellafield. **Holmes and Hall (1980)** presented logs of four boreholes from the Sellafield site which were drilled within a 30 metre radius of each other, yet show no apparent correlation. At Drigg, correlations have been made over scales of hundreds of metres or more (**Williams et al., 1985**).

2.5 Surface soils

The soils of the area are described by **Jarvis et al. (1984)**. The post-glaciation development of the soils on the coastal plain has depended upon both fluvial and coastal processes. On the coastal plain between St. Bees Head and the Ravenglass estuary, 8 different soil associations are identified. These can be roughly categorised into the very sandy coastal dunes towards the southern (estuary) end of the coastline (Sandwich association); well drained coarse or sandy loams developed on glaciofluvial drift over most of the coastal plain (Eardiston 1, Wick 1, Ellerbeck, Newport 1 and Blackwood associations); and fine silty or clayey river alluvium on flat land adjacent to some of the larger river channels (Hollington and Fladbury 3 associations). The river alluvium comprises loam or clay overlying gravel. Some terraces are cut into the Boulder Clay.

The distribution of upland soils is largely dependent upon elevation. Shallow acid peats (Bangor association) overlying acid crystalline rocks partially cover the high peaks, with about 20% of the land area consisting of exposed rock. In upland areas where the ground is flat or gently sloping, deeper waterlogged peats occur (Winter Hill association). On steep bouldery slopes on valley sides there are well-drained podzolic loamy soils (Malvern and Moretonhampstead associations). On some outlying moderately sloping land overlying sandstone there are seasonally waterlogged stagnohumic gley soils (Wilcocks 1 association).

For the purposes of modelling, the soils can be considered to be mostly easily draining, except for some areas of alluvium and peat. The soils can be generally divided into two groups: upland soils, which are shallow (soil depths are effectively zero where outcrop occurs), steeply sloping, and which rest directly on a low permeability bedrock; and lowland soils, which are on shallow slopes, and which overlie aquifers.

2.6 Hydrogeology

2.6.1 Regional hydrogeology

The general pattern of groundwater movement within the Cumbrian region is dominated by the radial geometry of the Cumbrian hills. The relatively impermeable rocks underlying the central area reduce recharge of the groundwater, and most precipitation is subsequently lost in the form of surface runoff.

Along the west Cumbrian coastal plain the sandstone aquifer is recharged inland where the overlying deposits are relatively thin (Fig. 2.2). Towards the coast the recharge is lower, and a general region of upflow discharges into rivers and to the coastal area. The freshwater/saline interface is assumed to occur at an angle from the seabed to underneath the onshore coastal plain.

2.6.2 Sandstone aquifer

The sandstone is the primary aquifer in the region. Water levels measured from the borehole surveys show a topographically-dominated system, with a generally coastward flow. Responses of monitored wells near the coast show evidence of tidal forcing.

The groundwater in the sandstone aquifer can be confined, semi-confined or unconfined, depending upon local conditions. Confined conditions occur where low permeability clay layers lie at the base of the overlying Quaternary deposits, especially where the deposits are thick. In areas where there are no extensive clay deposits, and particularly where the sandstone outcrops or is close to the ground surface, conditions are unconfined. (**Lloyd (1980)**, notes that Quaternary drift deposits in Britain, which are often assumed to consist of Boulder Clay and to therefore provide a confining layer, can in fact provide significant recharge to an aquifer, and in some cases can form significant extensions to the total storage of an aquifer.)

Patrick (1978) considered that most of the flow in the sandstone occurs through fissures (see Section 2.4).

2.6.3 Perched aquifers

Above the main regional aquifer, lying mostly in the sandstone, perched aquifers have been widely reported within the Quaternary deposits, both at the Sellafield and the Drigg sites (eg. **Holmes and Hall, 1980**; **Williams et al., 1985**; **Nirex, 1992a**). Some perching may also occur associated with interbedded siltstone within the sandstone on steep terrain (**Nirex, 1992b**). No quantitative information on the extent of perching or on lateral flows has been reported, although it is recognised that flow patterns are likely to be complex.

2.6.4 Surface water systems

Three major surface water catchments drain the Cumbrian hills and cross the west Cumbrian coastal plain near Sellafield: the Ehen, the Calder, and the Irt (Fig. 1.1). Many small streams rise in the coastal plain (often from a spring source) and drain the areas between the larger rivers, running mostly over the Quaternary deposits. The rivers incise deeply into the foothills, eroding through to the sandstone in places, and strongly affect the groundwater patterns. From the evidence of the water level maps, **Suttie (1989)** concluded that the Calder is a gaining river for most of its length over the sandstone aquifer.

2.6.5 Springs

A large number of springs have been identified on the coastal plain. Some of these emerge at or near the interface between the sandstone aquifer and the Borrowdale Volcanics (**Nirex, 1992a**). A significant number of springs also emerge from within the Borrowdale Volcanics. Some contact springs may emerge due to interbedded siltstone within the sandstone on steep terrain (**Nirex, 1992b**).

2.6.6 Anthropogenic influences

The River Ehen has its source in the Ennerdale valley; and low flows are artificially compensated for by discharges from Ennerdale Water. In addition, water from the Beckermet mines is discharged into the Ehen. A conjunctive use scheme is in operation on the River Calder, with groundwater abstraction being used for river augmentation to maintain levels for supply to the Sellafield industrial works. Low flows in the River Irt are artificially augmented by compensation water from Wastwater in Wasdale. Numerous shallow abstraction wells are sited in the Quaternary deposits and in the upper parts of the sandstone aquifer.

2.7 Conclusions

The following list is a summary of the main features of the Sellafield area relevant to modelling of the near-surface aquifers and soils in both the coastal plain and the upland areas, and forms the basis for specifying the operational requirements of the new VSS model.

1. The near-surface aquifer of the west Cumbrian coastal plain consists of sandstones of the Sherwood Sandstone Group (SSG), which may have undergone weathering in their upper layers, and the Quaternary deposits which overlie them.
2. The geology beneath the upland catchments in the Cumbrian hills above the west Cumbrian coastal plain consist of relatively impermeable units of the Borrowdale Volcanic Group, Skiddaw Slates, and Granites.
3. The surface soils of the upland catchments range from poorly drained peats to well-drained loams; there are significant areas of rock outcrops.
4. The Quaternary deposits consist of interbedded and in places glacio-tectonically modified sequences of sands, gravels and boulder clay, with lenses of peat and clay.
5. The regional groundwater flow is driven by recharge in the Cumbrian hills, and contributes a net upward flow to the base of the coastal plain near-surface aquifers.
6. The SSG is generally in hydraulic contact with the Quaternary deposits.
7. The regional aquifer shows both confined and unconfined characteristics, depending upon the local configuration of the Quaternary deposits.
8. There are likely to be complex three-dimensional flow patterns in the upper layers of the SSG and overlying Quaternary deposits.
9. Perched aquifers can develop over clay lenses.
10. The natural aquifer discharges are to a) river channels, b) springs, and c) the offshore seabed.
11. The natural flow pattern is affected by anthropogenic influences, through shallow well abstraction, and river abstraction and augmentation.

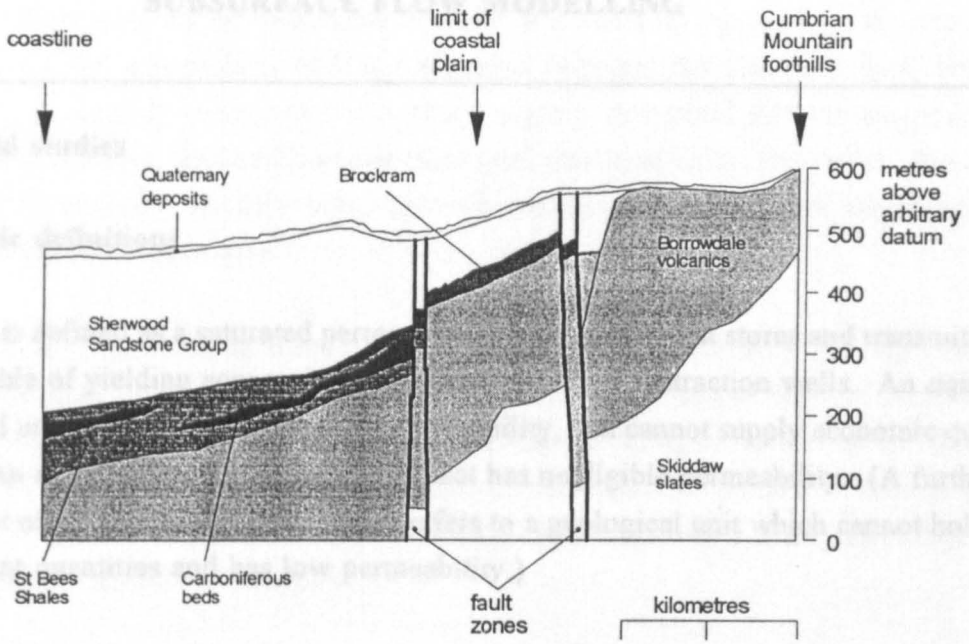

Figure 2.1 Schematic section of regional geology (after Black et al., 1981)

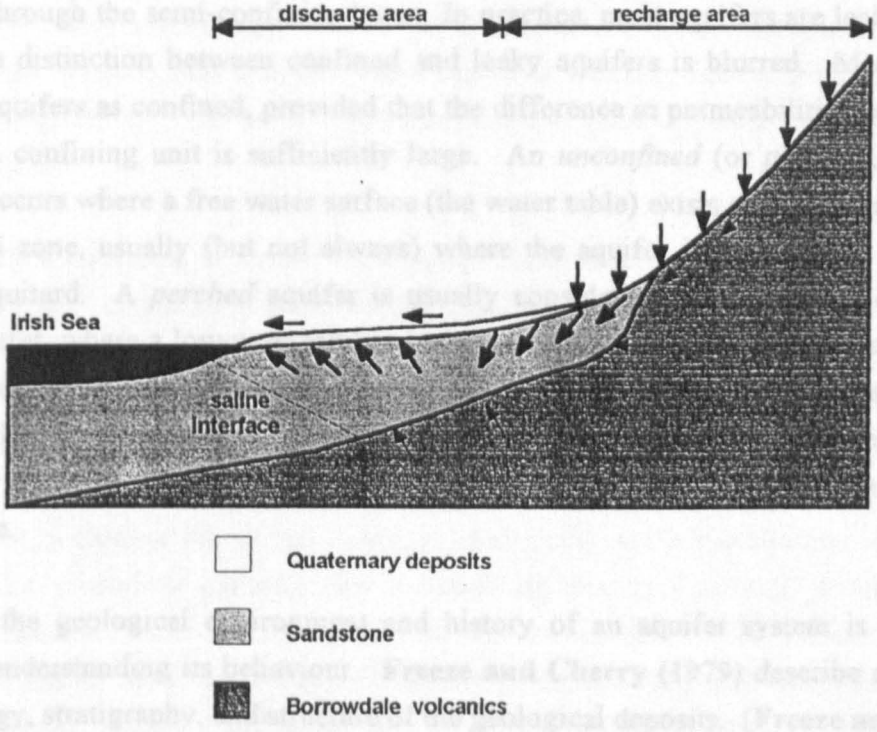

Figure 2.2 Schematic representation of regional groundwater flow

CHAPTER 3 LITERATURE REVIEW: SUBSURFACE FLOW MODELLING

3.1 Field studies

3.1.1 Basic definitions

An *aquifer* is defined as a saturated permeable geological unit that stores and transmits water, and is capable of yielding economic quantities of water to abstraction wells. An *aquitard* is a geological unit that has a relatively low permeability, and cannot supply economic quantities of water. An *aquiclude* is a geological unit that has negligible permeability. (A further term which is not often used is *aquifuge*, which refers to a geological unit which cannot hold water in significant quantities and has low permeability.)

Four types of aquifer can be defined: confined, unconfined, semi-confined, and perched (Fig. 3.1); see, for example, **Todd (1980)**. *Confined* (or *artesian*) aquifers develop where full saturation occurs within a potentially water-bearing rock which is overlain by a relatively impermeable layer (aquitard or aquiclude). A *semi-confined* (or *leaky*) aquifer is one where a layer of low (but not negligible) permeability medium overlies the aquifer, allowing some flow of water through the semi-confining layer. In practice, most aquifers are leaky to some degree, and the distinction between confined and leaky aquifers is blurred. Many authors refer to leaky aquifers as confined, provided that the difference in permeabilities between the aquifer and the confining unit is sufficiently large. An *unconfined* (or *phreatic*, or *water-table*) aquifer occurs where a free water surface (the water table) exists as the upper boundary of the saturated zone, usually (but not always) where the aquifer is not overlain by a low-permeability aquitard. A *perched* aquifer is usually considered to be a special case of an unconfined aquifer, where a low-permeability layer (often a localised lens) forms a barrier to infiltrating water within the unsaturated zone, and a saturated zone develops above, and separate from, the regional water table. *Multi-layered* aquifers consist of sequences of media with alternately high and low permeabilities, which may include any of the aquifer types described above.

Knowledge of the geological environment and history of an aquifer system is of crucial importance in understanding its behaviour. **Freeze and Cherry (1979)** describe aquifers in terms of lithology, stratigraphy, and structure of the geological deposits. (**Freeze and Cherry (1979)**, describe *lithology* as 'the physical makeup, including the mineral composition, grain

size, and grain packing, of the sediments or rocks that make up the geological systems', and *stratigraphy* as 'the geometrical and age relations between the various lenses, beds, and formations in geological systems of sedimentary origin'.) Structural features are produced by deformation of the rock, and may include cleavages, fractures, folds, and faults. **Freeze and Cherry (1979)** describe the following types of geological environments which may form significant aquifers or aquitards:

alluvial deposits (described as fluvial deposits by **Freeze and Cherry (1979)**) - these are materials deposited by rivers, in channels or on floodplains, and consist of non-cemented particles which may be coarse- or fine-grained, depending upon the mode of deposition. **Todd (1980)** estimated that 90% of all developed aquifers consist of coarse-grained unconsolidated alluvial deposits. Complex bedding of different types of deposits often occurs, which can lead to significant anisotropy.

aeolian deposits - these are relatively non-cohesive materials transported and deposited by wind action. Particle sizes are usually in the sand or silt ranges (extensive silt deposits, known as loess, are the most common type of aeolian deposit). Due to the sorting action of the transport mechanism, the aquifers are usually homogeneous and isotropic.

glacial deposits - these include glacial till, glaciofluvial, and glaciolacustrine sediments. Deposits are often layered, with coarse-grained materials forming aquifers, and silt or clay layers forming aquitards. The west Cumbrian coastal plain deposits are primarily of glaciofluvial origin.

sedimentary rocks (sandstone, carbonate rocks, coal, shale, mudstones)
- sandstone deposits, originating from marine, fluvial, or aeolian sources, often form significant aquifers. Porosities and permeabilities cover a wide range, depending upon the degree of compaction and cementation, and upon the amount of fracturing. Significant anisotropy between the horizontal and vertical directions can occur due to small-scale stratification caused by varying depositional conditions.
- carbonate rocks, including limestone, dolomite, and chalk, are often aquifers, commonly having significant secondary porosity and permeability due to fractures, which may be enlarged by dissolution.
- coal deposits can also have an increased secondary permeability due to fractures across or along bedding planes, but bulk porosities may be low. Most usually, coal deposits form aquitards.

- shale, originating from compacted mud deposits, generally has low permeability. Secondary permeabilities due to fractures, especially at shallower depths, can increase bulk permeabilities.
- mudstones, which are similar to shales (described as blocky or massive sediments, in contrast to shale which is fissile and laminated, **Pettijohn (1975)**), may also exhibit enhanced permeability due to fracturing when over-consolidated.

igneous and metamorphic rocks - unfractured rocks generally have very low porosity and permeability due to pore spaces being small and unconnected. Significant permeabilities are mostly due to fractures (although volcanic rocks can have high permeability due to the presence of gas vents, lava tubes, tree molds, cooling joints and clinker zones).

3.1.2 Flow in multi-layered aquifers

There are very few field investigations of contaminant movement and distribution in partially saturated multi-layered porous media, or contaminant transport modelling studies in this type of environment, reported in the literature. One of the few studies available is by **Maguire (1988)**. He investigated the movement of fuel oil (a non-aqueous phase liquid, or NAPL) following a subsurface spillage in a glacial till sequence in New Jersey. The site hydrogeology was characterised by a perched water table (sensitive to precipitation events) overlying a deeper regional water table. He found that the presence of a saturated horizon above a low permeability stratum acted to "significantly alter contaminant migration pathways as well as transport velocities". The transport of the NAPL was primarily lateral, and was driven by velocities approximately an order of magnitude greater than those of the underlying water table aquifer. He also found that the transport directions were both up and down the hydraulic gradient of the underlying regional aquifer.

Many studies have been made into flow and transport in multi-layered aquifers using fully saturated groundwater models (such as the USGS model of **Trescott (1975)** and **Trescott and Larson (1976)**). These have largely arisen out of the need to characterise contaminant migration accurately for recovery operations following spillages. An important area of research underpinning these types of study is into the spatial variability of hydraulic conductivity in complex aquifers. The magnitude and direction of transport velocities depends on accurate characterisation of the spatial distribution of physical properties of the aquifer. In particular, internal heterogeneity within geologic formations critically affects the dispersion

of contaminants. Invasive measurement of hydraulic parameters at a sufficiently detailed scale is not practicable for most field applications. The alternative approach most widely researched is the use of stochastically generated fields of parameter values, conditioned on available point measurements, using geostatistical methods.

One interesting and relevant result arising from such a stochastic modelling study is given by **Fogg (1986)**. He generated data for a three-dimensional groundwater flow and transport model (TERZAGI) based on field measurements of a fluvial depositional aquifer consisting of multiple elongated sand, silt and clay bodies, and concluded that the resulting flow fields were controlled by the continuity and interconnectedness of the sand bodies, rather than their actual values of hydraulic conductivity. For practical applications, he recognised that, although the interconnectedness of the high permeability layers is of critical importance, it is very difficult to estimate. This implies that there should be more interaction and understanding between geologists and hydrological modellers so that the hydrogeological characterisation and its effect on model predictions can be better assessed. He made the further observation that the hydraulic head field is not necessarily sensitive to the degree of connectedness of the high permeability bodies.

A conceptually simpler numerical modelling study of flow in multiple perched groundwater mounds was made by **Brock (1990)**, who compared the results from a radial multi-layer model with data from an artificial recharge pond for both confined and unconfined conditions and found that, under these simple conditions, a multi-aquifer model was adequate to reproduce the observed heads.

3.1.3 Flow in unsaturated media

The unsaturated zone can be defined as the region of soil or rock where the pressure potential is negative (**Nielsen et al., 1986**), with the reference zero potential taken to be equal to atmospheric pressure. However, for convenience, many authors include regions of temporary saturation near to the ground surface and associated with perched water tables in the unsaturated zone. Taking this extended definition, and noting that the *capillary fringe* (the zone of tension saturation immediately above a water table) is at a negative potential, the *unsaturated zone* is defined as the region between the main water table (ie. zero potential surface) and the ground surface. Typically, the thickness of the unsaturated zone is at most a few tens of metres, although in some cases it may extend to several hundred metres (eg. **Peters and Klavetter, 1988**). The thickness of the capillary fringe may be almost negligible

in coarse sand (less than a centimetre), but may extend to several metres in fine-textured media (**Gillham, 1984**).

The importance of the unsaturated zone lies in its role as a conduit and buffer for water and dissolved contaminants, and in its interfaces at the ground surface and at the water table. At the ground surface, the infiltration of precipitation is controlled by conditions within the top few centimetres of soil, and the rate of evaporation from the soil surface and of transpiration from plants is governed by the moisture availability in the soil. The rate of recharge to the water table is controlled by conditions in the unsaturated zone (which are often grossly simplified in groundwater models).

Although most representations of flow in the unsaturated zone have traditionally been based on the assumption that flow is predominantly vertical, there is a growing awareness that this may not be a valid assumption, except under particular conditions. Steeply sloping or layered soils can provide the causes for important lateral flows effects which would not be evident in one-dimensional models. **Miyazaki (1988)** described measurements of flows down sloping layered soils in a laboratory experiment; **Ross (1990)** investigated the lateral diversion capacity of capillary barriers (where fine-grained media overlie coarse-grained media); and **Montazer and Wilson (1984)** described the possibility of lateral flow in the unsaturated zone along the boundaries between dissimilar media, within strongly anisotropic media, or where fine-grained media overlie coarse-grained media. The work of **Ross (1990)** and **Montazer and Wilson (1984)** demonstrate the capillary barrier phenomenon, where the smaller pores in the fine-grained medium can retain more water than the lower coarse-grained medium, so that a zone of greater saturation develops at the boundary. It should be noted that the presence of strong anisotropy due to layering of soils may not be required for lateral unsaturated zone flows to occur; **McCord and Stephens (1987)** observed significant lateral flows in a relatively homogeneous sandy hillslope, and emphasised that 'a sloping soil surface in itself is sufficient cause for the development of a lateral component to unsaturated flow'. Lateral flows can also occur in the capillary fringe (**Gillham, 1984**), and, of course, in perched aquifers.

3.1.4 Flow in fractured aquifers

The term 'fracture' is used by most authors in a very general sense, to describe any conduit which provides a pathway for fast flow and transport, usually in consolidated rock

environments, which may include fissures, faults, or joints. **Barker (1990)** defines a *fracture* as 'any discrete discontinuity, natural or induced, which provides a conduit for the movement of fluid'. Similar flow behaviour may be seen in unconsolidated deposits (particularly in soils), where preferential flow takes place through large continuous openings (formed by soil fauna, plant roots, cracking, or subsurface erosion), often collectively termed macropores (**Beven and Germann, 1982**). The term 'fracture' will, however, be used here only to describe consolidated rock environments. Fractured porous media are often described as exhibiting two overlapping regions (each occupying the same bulk volume of the porous medium): a matrix, consisting of undisturbed rock, and an embedded fracture system which partitions the matrix into blocks.

The *aperture* of a fracture is the cross-sectional width of the fracture normal to the direction of flow. The aperture can vary significantly along the direction of flow within a single fracture. Apertures are decreased by increasing stress at depths within the rock. In fractures with a large aperture, flow may sometimes be turbulent.

The *spacing* between fractures can vary widely, and is usually several orders of magnitude greater than the fracture apertures. The measurement of a mean fracture spacing within a volume of rock can be used to determine the fracture *density* of the rock.

Flow through a fractured rock also depends upon the *inter-connectivity* of fractures. Separate fracture networks can exist within the same volume of rock, without intersecting. This can result in widely different responses of wells in close proximity to each other.

The *uniformity* of fracture characteristics, especially fracture densities, is often highly spatially variable. This can arise, for example, due to solution enlargement in exposed regions, or due to localised or regional stress patterns during deformation (high permeability fracture zones can occur along exposed crests of anticlines, with lower permeabilities in synclinal troughs, **Freeze and Cherry (1979)**).

The *orientation* of a fracture system determines the direction of hydraulic anisotropy of the rock. The primary fractures may be associated with bedding planes or joints. In sedimentary rocks, the bedding plane is aligned with the original depositional layers (this may be oriented in any plane, due to subsequent deformation). Joints are typically oriented in a sub-perpendicular direction to the bedding plane.

The effective *dimensionality* of the fracture system depends upon the complexity of types of fractures present, on the orientation of the fractures, and on their hydraulic properties (which in turn depend upon the physical properties of the individual fractures).

The interaction between water (and contaminants) in the fractures and in the matrix is strongly affected by the *surface characteristics* of the fractures. The surface of the fracture may have a layer of deposited material which retards rates of exchange. Such a layer is often referred to as a *fracture skin* (eg. **Moench, 1984**).

The *porosity* of a fracture system is often much less than the porosity of the matrix; the *permeability* of a fracture system, however, is usually much greater.

Much of the impetus for developing an understanding of flow and transport within fractured media has come from the need to develop safety cases for the disposal of radioactive waste in underground geologic formations. Research facilities exist in several countries, where detailed field investigations provide data to support model development and testing. For example, a large research programme at the Stripa mine in Sweden (the International Stripa Project) has been running since 1980, set in a granite body (**Fairhurst et al., 1993**; **Neretnieks and Rasmuson, 1984**); the Fanay-Augeres uranium mine research facility in France (**Cacas et al., 1990**) has generated data which has been used for a number of discrete fracture network models; and a substantial body of research into flow and transport in unsaturated fractured rock has been based on the Yucca Mountain experimental site in the USA (**Peters and Klavetter, 1988**).

A primary source of evidence for movement of water through fracture networks rather than through the rock matrix arises from the difference in hydraulic permeabilities measured by field tests which give bulk permeabilities, and those measured by laboratory analyses of rock samples taken from the same location which give matrix permeabilities. The difference in permeabilities from the two tests can often be several orders of magnitude, indicating that a high-permeability network exists in the field. For example, **Bibby (1981)** describes the Chalk formation in the United Kingdom as having a matrix permeability of 3 - 4 orders of magnitude less than the bulk permeability. Three of the main approaches for investigating the properties of fractured rock, and its flow and transport characteristics, are geophysical techniques (including core analyses), hydraulic pumping tests, and tracer tests (a more complete summary of methods is given in **Barker (1990)**).

In addition to providing a pathway for fast preferential flow, a fractured medium provides a reservoir in the matrix for storage and relatively slow release of water or contaminant. This can be seen in the enhancement of the tail of a breakthrough curve from a contaminant pulse tracer test (**Barker, 1990**), or in a distinct change in drawdown characteristics with time during a transient pumping test (**Kruseman and de Ridder, 1990**). The interpretation of the results of these types of investigations should be made with care, however, as similar effects can be seen in multi-layered aquifers.

In the unsaturated zone, fractures (or macropores) can act to retard as well as enhance flow rates. Fractures tend to drain rapidly, and due to their large aperture are not able to hold significant amounts of water, so have large pockets of air and relatively few continuous water phase contacts across the fracture (**Wang and Narasimhan, 1985**). The resistance to flow across the fracture is therefore large, and the fracture can act as a barrier to flow (especially if it is in the form of a fracture plane).

The relative importance of the fracture system and the matrix for flow and transport through fractured media depends upon the relative timescales for diffusion in the matrix and for flow and transport in the fracture system. If long timescales are being considered, and the matrix can reach equilibrium with the fracture system relatively quickly, then the effects of diffusion into and out of the matrix may be neglected. The physical properties of most media are such that pressure potentials reach equilibrium much more rapidly than contaminant concentrations; **Barker (1990)** suggests characteristic times for diffusive transport in matrix blocks over a distance of one metre of $10\text{-}10^4$s for pressure potential, and $10^9\text{-}10^{11}$s for contaminant concentration.

3.1.5 Streamflow generation mechanisms

The subsurface flow processes discussed above are mostly concerned with local phenomena. At the catchment scale, these processes can combine in a number of different ways to generate catchment runoff (ie. streamflow at the catchment outlet). There is a considerable amount of current research and debate into the relative importance of different streamflow generation mechanisms.

Historically, much of the debate on catchment runoff processes began with the theory of **Horton (1933)** that the soil surface acts to partition incoming precipitation into a surface and

a subsurface component, depending upon the infiltration capacity of the soil. The surface component provides the stormflow, and the subsurface component provides the baseflow, fitting in with the then prevalent theories of unit hydrographs and hydrograph separation (**Chorley, 1978**). The simplicity of the theory has resulted in its longevity, despite the fact that a growing body of contradictory evidence has been built up. The importance of subsurface stormflow was also recognised at an early date (eg. **Hursh, 1936**), but did not gain widespread acceptance until relatively recently. Current thinking is that there exists a 'continuum of surface and subsurface processes' (**Beven, 1989**) by which streamflow is generated within storm events. For example, **Chorley (1978)** defines 28 flow and storage components of the hillslope hydrological cycle.

The main components which may contribute to streamflow generation during storms are shown in Fig. 3.2. **Beven (1989)** noted that different mechanisms may contribute to a single storm response, either in different parts of the catchment, or at different times during the storm, and that the pattern of response during one storm event may not be repeated for other storms. For example, **George and Conacher (1993)** found that different mechanisms were responsible for streamflow generation during summer and winter periods in a small hillslope in Australia. The main streamflow generation components fall into three basic groups: surface runoff, subsurface interflow, and subsurface baseflow. Surface runoff and interflow are only associated with storm events; baseflow can occur both within and between storms. A summary of recent field studies which provide evidence for the different runoff mechanisms is given in **Anderson and Burt (1990)**.

The term *interflow* is used to describe the flow of subsurface water which contributes to stream discharge within the time-scale of a storm event. The term *baseflow* is used to describe the flow of subsurface water which has a response time in excess of the characteristic time for storm events. **Beven (1989)** considered that the term interflow is essentially equivalent to the other widely used terms *saturated interflow*, *throughflow*, and *subsurface stormflow*. Interflow, by this definition, includes contributions to storm runoff from lateral saturated flow within the main water table as well as within perched water bodies, and from lateral unsaturated flow; however, many authors (eg. **Freeze, 1972**) consider interflow to exclude any rapid responses from the main water table. Some authors discuss interflow as being generated by the development of a saturated perched water table, usually associated with a break in hydraulic properties at a soil horizon. For example, evidence for flow along the bedrock/soil interface, possibly through macropores, for a catchment on the Canadian Shield is given by **Wels et al. (1991)**. **Zaslavsky and Sinai (1981a-e)**, however, strongly

support the notion that a significant lateral component of flow can exist in unsaturated soils, and develop arguments on the importance of this premise for various aspects of catchment hydrology. **Zaslavsky and Sinai (1981a)** graphically illustrated this concept by using a 'straw roof' analogy (incoming rainfall runs off within the body of a sloping straw roof without creating a saturated region - note that this would not occur for a flat roof). Saturated or unsaturated flows may also occur very close to the ground surface, within organic A horizons (**McDonnell et al., 1991**), or within 'surficial surface material, such as forest litter and cultivated agricultural soil' (**Freeze, 1972**). The importance of the steepness of hillslopes in generating saturated or unsaturated interflow has been emphasised by many authors (**McCord and Stephens, 1987**; **Beven, 1981**).

Recognition that not all of a catchment contributes to stormflow formed the impetus for the development of the *partial source area* concept (described by **Chorley, 1978**), in which Hortonian infiltration excess runoff occurs from only part of a catchment. However, many precipitation events can generate significant runoff even for rates of precipitation which are too low to create infiltration excess runoff. A strong prevalent theory for streamflow generation under such circumstances is that of the *partial contributing area* concept, where saturation excess runoff (due to a combination of infiltrating precipitation and lateral subsurface flows) occurs over a variable sized part of the catchment near to the stream channel. The importance of topographic convergence in controlling the distribution of saturated areas has been emphasised by many authors.

Both surface and subsurface flows can generate a fast streamflow response from saturated areas. Surface flows can occur due to either *return flow* (where 'old' pre-event water flows upwards through the ground surface, **Dunne and Black (1970)**) or to direct precipitation onto saturated areas, where 'new' water runs off into the stream channel, or to a mixture of the two. (**Wels et al. (1991)** found that, for a snowmelt catchment on the Canadian Shield, the only component contributing to the storm hydrograph which consisted entirely of 'new' water came from direct precipitation onto saturated areas.) The mechanism most commonly invoked for generating a fast subsurface storm response is *groundwater ridging* (**Sklash and Farvolden, 1979**); the near-surface tension-saturated capillary fringe is converted to a pressure-saturated region by the addition of only a small amount of water, and the resulting increase in hydraulic head drives the fast subsurface response. However, although the mechanism has been observed in the field by several people, only groundwater ridging near to the stream channel can explain rapid subsurface runoff; the theory cannot explain the large volumes of subsurface water contributing to the storm hydrograph in some catchments (eg. **Wels et al., 1991**).

The importance or otherwise of macropores in streamflow generation has been widely debated. **Beven and Germann (1982)** note the difficulty in defining a *macropore*, but describe typical macropores as being formed by soil fauna (burrowing animals), plant roots, cracks and fissures, and natural soil pipes (the existence of larger pipe networks, not defined as macropores, which can contribute significant volumes of runoff during storm events has also been noted; eg. **Jones (1988)**). Macropores have been postulated as flow pathways to explain fast subsurface responses when the use of the more traditional translatory flows **(Hewlett and Hibbert, 1967)** would require unphysical values for soil parameters (*translatory* flows, or equivalently *displacement* or *piston* flows, occur when a mass of water added to a soil essentially remains intact as it moves through the soil). Vertical macropore flows in the unsaturated zone may increase the rate of infiltration into the soil **(Beven, 1989)**, and have been used to explain rapid lateral subsurface flows along locally saturated soil horizons **(Wels et al., 1991)**. **Anderson and Burt (1990)** considered that, since the field evidence appears to be in favour of 'old' soil water being the main contributor to stormflow, translatory flow must play a significant role.

Isotope and chemical hydrograph separation techniques have been widely used to investigate sources of storm water **(Sklash, 1990)**; the evidence from the numerous papers produced recently on this subject has not been reviewed in detail as part of this study. However, studies of concentrations of naturally occurring ^{18}O and deuterium in precipitation, groundwater, and stream water using simple mixing models have tended to demonstrate the importance of subsurface water in storm flow, supporting the more recent theories of streamflow generation mechanisms.

Finally, it is noted that most of the recent research into streamflow generation mechanisms has concentrated on humid, temperate catchments. Less attention appears to have been given to catchments in colder climates **(Obradovic and Sklash, 1986)** or in semi-arid or Mediterranean climates **(George and Conacher, 1993)**. Also, many of the papers cited above contain little discussion of the effects of making different assumptions about streamflow generation mechanisms on contaminant migration in catchments (these mechanisms do, however, play a critical role in determining migration pathways and residence times; **Sklash, 1990**).

3.2 Basics and definitions for variably-saturated flow modelling

3.2.1 Soil water potentials and Darcy-Buckingham flux law

The first recognition that the energy status of water in unsaturated soil could be represented by a measurable potential was made by **Buckingham (1907)**, who defined *capillary potential* as the reversible work per unit mass required to transfer water from a pure water reservoir to the soil, for a given water content, temperature, and bulk density (a concise description of Buckingham's work is given in **Sposito (1986)**). Alternative terms for capillary potential which have been, and continue to be, used in the literature are *soil water matric potential*, *matric potential*, and *pressure potential*. Following **Hillel (1980)**, the term *pressure potential* is used in this work, defined such that the pressure potential is positive in the saturated zone below the water table (this is sometimes called the *submergence potential*), and negative in the unsaturated zone.

The pressure potential ψ, which relates to the local pore pressure in the soil matrix due to capillary forces, is only one of many potentials which have been defined relating to the forces which may act upon water in unsaturated soil. The total potential has been described by various authors as being the summation of a number of components whose relative importance depends upon the field of application. The following list is taken from **Nielsen et al. (1986)** and **Feddes et al. (1988)**:

- ψ_p - pressure potential ($\equiv \psi$ as defined above);
- ψ_s - solute or osmotic potential;
- ψ_e - electrochemical potential;
- ψ_{ex} - potential arising from external gas pressure;
- ψ_{ov} - potential arising from external overburden load;
- ψ_g - gravitational potential.

In common with the approach taken in most subsurface flow models, all potentials other than the pressure potential ψ and the gravitational potential ψ_g are neglected. Writing the gravitational potential as $\psi_g = z$, where z is the vertical ordinate (measured positive upwards), the total potential (also termed the *hydraulic head*, h) can be written as

$$h = \psi + z \quad . \tag{3.1}$$

Buckingham related the rate of flow of water through an unsaturated soil to the pressure potential, by analogy with theories of heat and electrical conduction. As early as 1856, Henry Darcy (a French hydraulic engineer) had described the flow of water through saturated media by a similar linear relation between discharge and head gradient, based on results of experiments of flow through a sloping cylinder filled with sand; this can be written as

$$\underline{J} = -K(\theta)\nabla h \qquad (3.2)$$

where $\underline{J}$ is the soil water flux vector (or capillary current density), K is hydraulic conductivity, θ is the volumetric soil water content, and ∇ is the differential gradient operator. Eq. 3.2 is sometimes known, therefore, as the Darcy-Buckingham flux law, but is more often known simply as the Darcy equation (even for unsaturated conditions).

The main assumptions underlying Eq. 3.2 can be stated as **(Bear and Verruijt, 1987)**:

1. the water is at constant density (the density is not a function of temperature, pressure, or the concentration of dissolved substances);
2. flow is laminar;
3. flow is single phase;
4. inertia of the water is negligible.

These assumptions are generally approximately valid for groundwater flows. Exceptions are when flow rates are very large or very small. When flow rates are large, inertial effects become significant and turbulence can occur. Darcy's law is often assumed to be applicable for Reynolds numbers up to about 1-10. Large flows can occur, for example, near point sources or sinks such as strongly pumped wells or large point springs, or in coarse-grained media or fractures. When flow rates are very small, the relation between head and discharge can become non-linear, due mainly to molecular interactions between the water and the porous media.

The Darcy equation was originally based on saturated flow experiments, and has been widely verified under saturated conditions. However, it is assumed by most authors that it is applicable in the unsaturated zone, and that it can be extended in the obvious way to two or three dimensions.

3.2.2 Richards equation

Richards (1931) recognised that the Darcy equation could be combined with a mass continuity equation to give a single equation describing flow through an unsaturated porous medium, and that methods existed to measure all of the coefficients of the equation.

The continuity equation for a porous medium in the absence of sources or sinks can be written as

$$\nabla . \underline{J} + \frac{\partial \theta}{\partial t} = 0 \qquad (3.3)$$

where $\nabla .$ is the divergence operator, and t is time. This can be combined with the Darcy equation (Eq. 3.2, which, as well as being experimentally based, can also be derived from an underlying momentum conservation equation) to give Richards equation, written as

$$C \frac{\partial \psi}{\partial t} = \nabla . [k_r \underline{\underline{K}} . \nabla \psi] + \frac{\partial (k_r K_z)}{\partial z} \qquad (3.4)$$

where $C \equiv d\theta/d\psi$ is the soil water capacity (see Section 3.2.4), k_r is the relative conductivity (see Section 3.2.3), $\underline{\underline{K}}$ is the saturated hydraulic conductivity tensor (assumed to be diagonal, with vertical conductivity K_z, see Section 3.2.3), and z is the vertical ordinate (positive upwards).

There is an apparent inconsistency in the usual derivation of Richards equation (as given here), in that it is written in terms of energy potentials, but is derived using water mass balance. This was noted by **Sposito (1986)**, who demonstrated that the same equation could also be derived using energy balances based on thermodynamic principles.

3.2.3 Hydraulic conductivity

The hydraulic conductivity coefficient in Eq. 3.2 describes the ease with which a fluid can move through a porous medium, and is a function of the properties of both the medium and of the fluid. It is related to the properties of the medium (intrinsic permeability, k), and of the fluid (density, ρ; and viscosity, ν) by (**Bear and Verruijt, 1987**)

$$K = k\rho g / \nu \tag{3.5}$$

where g is the acceleration due to gravity.

In general, for an anisotropic heterogeneous porous medium, the hydraulic conductivity can be represented by a symmetric 3x3 tensor, with each component being a function of spatial position (see, for example, **Bear and Verruijt (1987)**). However, although fully heterogeneous media are often represented in models (within the limits of the model's resolution), anisotropy is usually limited to three principal directions, so that the conductivity tensor reduces to a diagonal form, with components K_x, K_y and K_z. Physically, this can be interpreted as saying that the directions associated with the model discretisation are coincident with the directions associated with the anisotropy of the medium. In the general case, for an anisotropic medium with cross-terms in the conductivity tensor, the flow resulting from a hydraulic head gradient need not be in the same direction as the head gradient. For the case of a diagonal tensor, the flow direction always coincides with the direction of the imposed head gradient.

In the unsaturated zone, hydraulic conductivity is a strongly non-linear function of pressure potential. This is handled by writing hydraulic conductivity as a product of relative conductivity, $k_r(\psi)$, a function of pressure potential, and saturated hydraulic conductivity, K (as in Eq. 3.4). Note that with this formulation the degree of anisotropy at any point is constant (it is not a function of pressure potential).

3.2.4 Storage coefficient

The *storativity* S of an aquifer is defined as the volume of water released from an area of aquifer per unit decline in head (**Bear and Verruijt, 1987**). (Note that a similar definition for gain of water as a result of an increase in head can also be made, although hysteresis effects can cause differences between aquifer responses to wetting and draining.) The water release mechanisms differ for unconfined and confined aquifers. For unconfined aquifers, water is physically drained from the pore space, and the storativity depends therefore on the porosity of the aquifer and on the drainage characteristics of the unsaturated zone above the water table (in traditional groundwater investigations, the term *specific yield* is usually used instead of storativity). For confined aquifers, the water is released by two mechanisms: a

decrease in head causes a decrease in the water pressure, so the water expands slightly; the decrease in water pressure is accompanied by an increase in the effective stress in the matrix (due to the overburden), so the matrix becomes slightly compressed.

The definitions given above describe the storativity of aquifers. For the development of a three-dimensional variably-saturated flow model, where the concept of a vertically-integrated aquifer is not used, the more fundamental parameters which describe the actual aquifer material properties need to be defined.

The development of an intrinsic storativity term is built upon the Terzaghi theory of effective stress (**Bear and Verruijt, 1987**). Essentially, this theory states that in a granular porous medium the water pressure is exactly balanced by a corresponding pressure from the material grains, and that deformation of the porous medium only comes from stresses at contact points between the grains (the *effective* or *intergranular stresses*). The total stress in the porous medium (eg. from the overburden) is the sum of the pore water pressure and the intergranular stress. If there is no change in the total stress, then an increase (or decrease) in pore water pressure results in an decrease (or increase) in the intergranular stress, and hence an expansion (or compaction) of the material skeleton. An increase (or decrease) in pore water pressure is also accompanied by a compaction (or expansion) of the water. The relations between the stresses and the resulting expansion or compaction are, for most practical applications, linear, and are used to define the coefficients of compressibility for the matrix (α) and the pore water (β) as (**Bear and Verruijt, 1987**)

$$\alpha = -\frac{1}{U_b}\frac{\partial U_b}{\partial \sigma_s}, \qquad \beta = \frac{1}{\rho_w}\frac{\partial \rho_w}{\partial p} \tag{3.6}$$

where U_b is a bulk volume of soil, σ_s is the effective stress within the volume, ρ_w is the density of water, and p is the pore water pressure.

For use in the model, these two parameters are combined into a single term, the *specific storage*, S_s, which is defined as (eg. **Freeze and Cherry, 1979**; **Bear and Verruijt, 1987**)

$$S_s = \rho_w g(\alpha + n\beta) \tag{3.7}$$

where ρ_w is the density of water, g is the acceleration due to gravity, α is the compressibility of the matrix, n is porosity, and β is the compressibility of water.

In the unsaturated zone, the storage is characterised by the soil water capacity (the rate of change of water content as a function of pressure potential), $C \equiv d\theta/d\psi$.

For a variably-saturated model, a storage co-efficient must be defined in both the saturated and the unsaturated zones. A storage coefficient η is defined, following the approach taken by **Huyakorn et al. (1986b)**, as

$$\eta = \frac{\theta S_s}{n} + \frac{d\theta}{d\psi} \quad . \tag{3.8}$$

The storage coefficient consists of two terms, the first relating to compressibility of the matrix and the pore water, and the second relating to changes in water content. In the saturated zone, $d\theta/d\psi$ is zero, $\theta = n$, so $\eta = S_s$; transient changes in pressure potential ψ are therefore entirely due to compressibility of the matrix and the pore water (the main contribution being usually due to matrix compressibility, **Younger (1993)**). In the unsaturated zone, the main contributor to the storage coefficient is usually the second term of Eq. 3.8.

In relatively dry regions of the unsaturated zone there can be large negative pressure potentials, but these do not convert to mechanical stresses on the matrix (**Narasimhan and Witherspoon, 1977**), so contribute little to the storage coefficient. In relatively wet regions of the unsaturated zone (including the capillary fringe), negative pressure potentials are partly converted to mechanical stresses (**Narasimhan and Witherspoon, 1977**). The relationship between negative pressure potential and effective stress is, in general, nonlinear. For simplicity (and since the first compressibility term of Eq. 3.8 is relatively small in the unsaturated zone), a simple product of soil saturation, θ/n, and specific storage, S_s, is used to represent compressibility effects in the unsaturated zone.

3.2.5 Unsaturated soil characteristic

The unsaturated soil characteristic function describes the relationship between pressure potential ψ and volumetric soil water content θ. This highly nonlinear function is central to the description of soil water behaviour, and reflects the capillary retention capability of the range of soil pore sizes. Its use in Richards equation (Eq. 3.4) arises through the gradient of the curve, termed the soil water capacity C, which forms the coefficient for the time derivative in the unsaturated zone, and through the sink terms which are given in terms of volumetric losses.

It has long been recognised that the soil characteristic function is not single-valued: the curve representing drying of a soil is different from that representing wetting. This effect is called hysteresis, and is mostly due to two causes: the different contact angle between the water and capillary walls during wetting and drying; and the so-called 'ink bottle' phenomenon, where large pores can drain suddenly, due to their incapacity to hold water. It is noted that hysteresis can also be seen in the relative hydraulic conductivity function, although this is small, and so is usually neglected (**Jaynes, 1990**). The incorporation of hysteresis effects into a simulation model requires that the previous history of wetting and drying of the soil is known and retained. This computational complexity, together with the recognition that few data exist to characterise hysteresis in field soils, and that the effects of hysteresis (especially on contaminant transport) may often be completely masked by uncertainty in hydraulic properties of the soil (**Jaynes, 1990**), leads to the conclusion that hysteresis effects need not be included in an operational hydrological model.

A phenomenon closely related to hysteresis is air entrapment. This occurs when a pocket of air (typically beneath an advancing wetting front, or beneath a perched water table) becomes totally surrounded by saturated pores. The effects of air entrapment are that the downward movement of water is retarded, and the resulting moisture content of the soil is reduced. These effects may be obscured, however, by the development of instability of the wetting front (**Hillel, 1987**), in which 'fingers' of percolating water bypass the unsaturated zone beneath the wetting front, a phenomenon which is likely to occur particularly in the presence of trapped air. Although these phenomena may be important under some conditions, especially for contaminant transport, they are still poorly understood, and process-based models do not exist which are suitable for inclusion within catchment scale models.

3.3 Three-dimensional flow models

3.3.1 Historical development

Models capable of handling flow in both saturated and unsaturated porous media have become increasingly frequently reported in the literature within the last few years, although there are still few which are fully three-dimensional (a summary of recent two- and three-dimensional saturated and variably-saturated flow and transport models is given in **Mangold and Tsang (1991)**). Many of these models build on the approach of **Freeze (1971)**, who extended the variably-saturated modelling theories of a number of previous researchers during a period of

rapid development in the late nineteen-sixties. **Freeze (1971)** presented a unified variably-saturated transient three-dimensional model, with the ground surface as the upper boundary, including anisotropy of layered geological formations, and general boundary conditions. The model was formulated as a parabolic partial differential equation in three spatial dimensions, using pressure head ψ as the independent variable, and was solved using a line successive over-relaxation (LSOR) iterative method, oriented in the vertical. He applied the model to a small (37m length) hypothetical basin represented using an orthogonal mesh system, with boundary conditions at the ground surface representing a rainstorm event, a snowmelt event, and ponded surface water. Examples of modelled catchment responses were given using a homogeneous medium. A low permeability clay layer was then introduced into the hypothetical basin in one of the rare examples (even in the intervening years since this paper was published) of the development of a perched water table in a three-dimensional model.

Further developments of this approach were made in the nineteen-seventies. **Narasimhan and Witherspoon (1977)** developed a three-dimensional model of flow in a variably saturated porous medium, including one-dimensional (vertical) deformation of the soil matrix. They noted the importance of recognising the equivalence of soil water diffusivity and the coefficient of consolidation of the soil in the capillary fringe. In this region, where the soil is saturated but soil tension is below air entry pressure, porosity is usually treated as a constant, with the implication that soil water diffusivity $D \equiv 1/(d\theta/d\psi)$ becomes infinite. In order to keep the diffusivity bounded for low values of tension, there must be a small change in soil porosity. For many practical applications a ψ-based equation is implemented, in which diffusivity is not directly used, and the implied small change in porosity is neglected. **Frind and Verge (1978)** investigated the practicality of application of a three-dimensional groundwater modelling system, evaluating the critical areas of the numerical solution of their finite element model that contributed most to the overall simulation time. They investigated two solution methods, Gaussian elimination and Cholesky decomposition, but came to no firm conclusions on the best numerical methods and matrix solvers for general application; the efficiency of the methods depended strongly upon the application. They noted the problems of application of three-dimensional models to the full catchment scale, due to the disparity of spatial scales required for accurate modelling in the saturated and the unsaturated zones.

The general form of the three-dimensional variably-saturated flow equation has remained unchanged in recent years, with most developments being in the area of improvements to numerical solution algorithms. The most active area of development of the underlying model equations has been for modelling of multiphase flow.

Huyakorn and Thomas (1984) investigated the application of the Picard and Newton-Raphson (N-R) iterative methods to solve the non-linearities of the variably-saturated flow equation in two dimensions (a vertical slice). They applied the model to several hypothetical situations, and found that the two algorithms were generally comparable in terms of overall simulation time, the Picard algorithm requiring less CPU time per iteration, but requiring more iterations to converge than the N-R scheme. The Picard scheme had problems converging during one of the steady-state tests. The results of this work were then used to develop a similar three-dimensional model (**Huyakorn et al., 1986b**). Picard iteration was used, with a vertical slice successive over-relaxation (SSOR) matrix solution scheme. The model (FLAMINCO) was applied to steady-state and transient one- and two-dimensional hypothetical examples, and to a steady-state three-dimensional example for a single unconfined aquifer.

Several further developments in the area of solution algorithms for the variably-saturated flow equation designed for implementation on parallel processors have recently emerged. **Faust et al. (1989)** presented a model for simulating the flow of immiscible fluids under saturated and unsaturated conditions in three dimensions. They used a (vertical) SSOR method embedded within N-R iteration, with alternate vertical slices of the SSOR algorithm being solved in parallel (ie. using odd-even or red-black ordering) on a shared-memory parallel computer. The model (SWANFLOW) was applied to several field transport problems in one, two and three dimensions. **Binley (1992)** developed a transient three-dimensional variably-saturated model using conjugate gradient methods implemented on a scalable local-memory parallel processing computer, and applied the model to a hypothetical unconfined aquifer.

3.3.2 Variably-saturated porous media flow equation

The governing equation for three-dimensional flow in a variably-saturated porous medium is based upon combining the Darcy equation and the continuity equations. This has been discussed by many authors (eg. **Narasimhan and Witherspoon, 1977; Frind and Verge, 1978; Huyakorn et al., 1986a; Huyakorn et al., 1986b**), and can be written in an integral form (**Narasimhan and Witherspoon, 1977**), or more commonly in a differential form as

$$\eta \frac{\partial \psi}{\partial t} = \frac{\partial}{\partial x}[K_x k_r \frac{\partial \psi}{\partial x}] + \frac{\partial}{\partial y}[K_y k_r \frac{\partial \psi}{\partial y}] + \frac{\partial}{\partial z}[K_z k_r \frac{\partial \psi}{\partial z}] + \frac{\partial (k_r K_z)}{\partial z} - q \qquad (3.9)$$

where x, y, and z are cartesian coordinates, q is a specific volumetric flow rate (volumetric flow rate per unit volume of porous medium) out of the medium representing sources or sinks,

and all other variables are defined in Section 3.2. The derivation of this equation, and its coefficients, is discussed in Section 3.2.

3.4 Quasi-three-dimensional flow models for multi-layered aquifers

A simplification often made in the development of numerical models for practical applications in groundwater flow problems is to assume that the dominant flow directions are essentially lateral in aquifers, and vertical in aquitards or aquicludes, since under these conditions flow is sharply refracted at the boundary between the two media. This approach reduces the three-dimensional problem to a set of coupled two-dimensional problems, with the resulting improvements in computational performance. The method relies on the use of known or assumed hydrogeological information to define aquifers and aquitards (the flow directionality is fixed once these definitions are made). **Neuman and Witherspoon (1969)** investigated the conditions when such an approximation can be made for a two-aquifer system, and found that if the ratio of hydraulic conductivities between the aquifer and the aquitard is greater than two orders of magnitude, the error introduced was negligible (less than 5%).

Several approaches can be taken to represent the (one-dimensional) flow through the aquitards. Early solutions to the problem of modelling flow in multi-aquifer systems assumed that the flow through the aquitards is a linear function of the head difference across the aquitard, and that the aquitard storage is negligible. This simple approach was used to produce a number of analytical solutions to idealised problems. One of the first numerical quasi-three-dimensional models was developed by **Bredehoeft and Pinder (1970)**. They assumed that storage effects within the aquitard were important, and showed the delaying effect of diffusion of a pressure wave arising from a step function change in head within one of the aquifers on the head in the other aquifer. They introduced these effects into their multi-aquifer model by considering two time periods, each with a different type of response. For early time, storage effects within the confining layer are important, but adjacent aquifers can be considered to be independent. After a transition time, flow through the aquitard is approximately steady, storage effects are no longer important, and adjacent aquifers are coupled through the aquitard flux terms.

A more rigorous approach to describing transient flows through an aquitard was presented by Herrera (eg. **Herrera, 1970**) in terms of a continuous representation of the diffusion of pressure waves through the finite thickness of the aquitard. This approach assumes uniform

properties across the thickness of the layer. An analytical solution to the diffusion equation for given boundary conditions can be written as an infinite series (**Carslaw and Jaeger, 1959**). The flux at the boundary (between the aquifer and the aquitard) can then be expressed using Duhamel's theorem as a convolution integral in terms of the historical head variations in the aquifers. The convolution integrals involve two kernels which have been termed 'memory function' and 'influence function'. This method was considered impractical by **Bredehoeft and Pinder (1970)**, but has since received considerable attention. The method has been made computationally feasible by: expressing the convolution integral as a recursive expression for each timestep, and restricting the infinite series to just the first few terms (eg. **Neuman et al., 1982**; **Huyakorn et al., 1986a**); expressing the memory and influence functions as negative exponentials (**Premchitt, 1981**); or using a Laplace Transform solution which removes the time dependence of the integrals (**Cheng and Ou, 1989**). An improvement to the method applicable to the early time period (ie. shortly after any changes in head in one of the aquifers) was implemented in a multi-aquifer model by **Gambolati et al. (1986)**.

For the (relatively few) cases where heterogeneity of the aquitards is considered to be important, a one-dimensional finite-difference or finite-element model of flow in the aquitard can be implemented. **Neuman et al. (1982)** implemented such a scheme, and considered that it compared favourably against the convolution integral approach for homogeneous aquitards. Their approach included an adaptive explicit-implicit finite element scheme, based on the fact that the diffusivity of aquitards is usually several orders of magnitude smaller than that of aquifers. For certain limits of spatial discretisation, the stability limits of the aquitard nodes are then much smaller than those of the aquifers. It is therefore possible to use an explicit representation of the head variation at many of the model nodes, with a subsequent reduction in computational cost.

3.5 Unsaturated zone models

The need to understand and model mechanisms of flow in the unsaturated zone arises in the branches of science and engineering of soil science, agricultural and environmental engineering, and groundwater hydrology (**Celia et al., 1990**), for the purposes of predicting the interaction of water availability and crop growth, transport of pollutants, and groundwater recharge. Most models are based on Richards equation (**Richards, 1931**; see Section 3.2.2), which uses pressure potential as the dependent variable, and are one-dimensional (eg.

UNSAT1, described by **van Genuchten (1978)**, and widely used). Alternative formulations of the equation governing unsaturated zone flow have been presented; for example, water content based models (eg. **Smith and Ferreira, 1989**) have been used, although these are generally avoided for partially-saturated flow problems (**Haverkamp et al., 1977**).

Improvements to numerical solution methods form a strong current interest in the literature (eg. **Paniconi et al., 1991**; **Hills et al., 1989**; and **Celia et al., 1990**). Alternatively, simplifications can be made by, for example, using quasilinear approximations (**Pullan, 1990**), or by using effective conductivities for flow through layered soils (**Weir, 1989**), although these approaches tend to limit the generality of the model. One-dimensional unsaturated zone models are often incorporated into quasi-three-dimensional models; however, substantial problems must be overcome when coupling a one-dimensional unsaturated zone model to a two-dimensional saturated zone model (eg. **van Bakel, 1986**). Two- and three-dimensional unsaturated zone models tend also to include the saturated zone (these are discussed in Section 3.3.1).

Although there is extensive and continuing research into unsaturated zone modelling, no well-proven alternative to Richards equation has been generally accepted for describing flow in partially-saturated porous media.

3.6 Fracture flow models

3.6.1 Dual porosity/permeability models

The most common and practicable method of modelling flow through many types of fractured media is to assume that the medium consists of two regions, a fracture network and a matrix, each of which can be represented as a continuum, and each occupying the same physical space (**Gerke and van Genuchten, 1993**). Early models of this type were proposed by **Barenblatt et al. (1960)**, and **Warren and Root (1963)**. The models that have been developed since that time can be divided into those in which water within the matrix as well as the fractures is mobile over large distances, and those in which large scale flows can only occur through the fractures. These are sometimes referred to as dual-permeability models and dual-porosity models respectively, although the term dual-porosity is now commonly used to describe either type. These types of models have been proposed to describe both fractured rock environments and structured soils (**Gerke and van Genuchten, 1993**).

The main feature which discriminates between models is in their treatment of the exchange flow between the matrix and the fractures. This depends critically upon the characteristic timescales for flow or transport through the matrix blocks. The simplest approach is to define a linear transfer term; the matrix blocks are assumed to be fully mixed, and the rate of transfer (of water or solutes) across the matrix-fracture interface is directly proportional to the difference between the head in the matrix and the head in the fracture. This quasi-equilibrium approach was used in a flow model by **Barenblatt et al. (1960)**. A similar method is used in the SHETRAN contaminant migration components for contaminant diffusion into dead-end pores (**Ewen, 1990**). For short timescales or large matrix block sizes, however, the time taken for diffusion into or out of the matrix may not be assumed to be negligible. **Bibby (1981)** considered that, for a chalk aquifer, 'it may be many days before the rate of mass transfer reduces to an approximately linear form'. **Moench (1984)** investigated the effect of a fracture skin on the exchange term, and considered that the existence of a fracture skin may help to justify the use of a quasi-equilibrium approach.

Models which are applicable over long timescales have been developed; for example, **Peters and Klavetter (1988)** presented a model for flow in a thick unsaturated zone at Yucca Mountain, Nevada, under slowly changing conditions, by assuming that the pressure heads in the fracture and the matrix were identical perpendicular to the direction of flow. As noted by **Dykhuizen (1990)**, this effectively results in a single effective porous medium model. **Dykhuizen (1990)** presented a model applicable for short timescale transient simulations by assuming a pressure distribution within the matrix blocks. The effect of the shape of the matrix blocks on flow and transport has also been extensively studied. **Berkowitz et al. (1988)** and many other authors have investigated flow in media where parallel fracture planes divide the matrix into periodically uniform blocks. Consideration of irregular block sizes and shapes has been made by **Neretnieks and Rasmuson (1984)**, who defined a 'pseudobody' to represent the irregular blocks; **Huyakorn et al. (1983)** idealised a 'blocky' fractured medium (ie. one with non-orthogonal intersecting fracture planes) by using spherical blocks.

3.6.2 Equivalent porous medium (EPM) models

Many single porous medium groundwater flow models (of which the subsurface flow component of SHETRAN is an example) have been used to model fractured environments, with effective parameters being used to represent the macroscopic hydraulic properties of an assumed equivalent porous medium. The use of equivalent porous medium (EPM) models

depends upon the assumption that an appropriate representative elementary volume (REV) can be defined, such that the hydraulic properties can be assumed to vary smoothly through space above the REV scale, and the medium can be treated as a continuum above that scale. (Note that the REV described here is not a rigorously defined concept.) **Neuman (1988)** pointed out that, in general, there is no guarantee that an REV can be defined for a given medium; and even if the scale of an appropriate REV is ascertained, standard techniques for the measurement of hydraulic properties often relate to rock volumes smaller than the REV.

Several successful examples of the use of EPM models for fractured environments have been reported. **Mercer and Faust (1979)** applied an EPM model to a fractured tuff in New Zealand at a regional scale. **Pankow et al. (1986)** investigated contaminant transport from two waste disposal sites with widely differing geological characteristics using an EPM model, and found, based on these two sets of results, that the use of an EPM model was effective for the medium with the smaller fracture spacing, higher fracture connectivity, and higher block porosity. **Peters and Klavetter (1988)** derived a continuum model for flow through unsaturated fractured porous media for application to Yucca Mountain, USA, under slowly changing conditions. They assumed, based on field and modelling evidence, that the pressure transients in the matrix blocks become insignificant after periods of a few months, so the pressure heads in the fractures and the adjacent matrix blocks could be assumed to be identical for the timescales being considered, and a single equivalent porous medium could be defined.

3.6.3 Discrete fracture models

Discrete or network fracture models have mostly been developed to study the physics of the movement of water and contaminants through fracture networks and the implications of data uncertainty on modelling results, in support of continuum models. For example, **Smith and Schwartz (1984)** investigated the effect of fracture network geometry on transport using a stochastic modelling technique.

Discrete fracture models are usually designed for detailed study of flow and transport within individual fractures, or within small-scale regions (for interpreting small scale measurements, for example; **Cacas et al. (1990)**); they are generally not practical for simulations of regional scale flow and transport (**Bear, 1993**).

3.6.4 Criteria for choice of a model

The choice of a model to represent the effects of fractures depends upon the scale of modelling. Four physical scales were identified by **Berkowitz et al. (1988)** for flow and transport through fractures relative to the contaminant source (similar divisions are discussed by many other authors):

very near field - representing single fractures close to the source;
near field - representing small numbers of interconnected fractures near to the source;
far field - representing regions further from the source where the effects of the fracture network and the matrix are still distinguishable; and
very far field - where the whole domain can be treated as an equivalent porous medium.

For the very near field and the near field, discrete fracture models are used. For the far field and the very far field (which are of interest in this case), dual porosity/permeability models or EPM models can be used.

Barenblatt et al. (1960) considered that an EPM approach can be used for simulating flow provided that the characteristic times for the flow processes are long compared with a delay time for the transient conditions in matrix blocks to decay. **Berkowitz et al. (1988)** investigated the conditions under which an EPM model could be used for simulating contaminant transport in fractured rocks, by using a continuum model of flow and transport in a medium consisting of two sets of uniformly spaced, orthogonally intersecting fractures, and inspected the resulting breakthrough curves for the cases when the flow is parallel to one of the fracture systems, and when flow is at 45° to both systems. They found that, at sufficiently large distances from the source, the breakthrough curves showed approximately Fickian behaviour for the 45° flow case, but not for the parallel flow case (similar results were found previously by **Schwartz et al. (1983)** and **Smith and Schwartz (1984)**). Conclusions about transport behaviour under field conditions based on these results should obviously be drawn with care (a point noted by the authors), since the geometry of any realistic fracture network will differ greatly from the simplified example used in the study.

The use of an EPM model depends upon identifying appropriate equivalent parameter values for the fractured medium. Several attempts have been made to quantify equivalent macroscopic hydraulic parameters. **Neuman (1988)** used a stochastic representation of the medium to estimate equivalent permeabilities based on results of hydraulic tests measured at the scale that is practical for obtaining the data. **Sagar and Runchal (1982)** derived

expressions for estimating permeability tensors for arbitrary fracture networks, and obtained conditions for ensuring that the tensors are symmetric. For the case where the fracture systems are nonextensive, **Sagar and Runchal (1982)** show that an equivalent permeability matrix cannot be defined, and therefore the medium cannot be regarded as a continuum for the purposes of establishing an EPM model.

There are three reasons for preferring an EPM model to a dual-porosity model, provided that its use can be justified by the field conditions: the uncertainty in the parameter values required for the model is likely to be less than for a dual porosity model **(Berkowitz et al., 1988)**; the implementation of the model is simpler; and the model is likely to be numerically more robust. **Gerke and van Genuchten (1993)** note that: the hydraulic conductivity function used in the exchange term in their dual-porosity model is a critical parameter, yet the underlying physical and chemical properties controlling its value are poorly understood; the values of the parameters required by their model are not easily measured experimentally (even though they are physical parameters); problems of stability and mass balance can occur, especially in the fracture region. The current state-of-the-art of dual-porosity models may be summarised by the view of **Gerke and van Genuchten (1993)** that 'The proposed dual-porosity model ... *eventually* may find application to practical field problems' (my italics).

In conclusion, an EPM model can be used to simulate flow and transport in a fractured medium only for the conditions when:

1. the fracture spacing is small;
2. the computational mesh size is large;
3. the region being modelled is sufficiently far from the contaminant source;
4. the fractures are sufficiently well connected across dimensions comparable to the computational mesh size;
5. the fracture orientations are sufficiently random;
6. the timescale of the macroscopic processes being simulated is long compared to the timescale for matrix block pressure transients to decay.

For the application of a variably-saturated flow and transport model to the shallow aquifers of west Cumbria, the choice of a model depends upon a knowledge of the types and scales of fracturing in each lithology, and on the types of simulations which will be run. The two main lithological types are the unconsolidated Quaternary deposits and the Sherwood Sandstone. The Quaternary deposits can be treated as single permeability / single porosity porous media. There is only limited evidence to quantify the scales and properties of

fractures in the Sherwood Sandstone (including its upper brecciated layer); the evidence available indicates that the scale of fracturing is small (typically of the order of a metre or less). The typical simulations that will be run for the shallow west Cumbrian aquifers are for contaminant migration from a diffuse source at a depth of several tens of metres within the Sherwood Sandstone (following migration through the deeper rocks from an original source at a greater depth), with a grid scale of the order of hundreds of metres.

It is concluded that an EPM model is adequate as a basis for modelling flow in the west Cumbrian aquifers, since: a) the scale of fracturing in the Sherwood Sandstone is small relative to the typical scales for modelling; and b) the use of a dual-porosity model would require additional data to characterise the porous media, and these data are not readily available. A mobile-immobile model for contaminant migration is already implemented in SHETRAN, which is capable of modelling migration with water flow through the region of primary porosity in a two-region porous medium, and diffusion of contaminants into and out of the matrix blocks.

3.7 Boundary conditions and source/sink terms

3.7.1 Stream-aquifer interaction

Interactions between aquifers and stream or river channels can occur in many different ways, depending upon the local ground and channel geometry, the lithology and geometry of the stream bed and underlying sediments, on the state of the channel (flowing or dry), and on the subsurface hydraulic gradients (saturated or unsaturated).

A stream or river may be perennial or ephemeral. *Perennial* streams or rivers are usually in hydraulic connection with the underlying aquifer, and may be *gaining* (ie. water flows from the aquifer to the channel), or *losing* (water flows from the channel to the aquifer) (see Fig. 3.3). For *ephemeral* streams, unsaturated materials can exist beneath a dry channel bed. When the stream initially starts flowing, large infiltration losses can occur, and recharge to the underlying aquifer can be substantially delayed.

A variety of methods have been used to represent stream or river channels in groundwater models. In two-dimensional saturated regional groundwater models, fully penetrating stream channels are often represented as fixed head boundary conditions for the computational nodes lying along the line of the channel. For partly penetrating channels, many models have a

computational node directly beneath the channel, and exchange flows are calculated as a linear Darcy flux between the head in the channel and the head in the aquifer. This simple approach neglects the fact that, for partially penetrating channels, subsurface streamlines converge towards the channel bed, and a three-dimensional flow pattern exists near the channel. Several mutually similar approaches have been developed to accommodate such flow patterns in regional groundwater models by different researchers (eg. **Herbert, 1970**; **Crebas et al., 1984**; **Miles, 1985**). In a typical formulation, **Herbert (1970)** assumed that the flow towards the channel is radial, and calculated the total discharge from the aquifer to the channel by integrating the radial Darcy flow equation. For the cases of layered or anisotropic aquifers, **Miles (1987a,b)** presented methods for calculating effective values for hydraulic conductivity.

None of these methods allows for the possibility of there being an unsaturated region beneath the channel above a deeper aquifer. **Reid and Dreiss (1990)** investigated the effect of unsaturated stratified sediments on groundwater recharge from intermittent streams, using a two-dimensional vertical slice model. They considered four possible cases of typical fluvial stratigraphy: (1) homogeneous sediments (as assumed by many groundwater models); (2) a low permeability channel lining; (3) a narrow lens of low permeability material embedded within the sediments beneath the channel bed; and (4) a laterally extensive low permeability layer. They simulated a wetting front infiltrating into unsaturated ground above a water table from a river channel which was represented by specified head nodes in the model. They found that for cases (1) and (3), where a continuous high permeability path exists between the channel and the water table, no recharge occurred until the saturated wetting front reached the water table. For cases (2) and (4), the wetting front was halted by the low permeability barrier, and a water table mound developed below the channel, eventually connecting with the wetting front. They did not consider it possible to reproduce the exchange flows in all of these cases with either of two simplified models which have been used in other studies to simulate channel losses (a model based on Darcian seepage through the saturated low-permeability stream bed sediments, and a model based on Green-Ampt infiltration into unsaturated sediments, **Green and Ampt (1911)**).

Other attempts have been made to investigate stream-aquifer interactions using numerical models. **Rovey (1975)** coupled a three-dimensional near-channel model to a two-dimensional aquifer model, and simulated monthly river discharges and water table elevations for a river in the Arkansas Valley of Southeastern Colorado. As a result of the long timesteps which were used in her model, she was able to make several simplifying assumptions (for example, that flow in the unsaturated zone for the hydraulically disconnected case was pseudo-steady-

state). However, these led to problems in simulating periods when significant flood events occurred. **Younger (1990)** developed a vertically-integrated two-dimensional model for part of the River Thames and the underlying aquifers. The use of a two-dimensional representation, however, restricts the ability of the model to simulate flows (and in particular, transported contaminants) through systems where the flows vary with depth (as in highly heterogeneous layered aquifers). **Reid and Dreiss (1990)** briefly reviewed some models for stream-aquifer interactions which include the effects of saturated and unsaturated stratified sediments, and concluded that none of the models had been used to investigate transient responses for intermittent streams.

The calculations of aquifer-channel exchange in the existing SHETRAN model are based on a similar approach to that of **Herbert (1970)**, except that the aquifer heads are at a distance from the channel, rather than directly beneath the channel. In addition, a low permeability channel lining is used, implemented as an additional resistance in series with the radial flow resistance. One-dimensional infiltration into unsaturated sediments beneath a dry channel bed is also a feature of the model.

In order to incorporate exchange flows into a multi-layered variably-saturated model, and to simulate flows in sufficient detail for contaminant transport under complex conditions, the governing flow equations must be solved for the near-channel region using a method which can incorporate the effects of stratification, and which can generate vertical flows. To do this for the general case would be impractical using any scheme other than employing a finer discretisation near to the channel. The approach taken, therefore, is to introduce the concept of a "stream column element" into the SHETRAN model structure. The existing SHETRAN structure allows for the inclusion of "bank elements", which are L-shaped in cross-section (Fig. 3.4a,b), and the stream-aquifer exchange uses a radially-convergent solution superimposed over the two-dimensional vertically-integrated flow. The structure for the new VSS model (Fig. 3.4c,d) involves only columns with a rectangular cross-section, and can generate lateral flows through layered media, and vertical flows near and beneath the channel. This approach fits naturally into the column-based structure of SHETRAN, so that the basic solvers for a column can be used for the new stream elements, and a detailed representation of the interactions at the stream bed under all conditions can be made (in particular, vertical and lateral flows through layered media can be represented, and a full Richards equation solution of unsaturated flow beneath an ephemeral or intermittent channel can be implemented - this is a substantial improvement over existing catchment-scale models, especially for simulations of contaminant movement into and out of stream channels).

Recognising that a stream channel (represented in the SHETRAN subsurface components with a rectangular cross-section) is a discontinuity in the surface soils within a catchment, consideration must be given to lateral exchange flows through the sides of a channel, and for flow into the channel through the seepage face above the stream water surface. To represent these, it is assumed that a hydrostatic pressure distribution exists in the stream (so that the hydraulic head at any depth equals the elevation of the stream water surface above datum), and that the pressure at a seepage face is equal to atmospheric pressure (the reference pressure). This pressure distribution is a (time-varying) prescribed lateral head boundary condition, given by

$$h = \begin{cases} z_s & z_b < z < z_s \\ z & z_s < z < z_p \end{cases} \qquad (3.10)$$

where z is the vertical ordinate (positive upwards), z_s is the elevation of the stream water surface (above datum), z_b is the elevation of the stream channel bed (above datum), and z_p is the elevation of the top of the seepage face (above datum). Above the seepage face, the pressure remains at the reference atmospheric pressure, but water is held in the soil by capillary forces, so no flow occurs through the soil-atmosphere boundary.

The specific volumetric flow rate, q_{ex}, into the stream channel through the channel side is given by

$$q_{ex} = k_r K_{ex}^{eff} \nabla h \qquad (3.11)$$

where K_{ex}^{eff} is the effective hydraulic conductivity (see below).

For a stream element, the role of bed sediments in reducing exchange flows and in retarding the movement of contaminants can be important (**Rovey, 1975**; **Younger et al., 1993**). These effects can be incorporated into the stream column by specifying appropriate parameters for the soils or sediments at the top of the column (hydraulic conductivities and sorption coefficients). However, sediments can also line the channel sides. In the new VSS model structure (Fig. 3.4c,d) it is necessary, therefore, to introduce a low permeability lining for the channel sides (otherwise, although flow was restricted through the channel bed, leakage would take place into the adjacent elements through the channel sides). This is achieved by adding an extra resistance to the flows through the channel sides. The effective hydraulic conductivity K_{ex}^{eff}, is defined as the weighted harmonic mean of the conductivities in the adjacent element and in the stream sediments as

$$K_{ex}^{eff} = \frac{(d_x + d_B)K_a K_B}{d_x K_B + d_B K_a} \quad (3.12)$$

where d_B is the thickness of the sediments, K_B is the saturated hydraulic conductivity of the sediments, d_x is the distance from the stream channel side to the adjacent computational node, and K_a is the saturated hydraulic conductivity of the aquifer (= K_x or K_y, depending upon the channel orientation).

3.7.2 Precipitation/evaporation

Under natural conditions in a catchment, precipitation and evaporation at the ground surface normally provide the driving conditions for subsurface flows. During periods of the simulation when no ponded water exists at the ground surface, the flux boundary condition is given by

$$k_r K_z \left(\frac{\partial \psi}{\partial z} + 1\right) = q_p - e_s \quad (3.13)$$

where q_p is net precipitation, and e_s is evaporation rate, at the ground surface.

3.7.3 Plant transpiration

Plant transpiration rates are controlled by a driving potential (governed by atmospheric conditions), a resistance of the vegetation material to the passage of water, and the availability of soil water. In SHETRAN, the transpiration rates are calculated in the evapotranspiration/interception (ET) component, and are extracted from the subsurface as a sink term, q_t, which is added to the overall sink term, q, in Eq. 3.9.

3.7.4 Interaction with ponded ground surface water

During periods of the simulation when ponded water exists at the ground surface, the head boundary condition is given by

$$\psi|_{z=z_s} = d_w \tag{3.14}$$

where z_s is the elevation of the ground surface (above datum), and d_w is the (time-varying) depth of ponded water.

The flux through the ground surface (negative for infiltration, positive for seepage) is then

$$I = -K_z\left(\frac{\partial\psi}{\partial z} + 1\right) \quad . \tag{3.15}$$

3.7.5 Well abstraction

Wells are important for near-surface hydrogeological modelling as they can affect flow paths both locally and regionally, and may provide fast pathways for the migration of contaminants through low permeability media. Depending upon the well design, pumping rates, and aquifer conditions, the local effects of a well may include: vertical flows induced by partially-penetrating wells; non-Darcy flows near the well (due to high local velocities); head losses due to friction or to momentum changes; and radial lateral flow patterns (associated with radial head distributions).

There are many types of well, used for various purposes. Most wells are used for water supply (domestic or industrial); other uses include subsurface hydrogeological investigations to determine rock characteristics (for potential water supply or petroleum extraction, for example), artificial recharge, and liquid waste disposal. Mine dewatering may also affect subsurface flow patterns in a similar way to well abstraction.

The design of a well depends upon its intended application. Shallow domestic water supply wells may be hand-dug and of a wide diameter (for example, hand-dug shallow pits which intersect the water table are used for water supply in some developing countries), or bored, driven, or jetted and of a smaller diameter. Deeper wells are drilled by cable-tool or rotary methods. Horizontal wells, or adits, may sometimes be constructed. Completion of a well can involve the use of a well casing and screen, a gravel pack, or a grouting cement, depending upon the type of aquifer. A well screen is a perforated length of a casing tube that

is used in unconsolidated aquifers to stabilise the well sides, and to prevent movement of coarse aquifer material into the well. In order to provide a good hydraulic contact between the well and the aquifer, a gravel pack may be introduced around the well screen, which also allows a coarser screen to be used. The parts of a well above and below the screen may be sealed using, for example, bentonite clay, to prevent the vertical movement of water along the well (this is particularly important in confined aquifers). Following completion, a well is 'developed' by pumping, surging, backwashing, or jetting, to remove the finer particles from the aquifer around the well, to prevent clogging of the well screen, and to provide a good hydraulic contact between the well and the surrounding aquifer. Further details of well construction methods, and references to comprehensive descriptions of water well technology, are given in **Todd (1980)** and **Freeze and Cherry (1979)**.

Many analytical solutions for flow to wells in simplified geological systems have been developed, mainly for the purpose of producing type curves for use in the analysis of pumping tests to determine aquifer characteristics (transmissivity and storage coefficients). These include solutions for steady-state flow (Thiem equation) and transient flow (Theis equation) in confined aquifers, and solutions for leaky, unconfined, and multi-layered aquifers under a wide variety of conditions (for example, bounded, sloping, anisotropic, or fractured aquifers, and partially penetrating or large diameter wells). A comprehensive treatment is given in **Kruseman and de Ridder (1990)**. Research in this area remains active.

Theoretical studies (both numerical and analytical) have also been made into the hydraulics of wells, including the local region of the aquifer. **Barker and Herbert (1992a,b)** presented a detailed set of theoretical formulae for well losses (ie. head reductions) associated with flow into a well for the case where the flow is uniformly distributed along the well screen. For the general case, they split the total head loss (between the aquifer near to the well and the pump intake) into six terms:

$$\textit{total head loss} = \textit{aquifer loss} + \textit{penetration loss} + \textit{gravel-pack loss} + \textit{slot loss} + \textit{screen loss} + \textit{losses above the screen.}$$

The aquifer and gravel-pack losses are head losses within the porous media. The penetration loss is the head loss incurred as a result of convergence of flow to a partially penetrating well. The slot loss is the head loss due to flow through the constrictions of the well screen slots. The screen loss and losses above the screen are losses within the well casing. They tested the formulae against data from 17 different types of well designs in Bangladesh, and concluded that only the slot losses are negligible.

There have been a number of different approaches taken to inclusion of wells in numerical groundwater models. These have varied greatly in complexity, depending upon the requirements and aims of each particular study. **Ramm and Chazan (1980)** presented a composite solution which incorporated analytical expressions for hydraulic head near wells (treated as singularities) within an overall smooth regional head field calculated by a numerical method. They noted that detailed solutions for hydraulic head near singularities are only required for certain purposes (such as providing a continuous flow field for some particle tracking applications). An alternative approach to providing a more detailed solution near wells is to use mesh refinement within the numerical model. Some numerical studies have been used to investigate local well effects which cannot be evaluated analytically; **Ehlig and Halepaska (1976)** used a numerical model to investigate the effects of transition from confined to unconfined conditions near to a well. The most common approach to modelling the effects of a well at the regional scale (ie. outside the cone of depression) in a groundwater model is to represent a well as a simple sink term. For a two-dimensional model, this is straightforward; for a multi-layer or three-dimensional model, the well acts as a conduit between layers (even if it is not pumped). **Bennett et al. (1982)** incorporated multi-layer wells into a finite-difference groundwater flow model by assuming a local region of the aquifer where storage changes do not occur, and calculating flows between layers as a function of the transmissivities of the layers using the Thiem equation (well screen losses were ignored). This approach appears, however, to depend heavily on the choice of the radius of the local aquifer region (an investigation into appropriate radii has been made by **Pritchett and Garg, 1980**). **Şen (1989)** also used the Thiem equation as a basis for modelling the composite drawdown in a well that intersects horizontal fractures. Often, a definition is made of a generalised well sub-model, with the transmitting capability of the region near to the well being characterised by a general coefficient (eg. the 'well index' of **Reeves and Cranwell (1981)**); the coefficient can then be related to the radial Thiem equation to represent a well, or to other parameters to represent different source/sinks such as streams or springs.

The minimum requirements for including a well in the new VSS model are relatively simple: within any model element containing a well, the prescribed abstraction rate needs to be partitioned between the cells of the element which intersect the well screen. It is not considered justifiable to include a more complex well representation within a regional model. The abstraction rates for each cell are included as part of the sink term, and can also be used by the SHETRAN contaminant components to define the contaminant sink terms. The hydraulic heads in each cell are calculated using the standard flow equation, and are assumed to be the effective heads for the element. Following the approach taken by **Şen (1989)** and

by **Bennett et al. (1982)**, we can write

$$q_w = \sum_{i=1}^{n_c} q_i \tag{3.16}$$

where q_w is the (time-varying) volumetric rate of abstraction from the well, and q_i are the volumetric rates of abstraction from each cell of the n_c cells which intersect the well screen (these are incorporated into the sink term, q, in Eq. 3.9).

Assuming that the q_i are weighted by the transmissivities of each cell, then

$$q_i = \frac{q_w K_i \Delta z_i}{\sum_{j=1}^{n_c} K_j \Delta z_j} \tag{3.17}$$

where K_i is the mean saturated lateral hydraulic conductivity and Δz_i is the thickness of cell *i*.

It is assumed for Eqs. 3.16 and 3.17 that:

a) only one well exists in any model element;
b) the well is vertical;
c) the head in the well is less than the head at any point in the part of the aquifer intersected by the well screen;
c) the well diameter is small relative to the size of the model element (so that well bore storage effects are negligible);
d) the aquifer resources are not depleted during a simulation (ie. the piezometric head at the well does not fall below the top of the well screen).

The more detailed well effects which are not included in this simple model are:

- flows from the well into aquifers; this can occur through either recharge wells, or through multi-layer wells where the hydraulic heads in two or more aquifers differ (whether or not pumping has started);
- head losses inside the well;
- storage within the well;
- non-Darcy flows near to the well screen.

3.7.6 Springs

A spring is defined by **Todd (1980)** as 'a concentrated discharge of groundwater appearing at the ground surface as a current of flowing water'. It should be noted that a spring is therefore defined in modelling terms as a point discharge, in contrast to seepage faces which are discharges of groundwater over larger areas.

Springs may occur due to gravitational or other forces (such as thermal upwellings in volcanic rocks). Gravity springs (which are the only type considered here) occur where a piezometric surface intersects the ground surface, and a conduit for flow from the aquifer to the ground surface exists. For an unconfined aquifer, springs occur therefore where the main water table or a perched water table intersects the ground surface, resulting in a *depression spring* (if a depression in the ground surface intersects the water table) or a *contact spring* (if the underlying aquitard intersects the ground surface) - see Fig. 3.5. For a confined aquifer, an *artesian spring* occurs where an opening in the confining bed provides the conduit for release of water under pressure (Fig. 3.5). Other types of spring may occur in fractured rocks (for example, tubular springs in karst regions, or fracture springs in hard rock aquifers), but these are generated by similar mechanisms to those described above, and are not explicitly considered further.

In many cases, where a water table or piezometric surface intersects the ground surface over a distance, a *spring line* occurs, consisting of a number of separate springs spaced at intervals along the side of a hillslope. Even under these conditions, the discharge of subsurface water usually occurs at individual points rather than along a continuous line. The actual location of a spring may be determined by the presence of an area of local weakness due to perhaps a fracture or a local area of subsurface inhomogeneity (**Lekhov, 1986**), or to a microtopographic depression.

Brassington (1988) notes that 'true' springs originate from groundwater, and can easily be confused in the field with discharges of near-surface water from drainage pipes, leaking water supply or sewerage pipes, or shallow throughflow. The source of spring discharge water may be identified by several methods: chemical analysis, temperature monitoring (groundwater temperatures usually remain around 10-15 °C throughout the year), or discharge monitoring (discharges from a deep groundwater source are likely to show little response to precipitation events).

The fate of water discharged from a spring depends upon the downslope conditions. In most cases, some form of channel will exist downslope of the spring, which may extend continuously down to a main drainage network, or may be poorly developed and of short length. Some or all of the water from low discharge or intermittent springs may infiltrate back into the ground, and re-emerge in a spring lower down the valley side (this was seen in a study of catchment responses at Åstdalen in Norway, **Englund (1986)**).

The essential elements of the mechanisms of spring discharge for inclusion in a catchment scale hydrological model (as opposed to a detailed hillslope spring discharge model such as that of **Lekhov (1986)**) are:

i) the spring discharge occurs at a point;

ii) there is a region of convergent subsurface flow towards the spring;

iii) there is a conduit for the passage of groundwater to the ground surface (this may be from a confined aquifer, or an unconfined aquifer; the springs in the Åstdalen valley in Norway **(Englund, 1986)**, for example, were fed from unconfined bedrock aquifers, but emerged at the ground surface through thin superficial sediments);

iv) there is a (small) stream channel which conveys water away from the spring (for catchment scale models, any minor springs which cannot sustain a stream over at least the scale of the model elements are considered to be negligible).

The approach adopted for the VSS model follows the simple representation of spring discharges in a groundwater model given by **Torak (1982)**. The spring discharge, q_{sp}, which is assumed to be linearly related to the difference between the head at the aquifer cell from which the discharge takes place, $\psi_c + z_c$, and the elevation of the spring, z_{sp}, is given by

$$q_{sp} = \begin{cases} C_s(\psi_c + z_c - z_{sp}) & \psi_c + z_c > z_{sp} \\ 0 & \psi_c + z_c \leq z_{sp} \end{cases} \qquad (3.18)$$

where the value of the spring coefficient, C_s, was obtained by **Torak (1982)** by calibration. It is assumed that a spring discharge is represented by a flow between a user-defined aquifer cell (located, for example, just above an outcropping aquitard; Fig. 3.5) and a channel link (this may be into the top of a stream channel, or into a channel reach if the spring discharge point is located along a valley side; Fig 3.6). This representation therefore provides a route for discharge of groundwater which bypasses surface soils (a route for groundwater discharge which flows through surface soils is provided by the interaction between subsurface flow and surface water).

3.8 Conclusions

The following list is a summary of the review of modelling techniques relevant to the development of the VSS model for simulating the shallow aquifers and soils near to the Sellafield site.

1. Computer modelling of saturated porous media flow in multi-layered aquifers has reached a stage of relative maturity; the two main approaches are a) fully three-dimensional, and b) quasi-three-dimensional (sub-horizontal flow in aquifers, vertical flow in aquitards).
2. The basic variably-saturated flow equations have been generally accepted and used for over twenty years; however, very few three-dimensional variably-saturated flow models have been presented in the literature.
3. Modelling of three-dimensional contaminant transport requires the use of a fully three-dimensional flow model.
4. Computer modelling of variably-saturated porous media flow for practical field situations has been historically restricted by a lack of computer speed; this restriction has only recently become less severe.
5. An equivalent porous medium (EPM) approach is adequate for modelling flow in the west Cumbrian coastal plain aquifers.
6. Aquifer-stream interactions should be modelled for both connected and disconnected conditions; low-permeability channel bed sediments can restrict the flows through the channel bed and sides.
7. A simple model of well hydraulics is adequate for modelling catchment scale flow and transport.
8. Only spring discharges which flow directly into a stream channel need be included in a catchment scale model.

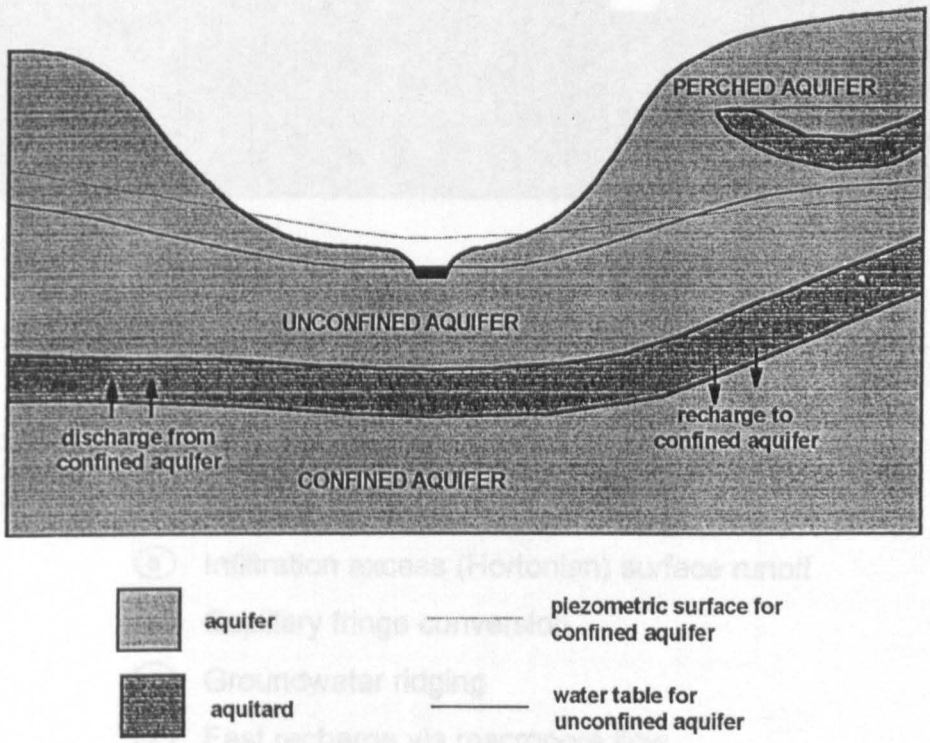

Figure 3.1 Schematic representation of aquifers and aquitards

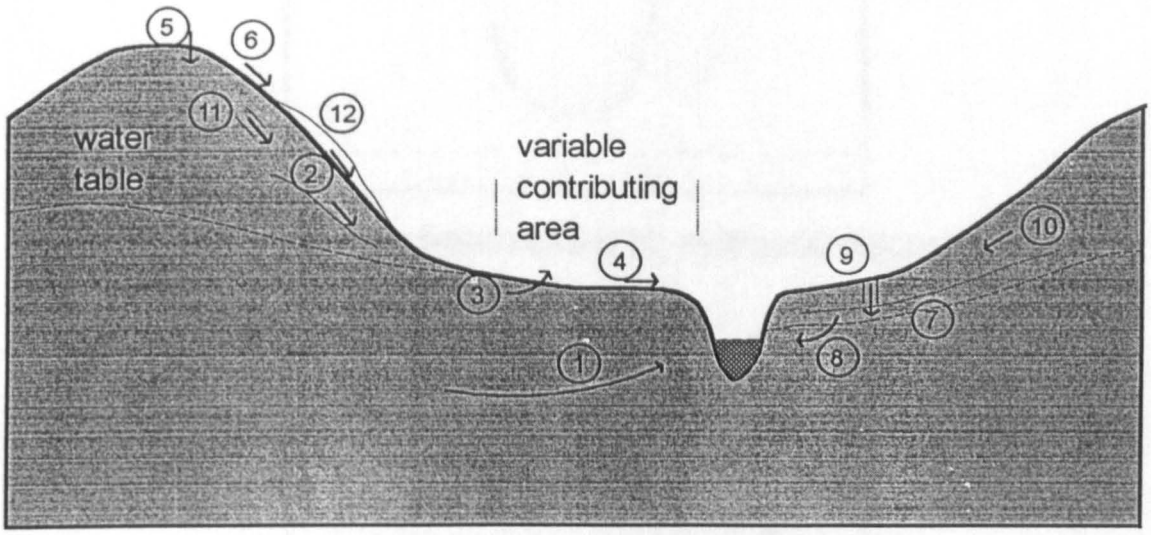

① Baseflow
② Saturated interflow
③ Return flow
④ Saturation excess surface runoff
⑤ Net infiltration
⑥ Infiltration excess (Hortonian) surface runoff
⑦ Capillary fringe conversion
⑧ Groundwater ridging
⑨ Fast recharge via macropore flow
⑩ Unsaturated interflow
⑪ Lateral pipe flow
⑫ Litter flow

Figure 3.2 Hillslope mechanisms for streamflow generation

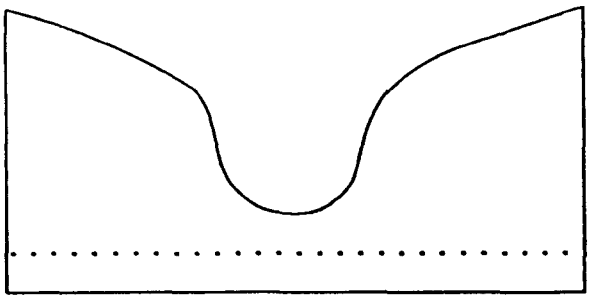

a) Dry stream channel, hydraulic disconnection

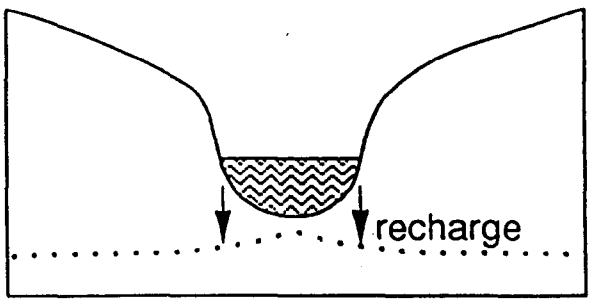

b) Losing stream, hydraulic disconnection

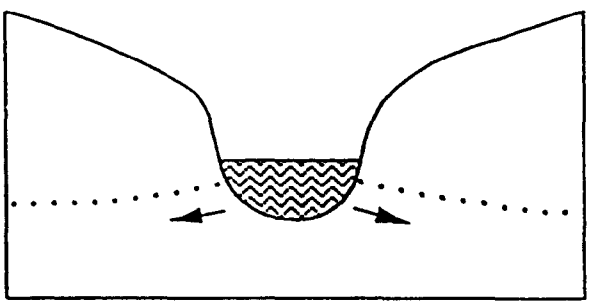

c) Losing stream, hydraulic connection

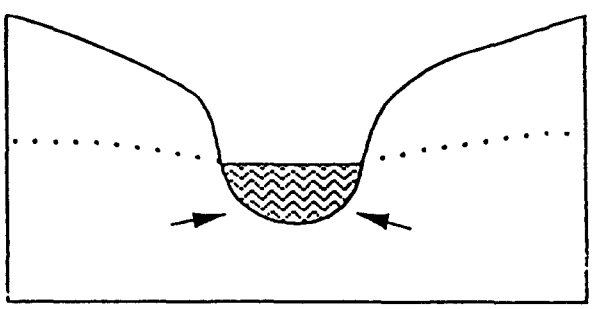

d) Gaining stream

Figure 3.3 Stream-aquifer interactions

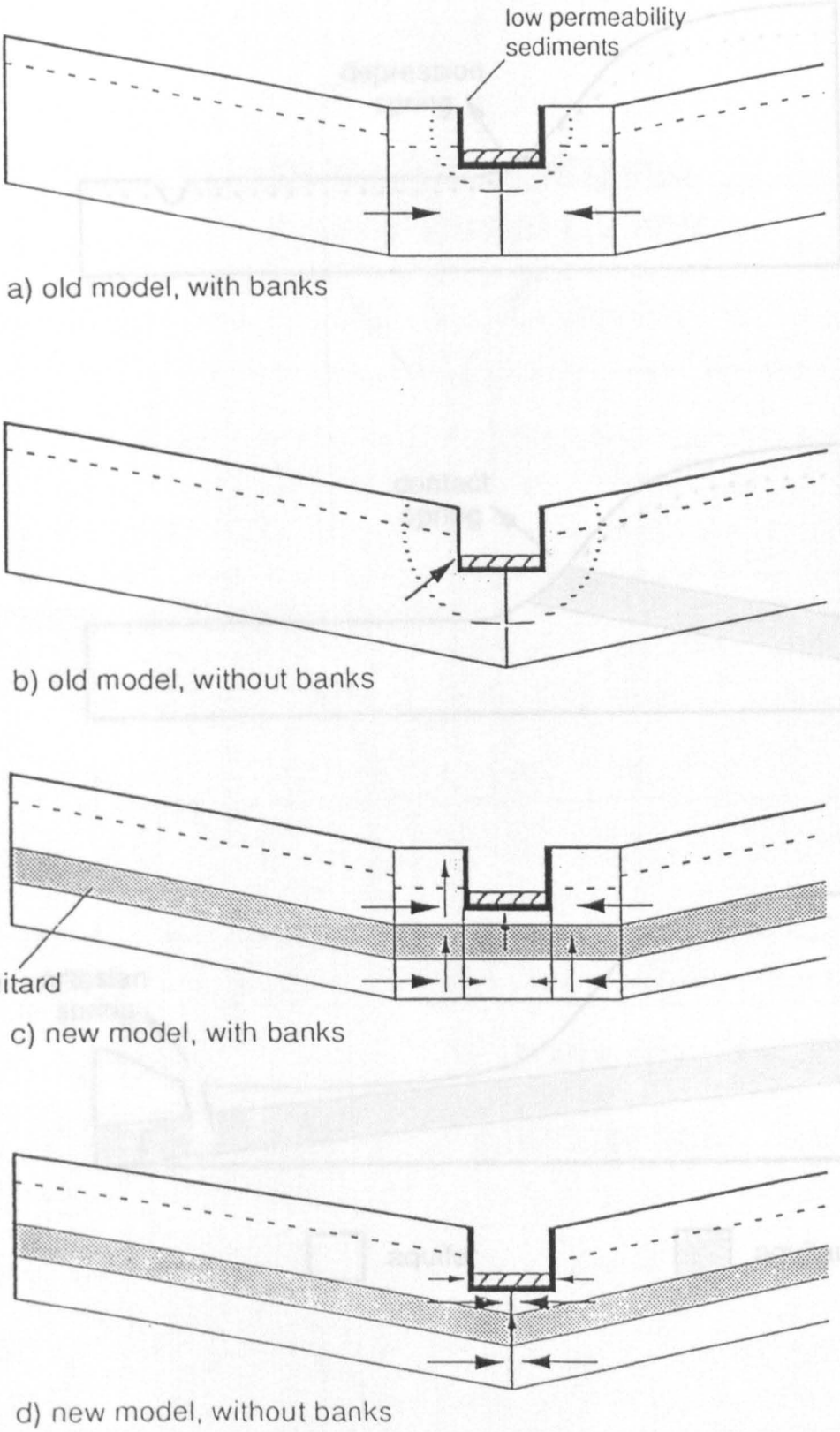

Figure 3.4 Stream column elements

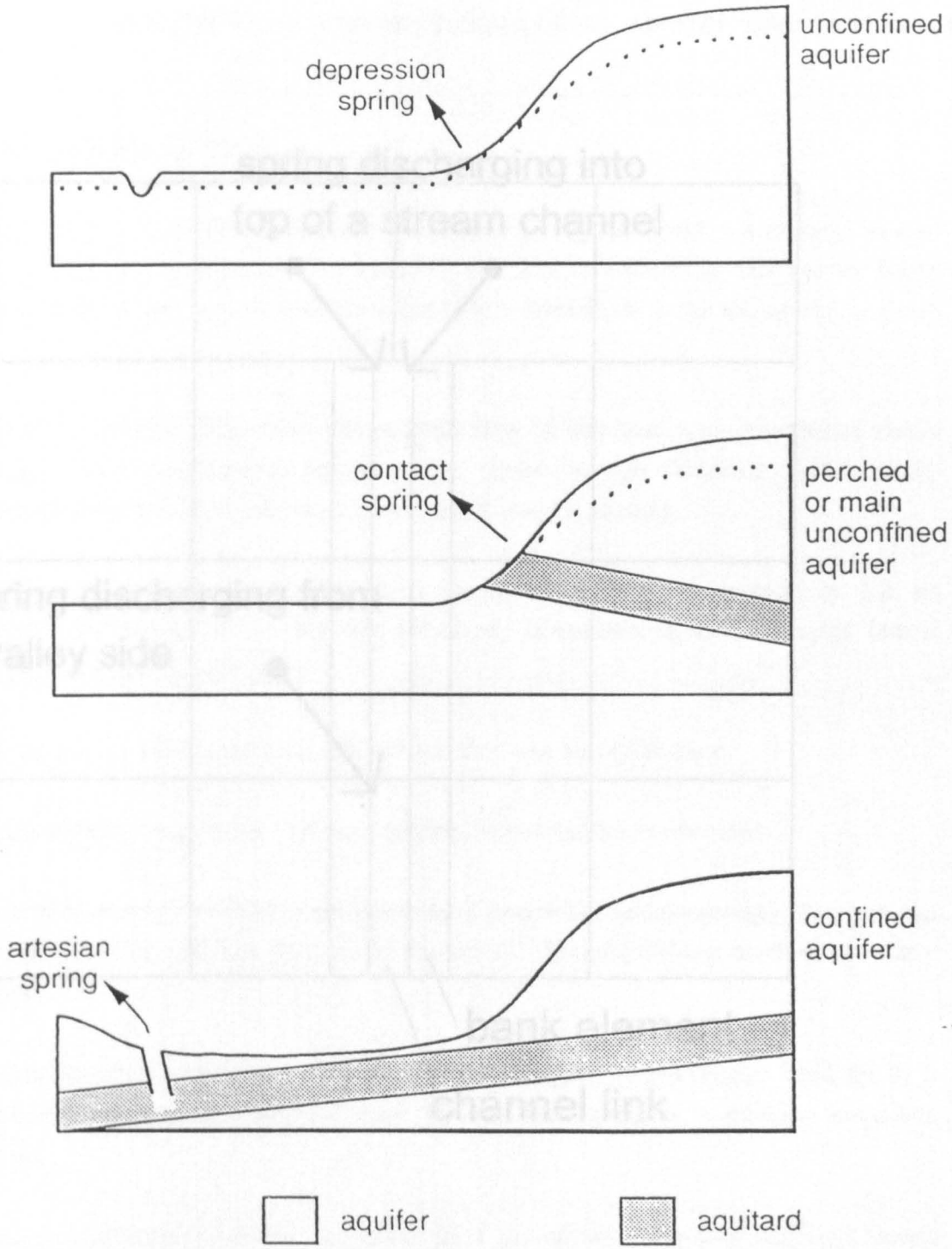

Figure 3.5 Types of gravity spring

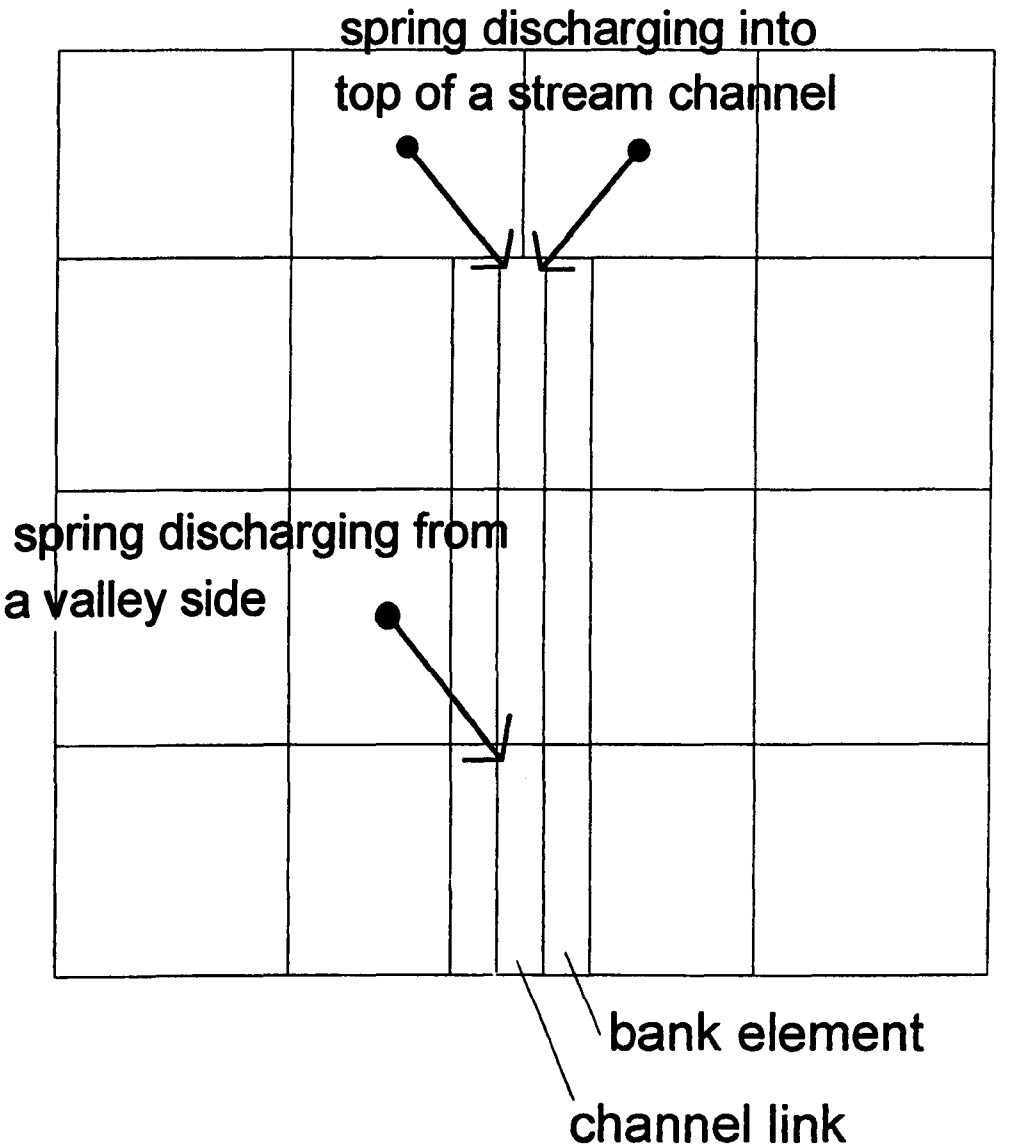

Figure 3.6 Representation of springs in SHETRAN V4

CHAPTER 4 CONCEPTUAL AND MATHEMATICAL MODEL SPECIFICATION

4.1 Model functional specification

Following the reviews of the characteristics of the west Cumbrian aquifers and soils, and of techniques for modelling complex aquifer systems, a model is defined in this section based on conclusions of the reviews. A descriptive functional specification for the model is given below.

i) The model simulates fully three-dimensional flow in saturated and unsaturated single porosity / single permeability porous media. (Flow through fractured media can be represented for conditions where an EPM model is appropriate.)

ii) Flow through multiple layers of porous media of differing characteristics can be simulated; the layers can be laterally extensive, discontinuous, or of limited lateral extent (for example, clay lenses).

iii) Confined, semi-confined, and unconfined aquifers can be represented.

iv) Groundwater perching above low permeability lenses can be represented.

v) The lower boundary conditions are either a) a prescribed (time-varying) flux into the model, or b) a free drainage flux out of the model. The default is a no-flow boundary condition.

vi) The edge boundary conditions are either a) a prescribed (time-varying) head, or b) a prescribed (time-varying) flux, for each layer. The default is a no-flow boundary condition.

vii) The upper boundary conditions are either a) a prescribed (time-varying) head, when ponded surface water is present, or b) a mixed type boundary condition, when no surface water is present, and there is precipitation and evaporation at the ground surface. Evaporative fluxes are calculated in the SHETRAN evapotranspiration/interception module, and are a function of pressure potential. The model automatically switches between the two types of boundary condition.

viii) The boundary conditions at a stream channel bed are identical to those at the ground surface (either a prescribed head, when stream water is present, or a flux representing precipitation and evaporation, when the channel is dry).

ix) Seepage faces can be generated both at the intersection of layers with a stream channel, and at the ground surface.

x) A distributed sink term in the upper soil layers is included for plant transpiration. The (time-varying) flux is calculated in the SHETRAN evapotranspiration/ interception component, and is a function of pressure potential.

xi) A distributed sink term is included for well abstraction, as a prescribed (time-varying) flux. Simple control mechanisms are included to prevent unphysical abstraction from dry wells.

xii) Springs are represented as point discharges of groundwater directly into a stream channel.

4.2 Variables and parameters

The dependent variable for the model is:

$\psi(\underline{x},t)$ pressure potential [L].

The independent variables are:

$\underline{x} = (x,y,z)$ space co-ordinates [L], where z is increasing positive upwards;

t time [T].

Note that hydraulic head, $h(\underline{x},t)$ [L], is used for defining some of the boundary conditions. Hydraulic head and pressure potential are related by

$$h = \psi + z \quad . \tag{4.1}$$

A list of the parameters which must be defined by the user is given in Table 4.1. A list of the model variables used for initial and boundary conditions is given in Table 4.2.

parameter		varies with
d_B	thickness of stream bed sediments [L]	x,y[1]
C_s	spring discharge coefficient [L^2 T^{-1}]	-
$\underline{K}=(K_x,K_y,K_z)$	saturated hydraulic conductivity [LT^{-1}]	$\underline{x}$
K_B	saturated hydraulic conductivity of stream bed sediments [LT^{-1}]	x,y[1]
k_r	relative hydraulic conductivity [-]	ψ
n	porosity [-]	$\underline{x}$
S_s	specific storage [L^{-1}]	$\underline{x}$
z_b	elevation of the model lower boundary above datum [L]	x,y
z_g	elevation of the ground surface above datum [L]	x,y
z_{Rs}	elevation of the stream channel bed above datum [L]	x,y[1]
z_r	elevation of the bottom of the root zone above datum [L]	x,y
z_{sp}	elevation of spring discharge point above datum [L]	x,y
$\Delta x,\Delta y,\Delta z$	dimensions of a column cell [L]	-
θ	volumetric soil water content [-]	ψ

[1] only defined for stream elements

Table 4.1 Model Parameters

variable		varies with	source[1]	non-zero range[2,3]
d_w	depth of ponded or stream water [L]	x, y, t	OC	-
e_s	evaporation rate at the ground surface [LT^{-1}]	x, y, t	ET	-
h_0	initial hydraulic head [L]	$\underline{x}$	ic	-
h_b	prescribed head at the model bottom boundary [L]	x, y, t	bc	-
h_l	prescribed head at the model boundary [L]	$\underline{x}$, t	bc	boundary only
q_b	rate of upflow from the deeper regional aquifer [LT^{-1}]	x, y, t	bc	-
q_l	prescribed lateral flux at the model boundary [LT^{-1}]	$\underline{x}$, t	bc	boundary only
q_p	net precipitation at the ground surface [LT^{-1}]	x, y, t	ET	-
q_t	specific volumetric sink term for plant extraction [T^{-1}]	$\underline{x}$, t	ET	$z_r \leq z \leq z_g$
q_w	specific volumetric flux out of an abstraction well [T^{-1}]	x, y, t	bc	well elements only
z_p	elevation of the top of the stream channel seepage face above datum [L]	x, y, t	OC[4]	channel only
z_s	elevation of stream water surface above datum [L]	x, y, t	OC	channel only

[1] ic = initial condition; bc = boundary condition or source/sink;
ET = evapotranspiration component; OC = overland/channel component.
[2] default non-zero range is the whole applicable model domain;
[3] z_r = elevation of bottom of root zone; z_g = elevation of ground surface (see Table 4.1);
[4] z_p is calculated within the VSS model using OC data

Table 4.2 Model Variables

4.3 Three-dimensional flow equation

The basic equation governing three-dimensional flow through a heterogeneous, anisotropic medium is

$$\eta \frac{\partial \psi}{\partial t} = \frac{\partial}{\partial x}[K_x k_r \frac{\partial \psi}{\partial x}] + \frac{\partial}{\partial y}[K_y k_r \frac{\partial \psi}{\partial y}] + \frac{\partial}{\partial z}[K_z k_r \frac{\partial \psi}{\partial z}] + \frac{\partial (k_r K_z)}{\partial z} - q \qquad (4.2)$$

where the storage coefficient, η, is defined as

$$\eta = \frac{\theta S_s}{n} + \frac{d\theta}{d\psi} \qquad (4.3)$$

and q is a specific volumetric flow rate (volumetric flow rate per unit volume of medium) out of the medium, given by

$$q = q_w + q_{sp} + q_t \qquad (4.4)$$

where q_w accounts for well abstraction (section 4.4.6), q_{sp} accounts for spring discharges (Section 4.4.7), and q_t accounts for transpiration losses (Section 4.4.4).

4.4 Initial and boundary conditions

4.4.1 Initial conditions

The initial conditions for a simulation are

$$h(\underline{x},0) = h_0(\underline{x}) \qquad (4.5)$$

where $h_0(\underline{x})$ is a prescribed hydraulic head field.

4.4.2 Stream-aquifer interaction

The exchange flows between an aquifer and a stream channel are composed of two parts: flow through the channel bed, and flow through the channel sides (including a seepage face).

Flow through the channel bed (which may be into or out of the channel) is handled in exactly the same way as flows at the ground surface, with a flowing stream channel corresponding to a ponded boundary condition at the ground surface (Section 4.4.5), and a dry channel corresponding to a flux boundary condition (Section 4.4.3). Low permeability sediments are handled by assigning appropriate values to the column cells at the stream bed.

For the channel sides, a pressure distribution is prescribed as a (time-varying) lateral head boundary condition, given by

$$h = \begin{matrix} z_s & z_{gs} < z < z_s \\ z & z_s < z < z_p \end{matrix} \quad . \tag{4.6}$$

The specific volumetric flow rate, q_{ex}, into the stream channel through the channel sides is then given by

$$q_{ex} = K_{ex}^{eff} k_r \nabla h \tag{4.7}$$

where K_{ex}^{eff} is the effective hydraulic conductivity, defined as the weighted harmonic mean of the conductivities in the adjacent element and in the stream sediments, given by

$$K_{ex}^{eff} = \frac{(d_x + d_B) K_s K_B}{d_x K_B + d_B K_s} \tag{4.8}$$

where d_x is the distance from the stream channel side to the adjacent computational node, and K_s is the saturated hydraulic conductivity of the aquifer (= K_x or K_y, depending upon the channel orientation).

4.4.3 Precipitation/evaporation

During periods of the simulation when no ponded water exists at the ground surface, the flux boundary condition is given by

$$k_r K_z \left(\frac{\partial \psi}{\partial z} + 1 \right) = q_p - e_s \quad . \tag{4.9}$$

4.4.4 Plant transpiration

Plant transpiration rates are controlled by a driving potential governed by atmospheric conditions, a resistance of the vegetation material to the passage of water, and the availability of soil water. In SHETRAN, the transpiration rates are calculated in the evapotransiration/interception (ET) component, and are extracted from the subsurface as a sink term, q_t.

4.4.5 Interaction with ponded ground surface water

During periods of the simulation when ponded water exists at the ground surface (including stream water for stream elements), the head boundary condition is given by

$$\psi|_{z=z_s} = d_w \quad . \tag{4.10}$$

The flux through the ground surface (negative for infiltration, positive for exfiltration) is then

$$I = -K_z\left(\frac{\partial \psi}{\partial z} + 1\right) \quad . \tag{4.11}$$

4.4.6 Well abstraction

For a well whose screen intersects n_c cells, the specific volumetric rate of flow from each cell, q_{wi}, is given by

$$q_{wi} = \frac{q_w \overline{K_i} \Delta z_i}{\sum_{j=1}^{n_c} \overline{K_j} \Delta z_j} \tag{4.12}$$

where $\overline{K_i}$ is the mean saturated lateral hydraulic conductivity of cell *i*.

4.4.7 Springs

In the VSS model it is assumed that water discharging from a spring flows into a stream channel (this may be into the top of a stream channel, or into a channel reach if the spring discharge point is located along a valley side). The specific volumetric spring discharge, q_{sp}, is given by

$$q_{sp} = \begin{cases} C_s(\psi_c + z_c - z_{sp}) & \psi_c + z_c > z_{sp} \\ 0 & \psi_c + z_c \leq z_{sp} \end{cases} \qquad (4.13)$$

where ψ_c is the pressure potential at the aquifer cell from which discharge takes place, and z_c is the elevation of the cell node (above datum).

4.4.8 Bottom boundary conditions

The lower boundary of the model should normally be located at a depth where substantial flows do not occur over the timescale of a simulation. To allow a small contribution of a deeper regional aquifer to the modelled region, a prescribed rate of inflow can be defined along the lower boundary by

$$-k_r K_z\left(\frac{\partial \psi}{\partial z} + 1\right) = q_b \qquad (4.14)$$

where the regional aquifer flow, q_b, is positive into the model. The default case is for the lower boundary to be an impermeable bed, so that $q_b = 0$.

To allow for the possible use of the model to simulate freely draining soil in a column, a free drainage flux lower boundary condition is included, given as a unit head gradient

$$\frac{\partial h}{\partial z}\Big|_{z=z_b} = 1 \quad . \qquad (4.15)$$

Alternatively, a prescribed time-varying spatially-varying head boundary condition can be defined, as

$$h\big|_{z=z_b} = h_b(x,y,t) \quad . \qquad (4.16)$$

4.4.9 Lateral boundary conditions

For some uses of the model, prescribed boundary conditions need to be given at the edge boundaries of a region, where a full catchment is not being modelled. These may be required, for example, in simulating experimental plots, sub-regions of a catchment (to define a locally finer grid for contaminant simulations), or catchments where the groundwater divide does not coincide with the surface water divide.

A head boundary condition can be defined along a part of the model boundary B_1, given by

$$h(\underline{x},t) = h_1(\underline{x},t) \quad \text{for } \underline{x} \text{ on } B_1 \ . \tag{4.17}$$

A flux boundary condition can be defined along a part of the model boundary B_2 as

$$\underline{n}.(k_r\underline{\underline{K}}.\nabla h) = q_1 \tag{4.18}$$

where $\underline{n}$ is the unit outward normal to the model boundary.

Note that, to maintain full flexibility, flux boundary conditions are allowed both into and out of the modelled region. No feedback is provided for specified fluxes out of the model (which could lead to unphysical dewatering of the aquifer), so particular care should be taken if this type of boundary condition is used.

4.5 Extensions to the SHETRAN V3 contaminant component

In **Ewen (1990)** and **Ewen (1991)**, the basis for lateral migration of contaminants between the saturated sections of columns was given. This can be extended to accomodate lateral migration in the unsaturated zone by simply extending the definition of q_j in **Ewen (1991)** to the whole region between the base of the modelled aquifer and the ground surface (q_j is defined in **Ewen (1991)**, as the volumetric rate of flow of water through face j of the saturated section of a column). Since the extended q_j is entirely consistent with the original q_j (the original q_j was undefined in the unsaturated zone, so was effectively equal to zero), no changes in the formulations given in **Ewen (1990)** and **Ewen (1991)** are required.

CHAPTER 5 NUMERICAL MODEL SPECIFICATION

5.1 Introduction

The equation used to describe flow in variably-saturated porous media is the extended Richards equation, which is given in its pressure form in three spatial dimensions in Eq. 4.2. The limitations of this equation as a description of the processes acting in field soils and rocks were discussed in Section 3. It is further assumed here that flow is non-hysteretic (ie. that the functions $K(\psi)$ and $C(\psi)$ in Eq. 4.2 are single-valued). The fact that there is continuing active research into methods of solution of the Richards equation, more than sixty years after its first appearance, is sufficient testimony to the difficulties it presents. These difficulties are mainly attributable to the non-linearity of the coefficients (hydraulic conductivity and storage terms). Some alternative approaches to solving the Richards equation are discussed in Section 5.2. In Sections 5.3 to 5.7, the numerical schemes for the VSS model are developed.

The approach which has been developed for the VSS model is intended to provide robust, mass-conservative solutions which are reasonably accurate under the ranges of conditions for which the model may be applied (these conditions are summarised in Section 1.6). In any numerical scheme, a balance has to be achieved between accuracy, mass conservation, and computational requirements. It is recognised that, for the types of engineering applications to which the new model will be applied as part of SHETRAN, and given the limitations of the Richards equation as a description of field processes (with the additional uncertainty of spatial heterogeneity of soil properties), a strong emphasis on obtaining a highly accurate solution to Eq. 4.2 cannot be justified. In the context of considering the utility of quasilinear approximations to the Richards equation (discussed in section 5.2.1), **Philip (1987)** stated that "... in most engineering contexts and in most field applications of soil physics, we should be surprised and delighted if our predictions held to 10% ...".

Of the many models which have been written to solve Eq. 4.2 (or its equivalent forms) in one, two, or three spatial dimensions, most have used finite-difference (FD) or finite element (FE) methods. (Recently, other methods have also been used, including boundary elements, methods of characteristics, and transform methods.) Investigations of the comparative behaviour of FD and FE methods (eg. **Celia et al. (1990)**; and studies reviewed by **Nielsen et al. (1986)**) have not tended to favour either method under all conditions. In order to remain consistent with the existing SHETRAN modelling system, only the finite difference method is considered in detail here.

5.2 Discussion of numerical methods

5.2.1 Simplified one-dimensional unsaturated zone models

Although most methods used to solve the Richards equation use finite difference or similar schemes, alternative approaches have been used, usually under restrictive conditions. Two approaches are briefly considered which can be used to reduce the computational complexity of obtaining solutions for Eq. 4.2: analytical solutions, and quasilinear approximations.

Closed-form analytical solutions for Eq. 4.2 have been developed under simplifying assumptions and used, in particular, for calculating infiltration rates, but also for verification of numerical algorithms. Analytical solutions can also provide insights into the behaviour of classes of solutions of Eq. 4.2 which may not be evident from numerical modelling results **(Milly, 1988)**.

Two of the analytical solutions for infiltration problems which have been most widely used, and which have been used as the basis for other solutions, are those of **Philip (1987)**, who developed a simple expression to characterise cumulative one-dimensional infiltration, and **Green and Ampt (1911)** who analysed the case of a distinct (step function) wetting front into initially dry soil. Even such simple methods as these can provide useful results under special circumstances; for example, **Beven and Clarke (1986)** investigated infiltration into a structured soil using Green-Ampt theory to describe the wetting front from a macropore into the soil matrix. There have been many other analytical solutions for one or more spatial dimensions, to handle more complex boundary conditions, or to handle heterogeneous soils (some examples are given in **Milly (1988)**). However, despite this continuing activity, it is usually recognised (eg. **Milly, 1988**; **Nielsen et al., 1986**), and it is concluded here, that currently available analytical solutions cannot handle the complex physical properties and general boundary conditions encountered near the ground surface in the field.

Another area in which analytical solutions may provide a means for simplification is in vertical one-dimensional flow deeper below ground, either within saturated aquitards (discussed earlier for multi-layered aquifer models), or in unsaturated regions below perched water tables. Under these conditions, boundary conditions for a vertical length of porous media are likely to change much more slowly than at the ground surface, and heterogeneity in the vertical is likely to be less than near the ground surface. However, within a simulation,

conditions change continually, so that a saturated aquitard may become unsaturated, or an unsaturated region below a perched water table may merge with the unsaturated region near to the ground surface as the perched water drains away. Any analytical solution defined under restricted conditions would then have to be modified or removed from the solution scheme dynamically within the simulation. In order to retain robustness of the model, and to avoid possible switches in behaviour by swapping between analytical and numerical methods of solution, it is concluded that only a single (numerical) solution method should be used for all cases.

Eq. 4.2 can be linearised for certain classes of functional forms for the non-linear hydraulic property coefficients. One method which has been extensively used is the 'quasilinear' approximation, the use of which is reviewed by **Pullan (1990)**. The basic quasilinear approximation depends upon the assumption that the soil is homogeneous, and is usually applied to steady-state or nearly steady-state problems. The approximation involves the use of an exponential form for the unsaturated hydraulic conductivity function ($K(\psi) \propto e^{\alpha\psi}$), with the consequence that Eq. 4.2 then reduces to a linear equation. This form for $K(\psi)$ has been extensively used to represent a wide range of field soils; and, although it cannot represent the soil hydraulic functions for many soils accurately (**Srivastava and Yeh, 1991**), the restrictions that it imposes on the possible solutions to Eq. 4.2 are considered by **Pullan (1990)** to be unimportant compared with the uncertainty in other aspects of unsaturated zone modelling.

Extension of the quasilinear form to transient problems involves the assumption of constant diffusivity, which also imposes strict limitations on its applicability. **Warwick (1991)** considered the transient quasilinear equation to be applicable for values of soil moisture which vary over only a small range about a steady-state case. Extensions of the quasilinear form to heterogenous soils have been made for specific boundary conditions. For example, **Weir (1989)** presented theoretical results for the asymptotic behaviour of infiltration into layered soils resulting from a step increase in water table height, under the quasilinear approximation, by assuming an effective conductivity over the soil layers; his solution did not allow for continuously varying water tables. It appears that, despite the possible benefits, the use of a linearised form of Eq. 4.2 would not be sufficiently general to adequately handle the range of conditions for which the model may be applied.

It is concluded, therefore, that neither analytical solutions to, nor linearised forms of, Eq. 4.2 are likely to be able to handle all of the conditions for which the model may be applied, and a numerical solution method must be employed.

5.2.2 Treatment of non-linearities in the Richards equation

The numerical solution of the nonlinear partial-differential Richards equation by finite difference (or indeed, other finite methods) involves transformation of the partial derivatives into algebraic expressions. If only the spatial derivatives are transformed, this results in a set of coupled ordinary differential equations. If the time derivatives are also transformed, the result is a set of coupled algebraic equations, with nonlinear coefficients (ie. the coefficients are functions of the dependent variable, ψ). In this case, one of the main problems in finding a solution is how to treat the nonlinear coefficients of the algebraic system.

The simplest approach to solving the algebraic system is to use a two-level explicit scheme, where all the coefficients are evaluated at time level n. This results in a system of linear equations which is relatively easily solved. However, the stability requirements of such an explicit scheme are usually quite severe (**Paniconi et al., 1991**), so that very small timesteps are needed, especially when steep wetting fronts occur. More commonly, unconditionally stable implicit methods have been used. In this case, the coefficients of the algebraic system are evaluated at time level $n+1$. There are two main methods by which the coefficients can be evaluated: iterative methods, where successive approximations to the solution vector $\underline{\psi}$ are calculated, until convergence is achieved (measured by comparing some norm $\|\underline{\psi}^{n+1} - \underline{\psi}^{n}\|$, where the superscripts denote iteration level, against a given criterion); and direct or noniterative methods, where the solution is calculated in a known number of steps. The most commonly used iterative methods (for the solution of the Richards equation in one, two, or three dimensions) are the Newton and the Picard methods (see, for example, **Murphy et al. (1988)** or **Woodford (1992)**).

Although iterative methods have been extensively used, and are generally robust (if well written, they are likely to find a solution eventually), they can require substantial amounts of processor time, as a linear algebraic system has to be solved at each iteration. Recognising this problem, **Paniconi et al. (1991)** investigated several non-iterative procedures for solving the Richards equation. For three test problems of one-dimensional unsaturated flow they compared the performance (in terms of processor requirements, accuracy, stability, and mass balance errors) of six iterative and non-iterative solution methods: iterative Newton; iterative Picard; single-iteration Newton; single-iteration Picard; implicit factored scheme; and three-level Lees scheme. The single-iteration Newton and Picard schemes consist of the first cycle of their fully-iterative counterparts, and are $O(\Delta t)$ accurate. The implicit factored and Lees

methods were introduced into the comparisons to provide $O(\Delta t^2)$ noniterative schemes. The implicit factored scheme involves taking the storage term $\eta(\psi)$ of Eq. 4.2 across to the right hand side, so that the time derivative term is linear. The Lees method involves use of three time levels to give a second-order accurate time derivative. **Paniconi et al. (1991)** concluded that: all the schemes, except the Lees method, were stable; of the iterative methods, the Picard scheme converges more slowly (linearly, compared to the quadratic convergence of the Newton method), but is computationally simpler, and gives symmetric matrices.

The use of a mixed form of the one-dimensional Richards equation was advocated by **Celia et al. (1990)**, who ran numerical tests on different forms of the Richards equation. They noted that, although the different forms of the time derivative in the Richards equation ($\partial\theta/\partial t$ and $\eta(\psi)\partial\psi/\partial t$) are equivalent in the continuous partial differential equation, their finite analogues are not equivalent. They re-derived the finite difference equations, and showed that the use of the mixed form of the equation produces perfect mass balance. (Note that the θ-based form of the equation, discussed in section 3, is not recommended for use under either non-homogeneous or saturated conditions.) This type of transformation of the ψ-based equation has been used by several other authors (eg. **Rathfelder and Abriola, 1994**), and is generally described as the chord-slope approximation, as it depends upon the use of a chord-slope, rather than a tangent, approximation to the storage term.

5.2.3 Spatial averaging of hydraulic conductivity

The evaluation of internodal mean values for hydraulic conductivity is an important control on solutions of the flow equations under both saturated and unsaturated conditions. In particular, quantitatively and qualitatively different solutions can be obtained using different methods for infiltration into dry soils, and for heterogeneous problems. A number of recent investigations have been critical of results obtained using numerical models with traditional methods for evaluating internodal hydaulic conductivities, but no universal method has been presented which will provide accurate solutions under all conditions.

Four of the most widely used methods for calculating mean conductivities (K) or conductances ($KA / \Delta x$) between two computational cells are:

arithmetic mean (conductivity)

$$<K_1,K_2>_a = 0.5\ (K_1 + K_2) \quad ; \tag{5.1}$$

geometric mean (conductivity)

$$<K_1,K_2>_g = \sqrt{(K_1 K_2)} \quad ; \tag{5.2}$$

harmonic mean (conductivity)

$$<K_1,K_2>_h = \frac{2\ K_1\ K_2}{(K_1 + K_2)} \quad ; \tag{5.3}$$

weighted harmonic mean (conductance)

$$<K_1,A_1,\Delta x_1,K_2,A_2,\Delta x_2>_{wh} = \frac{K_1 A_1 K_2 A_2}{(K_1 A_1 \Delta x_2 + K_2 A_2 \Delta x_1)} \quad ; \tag{5.4}$$

where K_1 and K_2 are hydraulic conductivities, A_1 and A_2 are cross-sectional areas in the direction of flow, and Δx_1 and Δx_2 are distances between the computional nodes and the computational cell boundaries in the direction of flow.

In a study of infiltration into dry soils, **Zaidel and Russo (1992)** investigated the use of different averaging expressions, including some which were weighted by the hydraulic heads or the water contents at the computational nodes, and demonstrated that the arithmetic mean smears the wetting front more than other means, and that the geometric mean gave the sharpest wetting front (for the particular hydraulic functions used in the test). The harmonic means also tend to give sharp wetting fronts. They proposed an asymptotic weighting formula, and demonstrated its accuracy for use in cases of infiltration into dry soil; however, the scheme performs less well for near-saturated conditions when using a relatively coarse grid.

Romeu and Noetinger (1995) investigated the effects of using different representations for internodal transmissivities in finite-difference models for saturated conditions (they noted the significant difference between the numerical requirements under saturated and unsaturated conditions), and discussed the interaction between grid scales and scales of natural heterogeneity. They concluded that harmonic schemes are inappropriate for three-dimensional problems with coarse grids, since the mean values are dominated by low conductivity values in heterogeneous cases (although the harmonic mean was shown to be correct at small scales).

Warrick (1991) presented a framework for comparing different weighting schemes for internodal unsaturated hydraulic conductivity for steady conditions in homogeneous soils, by comparing velocities from numerical cases with the correct Darcy velocities. The results were inconclusive for general application, as it was found that different averaging schemes gave the best results for different cases.

A general expression for the mean of two hydraulic conductivity values is the *w*-order mean, or the power-averaging formula (proposed by **Journal et al. (1986)**, and discussed by **Romeu and Noetinger (1995)**):

w-mean

$$\langle K_1, K_2 \rangle_w = \left(0.5 \left(K_1^w + K_2^w \right) \right)^{1/w} \quad . \tag{5.5}$$

A value of $w = 1.0$ corresponds to the arithmetic mean, $w = -1.0$ corresponds to the harmonic mean, and $w \rightarrow 0.0$ corresponds to the geometric mean (note that the expression is invalid for $w = 0.0$).

Romeu and Noetinger (1995) stated that the optimal value for *w* in a particular case depends upon the heterogeneity pattern; they discussed the results from an earlier study, where numerical experiments showed that, for a particular test case, a value of *w* of -0.23 gave the best representation of internodal hydraulic conductivites.

The *w*-mean provides a method for implementing a general formulation into a model, which can be controlled by a single parameter. Since the recent studies have not provided any justifiable conclusion on a single method for calculating internodal hydraulic conductivities under variably-saturated conditions, the *w*-mean gives a flexible approach to modelling which can be modified when further experience in use of the VSS model has been obtained.

5.2.4 Storage term for variably-saturated flow

The storage term $\eta(\psi)$ of Eq. 4.2 consists of two terms, representing the rate change of storage of water in the unsaturated zone with matric potential, and storativity in the saturated zone. It was noted earlier that the size of the storativity term S_s is small relative to the unsaturated storage term. The need to retain a non-zero coefficient in Eq. 4.2 is essential for variably-saturated flow modelling, to prevent the parabolic equation degenerating into an

elliptic equation in the saturated zone, with possible problems of indeterminacy (when the finite-difference system matrix becomes singular and therefore non-invertible) if Neumann boundary conditions are used (**Paniconi et al., 1991**). **Paniconi et al. (1991)** describe a method for extending the form of the soil characteristic function given by **van Genuchten and Nielsen (1985)** to incorporate storativity in the saturated zone.

5.2.5 Discussion of possible methods for catchment discretisation

The choice of a method for setting up a three-dimensional finite-difference mesh for catchment modelling is a compromise between simplicity, flexibility, and efficiency of solution of the resulting equations. A systematic approach to mesh generation facilitates both data input and graphical output; the method should be flexible enough to allow a reasonably accurate representation of the geological layering to be made; and a mesh design which results in a well structured matrix can provide the basis for efficient numerical algorithms.

To allow sufficient flexibility for the varied potential applications of SHETRAN, the mesh design should allow the following features to be accomodated:

1. small node spacings near to the ground surface;
2. shallow soils of spatially variable depths (typically less than one metre);
3. multilayered aquifers which follow the ground surface;
4. multilayered aquifers which form outcrops;
5. breaks in layers, and lenses.

The requirements for small node spacings in shallow soils can be met by dividing the subsurface region into two zones: a 'soil' zone, and an 'aquifer' zone. The computational mesh layers in the soil zone follow the ground surface. More complex arrangements are required to describe possible aquifer formations.

Three methods were considered for describing the lateral connections between adjacent elements in the aquifer zone to accomodate requirements 3, 4 and 5: *a*) continuous mesh layers following the stratigraphy; *b*) continuous mesh layers following the ground surface; and *c*) bifurcating layers. (More complex connectivities could be defined which would result in more complex numerical algorithms, but it is felt that these would not be justified given the high level of uncertainty in specifying aquifer geometries for most catchments.) Options *a* and *b* both have the disadvantage that any local lenses within an aquifer (an important part

of the functional requirements for the model) would need to be represented by 'ghost' or 'dummy' mesh cells within a layer extending across the entire model domain, with an associated computer memory and computational burden.

Option *c*, which involves any cell being uniquely connected to either one or two adjacent cells on each face, was therefore chosen; note that it includes both options *a* and *b* as special cases. A deformed co-ordinate system is used, so adjacent cells need not be of the same depth.

5.3 Catchment discretisation

5.3.1 Basic mesh design

The methods used to read in data describing the physical configuration of a catchment, and to process the data, are intended to provide a relatively simple facility for setting up catchments (especially subsurface layering) for default cases such as laterally extensive and continuous layers, while allowing full flexibility for setting up more complex systems. It is intended that separate pre-processing programs should be developed to establish layer boundaries and inter-connections between layers for each lithology for complex cases. The internal processing within SHETRAN will then establish the actual discretisation and inter-connections between computational cells used in the simulation.

Following the SHETRAN design of grid elements, bank elements, and channel elements (Fig. 1.2), a simple mesh design is adopted where each element consists of a column of cells which are variably spaced in the vertical (Fig. 5.1). A block-centred system is used for vertical discretisation, where the finite-difference computational node is at the centroid of each cell; this facilitates the siting of horizon boundaries on cell boundaries.

The subsurface region of a catchment is divided into two zones: a 'soil zone' and an 'aquifer zone' (Fig. 5.2); note that these terms are used for convenience only, and do not necessarily correspond with the actual soils and aquifer of the model set up. The soil zone consists of the upper region of the catchment subsurface to a specified depth below ground (constant over the whole catchment) where the cell spacing is identical for every element. The aquifer zone consists of the part of the catchment subsurface below the soil zone. This approach has been taken to allow small cell sizes to be implemented near to the ground surface, without involving complications of matching differing cell spacings between adjacent elements when

the cell spacings are very small (typically just a few centimetres near to the ground surface, to catch the fast dynamics of infiltration processes).

5.3.2 Soil zone

For the 'soil zone', the user defines a single sequence of cell sizes (depths) for the catchment. The soil zone is then defined as the upper region of the catchment subsurface to the base of the summed cell sizes (Fig. 5.2). Typically, the soil zone may be about 0.5 - 1.0 m depth (roughly corresponding to typical soil depths, although there is no requirement that it correspond in any way with actual soil depths, or with the plant rooting zone). A one to one connectivity is then established between corresponding cells in adjacent columns for all elements.

Note that, if required, the 'soil zone' may be defined to extend beyond the maximum aquifer depth in the catchment. In this case, the computational grid would consist of a uniform grid over the whole three-dimensional space of the modelled catchment. There would then be no aquifer zone, and any cells in the 'soil zone' defined below the lowest point of the aquifer at any element are simply excluded from the computations.

5.3.3 Aquifer zone

For the region below the soil zone (termed the 'aquifer' zone, though it will often include a significant unsaturated region), the vertical discretisation can vary from element to element (Fig. 5.1). The user input consists of the depth below ground or elevation above datum of the lower boundary of each layer, together with connectivity details where the stratigraphic sequence is not identical to the adjacent elements (Fig. 5.2a). Each layer is then automatically subdivided into computational cells by the VSS model (Fig. 5.2b). Each cell is connected to either one or two cells of the adjacent element on each face (Fig. 5.2b). For both the cell discretisation and the connectivities, a user-defineable cell-by-cell over-ride is allowed, subject only to the limitation that each cell is connected laterally to either one or two adjacent cells on each face.

The rules for connectivity between stratigraphic sequences in adjacent elements are as follows, where lower number rules over-ride higher number rules:

i use user-defined connectivities;
ii match corresponding adjacent stratigraphic sequences, starting from the lowest;
iii define null connectivities (ie. no-flow) where sequences do not match.

5.4 Soil hydraulic properties

5.4.1 Functional forms

Four representations of the soil hydraulic functions (the soil characteristic function, $\theta(\psi)$, and unsaturated hydraulic conductivity function, $K(\psi)$) are included in the first release of the VSS model, although the code is written so that further functional forms can easily be included at a later date, if required. The functional forms initially implemented are:

1 van Genuchten (**van Genuchten, 1980**);
2 tabulated functions;
3 exponential; and
4 Averjanov/tabulated (**Averjanov (1950)** for hydraulic conductivity; tabulated function for the soil characteristic).

Option 4 is included for consistency with SHETRAN V3. In each case, the functions are converted to internal look-up tables at the start of a simulation, which are subsequently used in the numerical computations.

5.4.2 Soil characteristic function

1 *van Genuchten*

The van Genuchten representation of the soil characteristic function, $\theta(\psi)$, is given by (**van Genuchten, 1980**)

$$\theta = \theta_r + \frac{(\theta_s - \theta_r)}{\left[1 + (\alpha |\psi|)^n\right]^m} \qquad (5.6)$$

where $m = 1 - 1/n$. This is converted to a look-up table by evaluating the function for each pre-defined value of ψ in the table.

2 *Tabulated functions*

This input data option for the soil characteristic function requires sufficient pairs of θ-ψ values to define the function. These values are then interpolated using cubic splines (**Press et al., 1992**), and values for the internal look-up table are evaluated using the spline functions.

3 *Exponential*

The exponential representation of the soil characteristic function, $\theta(\psi)$, is given by

$$\theta = \theta_r + (\theta_s - \theta_r)\, e^{\alpha\psi} \quad . \tag{5.7}$$

This is converted to a look-up table by evaluating the function for each ψ value in the table.

4 *Averjanov/tabulated*

The soil characteristic function for this input data option is evaluated in exactly the same way as for option 2.

5.4.3 Hydraulic conductivity function

1 *van Genuchten*

The van Genuchten representation of the hydraulic conductivity function, $K(\psi)$, is given by (**van Genuchten, 1980**)

$$K = K_s \Theta^{0.5}\left[1 - (1 - \theta^{1/m})^m\right]^n \tag{5.8}$$

where $\Theta = (\theta - \theta_r)/(\theta_s - \theta_r)$. This is converted to a look-up table by evaluating the function for each value of ψ in the table, using the previously established $\theta(\psi)$ relationship.

2 *Tabulated functions*

The hydraulic conductivity function for this input data option is evaluated in exactly the same way as for soil characteristic function option 2.

3 *Exponential*

The exponential representation of the hydraulic conductivity function, $K(\psi)$, is given by

$$K = K_s e^{\alpha\psi} \quad . \tag{5.9}$$

This is converted to a look-up table by evaluating the function for each ψ value in the table.

4 *Averjanov/tabulated*

The Averjanov representation of the hydraulic conductivity function, $K(\theta)$, is given by **(Averjanov, 1950)**

$$K = K_s \Theta^n \tag{5.10}$$

where $\Theta = (\theta - \theta_r)/(\theta_s - \theta_r)$. This is converted to a look-up table by evaluating the function for each value of ψ in the table, using the previously established $\theta(\psi)$ relationship.

5.4.4 Storage coefficient

There are two terms in the storage coefficient, relating to the compressibility of the aquifer in the saturated zone, and to the gradient of the soil characteristic in the unsaturated zone. Each time the storage coefficient has to be evaluated (within the iteration scheme for each column), each term is calculated for each cell, noting that the gradient of the soil characteristic is zero in the saturated zone. For the case of a partially saturated cell, however, the definition of a storage term is more difficult. For example, if the calculation node (at the mid-point of the cell) is at a positive pressure, the gradient of the soil characteristic (which defines the rate of drainage of pore space for unconfined aquifers) associated with that pressure is zero; whereas, taken over the whole depth of the cell, a non-zero gradient would be more appropriate.

The approach taken, therefore, is to define a storage coefficient for conditions in the capillary fringe as a representative value over a depth comparable with the typical depth of a computational cell. The storage coefficient for a cell is then

$$\overline{\eta}_i = \frac{1}{\Delta z'} \int_{z_i - 0.5\Delta z'}^{z_i + 0.5\Delta z'} \eta(\psi_i + z)dz \qquad (5.11)$$

where $\Delta z'$ is a distance representative of a typical cell depth. This approach of using a representative cell depth rather than the actual cell depth is used to permit the capillary fringe storage coefficients to be evaluated at the start of a simulation, without introducing the computational overhead of recalculating the value for the storage coefficient at each timestep of a simulation.

5.5 Numerical solution algorithms

5.5.1 Basic flow equation for a single cell

For cell *i* of a column element, with volume $V_i = \Delta x_i \Delta y_i \Delta z_i$, a finite-difference analogue for Eq. 4.2 can be developed by writing the equation in terms of the flows into a cell as

$$V_i \eta_i \frac{\partial \psi_i}{\partial t} = \sum_{j=1}^{4} Q_{i,j} + A_0(Q_{i+} + Q_{i-}) + V_i q_i \qquad (5.12)$$

where $Q_{i,j}$ is the lateral flow rate into face *j* of cell *i*, and Q_{i+} and Q_{i-} are the vertical flow rates into the top and bottom of cell *i* respectively.

Recognising the large difference in spatial scales between the vertical and the lateral discretisation for most catchments, it is convenient to treat the vertical and lateral spatial derivatives separately. This separate treatment forms part of the basis for the numerical solution algorithms.

5.5.2 Time derivative

The left-hand side of Eq. 5.12 can be approximated by a two-level finite-difference expression for cell *i* as

$$V_i \eta_i \frac{\partial \psi_i}{\partial t} \approx V_i \eta_i^{n+1} \frac{\psi_i^{n+1} - \psi_i^n}{\Delta t} \tag{5.13}$$

where the superscripts denote time level.

5.5.3 Vertical flows into a cell

The terms describing vertical flows into cell *i* in Eq. 5.12 can be related to hydraulic heads, and therefore to pressure potentials, using the Darcy equation as follows:

$$\begin{aligned} Q_{i+} &= \beta_{z+,i}((z+\psi)_{i+1} - (z+\psi)_i) \\ Q_{i-} &= \beta_{z-,i}((z+\psi)_{i-1} - (z+\psi)_i) \end{aligned} \tag{5.14}$$

where the vertical conductances are calculated using either the *w*-mean (Eq. 5.5, which includes the arithmetic, geometric, and harmonic means as special cases)

$$\begin{aligned} \beta_{z+,i} &= \frac{2A_0}{(\Delta z_i + \Delta z_{i+1})} \langle K_{z,i+1} , K_{z,i} \rangle_w \\ \beta_{z-,i} &= \frac{2A_0}{(\Delta z_i + \Delta z_{i-1})} \langle K_{z,i-1} , K_{z,i} \rangle_w \end{aligned} \tag{5.15}$$

or the weighted harmonic mean (Eq. 5.4)

$$\begin{aligned} \beta_{z+,i} &= 2 \langle K_{z,i+1}, A_0, \Delta z_{i+1} , K_{z,i}, A_0, \Delta z_i \rangle_{wh} \\ \beta_{z-,i} &= 2 \langle K_{z,i-1}, A_0, \Delta z_{i-1} , K_{z,i}, A_0, \Delta z_i \rangle_{wh} \end{aligned} \tag{5.16}$$

and where

$$K_{z,i} = K_{z,i}^s k_{r,i} \tag{5.17}$$

Note that in Eqs. 5.15 and 5.16 the distance between the computational node and the cell boundary is $\Delta z / 2$.

5.5.4 Lateral flows into a cell

The terms describing lateral flows into cell *i* in Eq. 5.12 can be related to hydraulic heads, and therefore to pressure potentials, using the Darcy equation. In general, each cell may be connected to either one or two adjacent cells on each face (Fig. 5.2). The flow into cell *i* through face *j* is then given by

$$\begin{aligned} Q_{i,j} = \; & \gamma^1_{i,j} \left[(z+\psi)_{k,j} - (z+\psi)_i \right] + \\ & \gamma^2_{i,j} \left[(z+\psi)_{(k+\delta kj),j} - (z+\psi)_i \right] \quad . \end{aligned} \tag{5.18}$$

The lateral conductances are given by

$$\gamma^1_{i,j} = \frac{1}{(\Delta L_j + \Delta L^1_j)} \langle K_{i,j} A'_{i,j} \, , \, K_{k,j} A'_{k,j} \rangle_w \tag{5.19}$$

and

$$\gamma^2_{i,j} = \begin{cases} 0 & \text{if } \delta_{k,j} = 0 \\ \dfrac{1}{(\Delta L_j + \Delta L^1_j)} \langle K_{i,j} A'_{i,j} \, , \, K_{(k+\delta kj),j} A_{(k+\delta kj),j} \rangle_w & \text{if } \delta_{k,j} \neq 0 \end{cases} \tag{5.20}$$

where the effective cross-sectional areas for flow are given by

$$A'_{i,j} = \begin{cases} A_{i,j} & \text{if } \delta_{k,j} = 0 \\ 0.5 \, A_{i,j} & \text{if } \delta_{k,j} \neq 0 \end{cases}$$

$$A'_{k,j} = \begin{cases} A_{k,j} & \text{if } \delta_{i,j} = 0 \\ 0.5 \, A_{k,j} & \text{if } \delta_{i,j} \neq 0 \end{cases} \tag{5.21}$$

and where

$$K_{i,j} = K_{i,j}^{s} k_{r,i} \text{ etc.} \quad . \tag{5.22}$$

In Eqs. 5.19 and 5.20 it is assumed that the cross-sectional area for flow into cell *i* is partitioned equally for the case where there are two connected adjacent cells in the current or the adjacent column. Subscripts *i,j* refer to the *j*th face of the current cell *i* ; subscripts *k,j* refer to a cell in an adjacent column connected to the *j*th face of the current cell *i* ; and

$\delta_{i,j}$ = 1 if both the *i*th and the (*i+1*)th cells of the current column are connected to cell *k* in the adjacent column on face *j*,

= -1 if both the *i*th and the (*i-1*)th cells of the current column are connected to cell *k* in the adjacent column on face *j*,

= 0 otherwise;

$\delta_{k,j}$ = 1 if both the *k*th and the (*k+1*)th cells of the adjacent column are connected to cell *i* in the current column on face *j*,

= -1 if both the *k*th and the (*k-1*)th cells of the adjacent column are connected to cell *i* in the current column on face *j*,

= 0 otherwise.

For clarity, where $\delta_{i,j}$ and $\delta_{k,j}$ are used in subscripts, they are written as δij and δkj. Note that $\delta_{i,j}$ and $\delta_{k,j}$ are mutually exclusive (ie. $\delta_{i,j} \neq 0 \Rightarrow \delta_{k,j} = 0$; $\delta_{k,j} \neq 0 \Rightarrow \delta_{i,j} = 0$); and neighbouring cells in the same column with non-zero values of $\delta_{i,j}$ or $\delta_{k,j}$ occur in pairs (eg. $\delta_{i-1,j} = 1 \Leftrightarrow \delta_{i,j} = -1$).

The cross-sectional area perpendicular to the direction of flow, $A_{i,j}$, is given by

$$A_{i,j} = W_j \, \Delta z_i \cos\phi \tag{5.23}$$

where W_j is the width of face *j* of the element, and φ is the angle between the line joining the nodes of adjacent cells and the horizontal (Fig. 5.2).

5.5.5 Finite difference equation for a single cell

Eqs. 5.13 to 5.23 can be substituted into the basic cell equation (Eq. 5.12) to give a non-linear algebraic equation in terms of ψ. Introducing a time-weighting factor σ, and rearranging the equation, yields

$$f(\psi) = 0 \tag{5.24}$$

where

$$\begin{aligned} f(\psi) \equiv\ & \sigma\, \beta_{z-i}\, \psi_{i-1}^{n+1} \\ & -(\sigma F_i + G_i)\, \psi_i^{n+1} \\ & +\sigma\, \beta_{z+i}\, \psi_{i+1}^{n+1} \\ & +(1-\sigma)\, \beta_{z-i}\, \psi_{i-1}^{n} \\ & -\left((1-\sigma)\, F_i - G_i\right)\psi_i^{n} \\ & +(1-\sigma)\, \beta_{z+i}\, \psi_{i+1}^{n} \\ & +\sigma \sum_{j=1}^{4} \left[\psi_{kj}^{n+1}\, \gamma_{ij}^{1} + \psi_{(k+\delta kj),j}^{n+1}\, \gamma_{ij}^{2}\right] \\ & +(1-\sigma) \sum_{j=1}^{4} \left[\psi_{kj}^{n}\, \gamma_{ij}^{1} + \psi_{(k+\delta kj),j}^{n}\, \gamma_{ij}^{2}\right] \\ & +\beta_{z-i}\, z_{i-1} \\ & +\beta_{z+i}\, z_{i+1} \\ & -F_i\, z_i \\ & +\sum_{j=1}^{4} \left[z_{kj}\, \gamma_{ij}^{1} + z_{(k+\delta kj),j}\, \gamma_{ij}^{2}\right] \\ & +V_i\, q_i \end{aligned} \tag{5.25}$$

and

$$\begin{aligned} F_i &= (\beta_{z+i} + \beta_{z-i}) + \sum_{j=1}^{4} \left[\gamma_{ij}^{1} + \gamma_{ij}^{2}\right] \\ G_i &= \frac{V_i \eta_i^{n+1}}{\Delta t} \quad . \end{aligned} \tag{5.26}$$

Definitions for $\beta_{z+,i}$, $\beta_{z-,i}$, $\gamma_{i,j}^{1}$, $\gamma_{i,j}^{2}$, $\delta_{i,j}$, and $\delta_{k,j}$ are given earlier in this section.

The coefficients have the following dependencies on ψ:

$$\begin{aligned} &\beta_{z+i} \quad (\psi_i \, , \, \psi_{i+1}) \\ &\beta_{z-i} \quad (\psi_i \, , \, \psi_{i-1}) \\ &F_i \quad (\psi_i \, , \, \psi_{i+1} \, , \, \psi_{i-1} \, , \, \psi_k \, , \, \psi_{k\pm1}) \\ &G_i \quad (\psi_i) \\ &\gamma_{i,j}^{1} \quad (\psi_i \, , \, \psi_k) \\ &\gamma_{i,j}^{2} \quad (\psi_i \, , \, \psi_{k\pm1}) \end{aligned} \tag{5.27}$$

where $\psi_{k\pm1}$ denotes either ψ_{k+1} or ψ_{k-1} depending upon the value of $\delta_{k,j}$.

The time-weighting factor, σ, can take values from zero to one, a value of zero corresponding to an explicit scheme, a value of one corresponding to a fully implicit scheme, and a value of 0.5 corresponding to the Crank-Nicholson scheme (**Press et al., 1992**). The Crank-Nicholson scheme is theoretically the most accurate ($O(\Delta t^2)$ rather than $O(\Delta t)$), but can produce oscillatory solutions for large timesteps. In all of the simulations reported in this thesis, a value of σ=1 (fully implicit) has been used.

5.5.6 Solution algorithm for a column

Eq. 5.24 is a non-linear equation in ψ (the coefficients are functions of the dependent variable). For a column iteration, all variables (and dependent physical coefficients) from adjacent columns in Eq. 5.24 are taken to be independent of the column variables at iteration level *m+1*. The non-linearities are thereby restricted to only the column cells; the reduced Eq. 5.24 can be solved using a Newton iteration scheme (described in **Murphy et al., 1988** and **Woodford, 1992**), which can be written as

$$f'(\underline{\psi}^{n+1,m})\Delta\underline{\psi}^{n+1,m+1} + f(\underline{\psi}^{n+1,m}) = 0 \tag{5.28}$$

where

$$\Delta\underline{\Psi}^{n+1,m+1} \equiv \underline{\Psi}^{n+1,m+1} - \underline{\Psi}^{n+1,m} \quad . \tag{5.29}$$

This can be written

$$A_i \, \Delta\psi_{i-1}^{n+1,m+1} + B_i \, \Delta\psi_i^{n+1,m+1} + C_i \, \Delta\psi_{i+1}^{n+1,m+1} = R_i \tag{5.30}$$

where

$$\begin{aligned} A_i &= \frac{\partial f}{\partial \psi_{i-1}} \\ B_i &= \frac{\partial f}{\partial \psi_i} \\ C_i &= \frac{\partial f}{\partial \psi_{i+1}} \\ R_i &= -f\,(\psi_i^{n+1,m}) \quad . \end{aligned} \tag{5.31}$$

Since all variables (and dependent physical coefficients) from adjacent columns are taken to be independent of the column variables, there are no functional dependencies on ψ_k or $\psi_{k\pm1}$ at iteration level $m+1$ in Eq. 5.30. The derivative terms in Eq. 5.31 are given in full in Appendix B.

Eq. 5.30 is solved using the Thomas algorithm, a standard direct solution method for tri-diagonal linear systems (**Press et al., 1992**).

5.5.7 Overall solution algorithm

The overall solution algorithm used in the VSS model consists of Newton-Raphson iteration, with an inner iteration for each one-dimensional column embedded within an outer iteration over all columns. The inner iteration treats non-linearities in the Richards equation for vertical flows; the most severe non-linearities which require accurate treatment are often likely to occur for vertical flows, during infiltration events, for example, or near interfaces between dissimilar porous media (the finite-difference mesh is constructed so that such interfaces are mostly for vertical flows). The outer iteration treats lateral flows. An adaptive convergence algorithm is introduced to reduce computational effort for those cases where convergence is

most difficult only for localised regions of the catchment (the experience gained with the VSS model to date indicates that such localised regions do often occur, for example near to springs where rapid changes in vertical flow rates can be generated).

Following extensive checks for global and local mass balance in preliminary VSS simulations, it was found that mass was generally conserved well (to within a fraction of a percent), except for some occasions when the small computational cells in link and bank columns near to stream channels showed some errors (at most a few percent). In these cases the cells were fully saturated, and large flows (in terms of cell volumes) moved through the cells. The errors were corrected for these cells only, by adjusting lateral flows towards the stream channel to ensure mass conservation in the link and bank cells.

The overall solution algorithm for each timestep can be summarised as follows.

[1] Repeat until globally converged (outer iteration):
- [2] Loop over all columns:
  - [3] For each column:
  - [4] Check if already converged (adaptive convergence algorithm)
  - [5] Update coefficients for adjacent columns (lateral flow approximation)
  - [6] Repeat until locally converged (inner iteration):
    - [7] Update coefficients for column
    - [8] Solve column equation using tri-diagonal solver
  - [9] Calculate auxiliary variables

[10] Check and adjust for mass balance

5.5.8 Adaptive convergence algorithm

During the outer iteration ([1] in the outline algorithm above), the criterion for convergence is that the difference in values of pressure potential, $\Delta\psi_o$, between two outer iteration calculations must be less than a specified value, ε_o , for all cells in all columns.

A minimum of two outer iterations are made for all columns. For subsequent outer iterations, the adaptive convergence algorithm is introduced ([4] in the outline algorithm above). For each column, a check is made on the column and each of its neighbours (maximum of five columns in all). If $\Delta\psi_o$ is less than ε_o for all of the cells in all of these columns, it can be

assumed that further iterations would not significantly change the lateral flows, and the column is not included in the next outer iteration loop. Otherwise, if $\Delta\psi_O$ is greater than ε_O for the column or any of its neighbours, further iterations may change the lateral flows, and the column is included in the next outer iteration loop.

During the inner iteration ([6] in the outline algorithm above), the criterion for convergence is that the difference in values of pressure potential, $\Delta\psi_I$, between two inner iteration calculations must be less than a specified value, ε_I , for all cells in a column.

The adaptive convergence algorithm is designed to ensure that computational effort is directed to where it is most needed. The idea is based upon methods used in the parallel processing literature, which in turn can be traced back to pioneering work into numerical methods for weather forecasting before the days of digital computers (**Richardson, 1922**). In his remarkable book[1], Richardson described the vision of a large team of people in a hall each working on separate calculations, with a 'conductor' controlling the rates of calculation by directing beams of red or blue light upon individuals in different areas of the hall representing spatial areas of the computational domain..

5.6 Boundary conditions

5.6.1 General comments

SHETRAN was originally designed to include several interacting components, with differing degrees of interaction between components depending upon the corresponding physical interactions. The interfaces were based on explicit (or external) coupling, where each component supplies head or flux variables to the subsequent components at each timestep, and there is no feedback between components. The alternative approach (internal coupling) usually involves iteration between components, until some error norm is minimised to within a specified tolerance. However, this is computationally very expensive.

---

[1]In addition to deriving the equations for atmospheric motion, and solving the finite-difference equations by hand on 'a heap of hay in a cold rest billet' near the front line in World War 1, Richardson also presented the mixed form of Richards equation for water flow through unsaturated soil, discussed methods for measuring the soil characteristic functions, and noted the need to consider macropore flow.

The introduction of the new VSS component into SHETRAN resolves some of the interface problems, by treating the whole of the subsurface region within a single implicit solver. However, external coupling is still used for interfaces at the ground surface, at the stream channel, and within the root zone, between the VSS component and the two other central SHETRAN components (the evapotranspiration, or ET, component, and the overland/channel, or OC, component). Potential problems may arise in the coupling where there is inappropriate feedback between the rate of extraction of water and the available water in a computational element (especially when the water storage in an element is small). For the integration of the VSS model as a component of SHETRAN, it has been assumed that appropriate feedback is included within the ET and OC components.

A general structure is used for all of the types of boundary conditions in the VSS component. Source/sink terms (for example, $Q_{i,j}^{sai}$) are added into the term $V_i q_i$ in the cell balance equation (Eq. 5.12) and equivalently in the function $f(\psi)$ (Eq. 5.25) and subtracted from R_i in Eq. 5.31. Head boundary conditions are defined at the edges or top or bottom surfaces of computational cells; flows are calculated based upon the difference between prescribed head at the boundary and head at the node, and are similarly subtracted from the term R_i in Eq. 5.31. Derivatives of boundary flows with respect to potential (for example, $dQ_{i,j}^{sai}/ d\psi_i$) are calculated in each case; these are added to B_i in Eq. 5.31.

5.6.2 Stream-aquifer interaction

There are two cases for which stream-aquifer interaction is modelled using VSS:

1 with bank elements included;

2 without bank elements included.

For case 1, the distance between computational nodes in the bank element column and the stream channel is assumed to be comparable to the depth of the aquifer; vertical components of flow are then modelled between the column cells. For case 2, the distance between computational nodes in the adjacent element and the stream channel is assumed to be large relative to the depth of the aquifer; under these circumstances the vertical flow components induced by the presence of the stream channel cannot be resolved at the scale of the model discretisation, and flows between the computational nodes and the stream channel are assumed to be sub-horizontal.

For case 1, stream-aquifer flows occur only for computational cells above the stream channel bed (vertical flows through the stream channel bed are calculated as the upper boundary condition for the link element). For case 2, it is assumed that all computational cells in the adjacent column are hydraulically connected to the stream channel (in effect, it is assumed that the channel can be considered to be fully penetrating at the modelled scale). In both cases, a head boundary condition is prescribed at the boundary with the stream channel, the head being defined by the stream water elevation, z_s. The flow into each aquifer cell i through face j from the stream channel is then given by

$$Q_{i,j}^{sai} = \frac{K_{i,j} A_{i,j}}{\Delta L_j} (z_s - (z_i + \psi_i)) \tag{5.32}$$

and the derivative of $Q_{i,j}^{sai}$ w.r.t. ψ_i is given by

$$\frac{\partial Q_{i,j}^{sai}}{\partial \psi_i} = \frac{A_{i,j}}{\Delta L_j} \left[(z_s - (z_i + \psi_i)) \frac{\partial K_{i,j}}{\partial \psi_i} - K_{i,j} \right] . \tag{5.33}$$

The total flow between the channel and the aquifer is then the sum of the flows through the channel sides (given by Eq. 5.32) for all cells above the channel bed plus the flows through the channel bed (for case 1), or the sum of the flows for all cells in the column through the face adjacent to the channel (for case 2).

5.6.3 Ground surface boundary conditions

For the top cell in an element, the boundary condition used depends upon the available water during a timestep (ponded water plus accumulated precipitation and snowmelt), the rate of evaporation at the soil surface, the pressure potential in the top cell, and the maximum possible rate of flow into or out of the cell (limited by the value for hydraulic conductivity).

Evaporation from surface soil is calculated (in the ET component of SHETRAN) in two ways, depending upon whether surface water exists at the start of a timestep. If surface water does not exist ($d_w = 0$), actual soil evaporation, e_s , is calculated as a function of pressure potential. If surface water does exist ($d_w > 0$), evaporation is assumed to occur at the potential rate from the surface water; if the total amount of evaporation over the timestep exceeds the amount of surface water, the net amount of evaporation occurs from the soil surface, limited by pressure potential.

The calculation sequence for the top cell (i = 'top') is as follows.

1 Calculate maximum possible rate of flow into the top cell from externally prescribed flows and water depths (positive for precipitation and ponded water, negative for evaporation):

$$q_1 = d_w/\Delta t + q_p - e_w \quad . \tag{5.34}$$

2 Calculate the maximum possible rate of flow out of the top cell as a function of soil hydraulic properties and pressure potential in the top cell at the current iteration, based on vertical Darcy flow between the computational node and the upper boundary of the top cell (assuming that the pressure at the ground surface is either atmospheric, or equal to the depth of ponded water plus accumulated net precipitation):

$$q_2 = \frac{K_z}{0.5\Delta z_{top}}(\psi_{top} - (\max(0,\ d_w + (q_p - e_w)\Delta t) + 0.5\Delta z_{top})) \quad . \tag{5.35}$$

3 Calculate the actual flow through the ground surface, q_{inf} , and the derivative of q_{inf} w.r.t. ψ_{top}, depending on the values of q_1 and q_2 for the following cases:

Case 1

$q_1 < -q_2$ (net evaporation, no exfiltration) or (net precipitation or ponding, limited by available water)

$$\begin{aligned} q_{inf} &= -q_1 \\ \frac{\partial q_{inf}}{\partial \psi_{top}} &= 0 \end{aligned} \quad . \tag{5.36}$$

Case 2

$q_1 \geq -q_2$ (net evaporation, exfiltration) or (net precipitation or ponding, limited by soil properties; including exfiltration)

$$\begin{aligned} q_{inf} &= q_2 \\ \frac{\partial q_{inf}}{\partial \psi_{top}} &= \frac{K_z}{0.5\Delta z_{top}} \end{aligned} \quad . \tag{5.37}$$

5.6.4 Plant transpiration

The rate of water loss due to plant transpiration, $A_0 q_t$, is subtracted from the source/sink term, $V_i q_i$, in eq. 5.12. For each timestep, the transpiration rate is calculated (in the ET component of SHETRAN) as a function of the pressure potential at the start of the timestep in each of the cells containing plant roots. There is no feedback during a timestep between the pressure potential and the rate of abstraction from a cell.

5.6.5 Well abstraction

For a well, the prescribed abstraction rate is assumed to be for the entire well depth, and the rate of flow from each computational cell intersected by the well screen is given by Eq. 4.12. If any cell becomes partially or entirely unsaturated during abstraction, the rate of flow from the cell is reduced according to the fraction of the cell which is saturated, and the total actual abstraction rate is reduced. If the water table falls below the bottom of the well screen, the actual abstraction rate is reduced to zero.

5.6.6 Springs

The discharge from a spring is proportional to the difference between the head in the computational cell from which discharge occurs and the elevation of the spring discharge point (Eq. 4.13). To allow for a smooth transition from saturated to partially saturated conditions (to avoid possible spurious numerical oscillations), the relative conductivity is introduced into the relationship, so the term representing spring discharge (defined as positive into the computational cell *i*) is given by

$$q^{sp} = C_s k_{r,i} (z_{sp} - (z_i + \psi_i)) \tag{5.38}$$

and the derivative of q^{sp} w.r.t. ψ_i is given by

$$\frac{\partial q^{sp}}{\partial \psi_i} = C_s \left[(z_{sp} - (z_i + \psi_i)) \frac{\partial k_{r,i}}{\partial \psi_i} - k_{r,i} \right] . \tag{5.39}$$

5.6.7 Bottom boundary conditions

The source/sink term, q_b , for the bottom cell (i = 'b') of a column can be calculated based on a prescribed flow rate, or a prescribed head.

For a prescribed flow boundary condition, the value of q_b is used directly, and the derivative of q_b w.r.t. ψ_b is zero (the flow rate at the boundary is independent of the pressure potential at the computational node).

For a prescribed head boundary condition, q_b is given by

$$q_b = \frac{2K_{z,b}}{\Delta z_b}(h_b - (z_b + \psi_b)) \tag{5.40}$$

and the derivative of q_b w.r.t. ψ_b is given by

$$\frac{\partial q_b}{\partial \psi_b} = \frac{2}{\Delta z_b}\left(\frac{\partial K_{z,b}}{\partial \psi_b}(h_b - (z_b + \psi_b)) - K_{z,b}\right) \quad . \tag{5.41}$$

5.6.8 Lateral boundary conditions

A flow boundary condition can be prescribed for any boundary element, either for the whole aquifer depth, or separate flow rates can be given for each distinct layer. For each computational cell i where a flow boundary condition is prescribed, the flow rate through the boundary face j, $Q_{i,j}$, is equal to the prescribed flow rate at the boundary, q_l multiplied by the cross-sectional area perpendicular to the direction of flow, $A_{i,j}$, and the derivative of $Q_{i,j}$ w.r.t. ψ_i is zero (the flow through the boundary is independent of the pressure potential at the computational node).

A head boundary condition can be prescribed for any boundary element, either for the whole aquifer depth, or separate heads can be given for each distinct layer. For each computational cell i where a head boundary condition is prescribed, the flow rate through the boundary face j, $Q_{i,j}$, is given by

$$Q_{i,j} = \frac{K_{i,j} A_{i,j}}{\Delta L_j} (h_l - z_i + \psi_i)) \tag{5.42}$$

and the derivative of $Q_{i,j}$ w.r.t. ψ_i is given by

$$\frac{\partial Q_{i,j}}{\partial \psi_i} = \frac{A_{i,j}}{\Delta L_j} \left(\frac{\partial K_{i,j}}{\partial \psi_i} (h_l - (z_i + \psi_i)) - K_{i,j} \right) . \tag{5.43}$$

5.7 Coupling with the contaminant component

5.7.1 General comments

The contaminant transport (CM) component of SHETRAN (**Ewen, 1995**) was developed as part of SHETRAN V3, and is consistent with the flow components of this previous version of SHETRAN. The CM component has been extensively tested, both as a component of SHETRAN, and independently of SHETRAN. In order to maintain continuity with these previous versions of the code, only the minimum possible modifications have been made to the CM component, and where possible the modifications have been made to the data interface between the VSS and CM components, rather than in the core CM calculation routines.

5.7.2 3D variably-saturated flow field

Two modifications have been made to the CM component to be consistent with the VSS component: the lateral transport of contaminants has been extended through the unsaturated zone to the ground surface; and the vertical and lateral flow rates calculated by the VSS component have been transferred to the CM component (previously, these flows were calculated within the CM component using some simplifying assumptions, **Ewen, 1995**).

5.7.3 Overlaps / interconnections

The interconnectivity matrix which forms the central basis for the spatial discretisation and calculations in the VSS component and which is designed to make best use of data on the geometry of aquifer units, can be related to the overlap system used in the contaminant component (**Ewen, 1991**) which did not necessarily relate similar adjacent aquifer units to each other.

The modifications made to the CM code were to set up the CM overlap variables using the VSS connectivity matrix during the initialisation phase of a simulation. No further modifications to the central calculation routines of the CM component were then necessary.

5.7.4 Vertical block-centred finite-differences

The change to a block-centred finite difference scheme in the vertical has been made so that the computational nodes are defined based on the locations of boundaries between soils or aquifer units. (In a mesh-centred finite difference scheme, such as that used in SHETRAN V3.4, the positions of the computational nodes are defined first; it is then often difficult to position the computational cell boundaries to coincide with the known positions of soil or aquifer unit boundaries.)

The modifications to the CM component were necessarily made at the core of the CM calculation routines, and involved a change in the calculation of mean inter-cell physical properties from an arithmetic mean to a weighted harmonic mean.

5.7.5 Stream-aquifer interactions

For simulations in which bank elements are used, two different methods of dicretisation of the subsurface are used in the CM and VSS components. In the CM component (as in the SHETRAN V3.4 water flow component), there are two bank elements associated with each stream link element, each being L-shaped in cross-section, with half of the soil or rock beneath the channel being assigned to each bank element. In the VSS component there are three subsurface elements associated with each stream link element: one stream element, and two bank elements, all of which are rectangular in cross section. Since the physical

definitions of each of these three elements are constrained to be consistent in SHETRAN V4.0 (ie. the two bank elements are identical, and the aquifer units are identical across the sub-channel parts of the elements), equivalent L-shaped bank elements can be defined, for use by the CM component.

The bulk flow rates through the channel bed and the channel faces are calculated by the VSS component (based on the summation of the individual cell flow rates), and are used by the CM component. Internal variables for the stream banks (soil moisture contents, flows) are made consistent between the two stream bank representations by simple mass balance accounting.

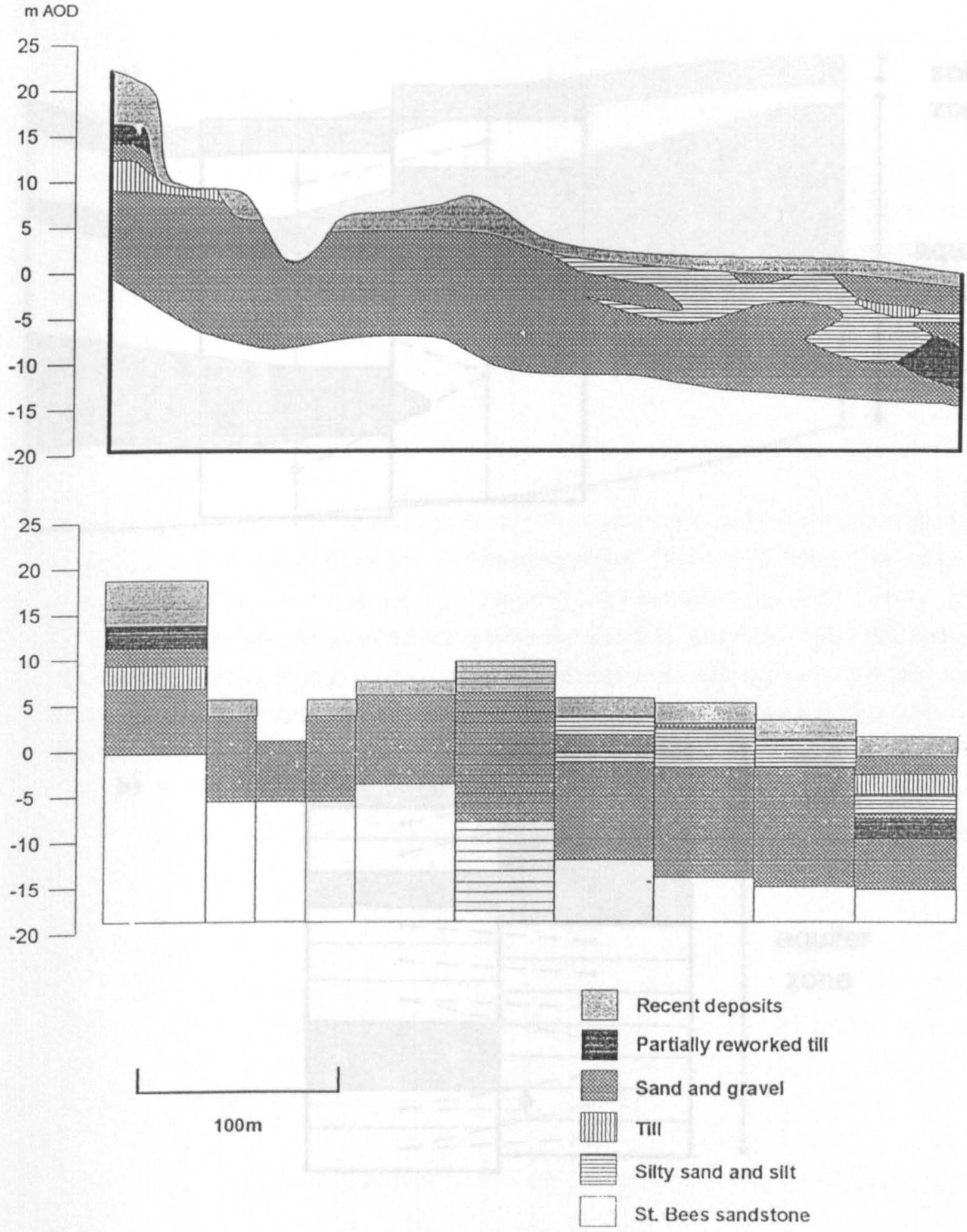

Figure 5.1 Typical complex drift lithology, and discretisation for VSS

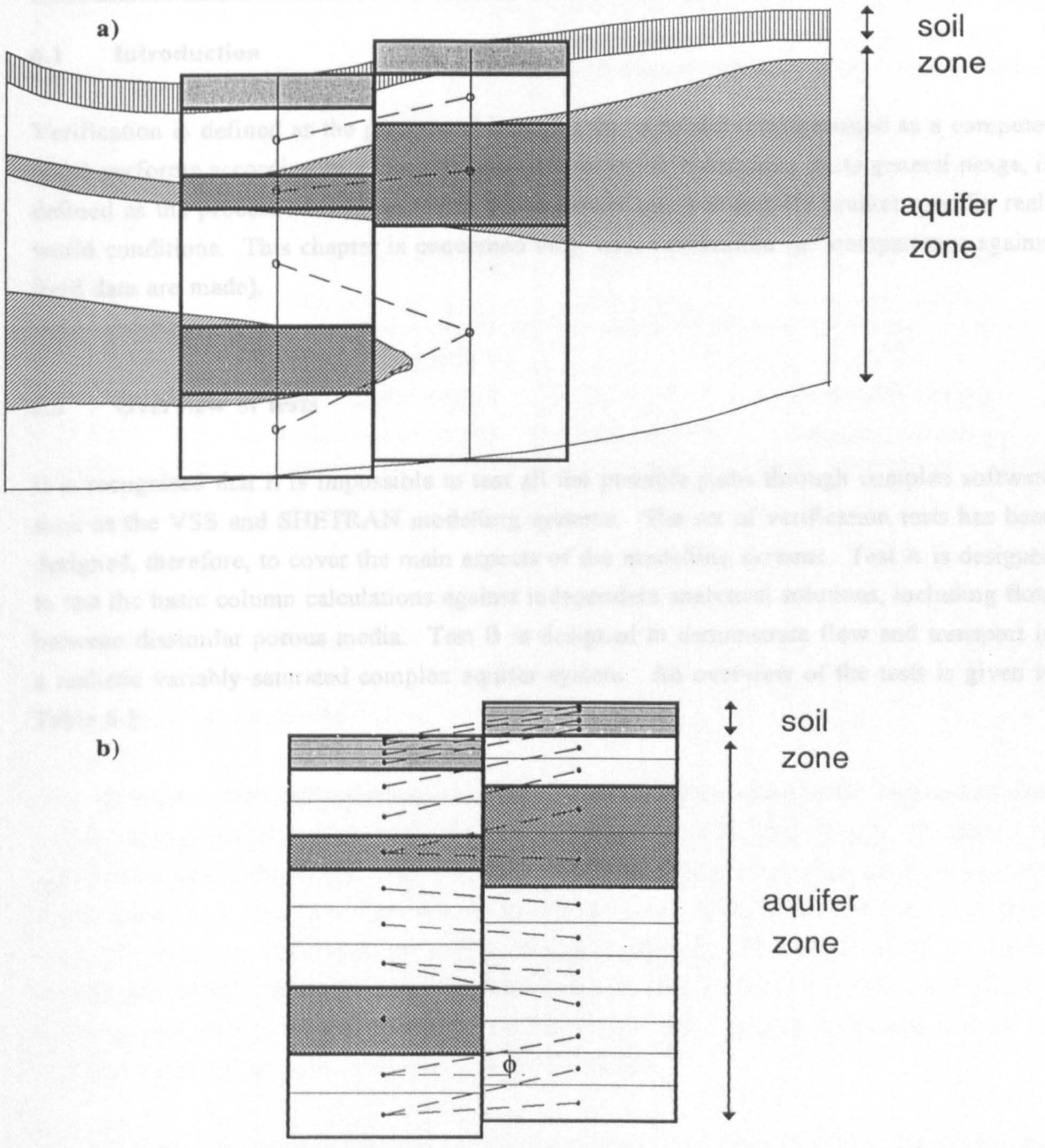

Figure 5.2 Discretisation scheme
a) Geological layering and connectivity
b) Computational cell definition and interconnections

CHAPTER 6 MODEL VERIFICATION

6.1 Introduction

Verification is defined as the process of ensuring that a model (implemented as a computer code) performs according to its specification. In contrast, validation, in its general usage, is defined as the process of demonstrating that a model can successfully predict specific real-world conditions. This chapter is concerned only with verification (no comparisons against field data are made).

6.2 Overview of tests

It is recognised that it is impossible to test all the possible paths through complex software such as the VSS and SHETRAN modelling systems. The set of verification tests has been designed, therefore, to cover the main aspects of the modelling systems. Test A is designed to test the basic column calculations against independent analytical solutions, including flow between dissimilar porous media. Test B is designed to demonstrate flow and transport in a realistic variably-saturated complex aquifer system. An overview of the tests is given in Table .6.1.

Test	Description	Flow/transport	Comparison against
Test A	1D column		
A1	Wetting, single soil	Flow only	Analytical solution
A2	Drainage, single soil	Flow only	Analytical solution
A3	Wetting, sand over silt	Flow only	Analytical solution
A4	Drainage, sand over silt	Flow only	Analytical solution
A5	Wetting, silt over sand	Flow only	Analytical solution
Test B	2D complex aquifer		
B1	Realistic aquifer system	Flow only	Physical reasoning
B2	Realistic aquifer system	Flow/transport	Physical reasoning

Table 6.1 Overview of VSS verification tests

6.3 Test A: 1D Column Tests

6.3.1 General comments

The 1D column tests use analytical solutions to the Richards equation for unsaturated flow under wetting and drainage conditions for homogeneous and layered soils, developed by **Srivastava and Yeh (1991)**. The analytical solutions represent transient pressure potential distributions in a vertical soil profile above a fixed water table, illustrated schematically in Fig. 6.1. Cases are considered for both wetting and drainage. The initial conditions are the steady-state profiles for constant infiltration at a rate of 0.1 cm/hour (wetting case) or 0.9 cm/hour (drainage case). At time t=0, the infiltration rate increases instantaneously to 0.9 cm/hour (wetting) or reduces to 0.1 cm/hour (drainage).

The hydraulic properties of the soils used in the examples are described using the exponential functional forms

$$K = K_s e^{\alpha \psi} \tag{6.1}$$

and

$$\theta = \theta_r + (\theta_s - \theta_r)\, e^{\alpha\psi} \qquad (6.2)$$

where ψ is negative in the unsaturated region above the water table (Fig. 6.2). The use of the exponential functional form for the soil hydraulic functions was chosen by **Srivastava and Yeh (1991)** since the Richards equation then reduces to a linear form, which can be solved analytically using Laplace transform techniques for certain initial and boundary conditions. It is recognised that these functions cannot be used to represent the hydraulic properties of many real soils accurately; however, they are useful for demonstrating the accuracy of numerical solutions to the Richards equation. The analytical solutions for each test case were evaluated using a FORTRAN program supplied by Prof. Yeh of the University of Tucson, Arizona, USA.

For all cases other than the second part of test A1, the value of α used is 0.1 cm^{-1}. Several further examples were given in **Srivastava and Yeh (1991)** using a value for α of 0.01 cm^{-1}; however, the examples used here have sharper wetting and drying fronts, and are a more severe test of the model.

The parameters used in the tests are given in Table 6.2; the soils used in each test are given in Table 6.3. The names given to the soils are used for convenience only, and are not intended to relate to any specific field soils.

Soil name	K_s (cm/hour)	α (cm^{-1})	θ_s	θ_r
Silt 1	1.0	0.1	0.4	0.06
Silt 2	1.0	0.01	0.45	0.2
Sand	10.0	0.1	0.4	0.06

Table 6.2 Soil hydraulic property parameter values for test A

Test	Soil (upper/lower)
A1 (α=0.1)	Silt 1
A1 (α=0.01)	Silt 2
A2	Silt 1
A3	Sand / Silt 1
A4	Sand / Silt 1
A5	Silt 1 / Sand

Table 6.3 Soils used in test A

For all of the cases other than the second part of test A5, a uniform cell size of 5 cm was used, with a timestep of 0.1 hours. The use of a fine resolution spatial grid and a small timestep is intended to show that the numerical solutions are consistent with the exact solutions to the governing equation.

6.3.2 Test A1: Wetting, homogeneous soil

The simulated pressure profiles for infiltration into a homogeneous soil (test A1), and the corresponding analytical solutions to the Richards equation, are shown in Fig. 6.3 for α=0.1 cm^{-1}, and Fig. 6.4 for α=0.01 cm^{-1}. In both cases there is good agreement between the simulated profiles and the analytical profiles, with the better results being for the case with α=0.01 cm^{-1} (Fig. 6.4).

At early times after the onset of the increased infiltration rate in the first case (Fig. 6.3) a sharp infiltration front moves down the soil profile. Both the rate of movement and the shape of this front are simulated accurately. The most significant differences between the simulated and analytical curves occur near to saturation at the end of the simulation (for equilibrium flow through the soil column at the higher rate of infiltration).

All subsequent results for the soil column tests are for α=0.1 cm^{-1}.

6.3.3 Test A2: Drainage, homogeneous soil

The simulated pressure profiles for drainage in a homogeneous soil (test A2), and the corresponding analytical solutions to the Richards equation, are shown in Fig. 6.5. There is good agreement between the simulated profiles and the analytical profiles. Consistent with the results for test A1, the most significant differences between the simulated and analytical profiles were near to saturation for equilibrium conditions for the higher infiltration rate (at the start of this simulation).

6.3.4 Test A3: Wetting, heterogeneous soil (sand over silt)

The simulated pressure profiles for infiltration into a heterogeneous soil (test A3), and the corresponding analytical solutions to the Richards equation, are shown in Fig. 6.6. In the early part of the simulation, a wetting front moves down through the upper (sandy) soil, with little change in the lower (silty) soil. The simulated wetting front is slightly more diffused than the analytical solution. Once the wetting front reaches the interface between the two soils, the pressure at the interface increases rapidly and the wetting front propogates into the silty soil. The pressure profile in the lower soil, and the pressures at the interface between the two soils, show good agreement with the analytical solution.

6.3.5 Test A4: Drainage, heterogeneous soil (sand over silt)

The simulated pressure profiles for drainage in a heterogeneous soil (test A4), and the corresponding analytical solutions to the Richards equation, are shown in Fig. 6.7. Consistent with the earlier results, the most significant differences between the simulated profiles and the analytical solutions are for conditions close to saturation.

6.3.6 Test A5: Wetting, heterogeneous soil (silt over sand)

The simulated pressure profiles for infiltration into a heterogeneous soil (test A5), consisting of a low permeable soil over a high permeable soil, and the corresponding analytical solutions to the Richards equation, are shown in Fig. 6.8. There is good agreement between the simulated and analytical results in both soils and at the interface at all times in the simulation.

6.4 Test B: 2D Tests for a Complex Stream-Aquifer System

6.4.1 General comments

The 2D tests for a complex stream-aquifer system use data sets representing possible realistic cross-sections of the glacial tills of the Calder and Newmill Beck catchments in west Cumbria. The simulations use spatial discretisation and timesteps typical of those likely to be used in future simulation studies of similar environments.

The aim is to demonstrate that the SHETRAN modelling system, including the VSS model as a component, is capable of providing physically reasonable solutions to the flow and transport equations in the types of hydrogeological environments seen in the west Cumbrian shallow aquifers, including interbedded and pinched-out layers, perched water tables, and stream-aquifer interactions.

The line of the cross-section is located almost parallel to the west Cumbrian coastline, between OS grid references NY032058 and NY062028 (Fig. 6.9). There are 18 basic grid elements, each of length 250 metres. (Since the simulation is of a two-dimensional vertical slice, the width of the elements is arbitrary and does not affect the results.) Two surface water channels, the River Calder, and Newmill Beck, cross the line (Fig. 6.10); these are represented in the simulation using two bank elements and one stream link element for each channel, giving a total of 24 elements in the simulation. The low-lying region towards the south end of the line is in a headwater area within the Newmill Beck catchment. The surface soils are all brown earths (Wick 1 association). The vegetation consists of pasture and mixed woodland.

The line lies in an area of generally shallow drift deposits, and crosses a rock-drumlin, a feature created from basal ice-sheet material being deposited and streamlined over a rockhead high. In a study of the occurence of glacial deposits in west Cumbria, **Jamieson (1994)** described these types of feature (which are common along the west Cumbria coastal plain) as having the steep stoss slopes and shallower lee slopes typically associated with drumlins (the direction of ice movement was from the north end to the south end of the cross-section line), and being covered with sheet-like tills, in contrast to the lens-shaped tills found in low-lying areas. In the study, **Jamieson (1994)** investigated the occurence and distribution of clay bodies (which are significant for defining contaminant transport pathways), and concluded that

clays generally form isolated elongated bodies, rarely greater than 500m in length, although extensive bodies of lodgement till could exist which would form significant barriers to flow (it should be noted that the work was based on only a very sparse data set in the immediate Sellafield area).

The geometry of the lithologies for test B was generated using a stochastic interpolation scheme similar to that used by **Molz and Boman (1993)**. They defined a method for interpolating values of porosity and hydraulic conductivity using sparse data sets, based on the properties of fractional Brownian motion and fractional Gaussian noise, which preserves data irregularities over a range of spatial scales. The method is based upon knowledge of the variance of the data, and identification of a value for the 'Hurst coefficient', a parameter which controls the spatial correlation scales for the interpolated variable.

In this approach, it is assumed that data for at least two borehole logs are available or can be defined, each consisting of a sequence of lithologies of known thicknesses The method involves interpolation of the thicknesses using the recursive 'Successive Random Addition' (SRA) algorithm (**Molz and Boman, 1993**), taking each lithology in turn. (Lithogies for each borehole must be identical; a lithology can be assigned a zero thickness if it is not present in one or both boreholes.) The SRA algorithm consists of repeated bisection of the distance between the two boreholes until sufficient interpolated points have been calculated, applying the following calculation sequence at each stage:

1 for each interval, calculate the thickness at the mid-point by linear interpolation of the thicknesses at the end-points of the interval;

2 for each interpolated point (including both the points calculated at the previous stages, and the newly-interpolated points), add a random additional thickness, taken from a Gaussian distribution with a mean of zero, and a defined variance, σ (note that the additional thickness may be negative);

3 calculate a new (reduced) variance for the next stage of the recursion, $\sigma' = \sigma / 2^{2H}$, where H is the Hurst coefficient.

Three synthetic boreholes were constructed, designed to be consistent with the understanding of the drift stratigraphy along the cross-section line, and located at either end and in the centre of the cross-section. The sequence of deposits for each borehole was based on those used in earlier SHETRAN simulation studies for the area. The sequence was identical for each borehole, and consisted of:

brown earth A-horizon (K_s = 0.36 m/day);
brown earth B-horizon (K_s = 4.79 m/day);
brown earth C-horizon (K_s = 4.99 m/day);
upper sand (K_s = 0.66 m/day);
silty clay (K_s = 0.0001 m/day);
lower sand (K_s = 1.9 m/day);
sandstone (K_s = 3.0 m/day).

The thicknesses of the drift lithologies (the lower sand, silty clay, and upper sand) were generated by interpolating between these borehole logs, using standard deviations of thickness of 4 m. The standard deviations of thicknesses of the A-, B-, and C-horizons, and the high permeability sandstone, were zero. A Hurst coefficient of 0.8 was used for each of the sand layers; and a higher value for the coefficient of 0.9 was used for the silty clay, resulting in an elongated clay body being generated for these demonstration simulations.

The lithological cross-section generated using these synthetic data is shown in Fig. 6.11. The cross-section is generally consistent with the interpretation of **Jamieson (1994)** and with a shallow seismic cross-section from a recent geophysical survey of the area (reference UKN92-2D-15) which was aligned close to the test B cross-section. The drift deposits are less than 5 metres in total thickness near the centre of the high ground, with thicker deposits in the low -lying regions. The deposits consist of mostly sand, with the clay forming an isolated body.

The meteorological data used in the simulations consists of hourly precipitation (Fig. 6.12) and potential evapotranspiration (Fig. 6.13) data for a five year period, obtained from local meteorological stations.

At the base of the modelled region, a steady uniform upflow velocity of 3.0×10^{-9} m/s was prescribed to represent the contribution from the regional aquifer to the near-surface aquifer. The lateral boundaries were assumed to be impermeable. Fixed head boundary conditions were set for surface flows for both stream channels and for the 'headwater' area towards the right hand end of the cross-section; these allowed flow of water out of the model. The initial conditions were given as values of head for each computational cell, defined following a number of preliminary simulations (the initial conditions were roughly comparable to the final conditions from the simulation). The contaminant source was given as a fixed uniform concentration of unity across the bottom boundary of the modelled region, advected into the region with the regional aquifer upflow. The simulation was run for a period of five years.

In order to demonstrate the capabilities of SHETRAN V4 to simulate the abstraction of contaminated groundwater through a screened well, and the contamination of surface soils with abstracted water used for irrigation, an abstraction well was included, screened between 20 and 40 metres below ground (within the sandstone aquifer), and the abstracted water was used to irrigate the land near to the abstraction point (Fig. 6.10). The prescribed well abstraction rate was 50 l/s over the summer months (equivalent to a constant irrigation rate of approximately 3 mm/hour). Note that the well abstraction and irrigation are included for illustrative purposes only, and do not necessarily represent a realistic scenario.

6.4.2 Test B1: Flow

The actual rates of groundwater abstraction from the well are shown in Fig. 6.14. In the model, when the water table in the aquifer falls below the top of the well screen, the abstraction rate is reduced as the wetted portion of the well screen reduces; the actual abstraction rates are therefore less than the prescribed rate of 50 l/s. The response of the phreatic surface to the abstraction is shown in Fig. 6.15. During pumping, there is a drawdown of the water table of several metres; following the cessation of pumping each year, the water table recovers to near its original level.

A vertical cross-section of the pressure distribution and phreatic surface levels at the end of the simulation is shown in Fig. 6.16. (The phreatic surface levels are shown only for the regional aquifer, and are defined as the first points above the model base where the pressure potentials change sign.) The phreatic surface intersects the ground surface at the River Calder and at the headwater area towards the right-hand side of the cross-section, providing a direct hydraulic connection between the contaminated lower part of the aquifer and the ground surface. There is no direct hydraulic connection between the sandstone aquifer and Newmill Beck. In the centre of the cross-section, the drawdown in the aquifer as a result of the abstraction of groundwater through the well can clearly be seen. There is a region of higher potentials in the perched water table above the clay layer, which develops as a result of the irrigation using water abstracted from the well.

Below the clay layer (and in areas where the clay layer is absent) the potentials are close to equilibrium in the vertical (Fig. 6.17) due to the sandy and well drained nature of the porous media. Below the clay layer, where recharge rates are reduced, potentials fall to the lowest

values in this simulation. Above the clay layer, and in particular in that part of the cross-section where precipitation is supplemented by irrigation waters, a perched water table develops during the simulation. There are sharp gradients in the potentials at the boundaries between the clay layer and the Quaternary sands (Fig. 6.17). Lateral flows above the clay layer are generated (Fig. 6.18), some of which run towards the Newmill Beck, and sustain flows in the channel. In the sandstone aquifer, flows are in the opposite direction, towards the abstraction well.

6.4.3 Test B2: Transport

A vertical cross-section of contaminant concentrations at the end of the simulation is shown in Fig. 6.19. There is a general upward movement of contaminants from the contaminant source at the base of the modelled region, carried by the boundary condition flow. Contaminants reach the ground surface at the River Calder channel, where there is a localised convergence towards the channel through the bank elements, and at the headwater area where the phreatic surface intersects the ground surface.

There is no direct contaminant pathway from the contaminant source through the aquifer to Newmill Beck.

Contaminated water is abstracted from the well and used to irrigate land near the centre of the high ground of the cross-section. The contaminated water can be seen to infiltrate into the upper sandy horizon, and move both downwards and laterally along the perched aquifer towards and away from Newmill Beck. Some contaminant moves down through the silty-clay horizon into the main aquifer.

6.5 Conclusions

A set of verification tests for SHETRAN V4 have been completed successfully. The tests were designed to cover the main aspects of the new VSS component, including its effects on contaminant migration. The results demonstrate the abilities of SHETRAN V4 to solve the Richards equation accurately, and to simulate flow and transport under complex aquifer conditions. It is recognised that verification/validation of a modelling system is a continuous process; future validation exercises and applications will build upon these initial tests in demonstrating confidence in the modelling system.

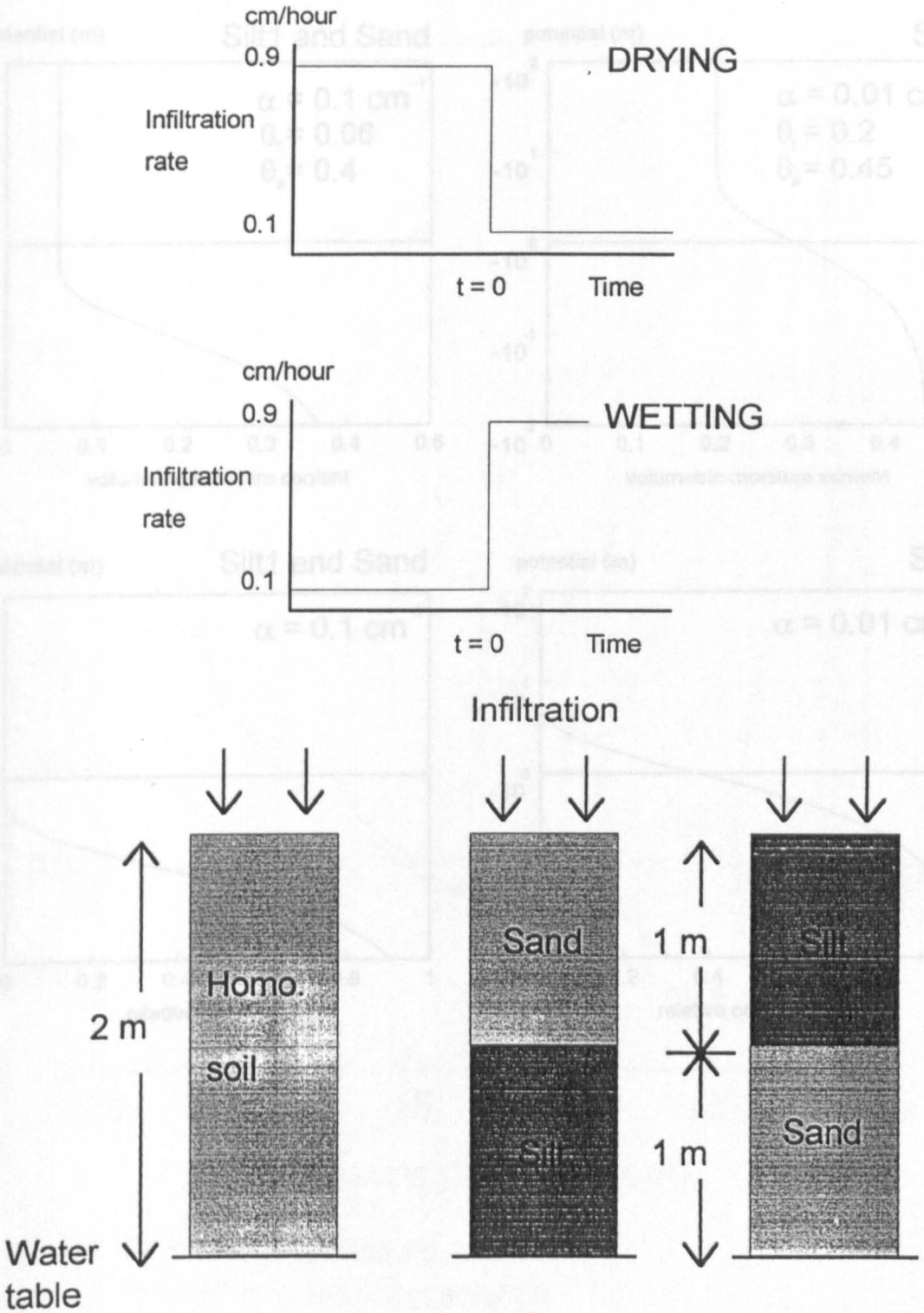

Figure 6.1 Test A: 1D column simulations

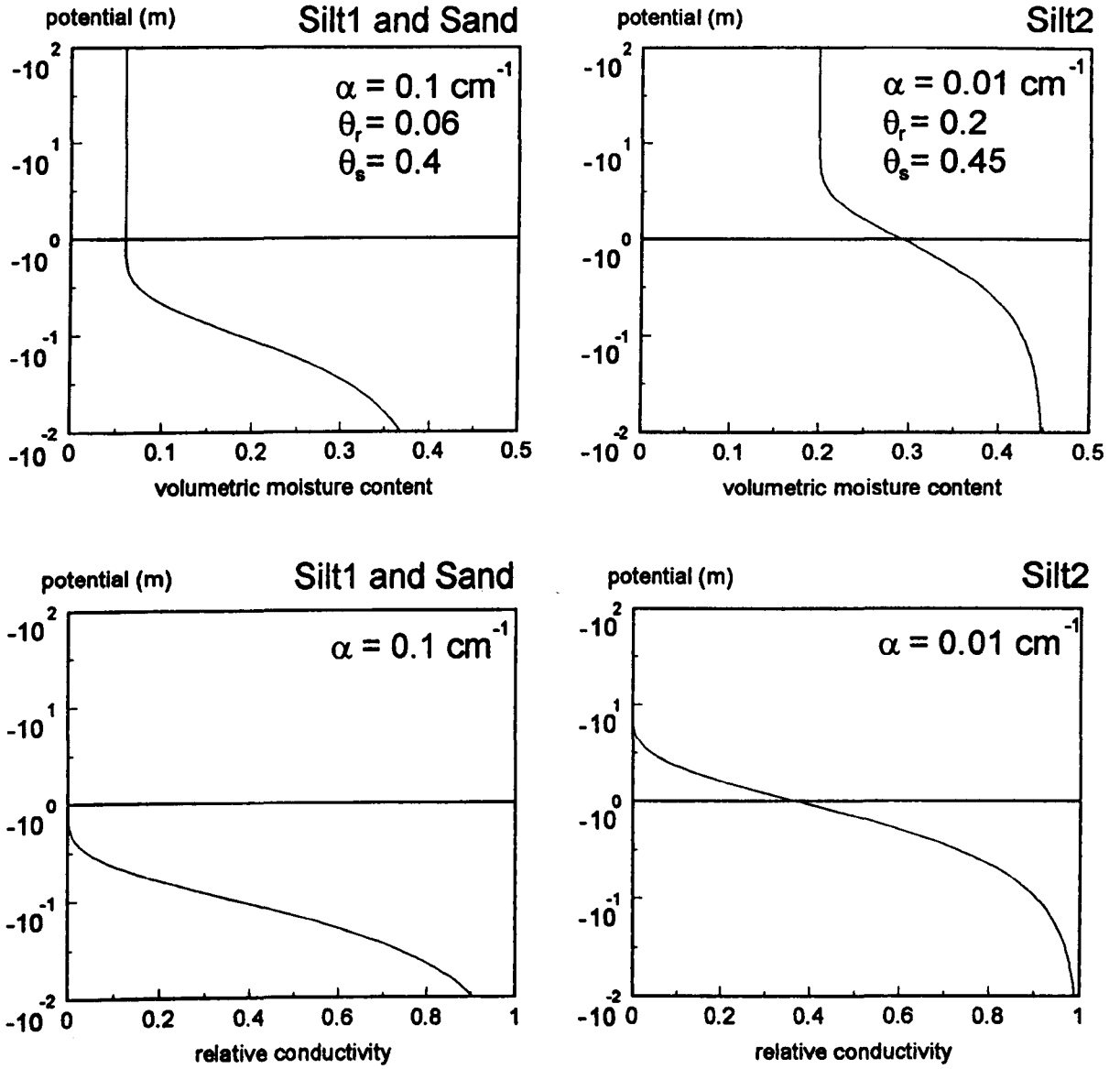

Figure 6.2 Soil hydraulic properties for test A

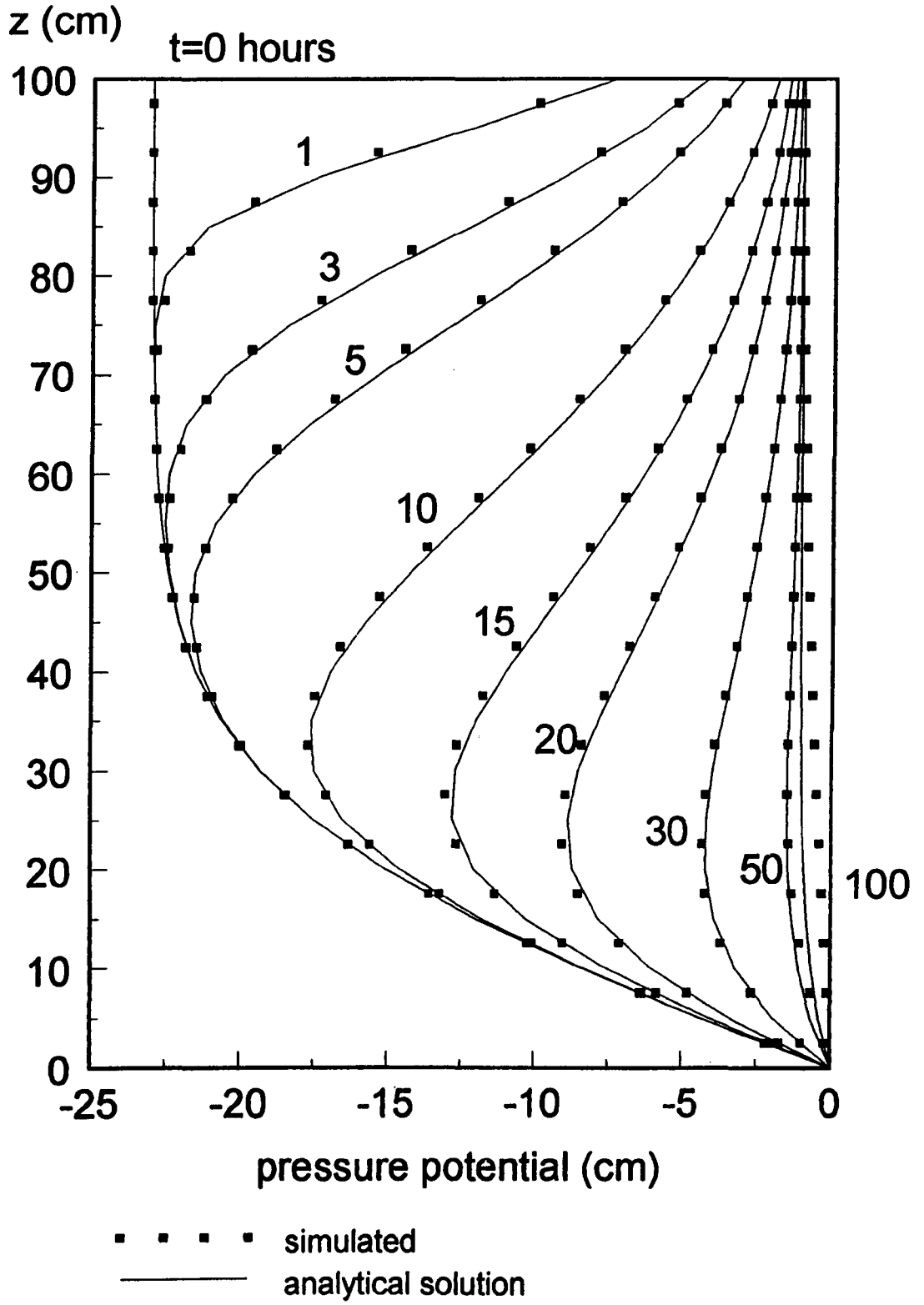

Figure 6.3 **Test A1: wetting pressure profiles for homogeneous soil, α = 0.1 cm^{-1}**

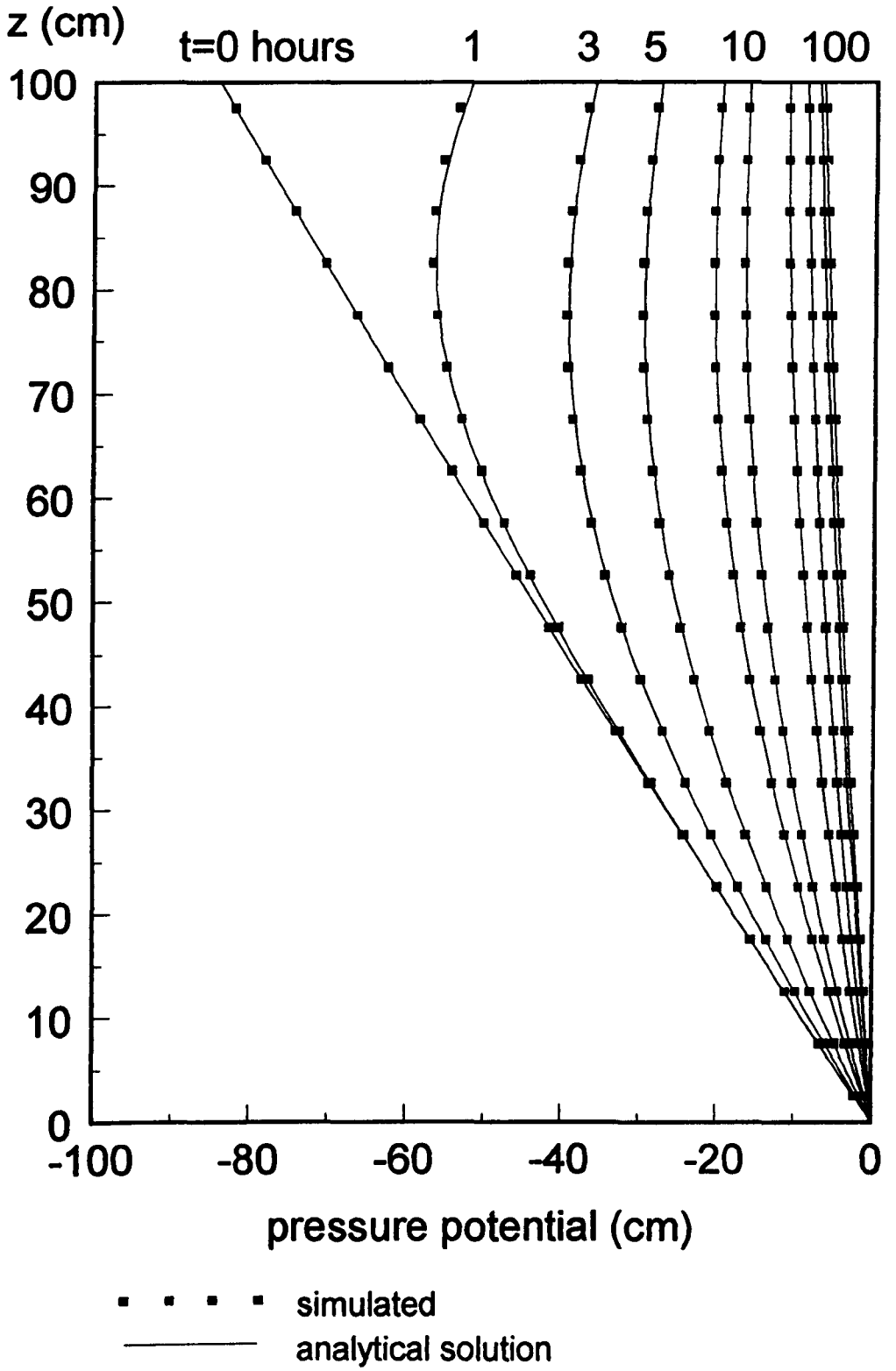

Figure 6.4 **Test A1: wetting pressure profiles for homogeneous soil, α = 0.01 cm^{-1}**

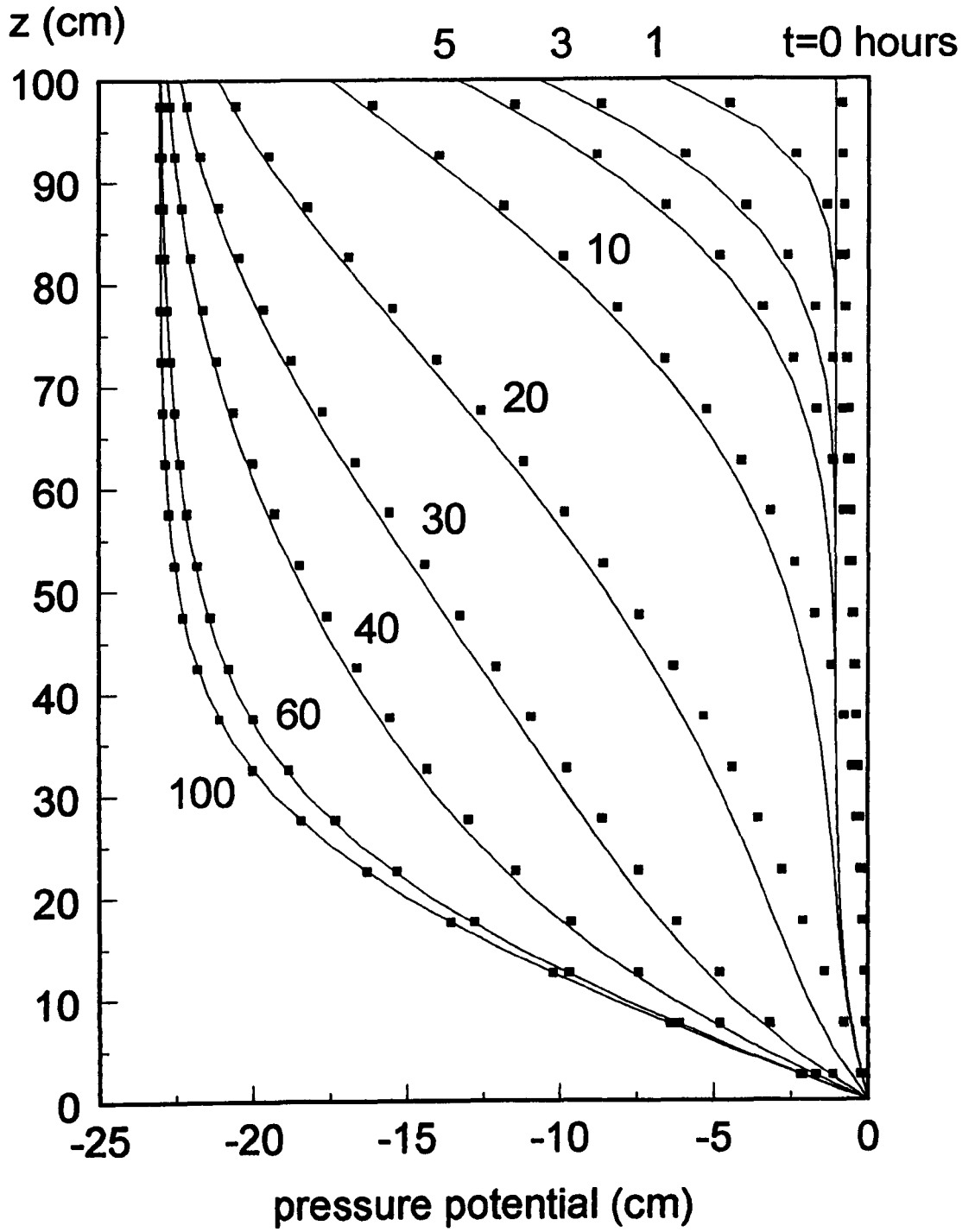

Figure 6.5 **Test A2: drainage pressure profiles for homogeneous soil**

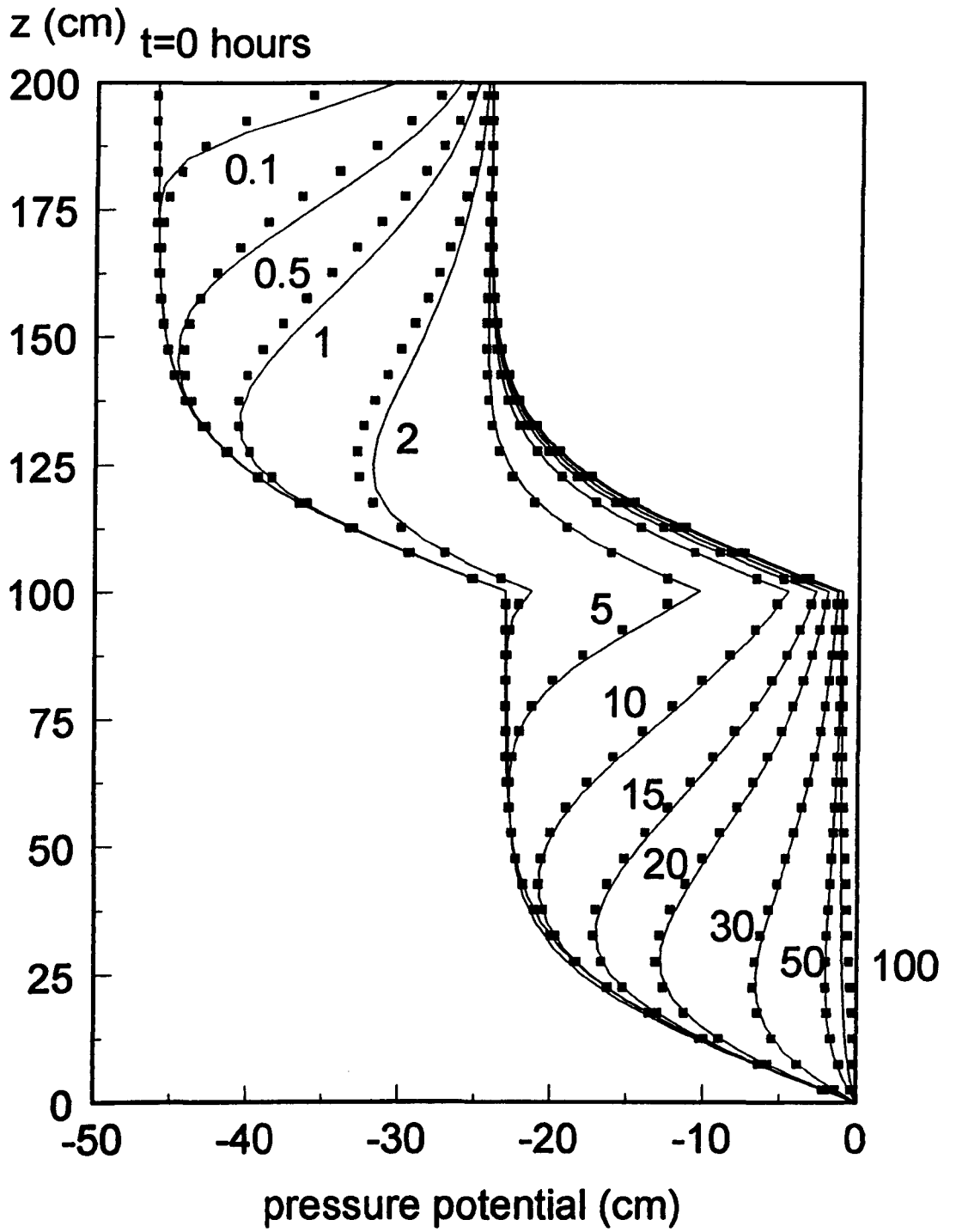

Figure 6.6 **Test A3: wetting pressure profiles for heterogeneous soils (sand over silt)**

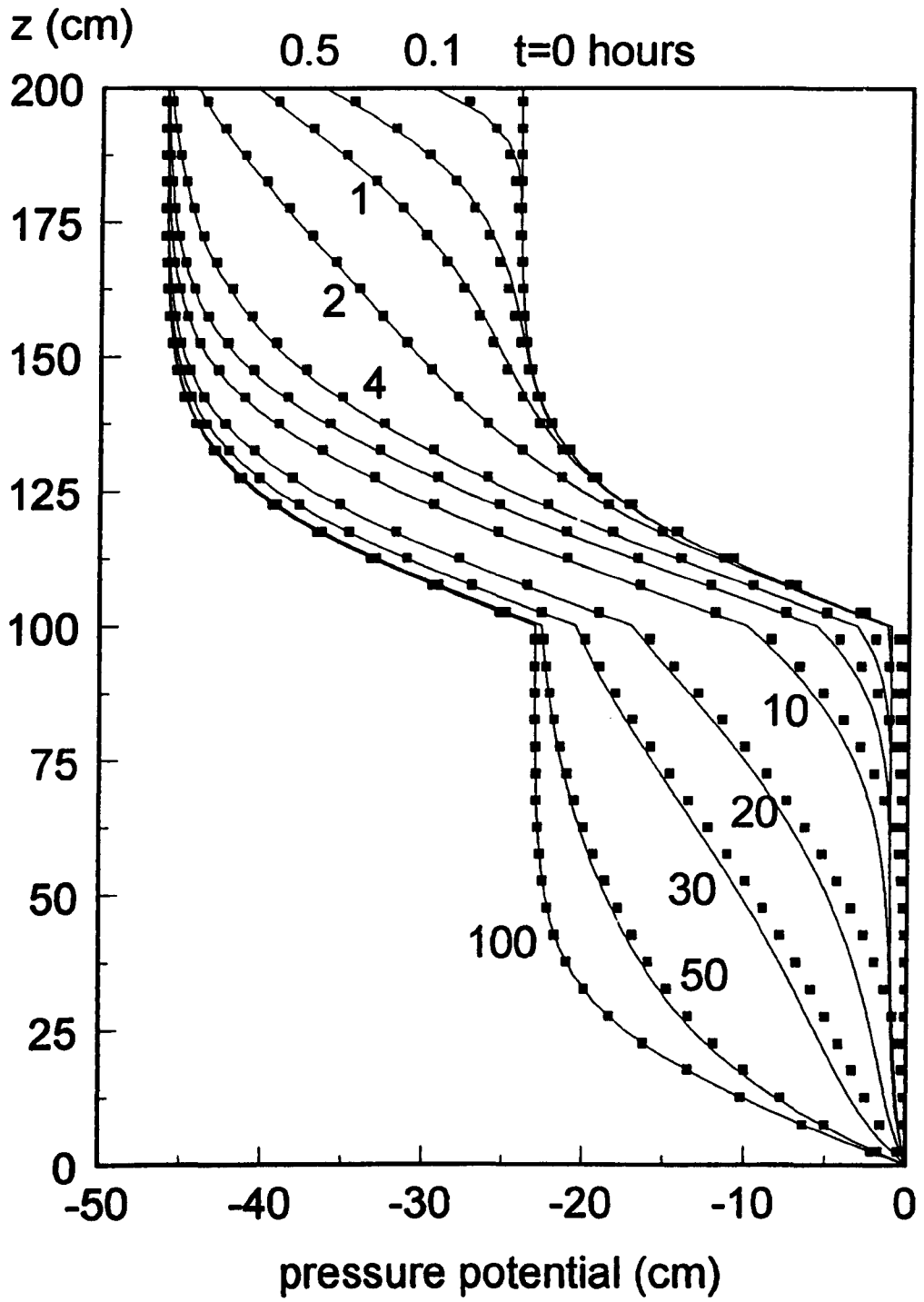

Figure 6.7 **Test A4: drainage pressure profiles for heterogeneous soils (sand over silt)**

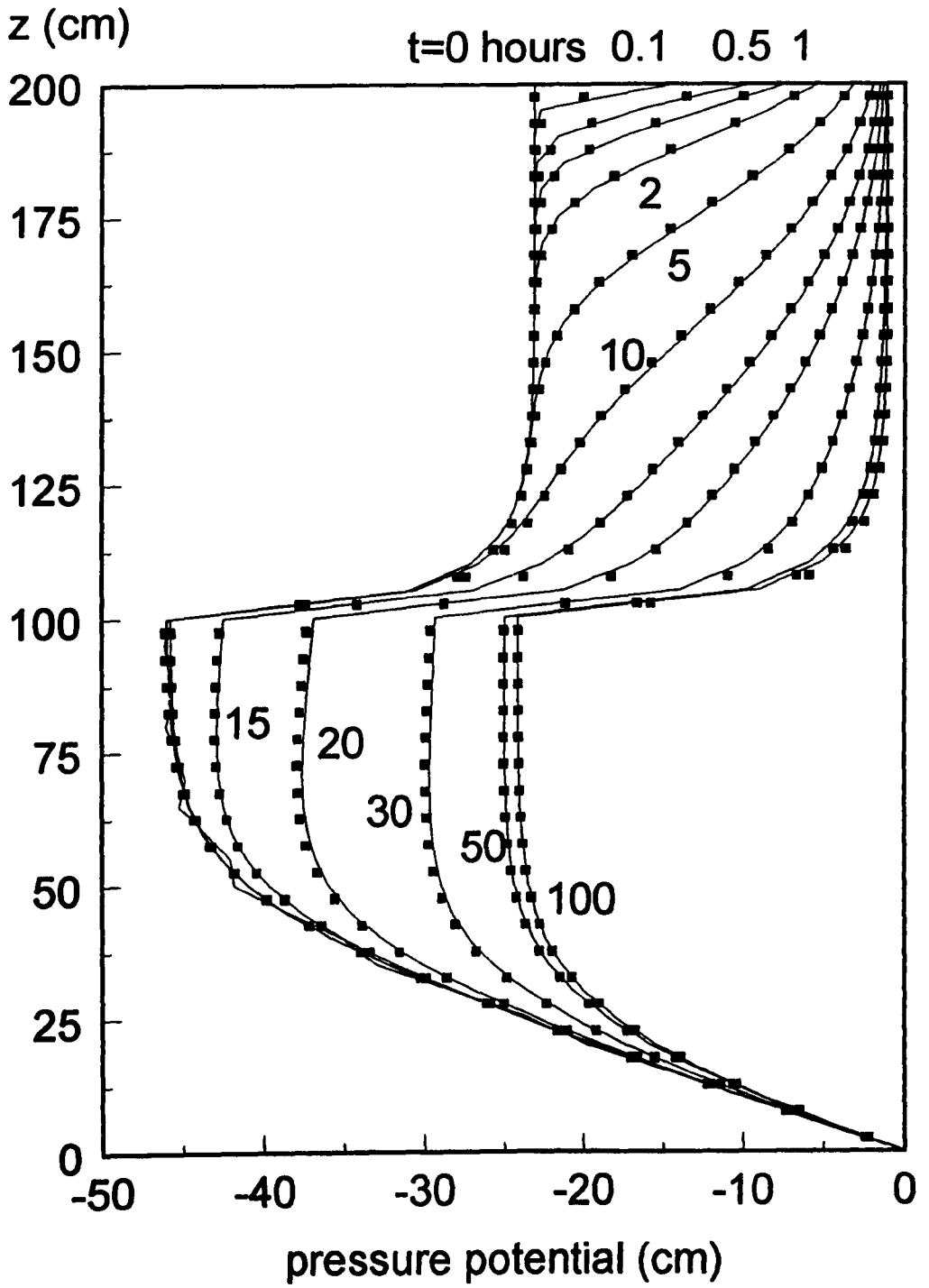

Figure 6.8 **Test A5: wetting pressure profiles for heterogeneous soils (silt over sand)**

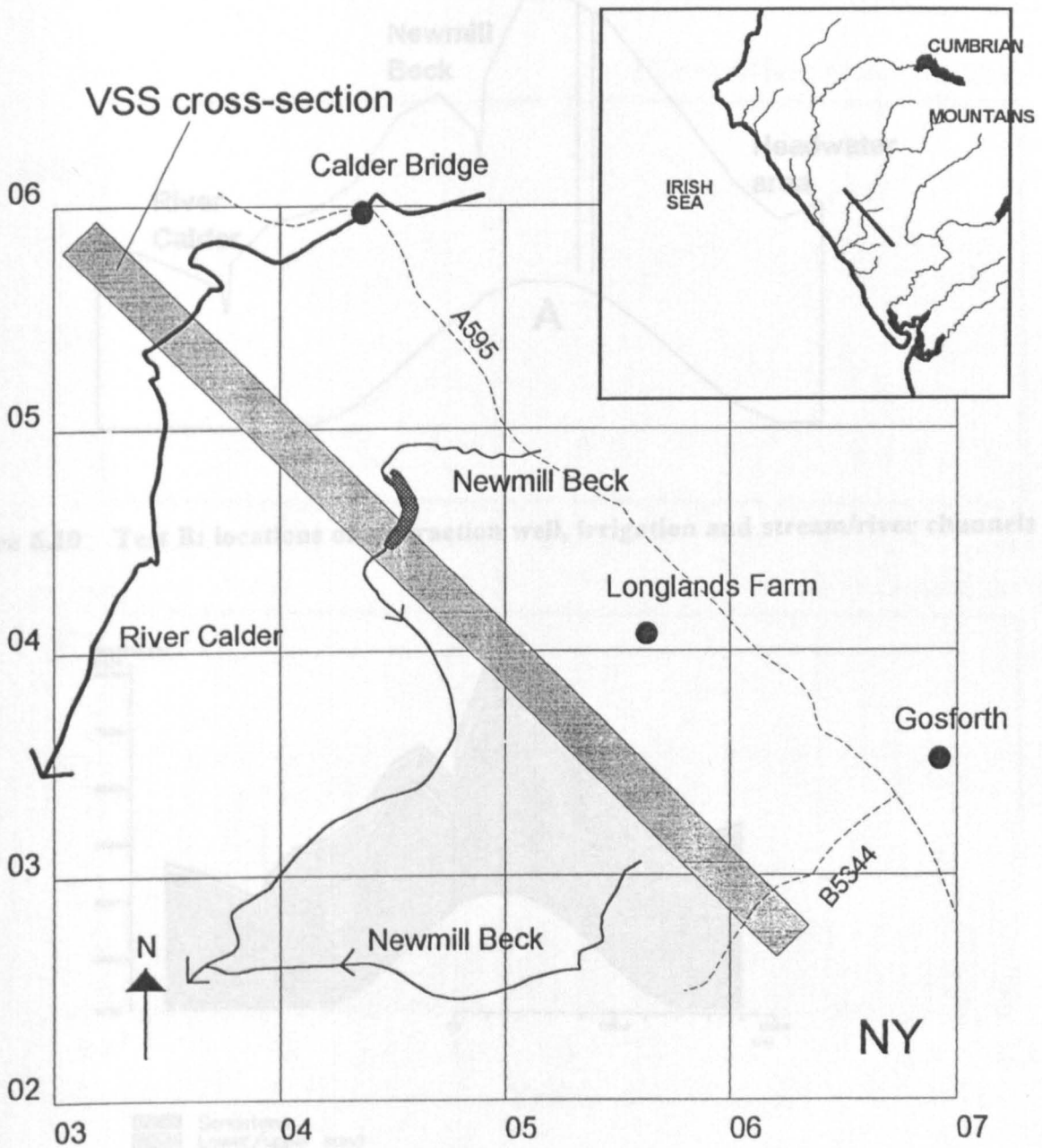

Figure 6.9 Test B: map showing cross-section location

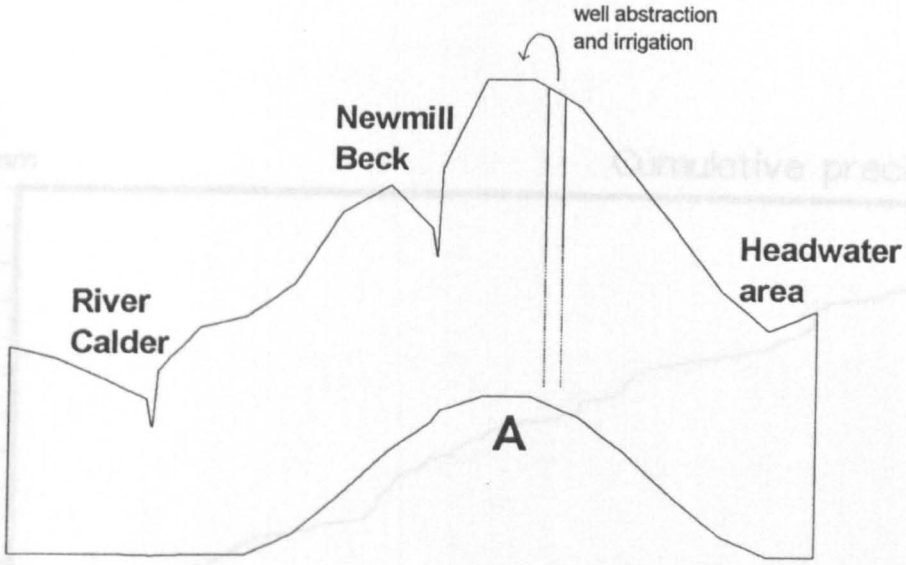

Figure 6.10 Test B: locations of abstraction well, irrigation and stream/river channels

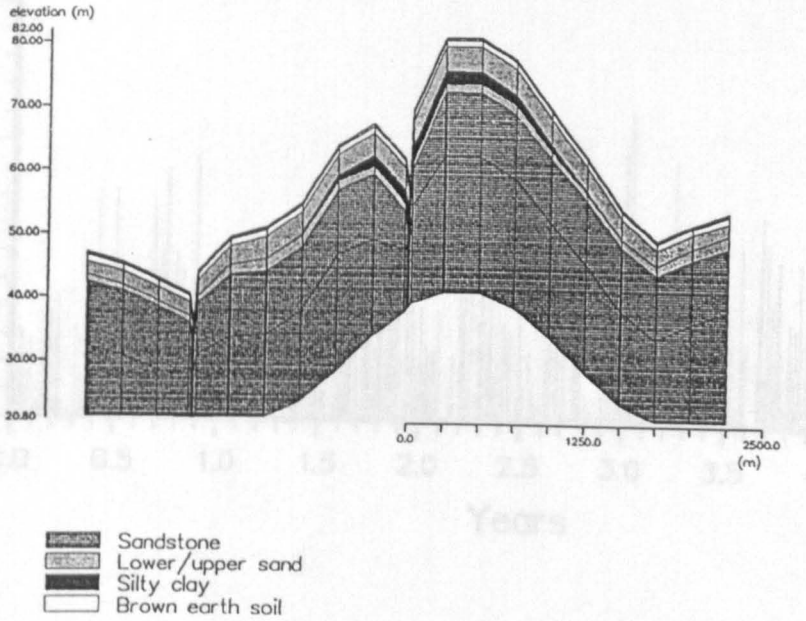

Figure 6.11 Test B: geological cross-section

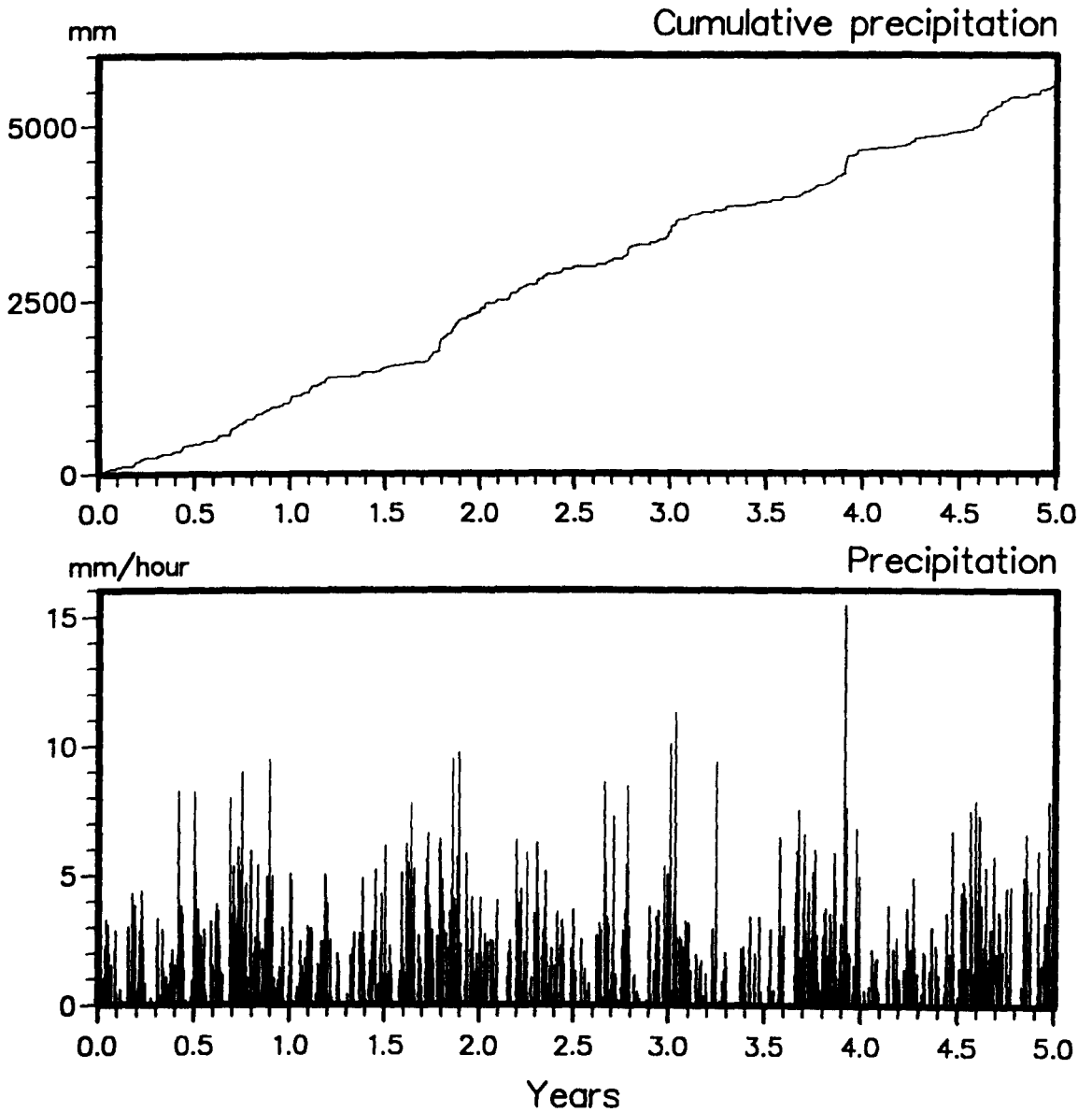

Figure 6.12 Test B: precipitation data

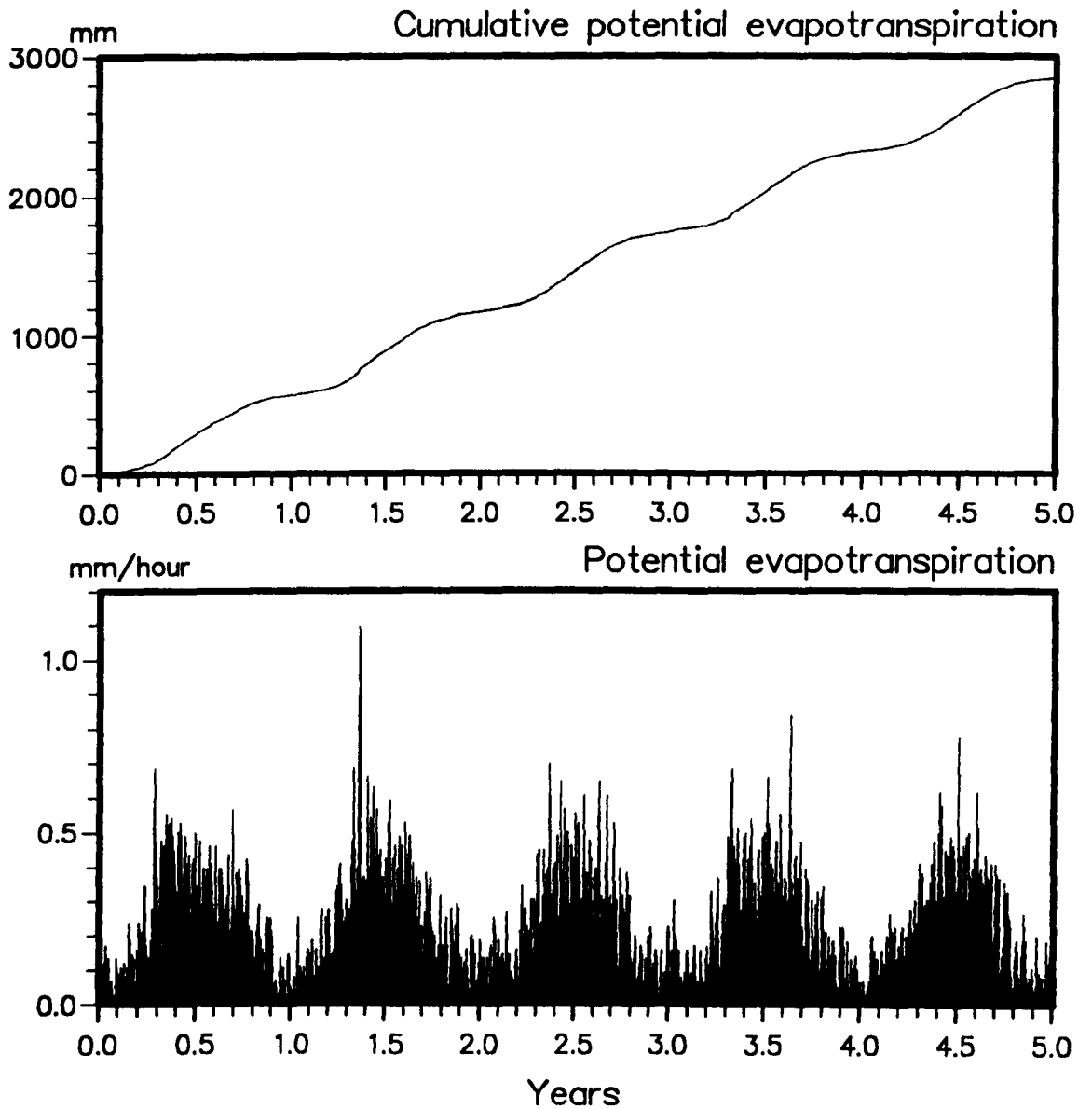

Figure 6.13 Test B: potential evapotranspiration data

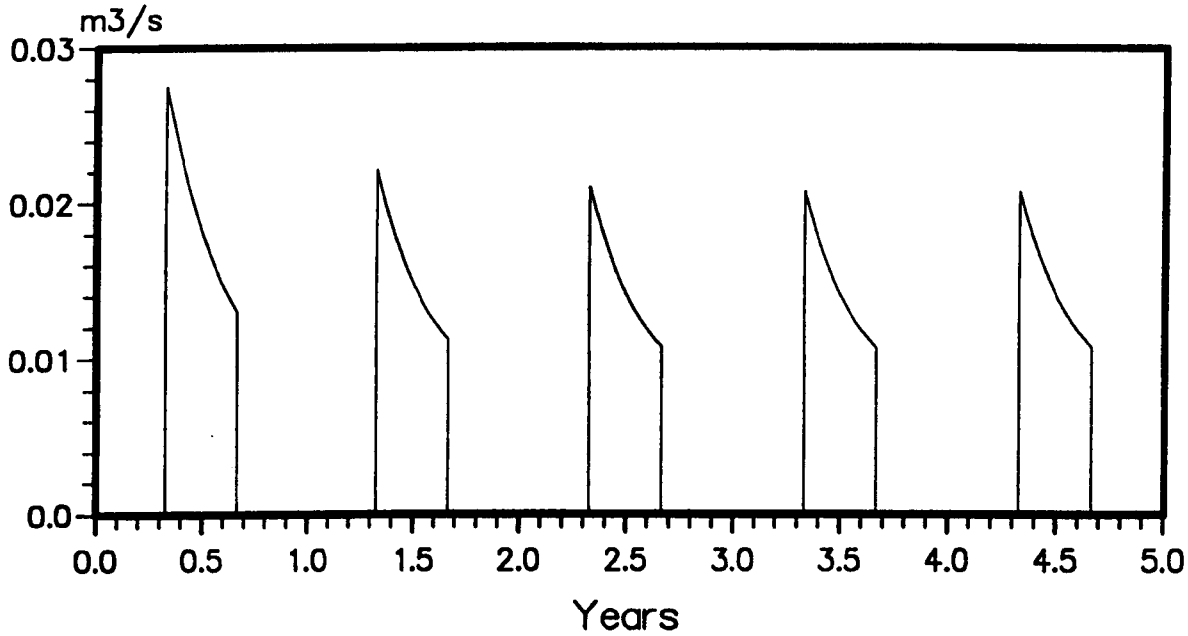

Figure 6.14 Test B1: well abstraction rates

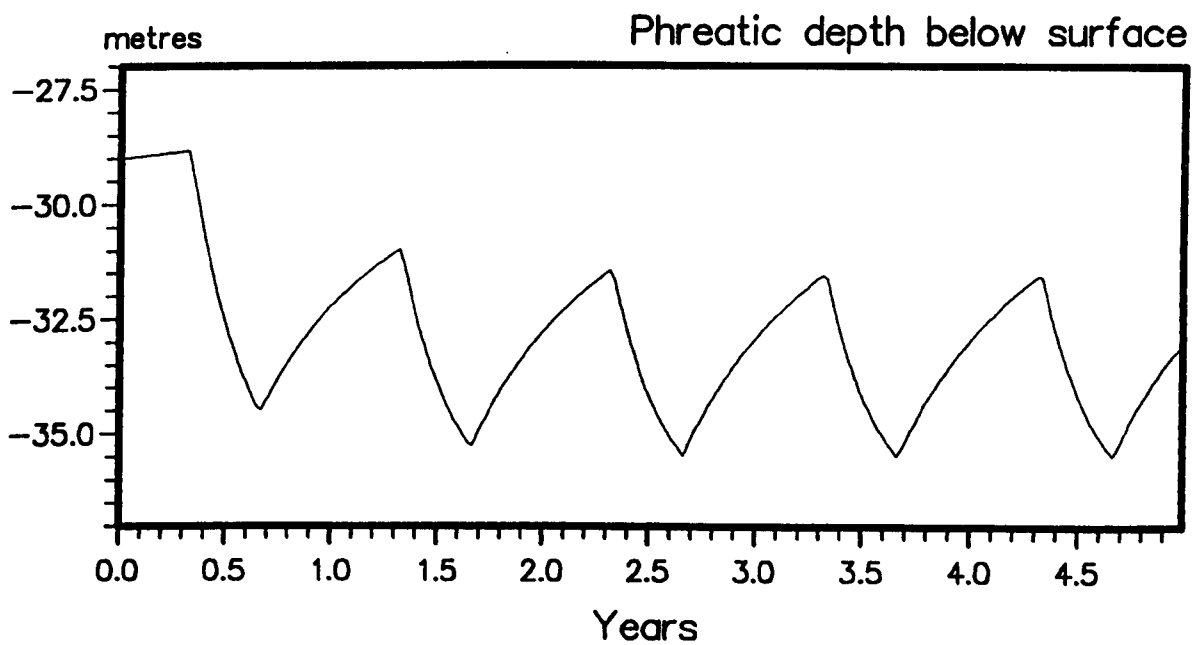

Figure 6.15 Test B1: phreatic surface levels at the abstraction well

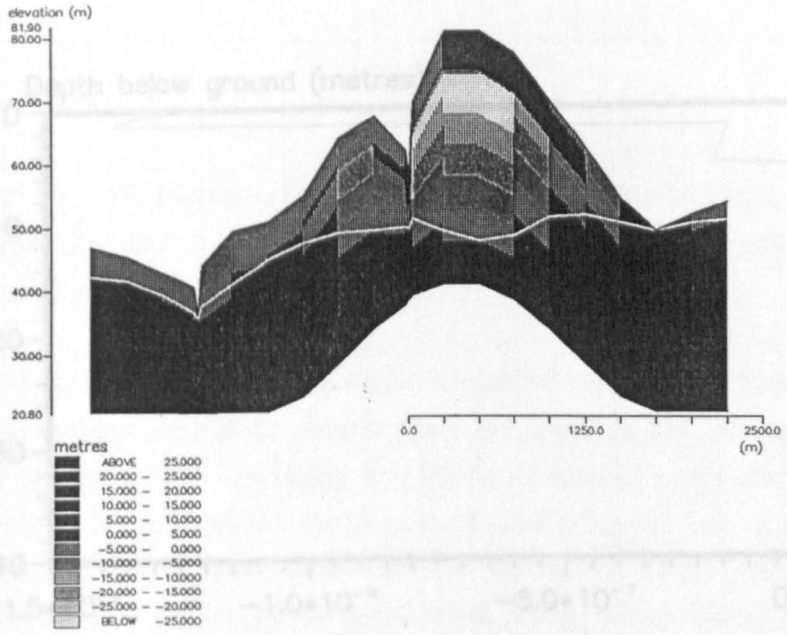

Figure 6.16 Test B1: cross-section of pressure potential and regional water table elevation at the end of the simulation

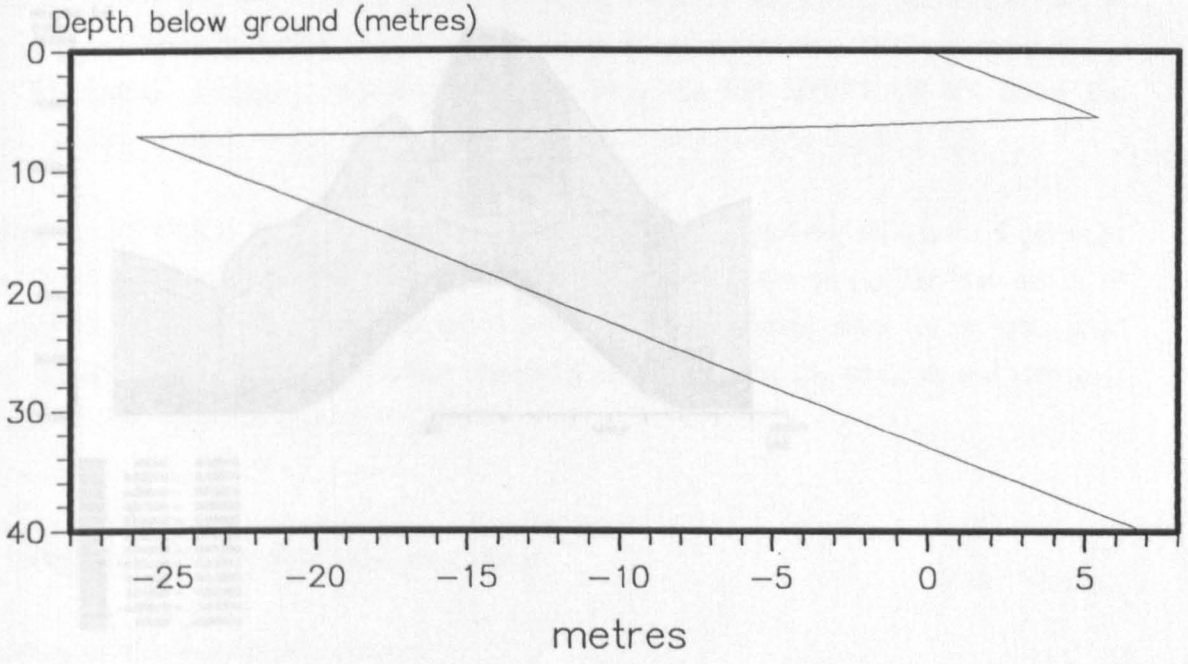

Figure 6.17 Test B1: pressure profile at location A (Fig. 6.10) at the end of the simulation

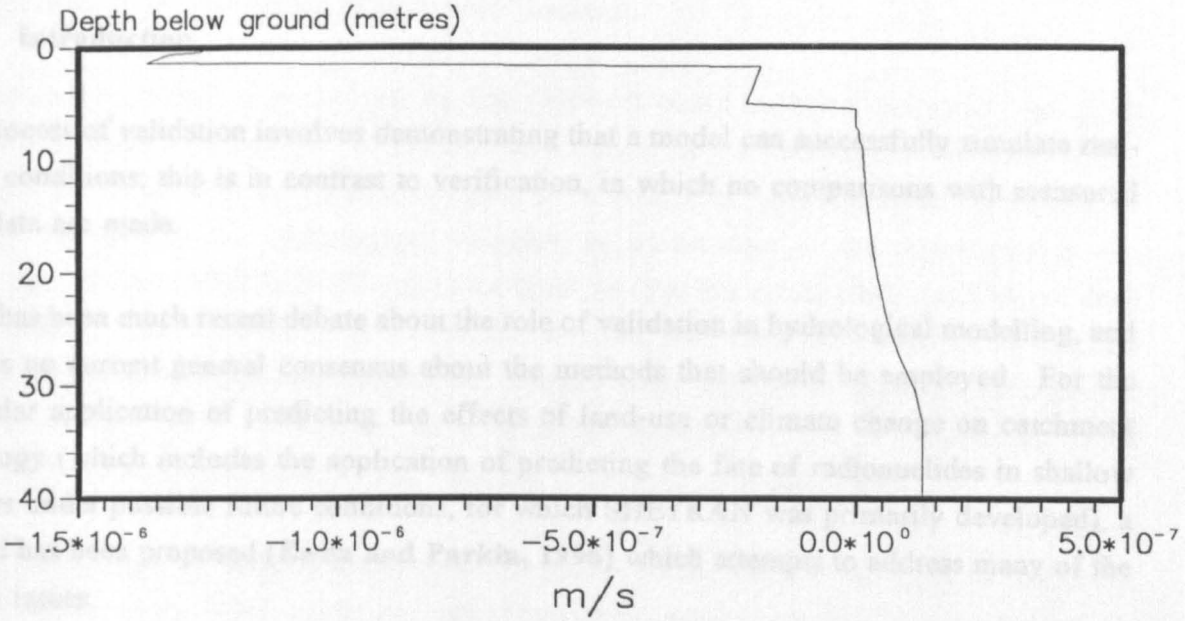

Figure 6.18 Test B1: lateral velocity profile at location A (Fig. 6.10) at the end of the simulation

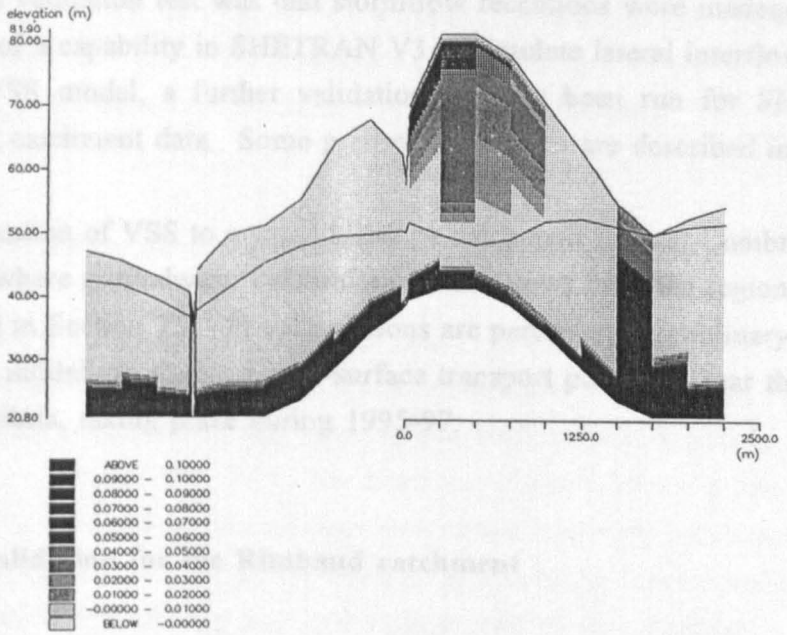

Figure 6.19 Test B2: cross-section of contaminant concentrations at the end of the simulation

CHAPTER 7 MODEL VALIDATION AND APPLICATION

7.1 Introduction

The process of validation involves demonstrating that a model can successfully simulate real-world conditions; this is in contrast to verification, in which no comparisons with measured field data are made.

There has been much recent debate about the role of validation in hydrological modelling, and there is no current general consensus about the methods that should be employed. For the particular application of predicting the effects of land-use or climate change on catchment hydrology (which includes the application of predicting the fate of radionuclides in shallow aquifers under possible future conditions, for which SHETRAN was primarily developed), a method has been proposed (**Ewen and Parkin, 1996**) which attempts to address many of the current issues.

This validation method has been applied for SHETRAN V3 using data from the Rimbaud catchment in south-eastern France (**Parkin et al., 1996**). One of the conclusions from the Rimbaud validation test was that stormflow recessions were inadequately simulated, due to the lack of a capability in SHETRAN V3 to simulate lateral interflow. With the availability of the VSS model, a further validation test has been run for SHETRAN V4 using the Rimbaud catchment data. Some preliminary results are described in Section 7.2.

An application of VSS to a small hillslope catchment in west Cumbria, chosen as a possible location where groundwater exfiltration (return flow) from the regional aquifer may occur, is described in Section 7.3. The simulations are part of the preliminary work for an integrated field and modelling study of near-surface transport pathways near the streams and rivers of west Cumbria, taking place during 1995-97.

7.2 Validation for the Rimbaud catchment

7.2.1 Aims of the validation exercise

The aim of the exercise is to demonstrate that SHETRAN V4, including VSS, is capable of providing improved predictions (relative to SHETRAN V3) of the stream discharges for the

Rimbaud catchment (in particular, the stormflow recessions), based on a sound conceptual interpretation of the catchment response mechanisms.

The validation method of **Ewen and Parkin (1996)** is based on 'blind' validation, in which the modeller does not have sight of the measured values for the hydrological variables which are being predicted until the simulations have been completed; and predictions are made of 'bounds' for each of the hydrological variables, as an estimate of the uncertainty in the predictions. In the SHETRAN V3 validation exercise (**Parkin et al., 1996**) predictions were made of hourly stream discharge at the catchment outlet, peak flow rates, monthly runoff, and total runoff over a three-year period; the bounds were calculated based on a series of SHETRAN simulations, consisting of a 'baseline' simulation, and a number of other simulations in which parameters were amended from their 'baseline' value.

For the SHETRAN V4 validation, the measured values for the stream discharges have already been inspected, so the blind validation method cannot be repeated for this catchment. Instead, direct comparisons are made between the SHETRAN V4 simulation of stream discharges and the corresponding observed data, for a sequence of storms during February 1968 (these storms were discussed in **Parkin et al., 1996**, and were analysed in detail in **Parkin et al., 1995**). The data set for the SHETRAN V4 simulation is based on the previous baseline simulation data set, with changes to the subsurface data in the light of the new capabilities of VSS, and new interpretations of the catchment response mechanisms.

7.2.2 Description of the Rimbaud catchment data set

The Rimbaud catchment is part of the Réal Collobrier collection of neighbouring and nested research catchments (**Beisson, 1985**) administered by the Centre National du Machinisme Agricole, du Génie Rural, des Eaux et des Forêts (CEMAGREF), located near Toulon in southeastern France (Fig. 7.1). Rimbaud was chosen from the Réal Collobrier catchments because: the soil and vegetation distributions are relatively homogeneous; there is relatively little topographic variation; it is thought to be watertight; it is located near to a meteorological station; and information on soil hydraulic properties was available.

The catchment area is 1.4 km^2, with elevations ranging from 620 m along the eastern crest to 470 m at the outlet to the northwest (Fig. 7.2). Slopes are steepest in the middle area west of the crest, and drain to a network of channels containing ephemeral streams. Towards the outlet there is a more level area, which also has the deepest soils, most of the rest of the catchment having only thin and rocky soils. The underlying rock is an impermeable gneiss. For the simulations, the catchment was represented by 144 grid squares of dimensions 100 m x 100 m, with the channel system running along the boundaries of the grid squares (Fig. 7.3).

The vegetation consists of: a dense natural cover of maquis (arbusier, fougère) about 2-4 m high, including grasses, shrubs and trees (green oak, pine, chestnut); subtree vegetation (grasses and small shrubs) along the roads where the natural cover has been cleared for fire protection; and a plantation of chestnuts. Parts of the catchment are clear of vegetation where the bedrock is exposed. The vegetation was represented for simulations by four types (Fig. 7.3): large maquis, with almost 100% cover throughout the year; small maquis, with a maximum cover of 80%, reduced during the summer as the grass dies; chestnuts, with 30% maximum cover in full leaf (underlain by grass), over the area of deeper soil; and bare rock, with no vegetation cover. Vegetation distributions and bedrock exposures were obtained from aerial photographs and a SPOT satellite image.

Photographs of the outlet weir structure, showing areas of bedrock exposed at the ground surface, and of an exposure of the thin soil horizons, are shown in Fig. 7.4.

Precipitation is measured at a site located in the middle of the catchment (Fig. 7.2) using a tipping bucket raingauge, giving values with a resolution down to 5 minutes. Precipitation for a sequence of storms during February 1968 is given in Fig. 7.5. Discharge is measured at the catchment outlet (Fig. 7.2) using a 90° triangular weir. Pan evaporation data were measured at a site immediately adjacent to the catchment, using a Colorado (sunken) evaporation pan, and were converted to potential evapotranspiration using a pan coefficient of 1.0 (which has been shown to apply as an annual figure by **Seguin, 1977**). Actual evapotranspiration was calculated in the simulations as a proportion of potential evapotranspiration, the ratio being a function of pressure potential (**Denmead and Shaw, 1962**).

Field visits were made by Dr. J.C. Bathurst of the University of Newcastle upon Tyne to measure some of the important soil hydraulic properties (some information being already

available from previous studies, **Demange, 1985**). Soil pits were dug and holes augered at three locations in the catchment (Fig. 7.2), and soil samples collected which were later analysed for particle size distribution in the laboratory. The soils are generally sandy, and contain a significant proportion of gravel and broken rock. Plant roots generally extend over the full depth of the shallow soils. The soil characteristic function (pressure potential versus moisture content) was obtained based on the formulation proposed by **Saxton et al. (1986)** which uses the gross particle size classification of the soil. Strickler roughness coefficients for overland and channel flow were evaluated on the basis of past experience in SHE simulations (e.g. **Bathurst, 1986**), taking into account values reported in the literature (e.g. **Engman, 1986**).

7.2.3 Previous simulations using SHETRAN V3

There have been two previous studies of the Rimbaud catchment using SHETRAN V3. The first application of the 'blind' validation method of **Ewen and Parkin (1996)** was to the Rimbaud catchment (**Parkin et al., 1996** and **Parkin et al., 1995**). Subsequently, a study of the possible impacts of vegetation loss on water flow and sediment erosion and transport was made, based on the previous work (**DM2E, 1994**).

From the first validation study (**Parkin et al., 1996**; **Parkin et al., 1995**), the main conclusion relevant to the SHETRAN V4 simulations was that SHETRAN V3 could not represent the discharge rates during stormflow recessions; the simulated peak discharges were too large, and the simulated hydrographs were sharper than those observed.

In August 1990, a forest fire removed 85% of the vegetation cover from the Rimbaud catchment. The aim of the vegetation loss study (**DM2E, 1994**) was to investigate the ability of SHETRAN to predict the impacts of fire on the hydrological response of the catchment, by running validation exercises for the pre-fire and the post-fire periods. Some simulations were also run for a small (75 m^2) erosion plot within the catchment, with the aim of determining values for soil property and overland flow parameters, although no conclusive results were achieved.

7.2.4 Conceptual understanding of possible runoff processes in the Rimbaud catchment

Simulated runoff in the SHETRAN V3 simulations was generated for most storms by saturation excess surface runoff and subsurface runoff, following the build up of a saturated zone at the base of the soil layer; for a single extreme storm in September 1968, Hortonian infiltration excess surface runoff also took place.

Since no additional relevant data on the catchment response mechanisms have become available since the inception of the first Rimbaud study, any improvements to the conceptual understanding of the runoff processes can only be inferred from inspection of the outlet hydrograph and the results of the SHETRAN simulations. The intention is to construct a physically reasonable conceptual representation of the catchment response mechanisms which, when translated into an actual data set of physical parameter values, will improve the simulations of the stream discharge hydrograph. It is recognised that, without independent field evidence, such a data set cannot be shown to more closely represent the actual field conditions even if the data set appears to be more physically reasonable.

Since the storm hydrographs simulated with SHETRAN V3 were too 'flashy' and the recessions were too steep, the general conclusion is made that a mechanism is present in the field which retains water during a storm event, only releasing the water slowly during the recession period. Two possible mechanisms are proposed. Firstly, the assumption made for the SHETRAN V3 simulations that the catchment contained a homogeneous soil overlying an impermeable gneiss bedrock may be invalid. It is postulated (following discussions with the local fieldwork staff at CEMAGREF) that the upper part of the gneiss may have undergone some weathering, and may be slightly permeable. This would provide a mechanism for the storage of water which would be released only slowly. Secondly, in the SHETRAN V3 simulations, the soil depth was uniform over large areas of the catchment, so the time taken for infiltrating water to build up a saturated region at the base of the soil which can generate subsurface runoff was similar for each area of the catchment. It is more likely to be the case, however, that the soil depths are much more variable over the catchment. If such variations were introduced into the model, the resulting times to saturation and to the generation of subsurface runoff would vary over a wider range.

7.2.5 SHETRAN V4 simulation

The SHETRAN data sets used for the V3 simulations were modified to accommodate the two proposed mechanisms affecting runoff generation. An additional sublayer was introduced beneath the surface soil; in the absence of any physical property data on the sublayer, all parameter values were made identical to those of the overlying soil, other than the lateral saturated hydraulic conductivity (which governs the rate of drainage from the sublayer). A uniformly random distribution of soil depths with no spatial correlation was introduced over the whole catchment. Soil depths for the surface layer varied between zero and 0.4 m. Soil depths for the sublayer varied between 0.1 and 0.5 m. Total soil depths (including surface soils and the sublayer) varied between 0.4 m and 0.9 m. Other than these changes, parameter values from the SHETRAN V3 baseline simulation were used (**Parkin et al., 1995**).

7.2.6 Simulation results

The simulated and observed discharges for a typical sequence of storms in February 1968 for a simulation where the lateral hydraulic conductivity in the upper soil layer was set to 50 m/day are shown in Fig. 7.6, together with the results from the earlier SHETRAN V3 simulation. The improved modelling of the storm recessions can clearly be seen. The total subsurface flow into the stream channel for the SHETRAN V4 simulation is also shown in Fig. 7.6. This highlights the main difference in response mechanisms between the V3 and V4 simulations - most of the storm runoff from the V4 simulation was due to subsurface lateral interflow (Fig. 7.7), whereas most of the contribution to storm runoff in the V3 simulation was from fast overland flow which tends to produce steep recessions during draining of surface water. For this simulation, the peak discharges were underestimated. Since the discharge peaks are mainly generated by saturation excess surface runoff, the extent of the contributing area of surface saturation during the storms may have been too small.

Lateral velocities within the soil profiles at a typical location within the catchment are shown in Fig. 7.8. Near to the start of the simulation the initial conditions have an effect on the subsurface flows: the soil is saturated into the upper horizon, and drainage takes place in the saturated zone and in the capillary fringe. The highest rates of flow occur at the base of the upper soil layer. At time 240 hours, following a storm event, the soil is saturated up to the ground surface, and near-uniform flow takes place in the upper soil (the slight variations are attributable to variations in lateral head gradients at different levels in the profile), with low

lateral flows in the lower horizon corresponding to the low hydraulic conductivities. At time 480 hours (just beyond the end of the sequence of storms described above), the soil horizon has begun to drain, and generally drier conditions have developed near to the ground surface, with corresponding reduction in hydraulic conductivity and hence lateral flow rates. Very close to the ground surface, however, there has been, at this location, some further infiltration from a small rainfall event; the soil moisture has increased, causing a small increase in hydraulic conductivity, and generating increased lateral flow in the top few centimetres of the soil.

7.2.7 Discussion and conclusions

The improved simulation of the only observed catchment response data for this catchment (the outlet hydrograph) was achieved through the use of two soil layers, the upper soil layer having a high lateral hydraulic conductivity, representing quickly responding mechanisms of subsurface flow (i.e. macropores). Although flow through macropores is not built explicitly into the model, these results demonstrate that the gross effects of rapid subsurface flow at the catchment scale can be represented in this way; this approach of using high conductivities in a Darcian model to represent fast subsurface flow has often been used by other modellers in a similar way.

In conclusion, it has been demonstrated that simulations of stream discharge in a Mediterranean catchment with shallow soils can be significantly improved, relative to those produced using a vertically-averaged subsurface flow model, through the use of the variably-saturated flow model described in this thesis.

7.3 Simulations of flow through layered deposits of Quaternary drift

7.3.1 Aims of the simulations

The simulations are a preliminary stage in an integrated field and modelling programme which is designed to improve understanding of stream-aquifer interaction and groundwater discharge in west Cumbria. The later stages of this programme will involve instrumentation of a field site (partly based on the results of these preliminary simulations), and a further programme of modelling using SHETRAN V4.

The aim of the preliminary simulations reported here was to gain experience in the use of VSS under the type of conditions for which it was designed. Further simulations (not reported here) will have the aim of refining understanding of discharge mechanisms in the light of field data.

7.3.2 Description and representation of the study site

The site chosen for the preliminary modelling study is located at Robertgate Bridge near to Calder Bridge, west Cumbria (Fig. 7.9). The site consists of a hillslope, draining into the Black Beck stream (Fig. 7.10), shown in photographs in Fig. 7.11.

The main characteristics of the site are summarised as follows:

- the site is approximately 850 by 750 m in size, and 0.4 km^2 in area;
- elevations range from approximately 80 to 160 m AOD;
- most of the site consists of Grade 3 agricultural land; some of the upper part of the site is Grade 4 land;
- the underlying bedrock for the whole site is St. Bees Sandstone;
- the Quaternary deposits on the lower part of the site are classified by the British Geological Survey as 'pre-Holocene valley infill'; the deposits on the upper part of the site are classified as 'thin till on rock (generally < 5m)';
- the soils on the site are classified on the 1:250000 scale Soil Survey map as Newport 1 (brown sand) and Wick 1 (brown earth) associations;

- there are several 'springs' (points of groundwater discharge) on the site; at least one of these is understood to be an old haematite exploration borehole, which is artesian and has, in the past, been used as a domestic water supply source; there is also evidence of wider areas of groundwater discharge to the ground surface;
- there are three NRA observation boreholes at or near to the site.

For the simulations, the topography was obtained from a 50 metre digital elevation model (DEM), and the SHETRAN grid network (Fig. 7.12) was chosen to coincide with the DEM data. A fixed head boundary condition was prescribed along the lower edge of the hillslope, to represent the Black Beck stream. Prior to the start of the detailed field surveys of the site, a simplified representation of the soils and geological layering was used, with a brown earth soil directly overlying permeable valley deposits in the lower part of the slope, and less permeable lodgement till over the rest of the slope (Fig. 7.12); these Quaternary sediments are underlain by sandstone. A silty clay horizon with low permeability was included, with different spatial distributions for each simulation. The vegetation was modelled as mostly rough pasture, with a small area of deciduous trees at the top of the hillslope. Precipitation data were taken from the Prior Scales raingauge, several kilometres from the site (Fig. 7.13), and potential evapotranspiration data were taken from the Meteorological Office MORECS system, based mainly on data from a meteorological station on the west Cumbrian coastal plain (Fig. 7.14).

For the representation of springs in VSS, three parameters are required:

z_c - the elevation relative to datum of the computational cell from which it is assumed that point spring discharge to the ground surface can occur;

z_{sp} - the elevation of the spring discharge point relative to datum;

C_s - a spring discharge coefficient, representing the resistance to flow of the notional conduit conducting flow to the ground surface.

In these preliminary simulations which are run to investigate the use of VSS, the 'springs' are treated as being natural. One spring (along the line C-C in Fig. 7.12) was implemented as a spring in VSS; the other was treated as a seepage area over one 50m by 50 m computational element. The parameter values used for the spring were: z_c = 73.75 m; z_{sp} = 81 m; and C_s = 0.01 m^{-1} s^{-1}. Ground elevation at the spring computational element is 82 m; the cell from which the spring discharges is located just above the top of the sandstone.

For each of the simulations, a small constant uniformly distributed vertical velocity of 1.0 10^{-9} m s^{-1} (approximately 30 mm/year) was prescribed as a lower boundary condition to represent a contribution from the regional aquifer to the hillslope discharge area.

The initial conditions for each simulation were prescribed as a three-dimensional field of pressure potentials. These were defined by taking the final pressure distribution from a preliminary simulation with arbitrary initial conditions; ie. the simulation was run twice, the first time having an estimate of appropriate initial conditions, the second starting from a state of approximate dynamic equilibrium. This approach was thought to be appropriate, since the final simulations showed realistic responses to the seasonal variations in meteorological conditions (some preliminary simulations which were run with initial conditions that were not in dynamic equilibrium tended to drain the upper part of the slope throughout the simulations, and not to respond to the increased effective precipitation during the Autumn period).

7.3.3 Simulations performed

Results from two simulations are presented, to demonstrate some of the possible mechanisms for groundwater discharge, each with a different representation of a hypothetical silty clay layer (Fig. 7.15):

1 no silty clay layer;

2 continuous, connected silty clay layer immediately above the sandstone, including a change in thickness of the layer, and a small break in the layer at one of the spring locations at the bottom of the hillslope.

Each simulation was run over a single calender year.

7.3.4 Simulation results

Phreatic surface levels relative to the ground surface during the whole simulation period at two locations in the catchment for simulation 2 are shown in Fig. 7.16. The phreatic surface is above the silty-clay horizon at location A (Fig. 7.12) and is below the silty-clay horizon at location B. The fast response to precipitation events at location A can be seen, where infiltrating rainwater drains quickly through the sandy upper drift layers. At location B, although responses to precipitation events can be seen, the recharge to the phreatic aquifer is

attenuated by the presence of the silty-clay horizon. Also, at location B there is a general drainage of the aquifer over the simulation year; this is due to the initial conditions representing wetter antecedant conditions than those of the simulation year. Better initial conditions to approximate equilibrium conditions could have been defined; this was not thought to be necessary, however, for these demonstration simulations.

Cross-sections of pressure potential for both simulations at the same time during Autumn are shown in Fig. 7.17, and vertical profiles of the same data at location B (Fig. 7.12) are shown in Fig. 7.18. Following the period of increased precipitation, a perched aquifer has developed above the silty-clay layer for simulation 2. The maximum depth of saturation occurs below a small hollow on the hillslope. The extent of the perched aquifer depends upon the characteristics of the silty-clay horizon, and the location of the regional water table. In the sandy deposits above the silty-clay layer, and in the permeable sandstone below the layer, near-equilibrium profiles of pressure potential can be seen. The transient nature of the perched aquifer can be seen in Fig. 7.19, which shows the pressure potential at a point just above the top of the silty-clay horizon for the whole simulation period (saturated conditions occur when the pressure potential is positive).

7.3.5 Discussion and conclusions

The preliminary simulations of the Robertgate experimental site are intended to demonstrate some of the capabilities of SHETRAN V4 for realistic conditions, and to gain experience in the use of the VSS component. Only information available from maps was used to set up the simulations. Only very general generic information was available on the nature and distribution of the Quaternary deposits. The simulations were intended to demonstrate some possible types of response of the hillslope.

Given the preliminary nature of this work, there remain many further aspects relating to representation of the potential experimental site that will be addressed in the future programme of work. These include the following.

- The bottom boundary condition, which is represented as a constant uniform upflow rate, needs to be refined.
- The lateral boundary conditions around the upper part of the catchment need to be improved. The use of a no-flow boundary condition in the preliminary simulations (where the catchment boundary was based on the ground surface catchment draining

into the reach of the Black Beck stream) is not likely to be representative of subsurface field conditions.

- The lateral boundary condition along the stream channel is set as a fixed head over the entire depth of the aquifer. Evidently, this is not realistic, since vertical head gradients are likely as flows converge upwards towards the channel.
- The representation of the springs in the preliminary simulations is intended only to demonstrate the processes included in the VSS model; at least one of the 'springs' is in fact an old haematite exploration borehole.

In conclusion, these simulations, which were run without any serious numerical difficulties, demonstrate the successful application of SHETRAN V4, including VSS, to a realistic field situation, and form a basis for subsequent work on the integrated field and modelling programme at the potential experimental site at Robertgate.

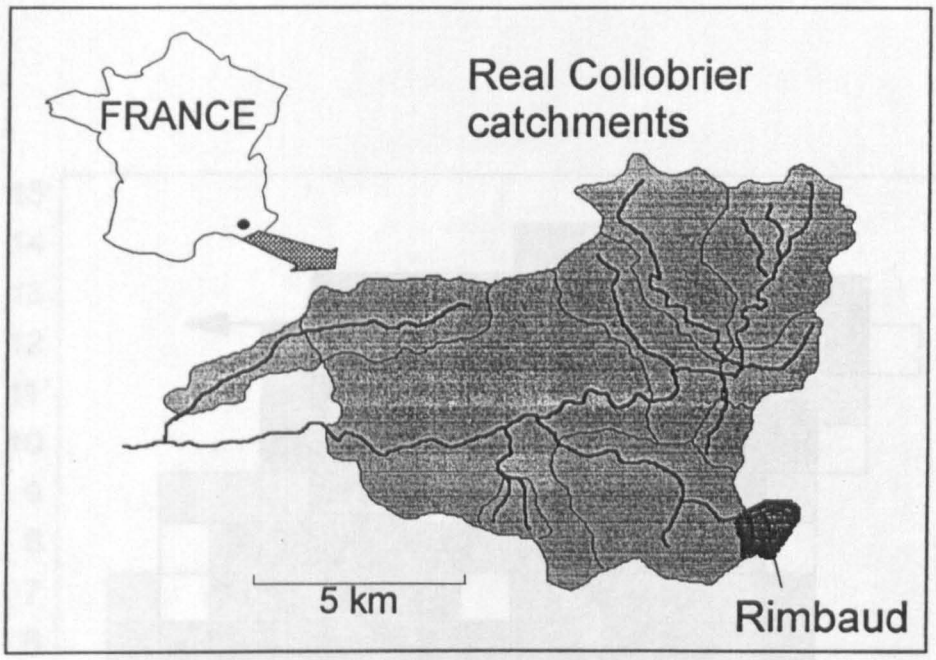

Figure 7.1 **Location map for the Réal Collobrier and Rimbaud catchments**

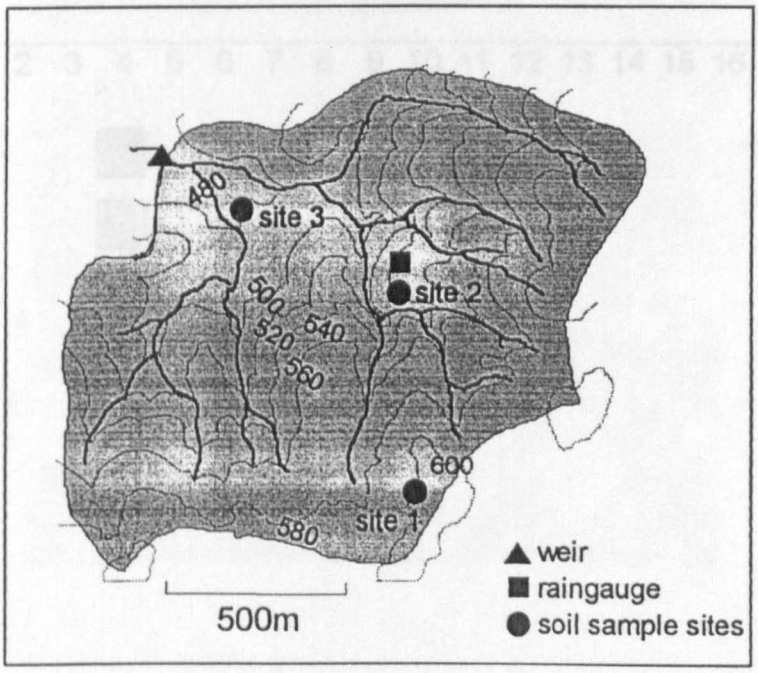

Figure 7.2 **Ground elevation contours (in metres), instrumentation, and field measurement sites for the Rimbaud catchment**

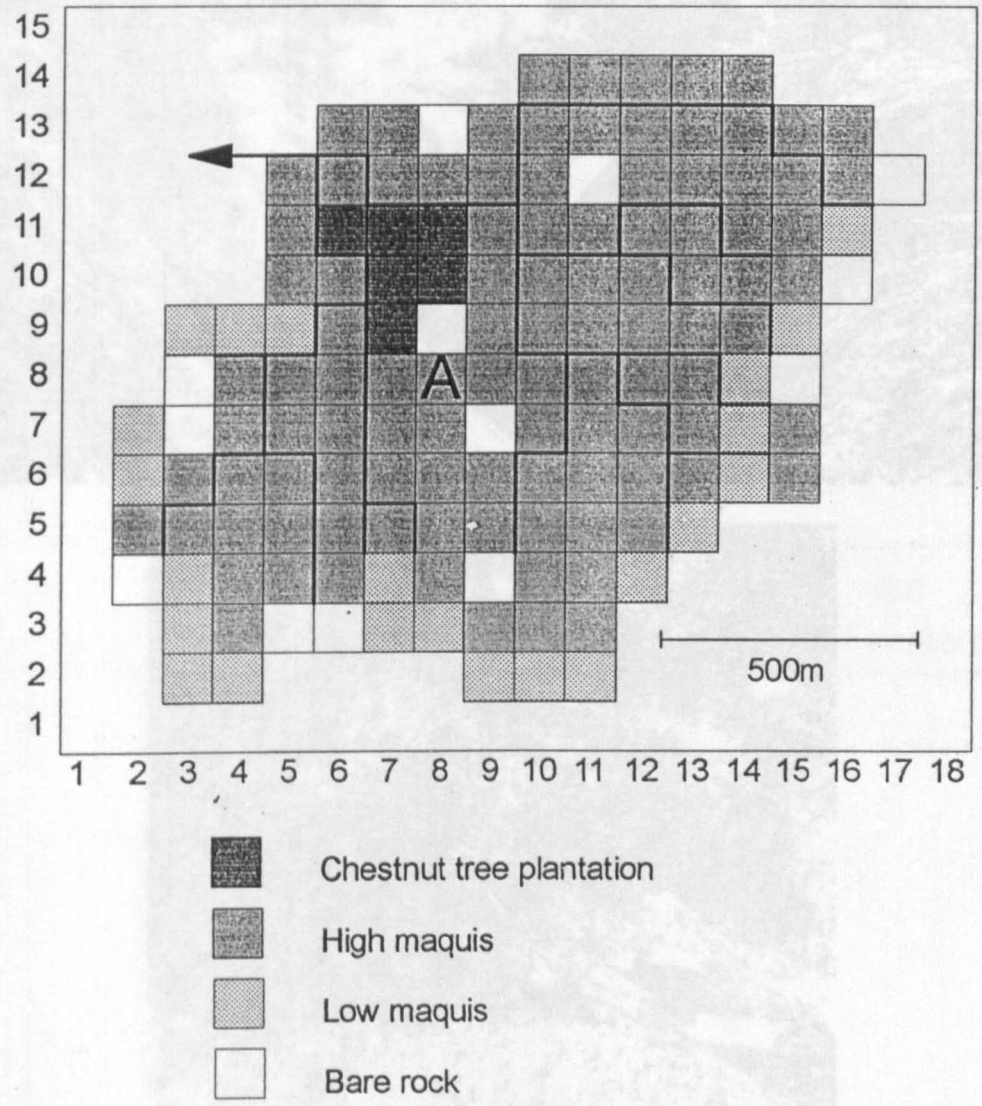

Figure 7.3 **SHETRAN grid network and channel system for the Rimbaud catchment, showing also the modelled vegetation distribution**

a)

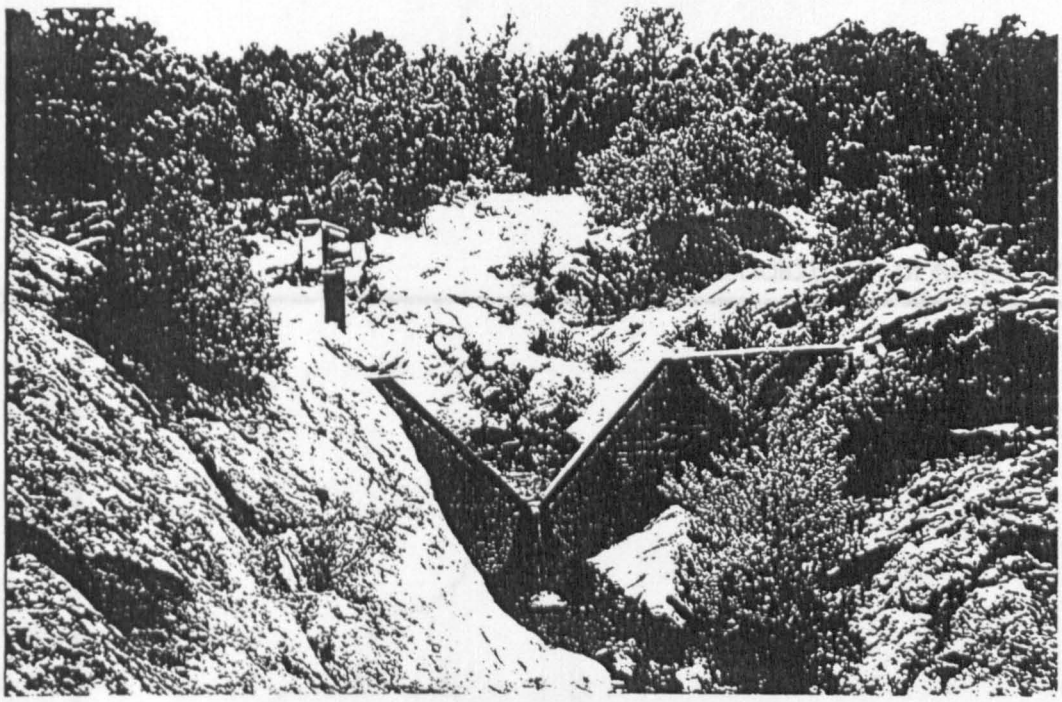

b)

Figure 7.4 **Photographs of the Rimbaud catchment**
a) the outlet weir, showing exposures of gneiss bedrock
b) an exposure of soil

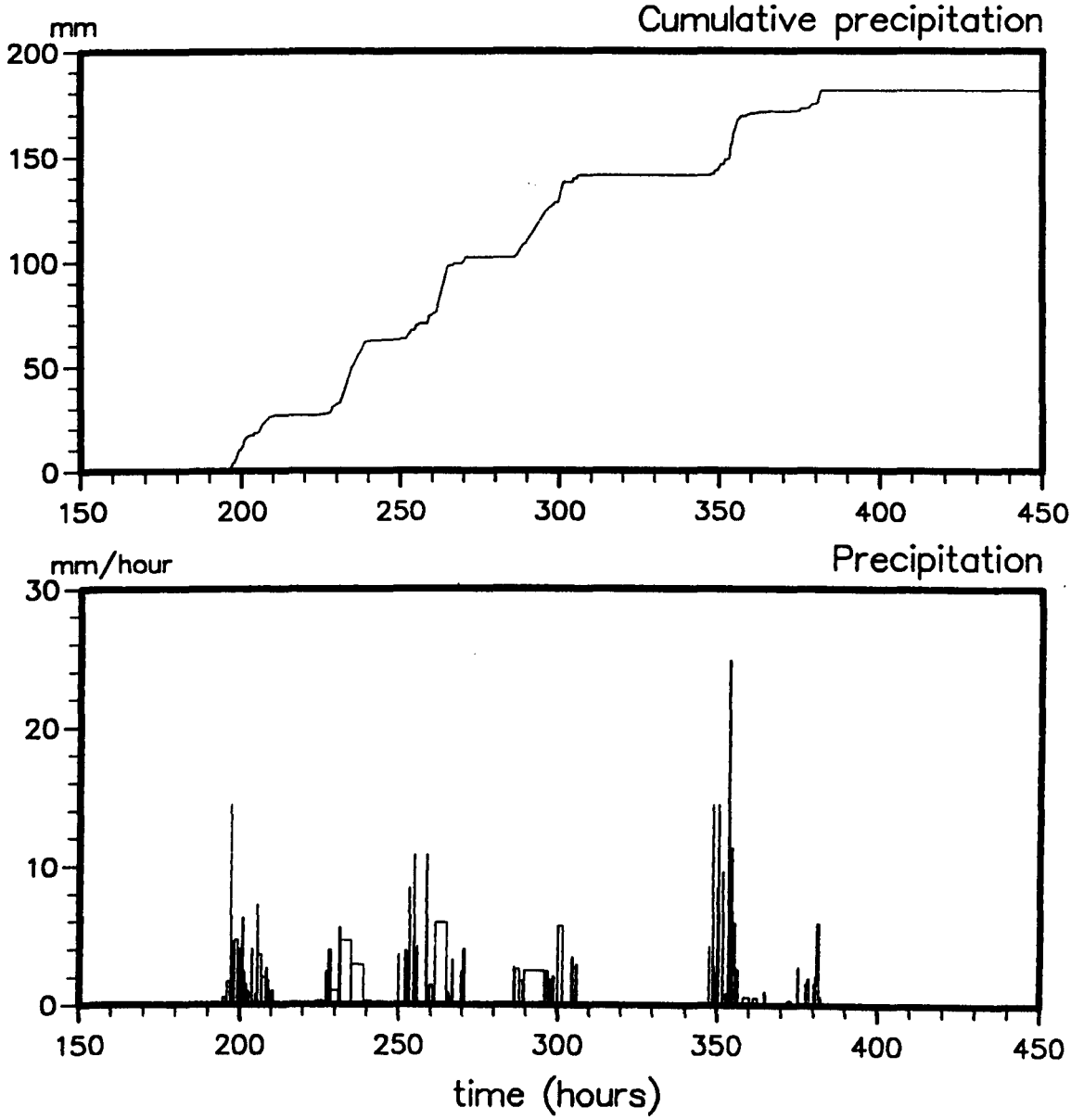

Figure 7.5 **Time-series of precipitation for a sequence of storms during February 1968 for the Rimbaud catchment**

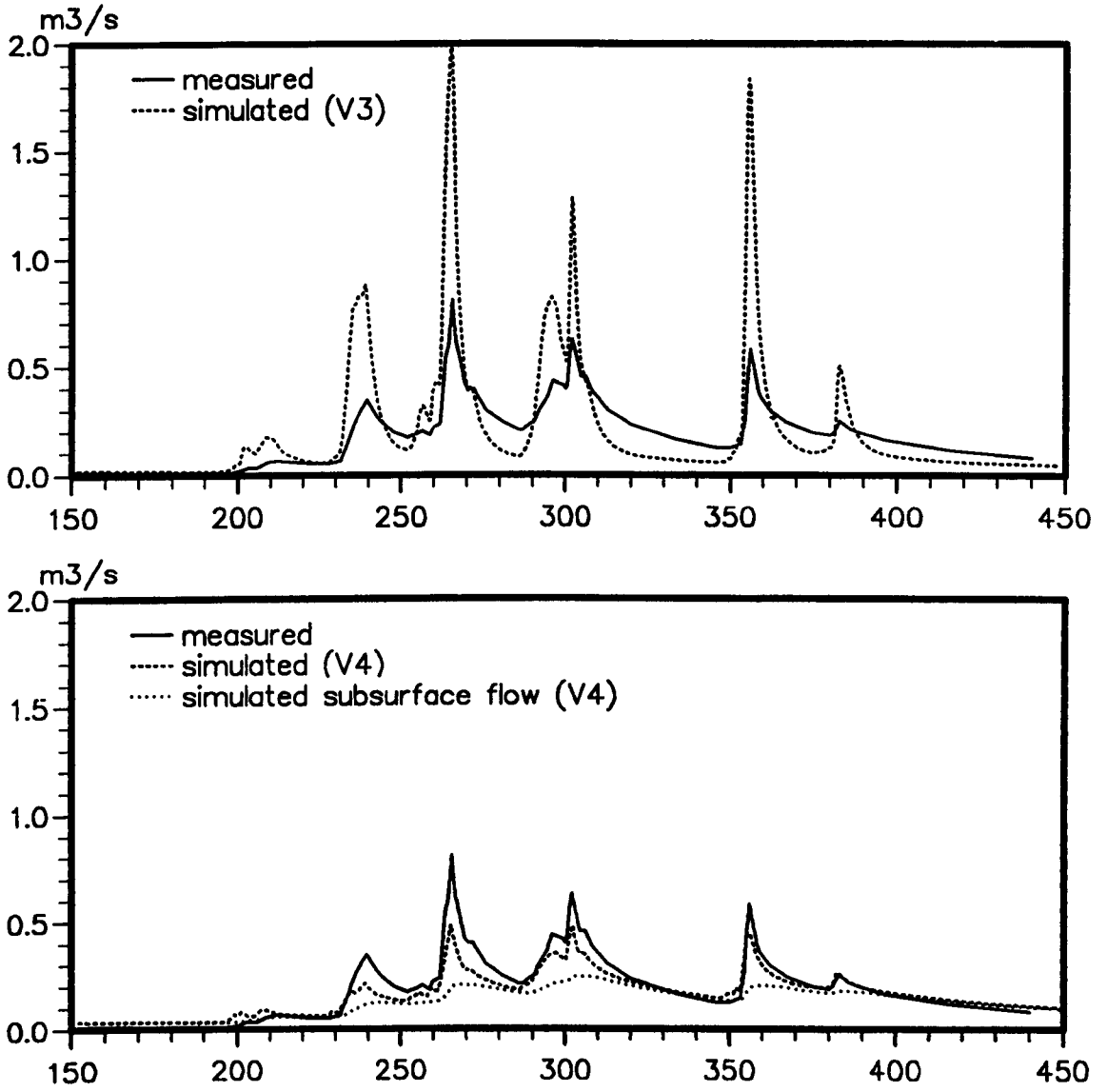

Figure 7.6 **Simulated and observed discharge for a sequence of storms during February 1968 for the Rimbaud catchment**

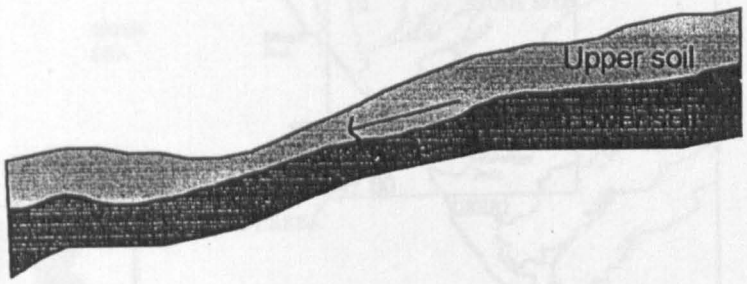

Figure 7.7 Schematic cross-section of soils for the Rimbaud catchment

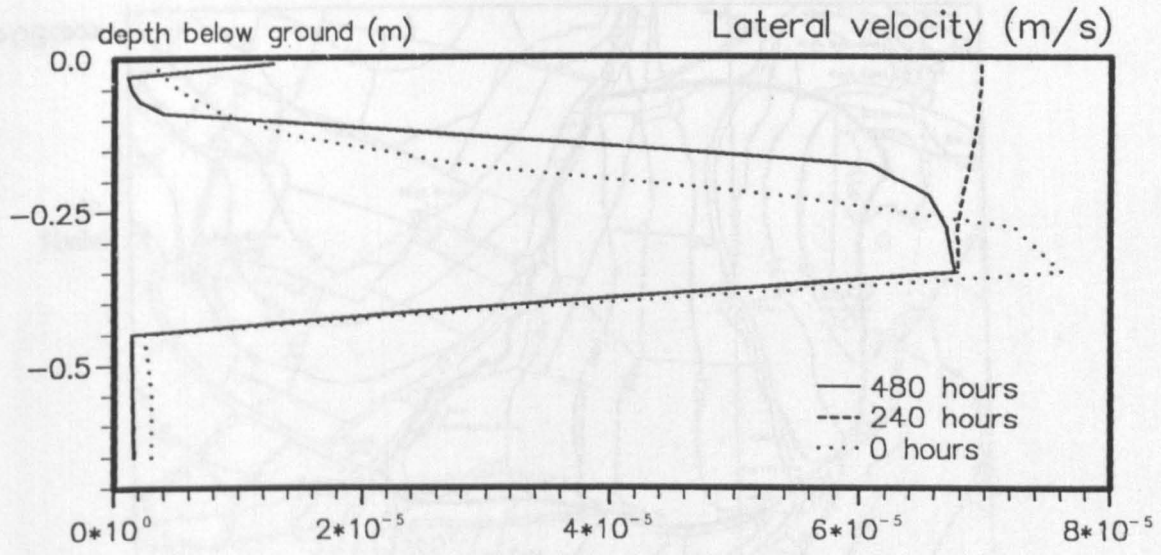

Figure 7.8 Lateral velocities at location A in Fig 7.3 for the Rimbaud catchment

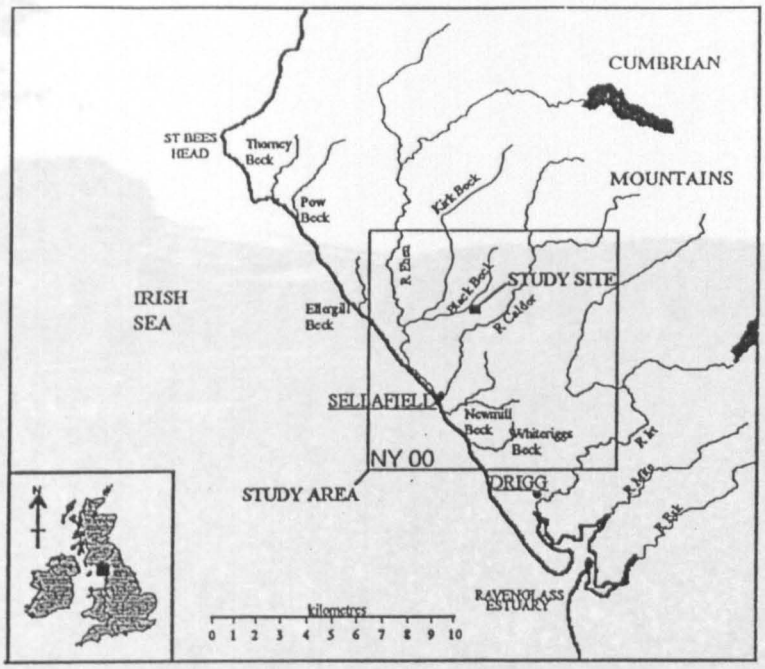

Figure 7.9 Location map for the Robertgate experimental site

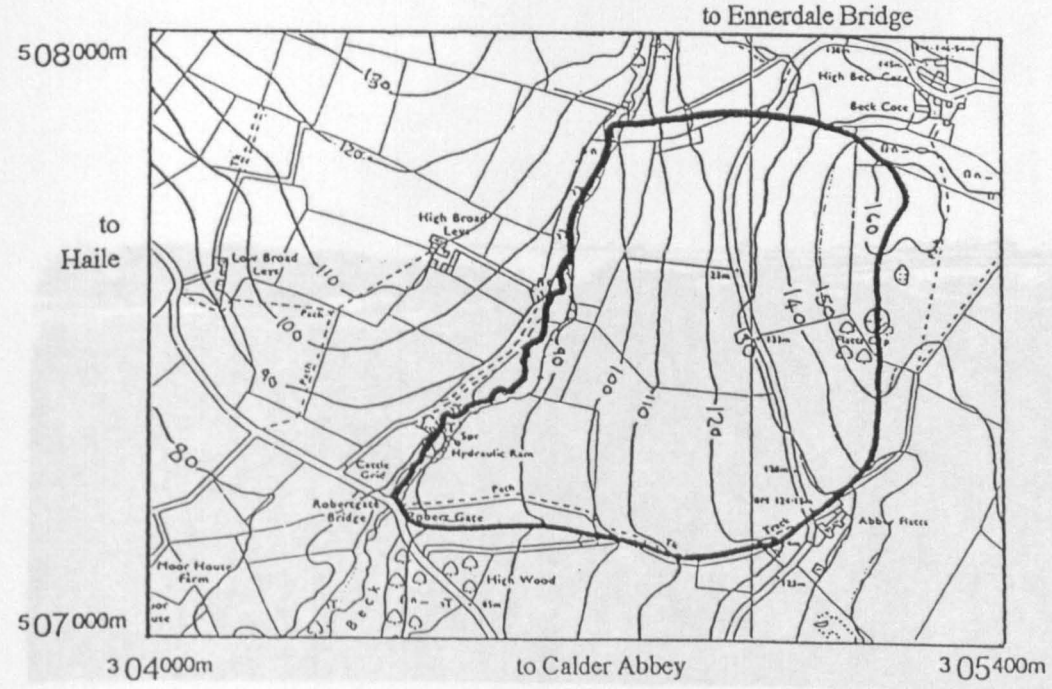

Figure 7.10 Map of the Robertgate experimental site

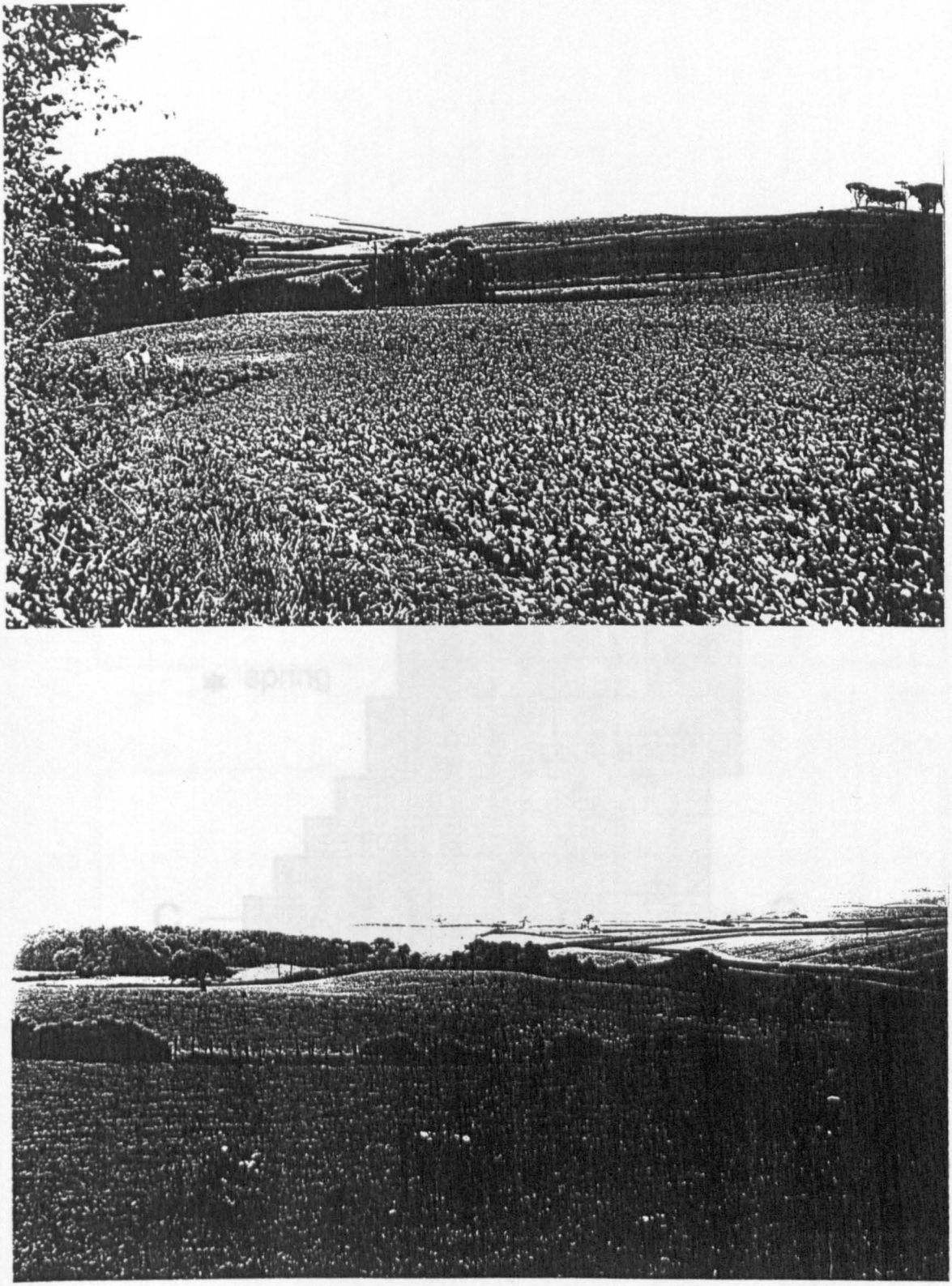

Figure 7.11 Photographs of the Robertgate experimental site

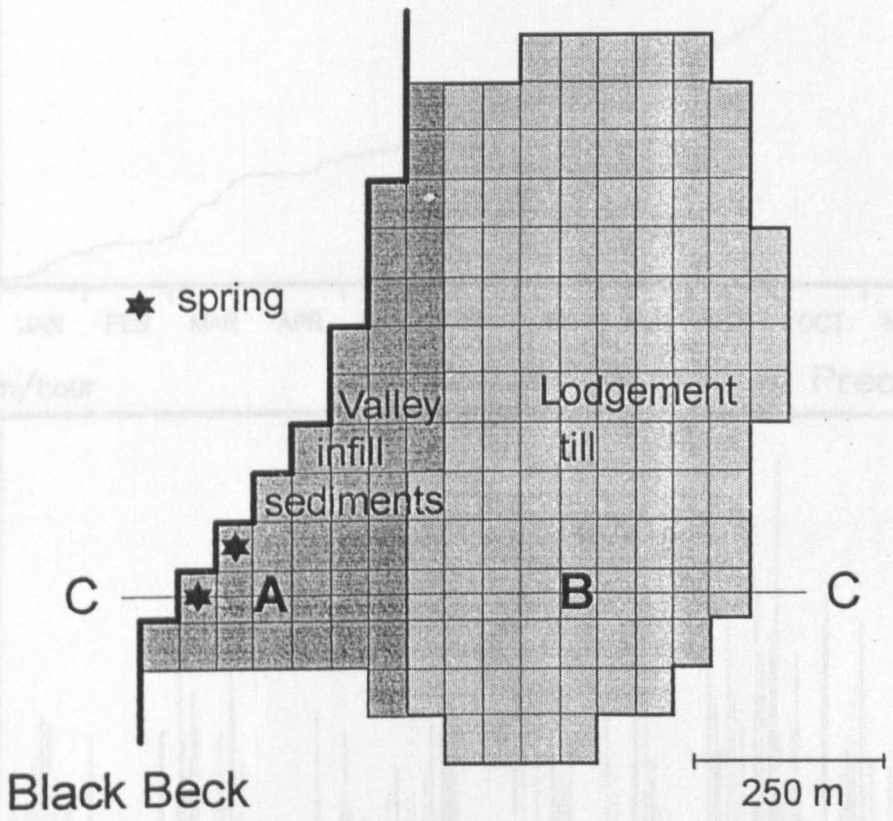

Figure 7.12 **Geological distribution and locations of springs, cross-sections and time-series plots for the Robertgate experimental site**

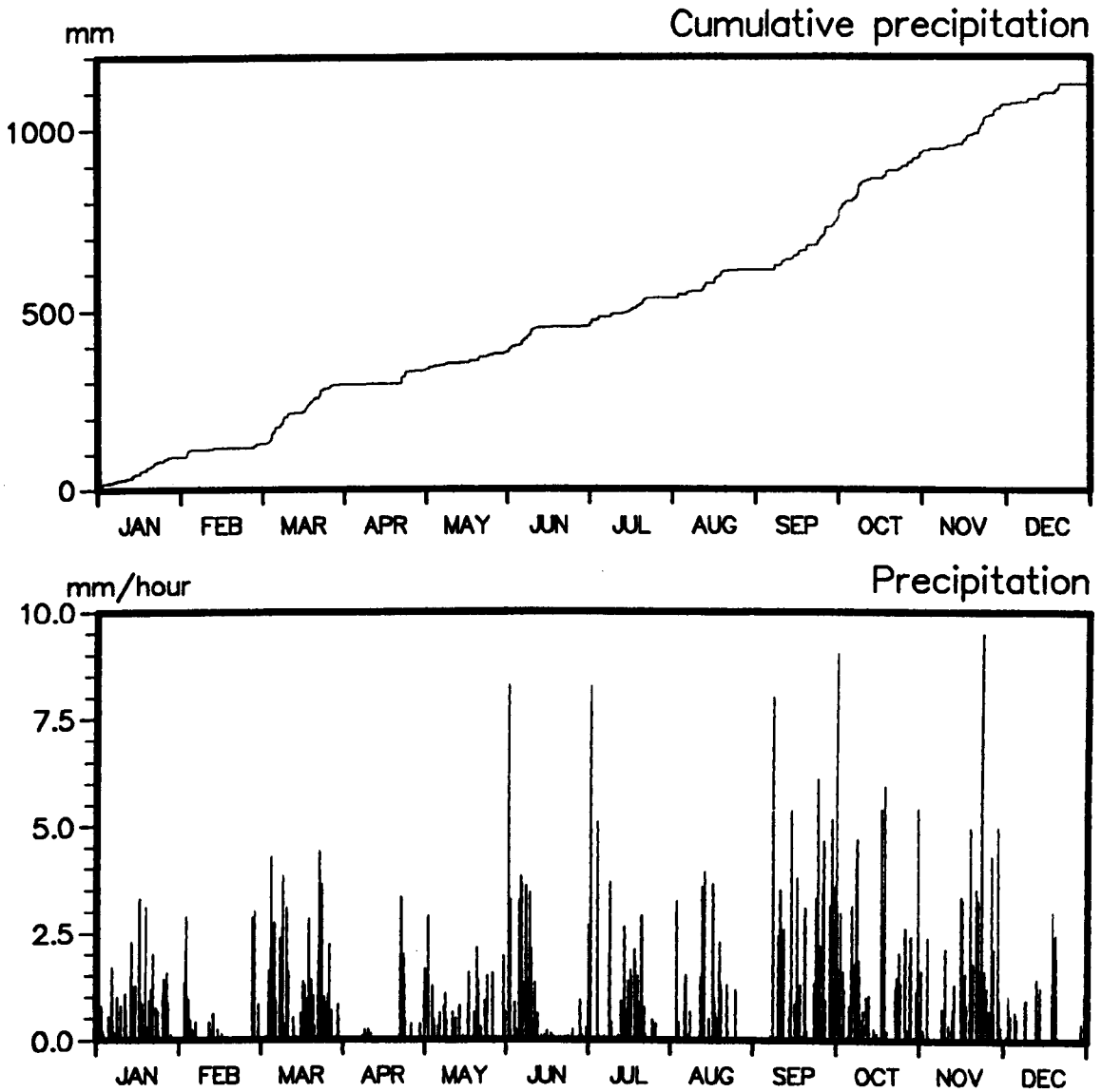

Figure 7.13 Precipitation data for the Robertgate simulations

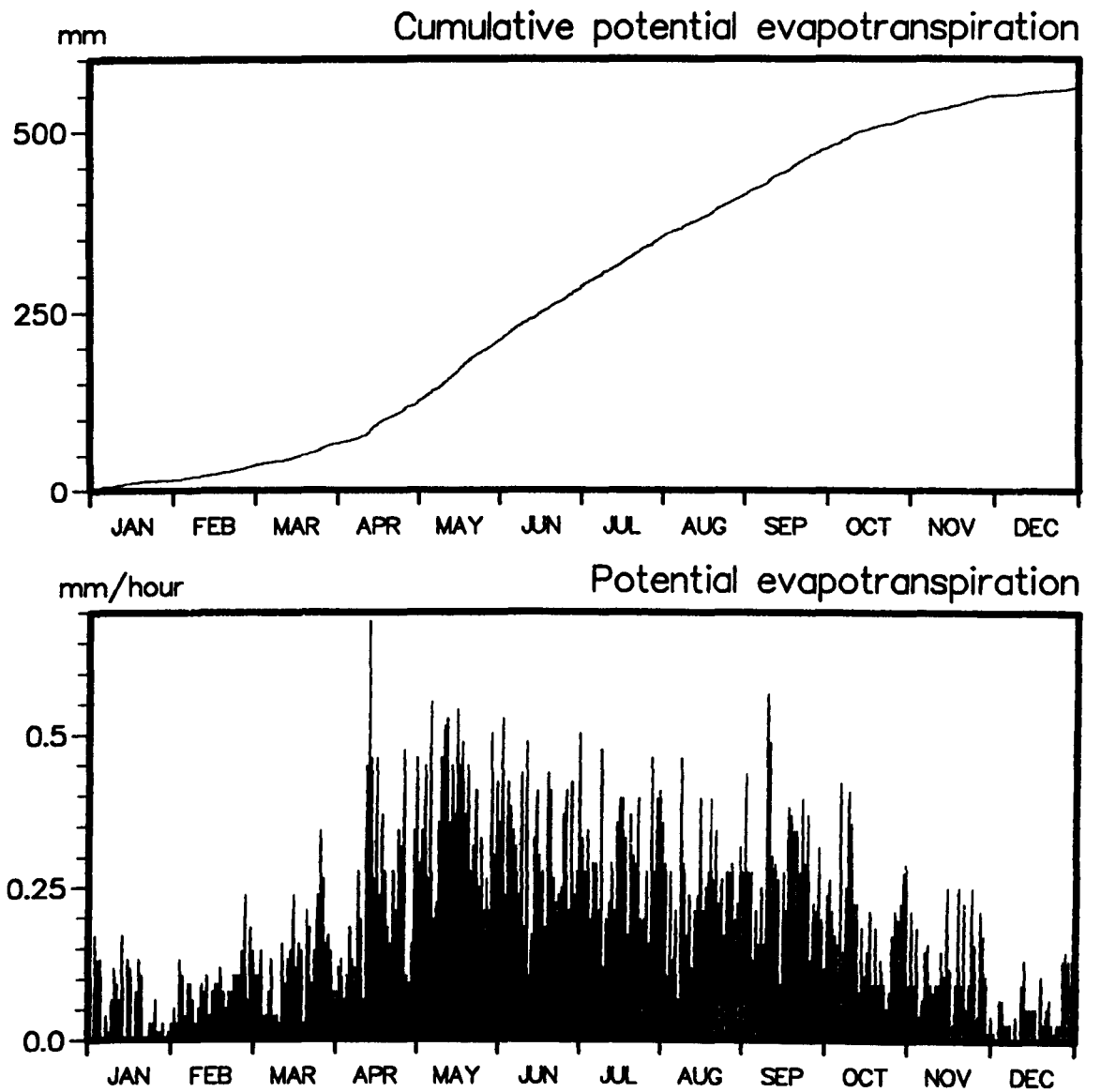

Figure 7.14 Potential evapotranspiration data for the Robertgate simulations

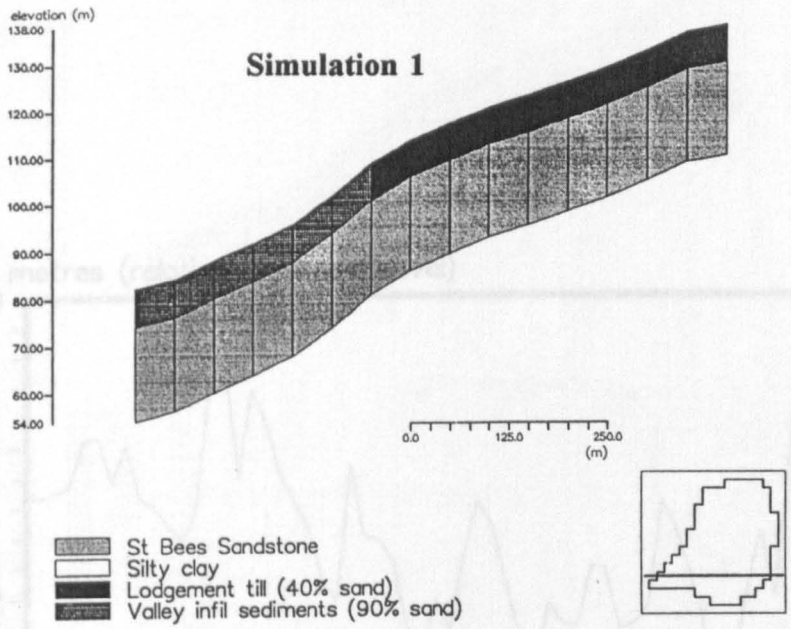

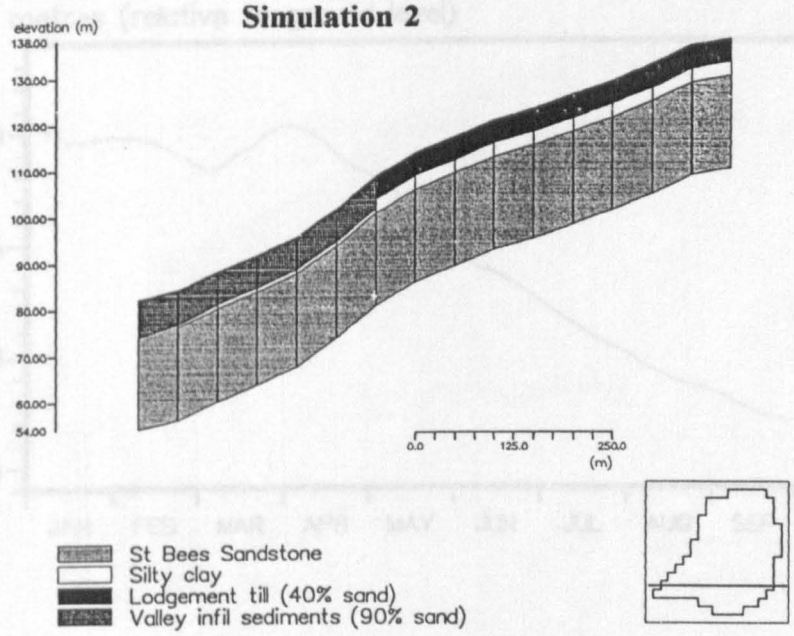

Figure 7.15 Cross-section of soils and geology (through C-C in Fig. 7.12) for the Robertgate simulations

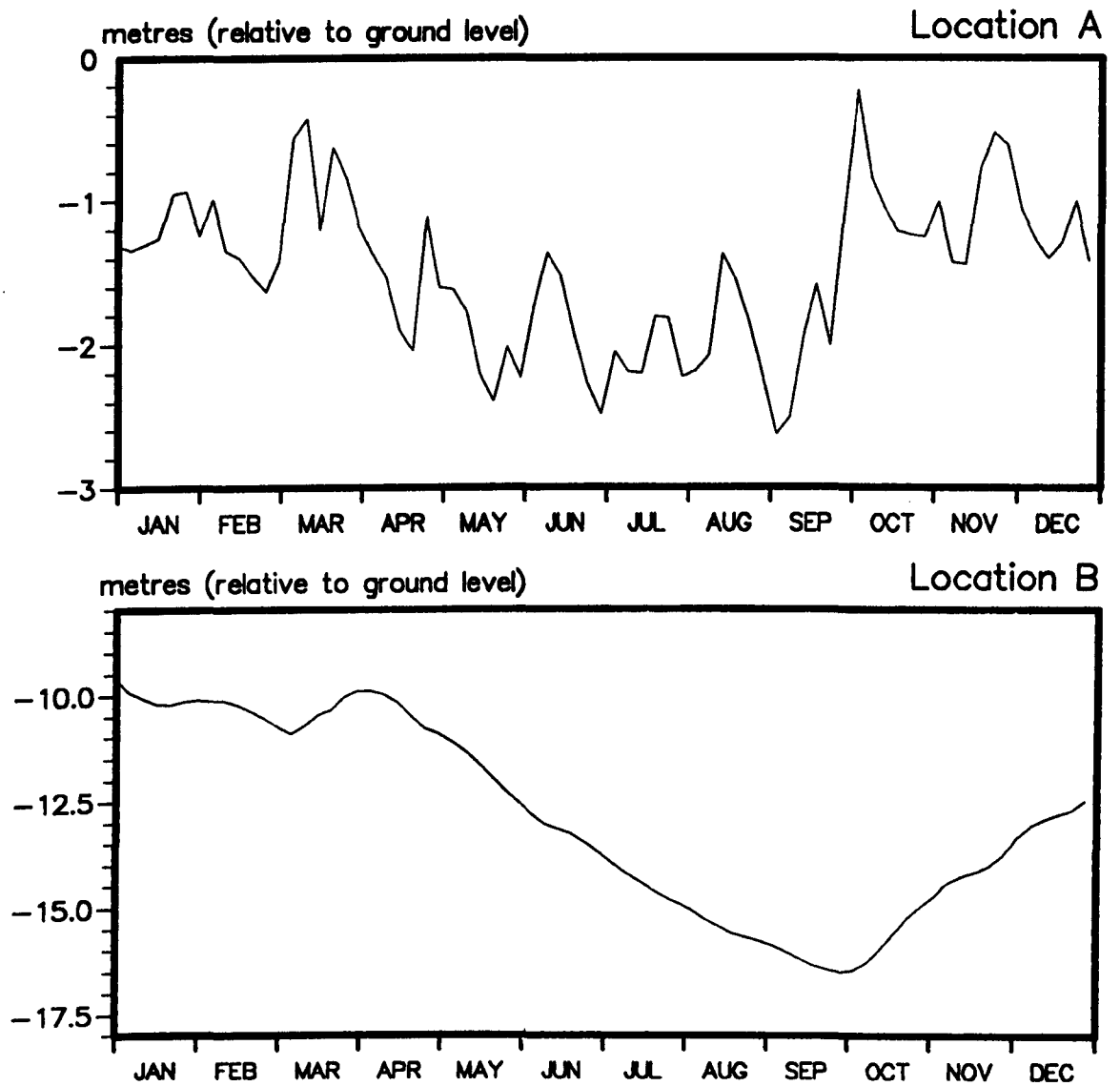

Figure 7.16 Phreatic surface level response to precipitation and lateral drainage at locations A and B in Fig. 7.12 for the Robertgate simulation 2

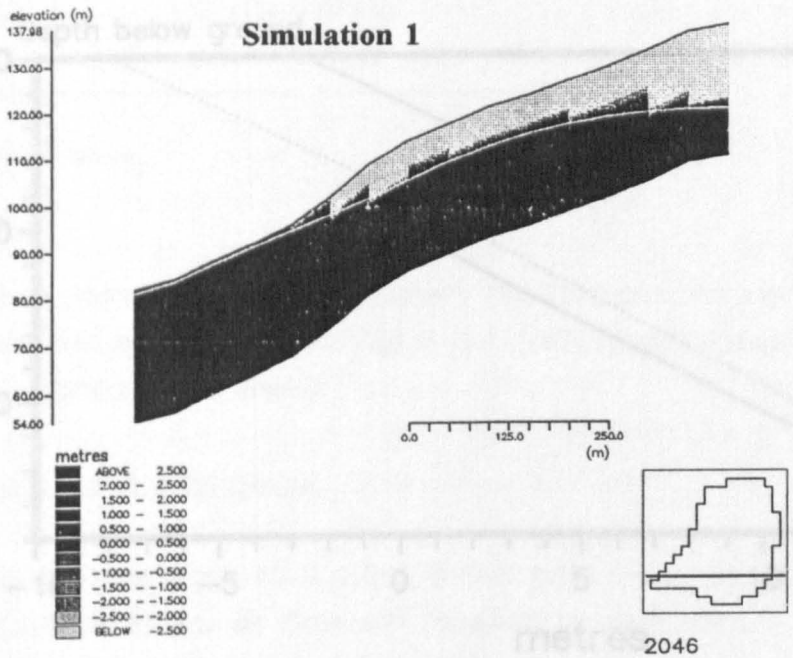

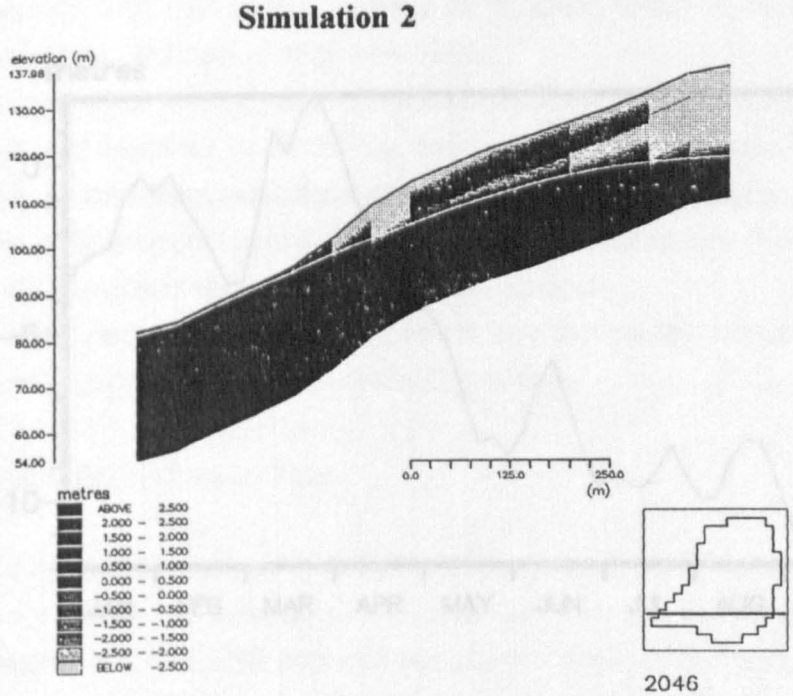

Figure 7.17 Cross-section of pressure potentials (through C-C in Fig. 7.12) at time 2046 hours for the Robertgate simulations

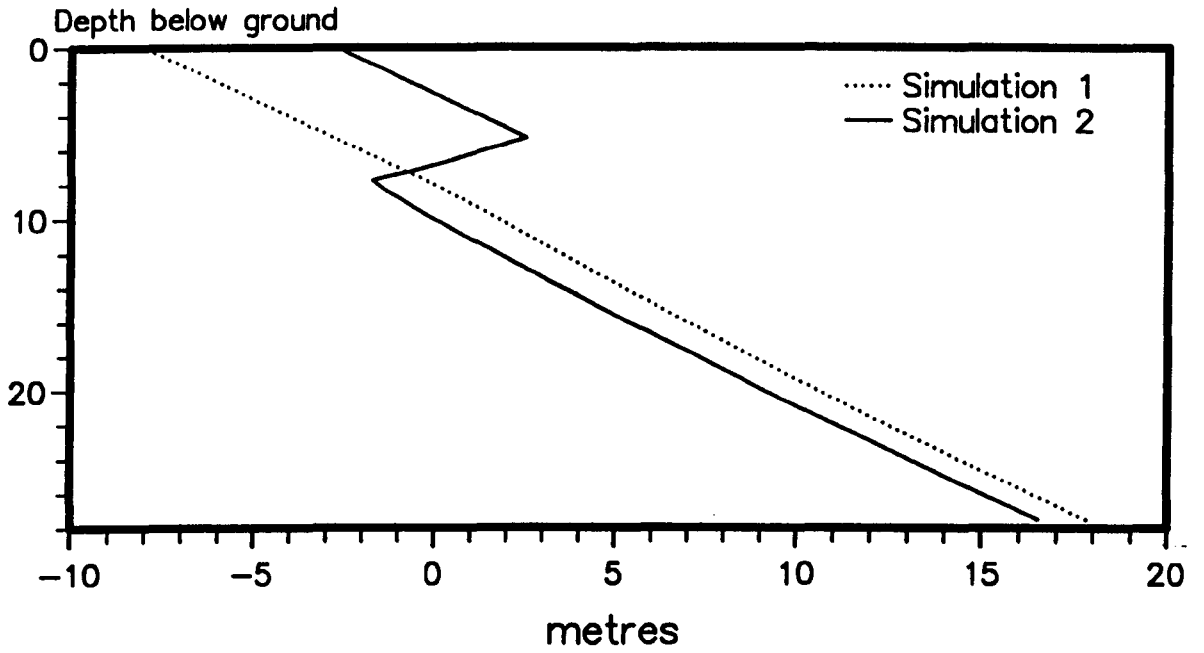

Figure 7.18 **Plot of pressure potential versus depth at location B in Fig. 7.12 at time 2046 hours for the Robertgate simulations**

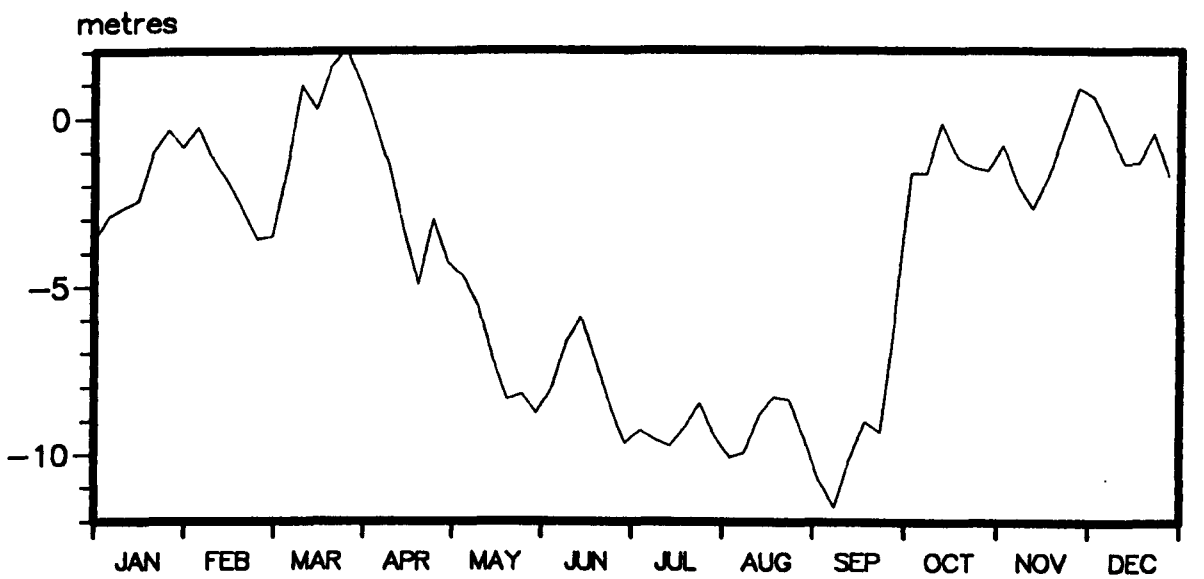

Figure 7.19 **Plot of pressure potential time-series at location B in Fig. 7.12 at 4.5 metres below ground for the Robertgate simulation 2**

CHAPTER 8 CONCLUSIONS

8.1 Conclusions

The following conclusions have been drawn from literature reviews and experience in the development and application of the VSS model (further detailed conclusions are contained in individual chapters of this thesis).

Basis for the model development

- Lateral flows in perched aquifers, surface soils, and in the unsaturated zone can have significant effects on flow and transport in catchments. These flows are often neglected in numerical modelling studies.
- There are several different mechanisms for streamflow generation in catchments, including partial source and contributing areas, baseflow, interflow, and groundwater ridging; these occur and interact in different ways at different places within a catchment, and may change over time.
- Near-channel conditions are important for catchment scale modelling.
- The best approach to modelling these many different effects is through the use of a fully three-dimensional variably-saturated physically-based model.
- The only proven mathematical basis for describing the flow in variably-saturated porous media is the extended Richards equation.
- A wide range of boundary conditions and source/sink terms must be defined for a general purpose subsurface modelling system.

Model capabilities and algorithms

- The integrated structure of SHETRAN has provided a suitable framework for building the VSS model; boundary conditions for VSS are provided by other SHETRAN components, and VSS provides boundary conditions for the other components. The inclusion of VSS has significantly enhanced the capabilities of SHETRAN.
- The boundary conditions for the VSS model have included: ponded water, infiltration, and evaporation at the ground surface; transpiration; stream-aquifer interactions; seepage of groundwater at the ground surface and at stream channels; well abstraction;

spring discharges; and general prescribed flux, gradient, or head boundary conditions.

- An approach has been developed which allows for general stream-aquifer interactions, including the presence of a low permeability channel lining, and the existence of an unsaturated region below the stream channel.
- The flexible-geometry finite-difference mesh used in VSS provides a better capability for representing the structure of complex sequences of Quaternary deposits than traditional fixed-geometry meshes.
- The column-based solution algorithm is a feasible method for solving the extended Richards equation under the type of conditions for which VSS was designed.
- The adaptive convergence algorithm used in the numerical solution scheme for VSS is a simple and effective way to reduce computational effort in a simulation.
- The potential for improving simulation run times using parallel processing systems has been demonstrated. A method has been established for implementing future versions of the SHETRAN code on parallel processing systems.
- Simulations of integrated surface and fully three-dimensional variably-saturated subsurface flow and transport using timesteps of about one hour have been run over periods of several decades; this represents the current state-of-the-art in physically-based catchment modelling.

Verification, validation, and application

- The results of the verification tests for VSS have demonstrated the abilities of SHETRAN to solve the underlying equations accurately for one-dimensional tests, and to provide physically reasonable simulations of flow and transport under complex geological conditions.
- The simulations of two very different small catchments and hillslopes have provided further confidence in the performance of the VSS model as part of SHETRAN V4.

8.2 Areas for further research

The development of the VSS model, and its integration into SHETRAN, forms part of a long-term plan of development, testing, and application of SHETRAN. As SHETRAN is used for a wide range of applications under several research programmes in countries around the world, all development and related work is undertaken under a quality assurance system, and development and testing is carefully planned with the long-term goals in mind. This thesis

can therefore be viewed as consisting of a synthesis of current understanding of certain catchment response mechanisms, and the development of a powerful tool for hydrological analysis and prediction. Although the model has already been verified against analytical solutions for simple cases, and has been applied to a catchment and an experimental hillslope, further validation tests and applications are planned as part of the long term SHETRAN programme, and new understanding of the processes of catchment response will continue to be incorporated into the SHETRAN. This further work falls into three main areas:

i) testing and validation;
ii) application to environmental problems; and
iii) further development of the modelling system.

Some of the areas of work which are already in progress, and my views on the most important issues to be addressed in further development of the modelling system, are briefly discussed below.

Validation of flow and transport at the plot scale

During the development of the VSS model, experimental field plots in the Quaternary drift deposits of west Cumbria have been instrumented and monitored by the Centre for Research into Environmental Systems and Statistics (CRES), Lancaster University, in a collaborative project designed with the specific aim of validating SHETRAN V4 including VSS. The data sets from this field study were not available in time for inclusion in this thesis; the validation exercise, which will be a rigorous examination of the internal flow and transport mechanisms in the model using a weakly sorbed tracer ($CuCl_3$) and a strongly sorbed tracer ($LaCl_3$) will commence in 1996.

Field and modelling investigations into mechanisms of groundwater discharge

The preliminary simulations for the Robertgate experimental site reported in Section 7.3 form part of an integrated field and modelling programme which is designed to improve understanding of stream-aquifer interaction and groundwater discharge in west Cumbria. This programme will involve selection and instrumentation of a field site (partly based on the results of these preliminary simulations), and a further programme of modelling using SHETRAN V4.

Other applications

SHETRAN V4 is being used to simulate radionuclide migration from subsurface sources in hypothetical catchments under boreal and temperate climates for UK Nirex Ltd., as supporting research for post-closure risk assessment studies for a potential low and intermediate radioactive waste repository near Sellafield, west Cumbria, UK. Simulations of flow and transport in a hypothetical catchment under a boreal climate over a period of thirty years have already been completed using SHETRAN V4 as part of this programme.

SHETRAN V4 will also become the standard simulation tool used in a wide range of studies within the Water Resource Systems Research Unit (WRSRU) at the University of Newcastle upon Tyne, and at other organisations with which WRSRU have formed collaborative research projects. These projects make use of the particular strength of SHETRAN in simulating integrated subsurface and surface catchment responses.

Improved process representation

The main areas where further work on basic processes is likely to be most fruitful for the application of VSS to a wide range of different types of catchment are:

1. macropores, especially for hillslope scale studies with shallow soils;
2. mesh refinement;
3. representation of sub-grid scale processes.

The importance of macropore flow (discussed in Section 3) is now generally recognised amongst the hydrological community. Macropores can be important both in the unsaturated zone, where they provide a route for fast recharge and for contaminant movement (bypassing much of the soil matrix), and in the saturated zone, where rapid runoff through shallow perched horizons can be a significant contributor to stormflow. Although macropore flow was considered to be a secondary issue from the perspective of this thesis, it is undoubtedly a significant factor in streamflow generation, and further research and model development in this area is probably the next essential step in the continuing development of SHETRAN.

The implementation of grid refinement would allow better representation of areas of a catchment where small-scale dynamics operate. These include riparian and groundwater discharge areas, where the concept of variable contributing areas may be useful, and areas

near to point sources of contaminant, where numerical dispersion in the subsurface could be reduced by a smaller mesh size. The use of a more flexible grid system would also allow larger catchments to be modelled efficiently, by increasing the mesh size in areas where soils and vegetation can be treated as homogeneous. The design of the program structure of VSS could be adapted relatively easily to a quadrature type of grid refinement, where each element can be subdivided into four elements, and each of these can again be subdivided into four, and so on.

An adequate representation of sub-grid scale processes in a variably-saturated subsurface model is a much more difficult proposition. The problem of how to represent natural heterogeneity at all scales is currently being hotly debated in the hydrological community, but is a topic in its infancy. Given the lack of any comprehensive and accepted theory, and the need to develop a practical fully working modelling system, this subject was not discussed at length in this thesis, but remains a subject for future research.

Numerical algorithms

An adaptive convergence algorithm has already been implemented for the VSS model, and tested. In addition, the VSS code structure was designed so that, potentially, the column iteration algorithm could adapt dynamically to the rates of convergence in different parts of the column. For example, this could be used to allow most iterations to occur in the unsaturated region where there is non-linearity in the governing equations, and fewer iterations in the saturated region. This could potentially result in a significant reduction in simulation times for certain cases (for example, where a deep aquifer system is overlain by a relatively thin unsaturated zone). This was not, however, explored in the studies reported in this thesis.

Parallel processing

The speed-up which can be obtained by parallelising SHETRAN at a coarse level, running the flow and contaminant components in parallel, has already been demonstrated for SHETRAN V3. The same approach (and the same parallel code, with only minor modifications to allow for changed common block variables) can be implemented for SHETRAN V4.

The numerical algorithms and the code structure for the VSS component of SHETRAN V4 were designed with the potential fine-grain parallelisation of the code in mind, based on

experience gained with the parallelisation exercise of SHETRAN V3. For VSS, the code involves a sweep over all columns, with each column being solved separately (within the outer iteration loop) by a call to a single subroutine with clearly defined variables in identifiable common blocks. The links between columns depend upon current values (within the outer iteration) of potentials for all adjacent columns; a farming approach could therefore be implemented in which columns are solved in parallel, providing a suitable ordering algorithm can be defined so that the column solver uses the most up to date values of pressure potential from the adjacent columns.

8.3 ACKNOWLEDGEMENTS

The work described in this thesis was carried out while being funded by UK Nirex Ltd.

I would like to thank my colleagues in the Water Resource Systems Research Unit, University of Newcastle upon Tyne, for their help and support during this work. In particular I would like to mention my supervisor, Professor Enda O'Connell, and John Ewen, Steve Anderton, and Greg O'Donnell, with whom I have worked over a period of several years on the development and application of SHETRAN. I would also like to thank the reviewers of this thesis, especially Mike Thorne, who have made many useful comments; and S.G. Seo who assisted with the parallel implementation of SHETRAN V3.

CHAPTER 9 REFERENCES

Abbott, M.B., Bathurst, J.C, Cunge, J.A., O'Connell, P.E. and Rasmussen, J. (1986a). An introduction to the European Hydrological System - Système Hydrologique Européen, "SHE", 1: History and philosophy of a physically-based, distributed modelling system. J. Hydrol., 87, 45-59.

Anderson, M.G. and Burt, T.P. (1990). Subsurface runoff. In: *Process Studies in Hillslope Hydrology* [M.G. Anderson and T.P. Burt, Eds.], J. Wiley. pp 365-400.

Averjanov, S.F. (1950). About permeability of subsurface soils in case of complete saturation. Eng. Collect., 7.

Barenblatt, G.I., Zheltov, Iu.P. and Kochina, I.N. (1960). Basic concepts in the theory of seepage of homogeneous liquids in fissured rocks [strata]. PPM Soviet Appl. Math. Mech. (English translation), 24, 1286-1303.

Barker, J.A. (1990). Transport in fractured rock. In: *Applied Groundwater Hydrology: A British Perspective* [R.A. Downing and W.B. Wilkinson, Eds.], Clarendon Press. pp 199-216.

Barker, J.A. and Herbert, R. (1992a). Hydraulic tests on well screens. Appl. Hydrogeology, 0/92, 7-19.

Barker, J.A. and Herbert, R. (1992b). A simple theory for estimating well losses with application to test wells in Bangladesh. Appl. Hydrogeology, 0/92, 20-31.

Bathurst, J.C. (1986). Sensitivity analysis of the Système Hydrologique Européen for an upland catchment. J. Hydrol., 87, 103-123.

Bathurst, J.C. and O'Connell, P.E. (1992). Future of distributed modelling: The Système Hydrologique Européen. Hydr. Proc., 6, 265-277.

Bear, J. (1993). Modeling flow and contaminant transport in fractured rocks. In: *Flow and Contaminant Transport in Fractured Rock* [J. Bear, C-F. Tsang, and G. de Marsily, Eds.], Academic Press.

Bear, J. and Verruijt, A. (1987). *Modelling Groundwater Flow and Pollution*. D. Reidel.

Beisson, T. (1985). Etude des écoulements sur le bassin versant du Réal Collobrier - Modelisation pluie-débit. Mémoire de 3ème année, CEMAGREF, Aix-en-Provence, France.

Bennett, G.D., Kontis, A.L. and Larson, S.P. (1982). Representation of multiaquifer well effects in three-dimensional ground-water flow simulation. Ground Water, **20**, 334-341.

Berkowitz, B., Bear, J. and Braester, C. (1988). Continuum models for contaminant transport in fractured porous formations. Water Resour. Res., **24**, 1225-1236.

Beven, K. (1981). Kinematic subsurface stormflow. Water Resour. Res., **17**, 1419-1424.

Beven, K. (1989). Interflow. In: *Unsaturated Flow in Hydrological Modelling* [H.J. Morel-Seytoux, Ed.], D. Reidel. pp 191-219.

Beven, K.J. and Clarke, R.T. (1986). On the variation of infiltration into a homogeneous soil matrix containing a population of macropores. Water Resour. Res., **22**, 383-388.

Beven, K. and Germann, P. (1982). Macropores and water flow in soils. Water Resour. Res., **18**, 1311-1325.

Bibby, R. (1981). Mass transport of solutes in dual-porosity media. Water Resour. Res., **17**, 1075-1081.

Binley, A. (1992). Exploiting parallelism in finite element models of flow in variably saturated porous media. In: *Computational Methods in Water Resources IX. Vol. 1: Numerical Methods in Water Resources* [T.F. Russell et al., Eds.], Elsevier. pp 687-694.

Black, J.H., Martin, B.A., Brightman, M.A., Robins, N.S. and Barker, J.A. (1981). The geology and hydrogeology of West Cumbria: Report No. ILWGDS(81)P28. Institute of Geological Sciences Environmental Protection Unit Report No. WE/81/20, Harwell, UK (Report available from British Geological Survey, Keyworth, UK).

Brassington, R. (1988). *Field Hydrogeology*. Open University Press.

Bredehoeft, J.D. and Pinder, G.F. (1970). Digital analysis of areal flow in multiaquifer groundwater systems: a quasi three-dimensional model. Water Resour. Res., 6, 883-888.

Brock, R.R. (1990). Multiple perched groundwater mounds. Hydrosoft, 3, 133-147.

Buckingham, E. (1907). Studies on the movement of soil moisture. USDA Bur. of Soils Bull. 38.

Cacas, M.C., Ledoux, E., de Marsily, G., Tillie, B., Barbreau, A., Durand, E., Feuga, B. and Peaudecerf, P. (1990). Modeling fracture flow with a stochastic discrete fracture network: Calibration and validation 1. The flow model. Water Resour. Res., 26, 479-489.

Carslaw, H.S. and Jaeger, J.C. (1959). *Conduction of Heat in Solids, 2nd ed.*, Oxford University Press.

Celia, M.A., Bouloutas, E.T. and Zarba, R.L. (1990). A general mass-conservative numerical solution for the unsaturated flow equation. Water Resour. Res., 26, 1483-1496.

Cheng, A. H-D. and Ou, K. (1989). An efficient Laplace transform solution for multiaquifer systems. Water Resour. Res., 25, 742-748.

Chorley, R.J. (1978). The hillslope hydrological cycle. In: *Hillslope Hydrology* [M.J. Kirkby, Ed.], J. Wiley. pp 1-42.

Crebas, J.I., Gilding, B.H. and Wesseling, J.W. (1984). Coupling of groundwater and open-channel flow. J. Hydrol., 72, 307-330.

Dagan, G. (1987). Theory of solute transport by groundwater. Ann. Rev. Fluid Mech., 19, 183-215.

Demange, Ph. (1985). Bassin d'investigation du Réal Collobrier, bassin versant du Haut Rimbaud. Mémoire de D.E.A., CEMAGREF, Aix-en-Provence, France.

Denmead, O.T. and Shaw, R.H. (1962). Availability of soil water to plants as affected by soil moisture content and meteorological conditions. Agronomy Journal, 54, 385-390.

DM2E (1994). Simulating impacts of vegetation loss using the SHETRAN water flow and sediment transport modelling system. Unpubl. Rep., DM2E/PR/9412/4, Water Resource Systems Research Unit, Dept. of Civil Eng., University of Newcastle-upon-Tyne, UK.

Dunne, T. and Black, R.D. (1970). Partial area contributions to storm runoff in a small New England watershed. Water Resour. Res., **6**, 1296-1311.

Dykhuizen, R.C. (1990). A new coupling term for dual-porosity models. Water Resour. Res., **26**, 351-356.

Ehlig, C. and Halepaska, J.C. (1976). A numerical study of confined-unconfined aquifers including effects of delayed yield and leakage. Water Resour. Res., **12**, 1175-1183.

Englund, J.O. (1986). Spring characteristics and hydrological models of catchments: A case study from Åstdalen, S.E. Norway. Nordic Hydr., **17**, 1-20.

Engman, E.T. (1986). Roughness coefficients for routing surface runoff. Proc. Am. Soc. Civ. Engrs., J. Irrig. Drain. Engrg., **112**, 39-53.

Ewen, J. (1990). Basis for the subsurface contaminant migration components of the catchment water flow, sediment transport, and contaminant migration modelling system SHETRAN-UK. NSS/R229, UK Nirex Ltd., Harwell, UK.

Ewen, J. (1991). Enhancement of the contaminant migration components of SHETRAN-UK since the publication of NSS/R229 and NSS/R232. Unpubl. Rep., WRSRU/TR/9109/21, Water Resource Systems Research Unit, Dept. of Civil Eng., University of Newcastle-upon-Tyne, UK.

Ewen, J. (1995). Contaminant transport component of the catchment modelling system SHETRAN. In: *Solute Modelling in Catchment Systems* [S.T. Trudgill, Ed.], J. Wiley. pp 417-441.

Ewen, J. and Parkin, G. (1996). Validation of catchment models for predicting land-use and climate change impacts: 1. Method. J. Hydrol., **175**, 583-594.

Fairhurst, C., Gera, F., Gnirk, P., Gray, M. and Stillborg, B. (1993). OECD/NEA *International STRIPA Project, Overview Volume 1: Executive Summary*. SKB, Stockholm, Sweden.

Faust, C.R., Guswa, J.H. and Mercer, J.W. (1989). Simulation of three-dimensional flow of immiscible fluids within and below the unsaturated zone. Water Resour. Res., **25**, 2449-2464.

Feddes, R.A., Kabat P., van Bakel, P.J.T., Bronswijk, J.J.B. and Halbertsma, J. (1988). Modelling soil water dynamics in the unsaturated zone - State of the art. J. Hydrol., **100**, 69-111.

Fogg, G.E. (1986). Groundwater flow and sand body interconnectedness in a thick, multiple-aquifer system. Water Resour. Res., **22**, 679-694.

Freeze, R.A. (1971). Three-dimensional transient saturated-unsaturated flow in a groundwater basin. Water Resour. Res., **7**, 347-366.

Freeze, R.A. (1972). Role of subsurface flow in generating surface runoff: 2. Upstream source areas. Water Resour. Res., **8**, 1272-1283.

Freeze, R.A. and Cherry, J.A. (1979). *Groundwater*. Prentice-Hall.

Frind, E.O. and Verge, M.J. (1978). Three-dimensional modeling of groundwater flow systems. Water Resour. Res., **14**, 844-856.

Gambolati, G., Sartoretto, F. and Uliana, F. (1986). A conjugate gradient finite element model of flow for large multiaquifer systems. Water Resour. Res., **22**, 1003-1015.

Gelhar, L.W. (1986). Stochastic subsurface hydrology from theory to applications. Water Resour. Res., **22**, 135S-145S.

George, R.J. and Conacher, A.J. (1993). Mechanisms responsible for streamflow generation on a small, salt-affected and deeply weathered hillslope. Earth Surf. Proc. and Landforms, **18**, 291-309.

Gerke, H.H. and van Genuchten, M.T. (1993). A dual-porosity model for simulating the preferential movement of water and solutes in structured porous media. Water Resour. Res., **29**, 305-319.

Gillham, R.W. (1984). The capillary fringe and its effects on water-table response. J. Hydrol., **67**, 307-324.

Green, W.H. and Ampt, G.A. (1911). Studies on soil physics, 1. The flow of air and water through soils. J. Agric. Sci., **4**, 1-24.

Haverkamp, R., Vauclin, M., Touma, J., Wierenga, P.J. and Vachaud, G. (1977). A comparison of numerical simulation models for one-dimensional infiltration. Soil. Sci. Soc. Am. J., **41**, 285-294.

Herbert, R. (1970). Modelling partially penetrating rivers on aquifer models. Ground Water, **8**, 29-36.

Herrera, I. (1970). Theory of multiple leaky aquifers. Water Resour. Res., **6**, 185-193.

Hewlett, J.D. and Hibbert, A.R. (1967). Factors affecting the response of small watersheds to precipitation in humid areas. In: *Proc. Int. Symp. on Forest Hydrology* [W.E. Sopper and W.H. Lull, Eds.], Pergamon Press. pp 275-290.

Hillel, D. (1980). *Fundamentals of Soil Physics.* Academic Press.

Hillel, D. (1987). Unstable flow in layered soils: A review. Hydr. Proc., **1**, 143-147.

Hills, R.G., Porro, I., Hudson, D.B. and Wierenga, P.J. (1989). Modeling one-dimensional infiltration into very dry soils. 1. Model development and evaluation. Water Resour. Res., **25**, 1259-1269.

Holmes, D.C. and Hall, D.H. (1980). The 1977-1979 geological and hydrogeological investigations at the Windscale Works, Sellafield, Cumbria. Institute of Geological Sciences Report 80/12 (Report available from British Geological Survey, Keyworth, UK).

Horton, R.E. (1933). The role of infiltration in the hydrologic cycle. Trans. Am. Geophys. Union, **14**, 446-460.

Hursh, J. (1936). Storm-water and adsorption. Trans. Am. Geophys. Union, **17**, 301-302.

Huyakorn, P.S., Lester, B.H. and Faust, C.R. (1983). Finite element techniques for modeling groundwater flow in fractured aquifers. Water Resour. Res., **19**, 1019-1035.

Huyakorn, P.S., Jones, B.G. and Andersen, P.F. (1986a). Finite element algorithms for simulating three-dimensional groundwater flow and solute transport in multilayer systems. Water Resour. Res., **22**, 361-374.

Huyakorn, P.S., Springer, E.P., Guvanasen, V. and Wadsworth, T.D. (1986b). A three-dimensional finite-element model for simulating water flow in variably saturated porous media. Water Resour. Res., **22**, 1790-1808.

Huyakorn, P.S. and Thomas, S.D. (1984). Techniques for making finite elements competitive in modeling flow in variably saturated porous media. Water Resour. Res., **20**, 1099-1115.

Jamieson, H. (1994). The characterisation of glacial sediments in the Sellafield region, to delineate large scale geological heterogeneity and identify potential contaminant flow paths. Unpubl. MSc thesis, Dept. of Civil Engineering, University of Newcastle-upon-Tyne, UK.

Jarvis, R.A., Bendelow, V.C., Bradley, R.I., Carroll, D.M., Furness, R.R., Kilgow, I.N.L. and King, S.J. (1984). *Soils and their use in Northern England*. Soil Survey of England and Wales, Bull. No. 10, Harpenden, Herts., UK.

Jaynes, D.B. (1990). Soil water hysteresis: models and implications. In: *Process Studies in Hillslope Hydrology* [M.G. Anderson and T.P.Burt, Eds.], J. Wiley. pp 93-126.

Jones, J.A.A. (1988). Modelling pipeflow contributions to stream runoff. Hydr. Proc., **2**, 1-17.

Journal, A.G., Deutsch, C. and Desbarats, A.J. (1986). Power averaging for block effective permeability. Paper SPE 15128, 56th California Regional Meeting of SPE, Soc. of Pet. Eng., Long Beach, USA.

Kruseman, G.P. and de Ridder, N.A. (1990). Analysis and evaluation of pumping test data. International Institute for Land Reclamation and Improvement Publ. No. 47, Wageningen, Netherlands.

Lekhov, M.V. (1986). Experimental model of a spring discharge on a slope. Wat. Resour., **12**, 513-521.

Lloyd, J.W. (1980). The importance of drift deposit influences on the hydrogeology of major British aquifers. Inst. Water Engineers and Scientists J., **34**, 346-356.

Lovelock, P.E.R. (1977). Aquifer properties of Permo-Triassic sandstones in the United Kingdom. Bull. Geol. Surv. G.B. No. 56.

Maguire, T.F. (1988). Transport of a non-aqueous phase liquid within a combined perched and water table aquifer system. In: *Proc. of the FOCUS Conf. on Eastern Regional Ground Water Issues, Sept. 1988, Stamford, Connecticut, USA.* pp 539-558.

Mangold, D.C. and Tsang, C. (1991). A summary of subsurface hydrological and hydrochemical models. Reviews of Geophysics, **29**, 51-79.

McCord, J.T. and Stephens, D.B. (1987). Lateral moisture flow beneath a sandy hillslope without an apparent impeding layer. Hyd. Proc., **1**, 225-238.

McDonnell, J.J., Owens, I.F. and Stewart, M.K. (1991). Case study of shallow flow paths in a steep zero-order basin. Wat. Resour. Bull., **27**, 679-685.

Mercer, J.W. and Faust, C.R. (1979). Geothermal reservoir simulation, 3: Application of liquid- and vapor-dominated hydrothermal modeling techniques to Wairakei, New Zealand. Water Resour. Res., **15**, 653-671.

Miles, J.C. (1985). The representation of flows to partially penetrating rivers using groundwater flow models. J. Hydrol., **82**, 341-355.

Miles, J.C. (1987a). The representation of flows to partially penetrating rivers from layered and anisotropic aquifers. J. Hydrol., **95**, 113-129.

Miles, J.C. (1987b). Simulating the interaction between groundwater and surface water. In: *British Hydrological Society Nat. Hydrol. Symp., Univ. of Hull., UK.* pp 13.1-13.8.

Milly, P.C.D (1988). Advances in modeling of water in the unsaturated zone. In: *Groundwater Flow and Quality Modelling* [E. Custodio, Ed.], Committee of U.S.A. Members of JAM, Tucson, Ariz., USA. pp 489-514.

Miyazaki, T. (1988). Water flow in unsaturated soil in layered slopes. J. Hydrol., **102**, 201-214.

Moench, A.F. (1984). Double porosity model for a fissured groundwater reservoir with fracture skin. Water Resour. Res., **20**, 831-846.

Molz, F.J. and Boman, G.K. (1993). A fractal-based stochastic interpolation scheme in subsurface hydrology. Water Resour. Res., 29, 3769-3774.

Montazer, P. and Wilson, W.E. (1984). Conceptual hydrologic model of flow in the unsaturated zone, Yucca Mountain, Nevada. USGS Water-Resources Investigations Report 84-4345, Lakewood, Colorado.

Moseley, F. (1978). *The Geology of the Lake District.* Yorkshire Geological Society Occasional Publ. No. 3.

Moseley, F. and Ahmed, S.M. (1967). Carboniferous joints in the north of England and their relation to earlier and later structures. Proc. Yorks. Geol. Soc., **36**, 61-90.

Murphy, J., Ridout, D. and McShane, B. (1988). *Numerical Analysis, Algorithms and Computation.* J. Wiley.

Narasimhan, T.N. and Witherspoon, P.A. (1977). Numerical model for saturated-unsaturated flow in deformable porous media, 1: Theory. Water Resour. Res., **13**, 657-664.

Neretnieks, I. and Rasmuson, A. (1984). An approach to modelling radionuclide migration in a medium with strongly varying velocity and block sizes along the flow path. Water Resour. Res., **20**, 1823-1836.

Neuman, S.P. (1988). Stochastic continuum representation of fractured rock permeability as an alternative to the REV and fracture network concepts. In: *Groundwater Flow and Quality Modelling* [E. Custodio, Ed.], Committee of U.S.A. Members of JAM, Tucson, Ariz., USA. pp 331-362.

Neuman, S.P. and Witherspoon, P.A. (1969). Theory of flow in a confined two-aquifer system. Water Resour. Res., 5, 803-816.

Neuman, S.P., Preller, C. and Narasimhan, T.N. (1982). Adaptive explicit-implicit quasi three-dimensional finite element model of flow and subsidence in multiaquifer systems. Water Resour. Res., 18, 1551-1561.

Nielsen, D.R., van Genuchten, M.Th. and Biggar, J.W. (1986). Water flow and solute transport processes in the unsaturated zone. Water Resour. Res., 22, 89S-108S.

Nirex (1992a). The geology and hydrogeology of Sellafield: March 1992 interpretation. Report 263 [U. McL Michie, Ed.], UK Nirex Ltd., Harwell, UK.

Nirex (1992b). Sellafield hydrogeology: Report of the hydrogeology joint interpretation team. Report 268 [J.H. Black, Ed.], UK Nirex Ltd., Harwell, UK.

Obradovic, M.M. and Sklash, M.G. (1986). An isotopic and geochemical study of snowmelt runoff in a small Arctic watershed. Hydr. Proc., 1, 15-30.

Paniconi, C., Aldama, A.A. and Wood, E.F. (1991). Numerical evaluation of iterative and noniterative methods for the solution of the nonlinear Richards equation. Water Resour. Res., 27, 1147-1163.

Pankow, J.F., Johnson, J.P., Hewetson, J.P. and Cherry, J.A. (1986). An evaluation of contaminant migration patterns at two waste disposal sites on fractured porous media in terms of the equivalent porous medium (EPM) model. J. Cont. Hydrol., 1, 65-76.

Pantin, H.M. (1977). Quaternary sediments of the northern Irish Sea. In: *The Quaternary History of the Irish Sea*, Geol. J. Special Issue No. 7 [C. Kidson and M.J. Tooley, Eds.]. pp 27-54.

Parkin, G., O'Donnell, G., Ewen, J., Bathurst, J.C. and O'Connell, P.E. (1995). Validation of SHETRAN-UK for a Mediterranean catchment. NSS/R378, UK Nirex Ltd., Harwell, UK.

Parkin, G., O'Donnell, G., Ewen, J., Bathurst, J.C., O'Connell, P.E. and Lavabre, J. (1996). Validation of catchment models for predicting land use and climate change impacts: 2. Case study for a Mediterranean catchment. J. Hydrol., 175, 595-613.

Patrick, C.K. (1978). Hydrogeology, Chapter 17. In: *The Geology of the Lake District*, Yorks. Geol. Soc. Occasional Publication No. 3 [F. Moseley, Ed.]. pp 250-261.

Peters, R.R. and Klavetter, E.A. (1988). A continuum model for water movement in an unsaturated fractured rock mass. Water Resour. Res., 24, 416-430.

Pettijohn, F.J. (1975). *Sedimentary Rocks (3rd Ed.)*. Harper and Row.

Philip, J.R. (1987). An analog for infiltration and unsaturated seepage. Eos Trans. AGU, 68, 153-154.

Premchitt, J. (1981). A technique in using integrodifferential equations for model simulation of multi-aquifer systems. Water Resour. Res., 17, 162-168.

Press, W.H., Teukolsky, S.A., Vetterling, W.T. and Lannery, B.P. (1992). *Numerical Recipes in FORTRAN: The Art of Scientific Computing*. Cambridge University Press.

Pritchett, J.W. and Garg, S.K. (1980). Determination of effective well block radii for numerical reservoir simulations. Water Resour. Res., 16, 665-674.

Pullan, A.J. (1990). The quasilinear approximation for unsaturated porous media flow. Water Resour. Res., 26, 1219-1234.

Ramm, D. and Chazan, D. (1980). A mixed numerical analytical method for groundwater flow simulation. Water Resour. Res., 16, 871-880.

Rathfelder, K. and Abriola, L.M. (1994). Mass conservative numerical solutions of the head-based Richards equation. Water Resour. Res., 30, 2579-2586.

Reeves, M. and Cranwell, R.M. (1981). User's manual for the Sandia Waste-Isolation Flow and Transport model (SWIFT) release 4.81 (US Nuclear Regulatory Commision). Sandia Report NUREG/CR-2324, SAND81-2516.

Reid, M.E. and Dreiss, S.J. (1990). Modelling the effects of unsaturated, stratified sediments on groundwater recharge from intermittent streams. J. Hydrol., **114**, 149-174.

Richards, L.A. (1931). Capillary conduction of liquids through porous mediums. Physics, **1**, 318-333.

Richardson, L.F. (1922). *Weather Prediction by Numerical Process*. Cambridge University Press.

Romeu, R.K. and Noetinger, B. (1995). Calculation of internodal transmissivities in finite difference models of heterogeneous porous media. Water Resour. Res., **31**, 943-959.

Ross, B. (1990). The diversion capacity of capillary barriers. Water Resour. Res., **26**, 2625-2629.

Rovey, C.E.K. (1975). Numerical model of flow in a stream-aquifer system. Colorado State University Hydrology Paper 74, Fort Collins, Colorado.

Sagar, B. and Runchal, A. (1982). Permeability of fractured rock: Effect of fracture size and data uncertainties. Water Resour. Res., **18**, 266-274.

Saxton, K.E., Rawls, W.J., Romberger, J.S. and Papendick, R.I. (1986). Estimating generalised soil-water characteristics from texture. Soil Sci. Soc. Am. J., **50**, 1031-1036.

Schwartz, F.W., Smith, L. and Crowe, A.S. (1983). A stochastic analysis of macroscopic dispersion in fractured media. Water Resour. Res., **19**, 1253-1265.

Seguin, B. (1977). Estimation de l'ETP en climat méditerranéen du sud-est de La France. La météorologie, **6**, 33-40.

Şen, Z. (1989). Volumetric approach to multiaquifer and horizontal fracture wells. ASCE J. Hydr. Eng., **115**, 1646-1666.

Sklash, M.G. (1990). Environmental isotope studies of storm and snowmelt runoff generation, Chapter 12. In: *Process Studies in Hillslope Hydrology* [M.G. Anderson and T.P. Burt, Eds.], J. Wiley. pp 401-435.

Sklash, M.G. and Farvolden, R.N. (1979). The role of groundwater in storm runoff. J. Hydrol., **43**, 45-65.

Smith, L. and Schwartz, F.W. (1984). An analysis of the influence of fracture geometry on mass transport in fractured media. Water Resour. Res., **20**, 1241-1252.

Smith, R.E. and Ferreira, V.A. (1989). Comparative evaluation of unsaturated flow methods in selected USDA simulation models. In: *Unsaturated Flow in Hydrologic Modelling* [H.J. Morel-Seytoux, Ed.], D. Reidel. pp 391-412.

Sposito, G. (1986). The "physics" of soil water physics. Water Resour. Res., **22**, 83S-88S.

Srivastava, R. and Yeh T.-C. J. (1991). Analytical solutions for one-dimensional, transient infiltration toward the water table in homogeneous and layered soils. Water Resour. Res., 27, 753-762.

Suttie, W. (1989). An integrated study of the hydrogeology of the coastal strip of the St. Bees sandstone aquifer west Cumbria. Unpublished MSc thesis, University College, London, UK.

Todd, D.K. (1980). *Groundwater Hydrology*. J. Wiley.

Torak, L.J. (1982). Modifications and corrections to the finite-difference model for simulation of three-dimensional ground-water flow. USGS Water Resources Investigations Rep. 82-4025.

Trescott, P.C. (1975). Documentation of finite-difference model for simulation of three-dimensional ground-water flow. USGS Open-File Report 75-438.

Trescott, P.C. and Larson, S.P. (1976). Documentation of finite-difference model for simulation of three-dimensional ground-water flow, supplement to Open-File Report 75-438. USGS Open-File Report 76-531.

Trotter, F.M., Hollingworth, S.E., Eastwood, T. and Rose, W.C.C. (1937). Gosforth District. Mem. Geol. Surv. UK, Sheet 37.

van Bakel, P.J.T. (1986). A systematic approach to improve the planning, design and operation of regional surface water management systems: a case study. Rep. 13, Inst. for Land and Water Management Research, Wageningen, Holland.

van Genuchten, M. Th. (1978). Numerical solutions of the one-dimensional saturated-unsaturated flow equation. Research Rep. 78-WR-09, Dept. of Civil Engineering, Princeton University.

van Genuchten, M. Th. (1980). A closed-form equation for predicting the hydraulic conductivity of unsaturated soils. Soil Sci. Soc. Am. J., **44**, 892-898.

van Genuchten, M. Th. and Nielsen, D.R. (1985). On describing and predicting the hydraulic properties of unsaturated soils. Ann. Geophys., **3**, 615-628.

Wang, J.S.Y. and Narasimhan, T.N. (1985). Hydrologic mechanisms governing fluid flow in a partially saturated, fractured, porous medium. Water Resour. Res., **21**, 1861-1874.

Warren, J.E. and Root, P.J. (1963). The behaviour of naturally fractured reservoirs. J. Soc. Petr. Eng., **9**, 245-255.

Warrick, A.W. (1991). Numerical approximations of Darcian flow through unsaturated soil. Water Resour. Res., **27**, 1215-1222.

Weir, G.J. (1989). Unsaturated vertical flows above a water table. Water Resour. Res., **25**, 55-60.

Wels, C., Taylor, C.H., Cornett, R.J. and Lazerte, B.D. (1991). Streamflow generation in a headwater basin on the Precambrian Shield. Hydr. Proc., **5**, 185-199.

Williams, G.M., Stuart, A. and Holmes, D.C. (1985). Investigation of the geology of the low-level radioactive waste burial site at Drigg, Cumbria. British Geological Survey report Vol. 17, No. 3. Keyworth, UK.

Woodford, C. (1992). *Solving Linear and Non-linear Equations*. Ellis Horwood Ltd., Chichester, UK.

Younger, P.L. (1990). Stream-aquifer systems of the Thames basin: Hydrogeology, geochemistry and modelling. Unpubl. Phd thesis, Dept. of Civil Eng., University of Newcastle-upon-Tyne.

Younger, P.L. (1993). Simple generalised methods for estimating aquifer storage parameters. Quart. J. Eng. Geol., **26**, 127-135.

Younger, P.L., Mackay, R. and Connorton, B.J. (1993). Streambed sediment as a barrier to groundwater pollution: Insights from fieldwork and modelling in the River Thames basin. J. Inst. Water and Env. Management, **7**, 577-587.

Zaidel, J. and Russo, D. (1992). Estimation of finite difference interblock conductivities for simulation of infiltration into initially dry soils. Water Resour. Res., **28**, 2285-2295.

Zaslavsky, D. and Sinai, G. (1981a). Surface hydrology: I - Explanation of phenomena. J. Hydraul. Div, Proc. ASCE, **107**, 1-16.

Zaslavsky, D. and Sinai, G. (1981b). Surface hydrology: II - Distribution of raindrops. J. Hydraul. Div, Proc. ASCE, **107**, 17-35.

Zaslavsky, D. and Sinai, G. (1981c). Surface hydrology: III - Causes of lateral flow. J. Hydraul. Div, Proc. ASCE, **107**, 37-52.

Zaslavsky, D. and Sinai, G. (1981d). Surface hydrology: IV - Flow in sloping, layered soil. J. Hydraul. Div, Proc. ASCE, **107**, 53-64.

Zaslavsky, D. and Sinai, G. (1981e). Surface hydrology: V - In-surface transient flow. J. Hydraul. Div, Proc. ASCE, **107**, 65-93.

APPENDIX A IMPLEMENTATION OF SHETRAN ON PARALLEL PROCESSING SYSTEMS

A.1 Introduction

One of the main limiting factors for the use of SHETRAN version 3 or version 4 is the high computational cost of solving the governing equations over a three-dimensional domain. There is a high computational cost associated, in particular, with modelling water flow and the subsurface movement of contaminants. With this in mind, there were two aims to the work described in this study:

a) to assess the performances of the Network LINDA and transputer parallel processing systems, as part of a feasibility study for the new subsurface flow component for SHETRAN V4;

b) to implement the existing SHETRAN V3 code on Network LINDA, both as part of a learning process in using parallel systems, and to provide an increase in computational performance for SHETRAN applications.

LINDA is a parallel processing system that is available for both the C and Fortran languages. LINDA has a number of features that make it a suitable environment for implementation of an existing serial code (**LINDA, 1992a,b**):

- it is an extension to the underlying serial language (no existing code is made obselete);
- it supports both process creation and interprocess communication at a high level;
- it is portable across many currently available processors;
- it is easy to use.

A version of LINDA called Network LINDA is currently implemented at Newcastle University, where data communications between HP9000/710 processors take place over the campus ethernet network.

A parallel computing system consisting of eight T800 transputers linked to a SUN Sparcstation 1+ via an Sbus interface board is installed in the Water Resource Systems Research Unit (WRSRU), Department of Civil Engineering. A transputer is an integrated chip containing both a processing unit and four communication links, which is designed for building scalable parallel processing systems. A parallel operating system called Genesys runs on the hardware.

The SHETRAN code is written in a structured format, with separate components handling calculations for particular hydrological processes (**Abbott et al., 1986a,b**). The contaminant migration component has only recently been added to the system (**Ewen, 1990**), and has been written with a very clearly defined interface to the hydrological flow component. This clear interface between two large blocks of serial code helps to make it an ideal candidate for parallelism using LINDA.

A.2 Parallelism

A.2.1 Measures of performance of a parallel program

The basic measures of performance of parallel codes are speed-up and efficiency (**Modi, 1988**), although other factors sometimes also need to be taken into account (such as individual processor performance, if comparisons are to be made against serial machines). The time taken for a parallel machine to execute a program contains three main elements:

T_s - time taken for the serial part of the program;

T_p - time taken for the parallel parts of the program;

T_c - time taken for parallel communications.

Thus the total time, T, taken to execute a program on n_p processors is given by

$$T = T_s + T_p/n_p + T_c .$$

The *speed-up* of running a program on a system of n_p processors is the ratio of execution time for one processor to the execution time for n_p processors. Noting that no communication time is required for a single processor, the speed-up is given by[1]

$$S(n_p) = (T_s + T_p) / (T_s + T_p/n_p + T_c) .$$

For an algorithm which is dominated by an inherently sequential section, the speed-up can be severely restricted, even given an unlimited number of processors. This limitation is

[1]Note that some authors (eg. **Bertsekas and Tsitsiklis, 1989**) define speed-up as the ratio of the computational time required by the best possible serial algorithm required to solve a problem to the computational time required by the parallel algorithm.

described by *Amdahl's law* (**Bertsekas and Tsitsiklis, 1989**)

$$S(n_p) \leq 1 / f$$

where $f = T_s/T$ is the fraction of the algorithm which is sequential .

The *efficiency* is the ratio of the speed-up to the number of processors, given as a fraction or a percentage. The percentage efficiency is therefore

$$E = 100 \times S(n_p) / n_p .$$

The efficiency of any algorithm using a single processor is 100%. Ideally, the efficiency of an algorithm using n_p processors would approach 100%. In practice, this is not attained due to communication overheads and processor idle time. **Bertsekas and Tsitsiklis (1989)** define a more realistic objective as an efficiency that stays bounded away from zero as n_p increases! A plot of efficiency against number of processors is usually made to indicate the relative performance of an algorithm depending on problem size.

A.2.2 Implementation of parallelism using Network LINDA

LINDA is a general model of MIMD (Multiple Instruction Multiple Data) parallel computing based on distributed data structures (**LINDA, 1992a,b**). A shared data space, called the *tuple space*, is used, which may exist on one or more machines. The user need not know the structure or physical location of the tuple space. A *tuple* is a collection of logically-ordered sets of data. There are two types of tuple: *process tuples* which are under active evaluation; and *data tuples*, which are passive.

The Fortran-LINDA system consists of four operations (as an additional set to the standard Fortran 77 operations):

- *out* place a tuple in tuple space;
- *eval* create a live tuple (usually, create a new process);
- *in* remove a tuple from tuple space;
- *rd* read the data from a tuple in tuple space (do not remove the tuple).

Network LINDA is an implementation of LINDA which uses a distributed network of processors, linked via ethernet. The implementation at Newcastle University currently consists of 10 HP9000/710 processors. The tuple space is distributed over all machines that are involved in a given application (see Fig. A.1).

A.2.3 Implementation of parallelism using transputers

A transputer is a VLSI (Very Large Scale Integrated) chip, containing both a processing unit (including a floating-point unit on the T800 series models) and four communication links. Transputers can be connected in a variety of topologies to assemble potentially large scale parallel processing machines. A major advantage of transputers (and similar 'building block' chips such as the Intel i860 or the transputers successor, the T9000) is that initially only a few processors can be connected together to give parallel processing capability at relatively little cost; further processors can be added as required. (**Jong, 1989** compared the performance of transputer systems with several shared-memory machines for a computational fluid dynamics problem, and concluded that transputer systems had the best price-performance ratio.)

The main difference between the implementation of parallelism on transputers and implementations using LINDA is that the transputers use 'message passing' protocols to communicate, whereas LINDA uses (virtual) shared memory.

The WRSRU transputer system was supplied by Transtech Devices Ltd., and uses Transtech's Genesys parallel operating system (based on the Trollius operating system developed at Cornell and Ohio State Universities). A small kernel of the operating system resides on each compute node. Implementation of communications can take place at four levels, representing different balances between functionality, simplicity of implementation, and communication overhead. An intermediate level, the 'network layer', was used, which provides automatic message routing through intermediate compute nodes whilst avoiding excessive overhead costs.

An alternative transputer system is also available at Newcastle University, which is based on the more commonly used Meiko operating system. Unfortunately this was not explored as a Fortran compiler was not available on the host computer.

A.3 Algorithmic structure of SHETRAN

The SHETRAN modelling system simulates hydrological flow, and is also capable of simulating sediment transport and/or contaminant migration. The high-level structure of the flow and contaminant components of SHETRAN is shown in Fig. A.2. This consists of an initialisation phase, followed by a repeated cycle of flow and contaminant calculations for each timestep, until the simulation is completed. The contaminant component is capable of simulating the migration of several interacting or non-interacting contaminants. The sediment and contaminant components use the results from the water flow components, but there is no feedback from the sediment or contaminant components to the water flow component.

Based on experience of running the SHETRAN V3 serial code, it has been noted that the computational requirements for the water flow component and the contaminant migration component (for each contaminant) are roughly comparable (the balance between each of the computational requirements varies from application to application). The computational requirements of the sediment transport component (which represents only two-dimensional transport) are relatively small.

Given this algorithmic structure, and given the very clear data interface between the flow and the contaminant components, an obvious parallelism exists, where the contaminant calculations for timestep N can be carried out in parallel with the water flow calculations for timestep $N+1$. For non-interacting contaminants, this method can be extended to calculate the migration of any number of contaminants, each of which can be processed in parallel (Fig. A.3).

The implementation of this method depends upon accurately identifying the data requirements of the contaminant component, and ensuring that the appropriate data are available for the contaminant calculations, whilst also ensuring that the minimum amount of data are transferred. Within Fortran-LINDA, data within a single common block can be transferred to/from tuple space with a single instruction. Communication overheads are incurred each time a block of data is transferred, with increasing overhead costs for larger amounts of data, and also each time a process is spawned (ie. *eval*ed).

After several methods had been tried, the final implementation involved spawning a process for each contaminant at the start of the simulation, which continued to run until the simulation is completed. This had the advantage that all initialisation data, and contaminant data which

needed to be preserved from timestep to timestep, remained local to each worker process, thus reducing communication overheads. The disadvantage of this approach was that, if a processor became heavily used during the simulation (by other users of the network), no dynamic load balancing was possible to utilise processors with a lighter load. Some additional code was added to compress large arrays where there were known to be large numbers of zero value array elements.

The parallel implementation was based on SHETRAN V3.4 and Network LINDA version 2.5.2. Amendments to the SHETRAN code were kept to a minimum, so that future versions of SHETRAN can be parallelised in a similar way. A summary of the code amendments is given in Section A.7. The details of the parallel algorithm are given in Fig. A.4, and the source code for the parallel subroutines is given in Section A.8.

A.4 Investigation of the performance of Network LINDA

Simple prototype codes were written during the development of the parallel algorithms for SHETRAN to mimic the high-level structure of SHETRAN. Prototype codes were used so that the parallel algorithms could be visualised easily, and the feasibility of various approaches could be explored without the possible implementation problems of using the full code. The amount of computation and data in the prototype code could also be scaled either to run test simulations very quickly, or to evaluate the possible performance of a typical SHETRAN application.

A suite of tests was run using one of the prototype codes, which mimics the implementation of a generic parallel algorithm involving a variable (but fixed for each run) amount of central processor unit (CPU) time per timestep of a simulation (C), and a variable (but fixed for each run) amount of data passed between processors (D). Each test consisted of several runs of the code for the number of processors (n_p) from one up to six or more. The speed-up (S) was calculated for each n_p, and if S increased sufficiently with n_p, the test was considered to be successful (ie. an algorithm using that data size, D, and CPU time per timestep, C, is likely to yield a successful speed-up). Typical results for successful and unsuccessful cases are given in Fig. A.5.

The final results are shown in Fig. A.6. The points marked with a dot represent successful tests, and the points marked with a circle represent unsuccessful tests. An approximate line

has been drawn to divide the successful and unsuccessful regions. The region above the line therefore represents algorithms which are likely to parallelise successfully. The further an algorithm is from the line in this region, the higher a speed-up may be expected.

A.5 Investigation of the performance of a transputer system

A similar feasibility study to that given in Section A.4 for Network LINDA was made for the WRSRU Transtech transputer system. In this case, a slightly different approach was taken. The efficiency was calculated for different combinations of CPU time and data size, and the exercise repeated for 1, 2, 4, and 8 processors. The results for the case with 8 processors are given in Fig. A.7 (results for 1, 2, and 4 processors were broadly similar). Successful speed-ups may be expected for the region where the efficiency is high (greater than, say, 70%); i.e. for the region with large CPU times and low amounts of transferred data.

A.6 Parallel implementation of SHETRAN V3

A typical SHETRAN application was chosen which has already been run using the serial code, with the following features:

- the simulation involves the simultaneous migration of 5 non-interacting contaminants;
- the simulation is run over a sufficiently long period, so that the CPU time involved in initialisation is negligible;
- the array sizes are sufficiently small, so that the whole program size is less than 16Mb (16Mb is the memory capacity of the HP9000/710 workstations).

The parallel SHETRAN simulation was run, using from one to six worker processors, and the results compared with those from a serial run using the original code. The results (contaminant concentrations in stream water at the catchment outlet) were inspected and found to match those from the serial simulation.

The best theoretical speed-up, based on the results from the prototype code, was 4.3. The best actual speed-up achieved was 3.5, corresponding to an efficiency of 58%. The best possible speed-up for this particular case was limited by the disparity in CPU time required for flow and contaminant calculations per timestep. The CPU times required for a single timestep of the flow and contaminant calculations respectively were 0.462 and 0.260 s. Since

synchronisation occurs at every timestep, each of the worker nodes idles for 0.202 s at every timestep, and the maximum possible speed-up is therefore only 3.85, corresponding to a maximum possible efficiency of 64%. The speed-up achieved was therefore 90% of this theoretical maximum, the difference being due to communications overheads. In theory, therefore, a simulation where the CPU requirements for the flow component exactly matched those for the contaminant component would potentially be able to achieve an efficiency approaching 90%.

A.7 Source code changes made to SHETRAN V3

The following list includes all changes made to the source code of SHETRAN V3.4, and is given to facilitate any similar parallelisation of future versions of SHETRAN.

Source code	Amendments
AL.C	- new common block added /linda1/ icon, icont icon = total no. of contaminants icont = contaminant no. passed to each process - tth, bexsy, and all variables associated with RES output, moved from AL.D - vuz removed - new variables eruz1, th31 added to common block alccb8 - variables dummy, earray, eruz, th3 moved to new common block alccb9
AL.D	- tth, bexsy, and all variables associated with RES output, moved to AL.C
fr.f/fr.fl	- source code fr.f renamed fr.fl (so that it has the correct syntax for the LINDA flc compiler) - main program renamed 'subroutine real_main' - calls to parallel LINDA routines added - contaminant result output removed from frame - code added to set up compressed arrays eruz1, th31
li.fl	- new parallel subroutines, including all LINDA operations

muz.f
- calls to parallel LINDA routines added
- ncon (no. of contaminants in contaminant component) initialised to 1
- global variables initialised only for local contaminant no. 1
- contaminant source location set depending upon global contaminant no.
- code added to set up arrays eruz/th3 from transferred arrays eruz1/th31

A.8 Source code listing of SHETRAN parallel subroutines *li.fl*

The following source code listing consists of the parallel code which, together with the changes to the SHETRAN source code outlined in the previous section, is the full code required to implement SHETRAN on the Network LINDA parallel processing system.

```
C
C     "li.fl"
C
c linda parallel routines for SHETRAN V3.4
c written by G Parkin, 24/3/93
c rewritten 16/4/93
c updated for >1 contaminant 29/4/93

c------------------------------------------------------------      subroutine linit
      include 'SPEC.AL'

      icon = 5

c flow initialisation data

      out('alccb1',/alccb1/)
      out('alccb3',/alccb3/)
      out('alccb5',/alccb5/)
      out('alccb7',/alccb7/)
      out('algcb1',/algcb1/)
      out('algcb2',/algcb2/)
      out ('alccb2',/alccb2/)
      out ('alccb6',/alccb6/)
```

```
      out ('alccb8',/alccb8/)

      ione = 1
      out('icont 1',ione)

c eval contaminant routine

      do 10 icont=1,icon
        out('icon',icon)
 10     eval('cmmain',cmmain())

      in('Flag for Data',ione)
      in('alccb1',?typeof(/alccb1/))
      in('alccb3',?typeof(/alccb3/))
      in('alccb5',?typeof(/alccb5/))
      in('alccb7',?typeof(/alccb7/))
      in('algcb1',?typeof(/algcb1/))
      in('algcb2',?typeof(/algcb2/))
      out('Flag for Data',ione+ione)

      return
      end

c------------------------------------------------------------  subroutine lisim

      include 'SPEC.AL'
      ione = 1

c out time-varying flow data

      in('Flag for Data',ione+ione)
      in('alccb2',?typeof(/alccb2/))
      in('alccb6',?typeof(/alccb6/))
      in('alccb8',?typeof(/alccb8/))

      out ('alccb2',/alccb2/)
```

```
      out ('alccb6',/alccb6/)
      out ('alccb8',/alccb8/)

      ione = 1
      out('icont 2',ione)

      return
      end

c-------------------------------------------------------------  subroutine lifin

      include 'SPEC.AL'
      ione = 1

c clear contaminant worker process from tuple space

      do 100 icont=1,icon
  100 in ('cmmain',0)
      in('Flag for Data',ione+ione)
      in('alccb2',?typeof(/alccb2/))
      in('alccb6',?typeof(/alccb6/))
      in('alccb8',?typeof(/alccb8/))

      return
      end

c-------------------------------------------------------------
      subroutine cmmain()
      include 'SPEC.AL'
      CHARACTER*50 AIOSTO

      ione = 1
      in('icon',?icon)

c get flow initialisation data
```

```
      in('icont 1',?icont)
      if (icont.le.icon-ione) out('icont 1',icont+ione)

      rd('alccb1',?/alccb1/)
      rd('alccb3',?/alccb3/)
      rd('alccb5',?/alccb5/)
      rd('alccb7',?/alccb7/)
      rd('algcb1',?/algcb1/)
      rd('algcb2',?/algcb2/)
      rd('alccb2',?/alccb2/)
      rd('alccb6',?/alccb6/)
      rd('alccb8',?/alccb8/)

      if (icont.eq.icon) out('Flag for Data',ione)

c call contaminant initialisation routine

      call incm(bexsy)

c get flow time-varying data (for each timestep)

  100 in('icont 2',?icont)
      if (icont.lt.icon) out('icont 2',icont+ione)

      rd('alccb2',?/alccb2/)
      rd('alccb6',?/alccb6/)
      rd('alccb8',?/alccb8/)

      if (icont.eq.icon) out('Flag for Data',ione+ione)

c call contaminant simulation routine

      call cmsim(bexsy)

c output contaminant results
```

```
200  AIOSTO = '00000000000000000000000000000001111111111'
     CALL FRRESP (AIOSTO)

c test for end of simulation

     IF (UZNOW .LT. (TTH - TIH)) GO TO 100

     return
     end
```

A.9 Summary and conclusions

The hydrological simulation model, SHETRAN V3.4, has been successfully implemented on the Network LINDA parallel processing system. The simple approach of LINDA meant that a parallel implementation of the SHETRAN code could be made with the minimum of effort.

Prototype codes were found to be useful in developing parallel algorithms, and in determining the feasibility and potential speed-up of various approaches. Figures have been produced to assist determination of when a parallel algorithm may be feasible for the Transtech T800 transputer system and the Network LINDA system implemented on HP9000/710 workstations, in terms of CPU and data transfer requirements. In general, it is recommended that coarse-grained algorithms are used on these systems in preference to fine-grained algorithms.

The speed-up of a particular SHETRAN application was predicted reasonably well using the results from the feasibility study. A speed-up of 3.50 was achieved using 6 processors, corresponding to an efficiency of 58%. The maximum possible speed-up achievable for a simulation depends upon the disparity between CPU requirements for flow and contaminant calculations. For some simulations, efficiencies approaching 90% should be achievable.

A.10 References

Abbott, M.B., Bathurst, J.C, Cunge, J.A., O'Connell, P.E. and Rasmussen, J. (1986a). An introduction to the European Hydrological System - Système Hydrologique Européen, "SHE", 1: History and philosophy of a physically-based, distributed modelling system. J. Hydrol., 87, 45-59.

Abbott, M.B., Bathurst, J.C., Cunge, J.A., O'Connell, P.E. and Rasmussen, J. (1986b). An introduction to the European Hydrological System - Système Hydrologique Européen, "SHE", 2: Structure of a physically-based, distributed modelling system. J. Hydrol., 87, 61-77.

Bertsekas, D.P. and Tsitsiklis, J.N. (1989). *Parallel and Distributed Computation : Numerical Methods.* Prentice-Hall, New Jersey, USA.

Ewen, J. (1990). Basis for the subsurface contaminant migration components of the catchment water flow, sediment transport, and contaminant migration modelling system SHETRAN-UK. NSS/R229, UK Nirex Ltd., Harwell, UK.

Jong, J-M. (1989). A comparison of parallel implementations of the flux corrected transport algorithm. Msc thesis, Utah State University, USA.

LINDA (1992a). *C-Linda User's Guide and Reference Manual, version 2.0.* SCIENTIFIC Computing Associates, Inc., New Haven, CT, USA.

LINDA (1992b). *Fortran-Linda Reference Manual.* SCIENTIFIC Computing Associates, Inc., New Haven, CT, USA.

Modi, J.J. (1988). *Parallel Algorithms and Matrix Computation.* Clarendon Press, Oxford, UK.

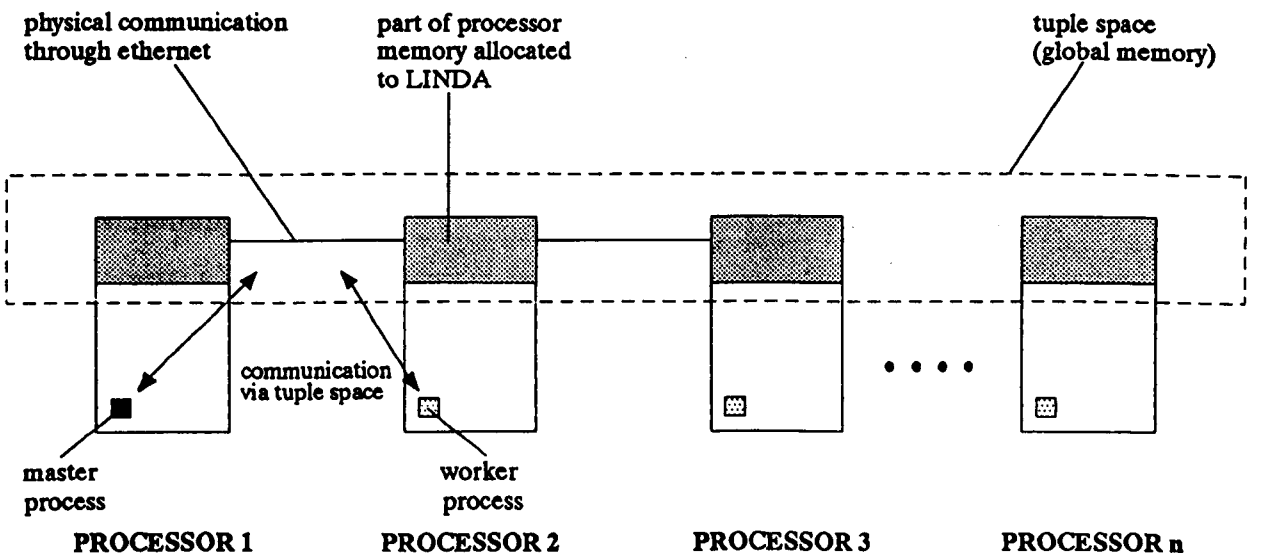

Figure A.1 Implementation of Network LINDA

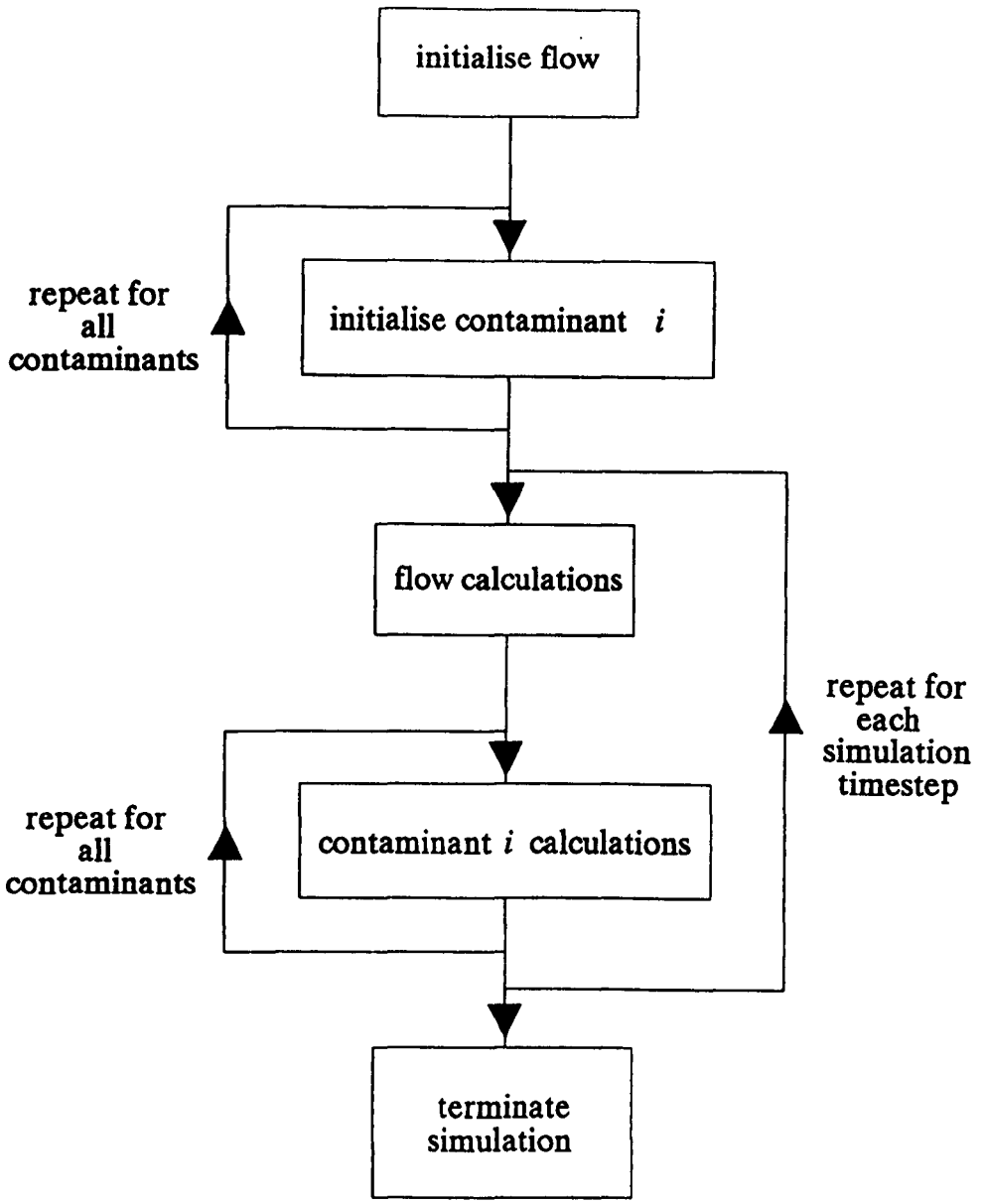

Figure A.2 High-level algorithmic structure of SHETRAN: serial code

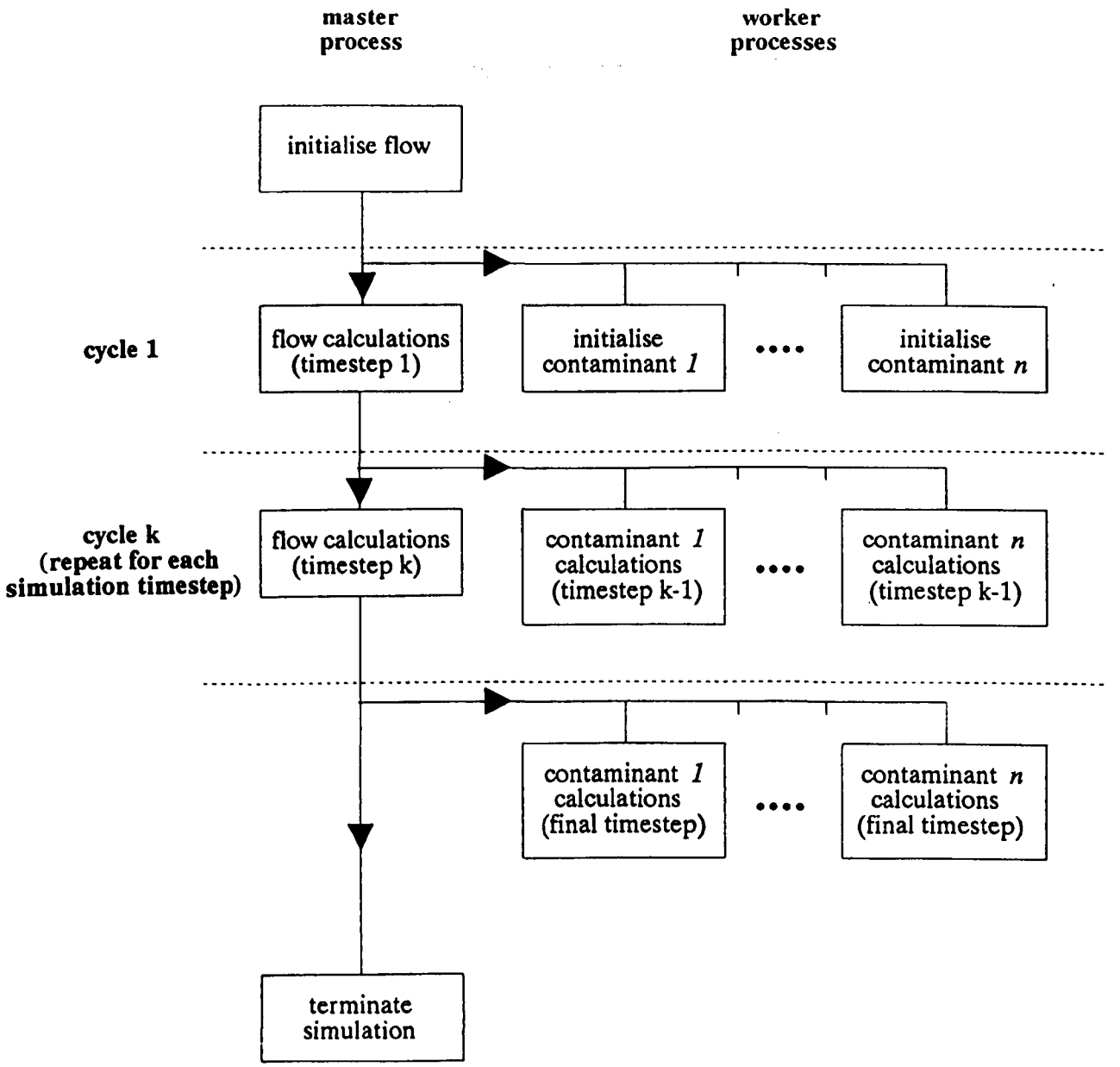

Figure A.3 High-level algorithmic structure of SHETRAN: parallel code

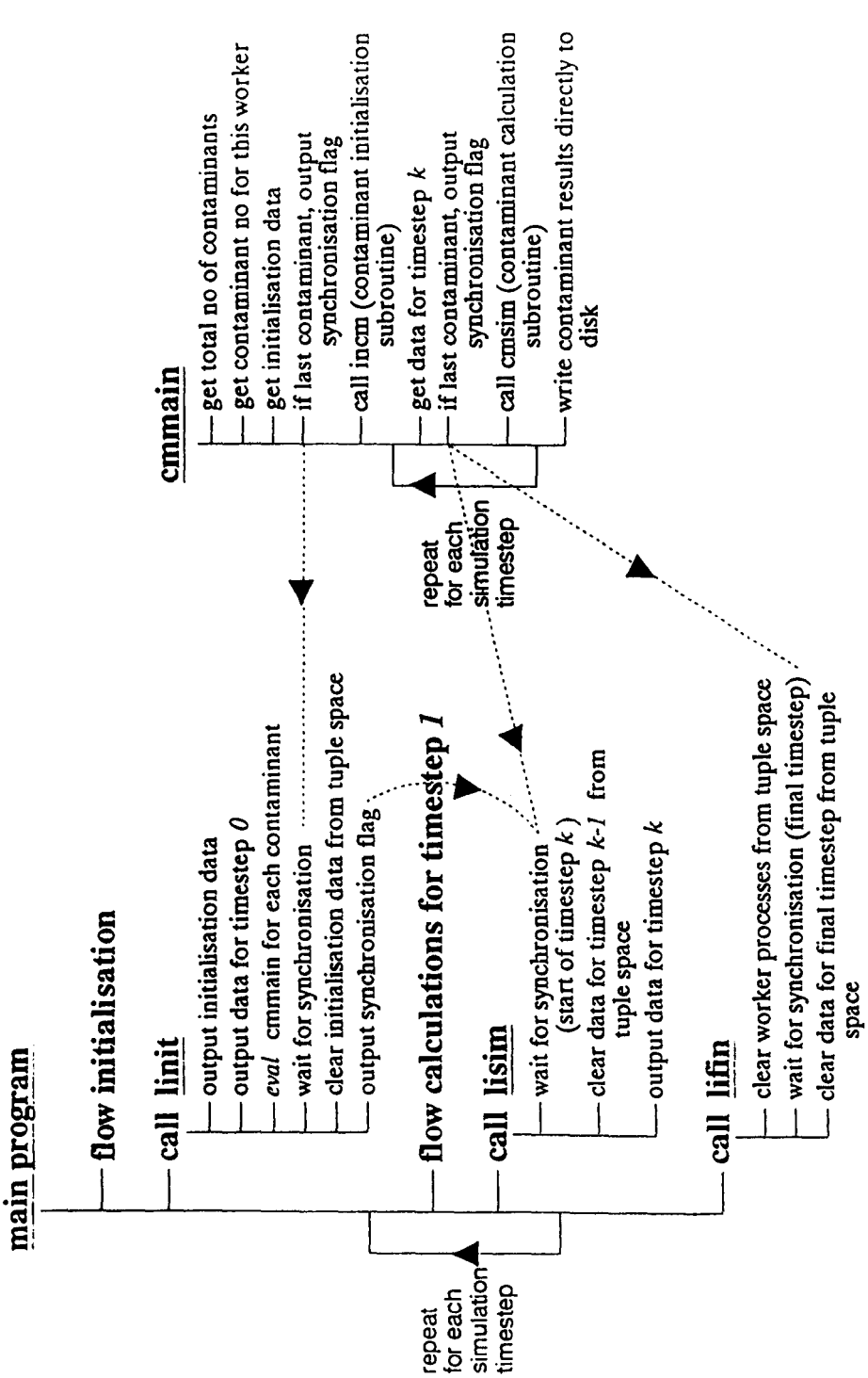

Figure A.4 Detailed parallel algorithm for SHETRAN

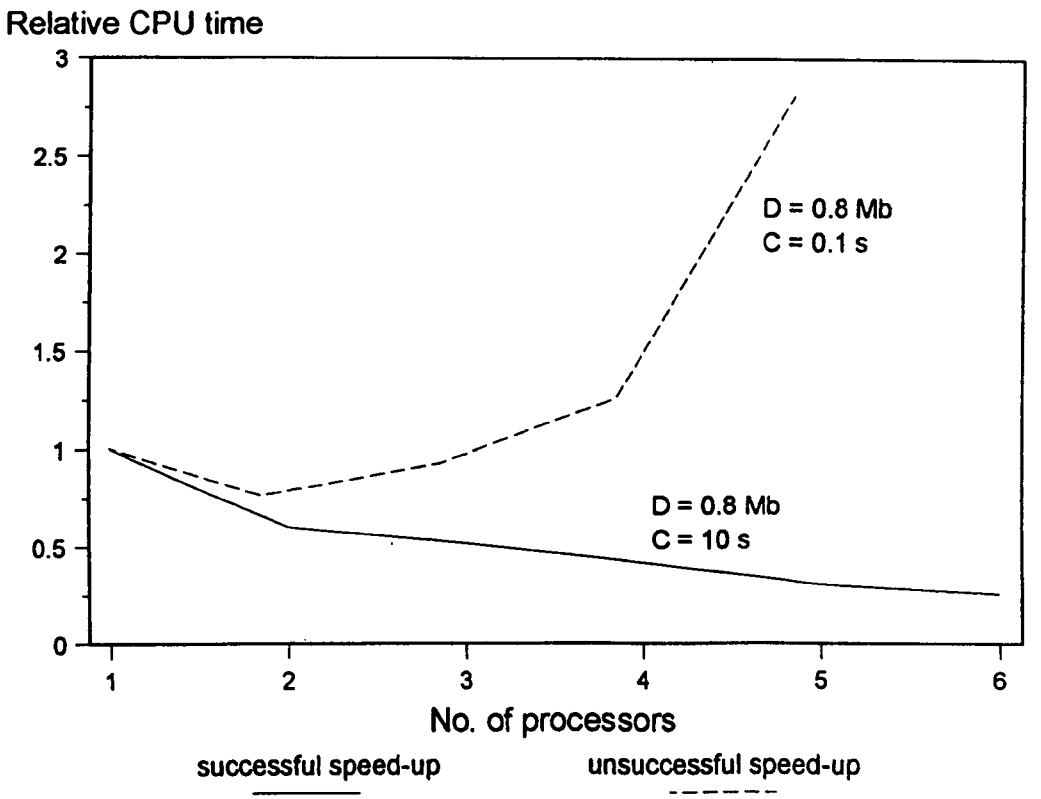

Figure A.5 Examples of successful and unsuccessful speed-up (Network LINDA)

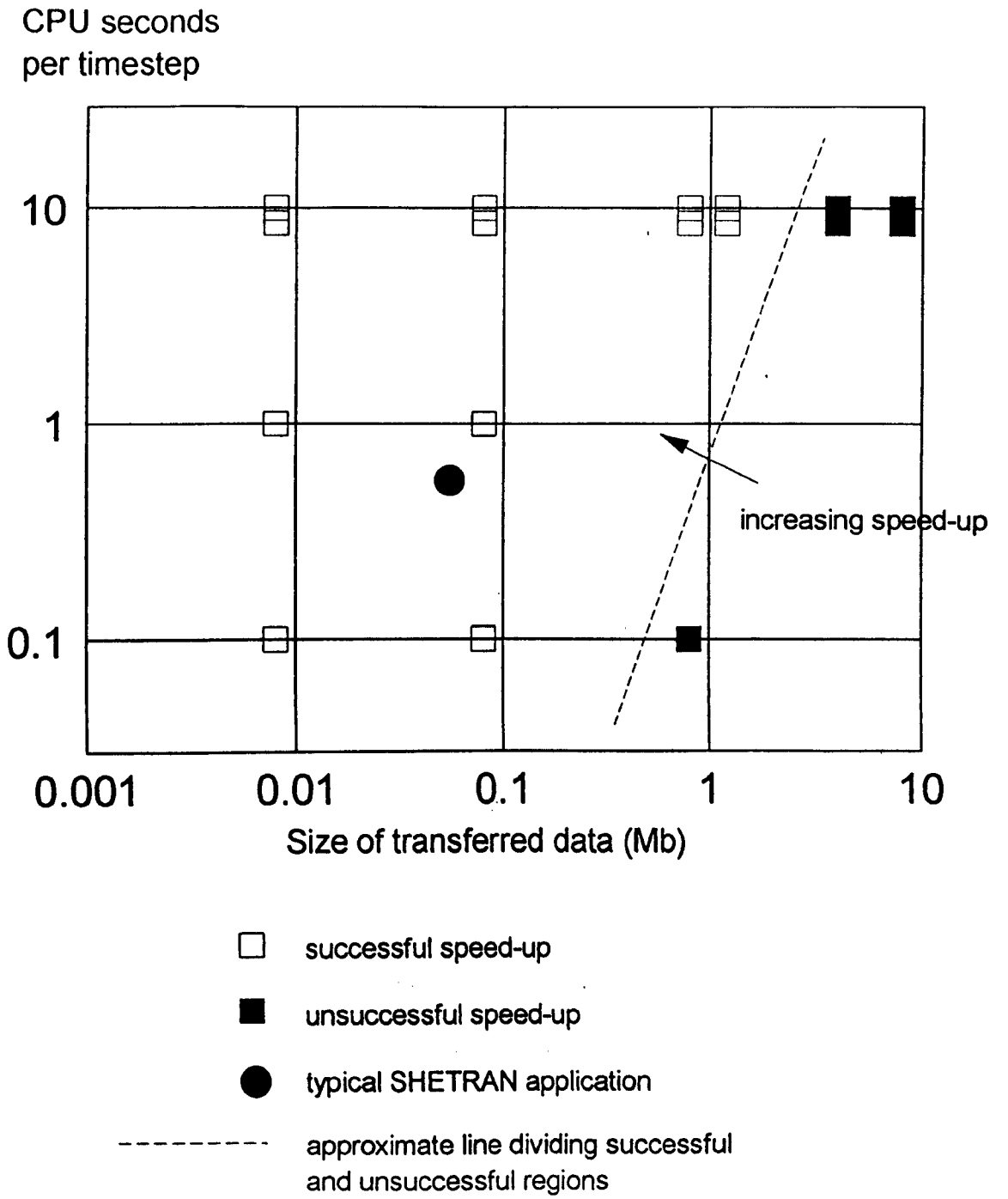

Figure A.6 Feasibility region for parallel implementation on Network LINDA

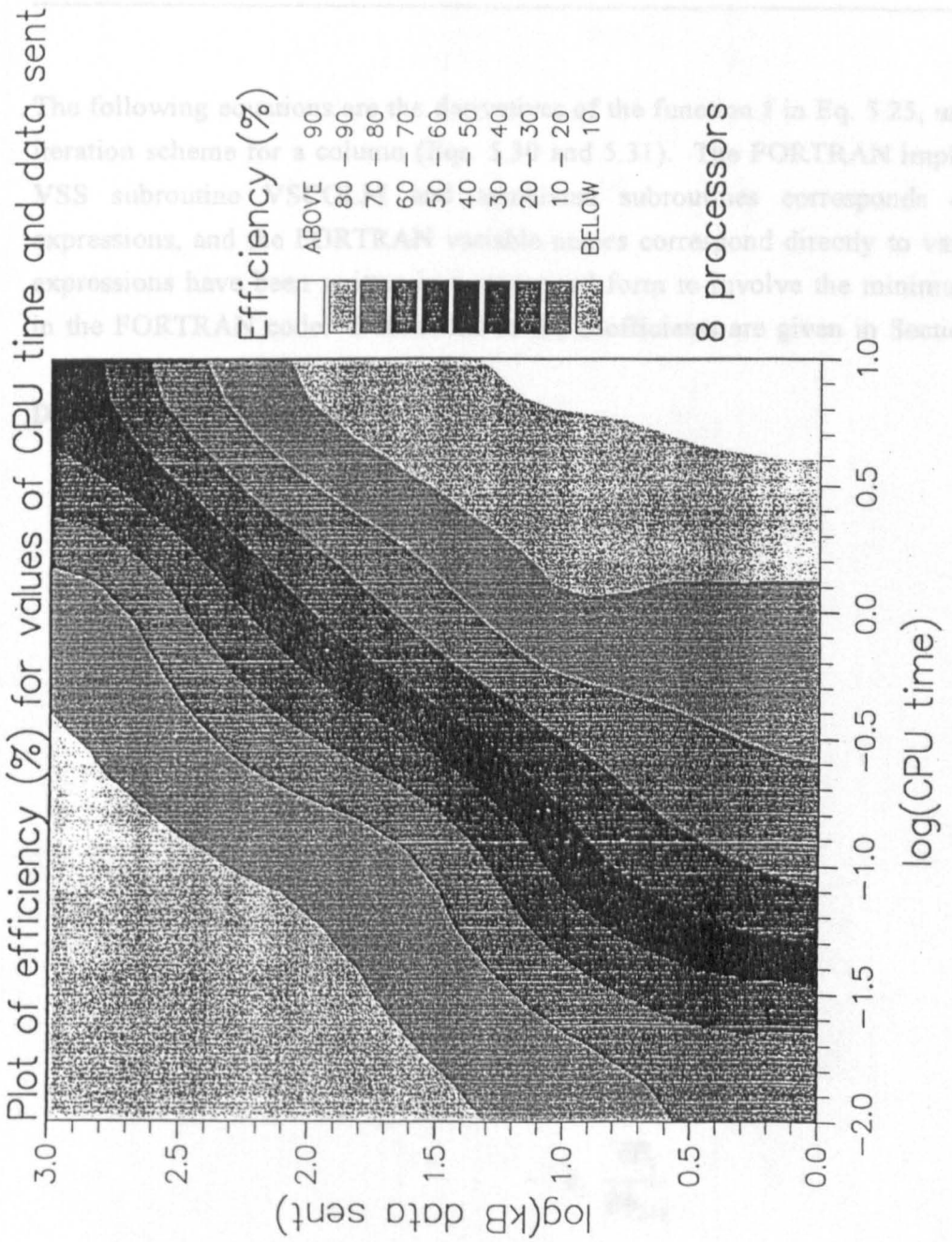

Figure A.7 Feasibility region for parallel implementation on a transputer system

APPENDIX B DERIVATIVE TERMS FOR NEWTON ITERATION FOR A COLUMN

The following equations are the derivatives of the function f in Eq. 5.25, used in the Newton iteration scheme for a column (Eqs. 5.30 and 5.31). The FORTRAN implementation in the VSS subroutine VSCOLM and associated subroutines corresponds directly to these expressions, and the FORTRAN variable names correspond directly to variables used. The expressions have been written in a structured form to involve the minimum of calculations in the FORTRAN code. Definitions of the coefficients are given in Section 5.5.

Derivative of f w.r.t. ψ_{i-1}

$$\begin{aligned}
\frac{\partial f}{\partial \psi_{i-1}} &= \sigma\, \beta_{z-,i} \\
&+ \sigma\, \psi_{i-1}^{n+1} \frac{\partial \beta_{z-,i}}{\partial \psi_{i-1}} \\
&- \sigma\, \psi_{i}^{n+1} \frac{\partial F_i}{\partial \psi_{i-1}} \\
&+ (1-\sigma)\, \psi_{i-1}^{n} \frac{\partial \beta_{z-,i}}{\partial \psi_{i-1}} \\
&- (1-\sigma)\, \psi_{i}^{n} \frac{\partial F_i}{\partial \psi_{i-1}} \\
&+ z_{i-1} \frac{\partial \beta_{z-,i}}{\partial \psi_{i-1}} \\
&- z_i \frac{\partial F_i}{\partial \psi_{i-1}}
\end{aligned} \qquad \text{(B.1)}$$

Derivative of f w.r.t. ψ_i

$$
\begin{aligned}
\frac{\partial f}{\partial \psi_i} &= \sigma\, \psi_{i-1}^{n+1}\, \frac{\partial \beta_{z-,i}}{\partial \psi_i} \\
&\quad - (\sigma F_i + G_i) \\
&\quad - \psi_i^{n+1} \left(\sigma\, \frac{\partial F_i}{\partial \psi_i} + \frac{\partial G_i}{\partial \psi_i} \right) \\
&\quad + \sigma \psi_{i+1}^{n+1}\, \frac{\partial \beta_{z+,i}}{\partial \psi_i} \\
&\quad + (1-\sigma)\, \psi_{i-1}^{n}\, \frac{\partial \beta_{z-,i}}{\partial \psi_i} \\
&\quad - \psi_i^{n} \left((1-\sigma)\, \frac{\partial F_i}{\partial \psi_i} - \frac{\partial G_i}{\partial \psi_i} \right) \\
&\quad + (1-\sigma)\, \psi_{i+1}^{n}\, \frac{\partial \beta_{z+,i}}{\partial \psi_i} \\
&\quad + \sigma \sum_{j=1}^{4} \left[\psi_{k,j}^{n+1}\, \frac{\partial \gamma_{i,j}^{1}}{\partial \psi_i} + \psi_{(k+\delta kj),j}^{n+1}\, \frac{\partial \gamma_{i,j}^{2}}{\partial \psi_i} \right] \\
&\quad + (1-\sigma) \sum_{j=1}^{4} \left[\psi_{k,j}^{n}\, \frac{\partial \gamma_{i,j}^{1}}{\partial \psi_i} + \psi_{(k+\delta kj),j}^{n}\, \frac{\partial \gamma_{i,j}^{2}}{\partial \psi_i} \right] \\
&\quad + z_{i-1}\, \frac{\partial \beta_{z-,i}}{\partial \psi_i} + z_{i+1}\, \frac{\partial \beta_{z+,i}}{\partial \psi_i} - z_i\, \frac{\partial F_i}{\partial \psi_i} \\
&\quad + \sum_{j=1}^{4} \left[z_{k,j}\, \frac{\partial \gamma_{i,j}^{1}}{\partial \psi_i} + z_{(k+\delta kj),j}\, \frac{\partial \gamma_{i,j}^{2}}{\partial \psi_i} \right]
\end{aligned}
\tag{B.2}
$$

Derivative of f w.r.t. ψ_{i+1}

$$\frac{\partial f}{\partial \psi_{i+1}} = - \sigma \, \psi_i^{n+1} \frac{\partial F_i}{\partial \psi_{i+1}}$$

$$+ \sigma \, \beta_{z+,i}$$

$$+ \sigma \, \psi_{i+1}^{n+1} \frac{\partial \beta_{z+,i}}{\partial \psi_{i+1}}$$

$$- (1-\sigma) \, \psi_i^n \frac{\partial F_i}{\partial \psi_{i+1}} \qquad \text{(B.3)}$$

$$+ (1-\sigma) \, \psi_{i+1}^n \frac{\partial \beta_{z+,i}}{\partial \psi_{i+1}}$$

$$+ z_{i+1} \frac{\partial \beta_{z+,i}}{\partial \psi_{i+1}}$$

$$- z_i \frac{\partial F_i}{\partial \psi_{i+1}}$$

Derivative of $\beta_{z+,i}$ and $\beta_{z-,i}$ w.r.t. ψ_i , ψ_{i+1} , and ψ_{i-1}

w-mean

$$\frac{\partial \beta_{z+,i}}{\partial \psi_i} = \frac{w\, A_0\, K_{z,i}^{w-1}}{\Delta z_i + \Delta z_{i+1}} \left[0.5(K_{z,i}^{w} + K_{z,i+1}^{w})\right]^{\frac{1-w}{w}} \frac{\partial K_{z,i}}{\partial \psi_i}$$

$$\frac{\partial \beta_{z+,i}}{\partial \psi_{i+1}} = \frac{w\, A_0\, K_{z,i+1}^{w-1}}{\Delta z_i + \Delta z_{i+1}} \left[0.5(K_{z,i}^{w} + K_{z,i+1}^{w})\right]^{\frac{1-w}{w}} \frac{\partial K_{z,i+1}}{\partial \psi_{i+1}} \qquad \text{(B.4)}$$

$$\frac{\partial \beta_{z-,i}}{\partial \psi_i} = \frac{w\, A_0\, K_{z,i}^{w-1}}{\Delta z_i + \Delta z_{i-1}} \left[0.5(K_{z,i}^{w} + K_{z,i-1}^{w})\right]^{\frac{1-w}{w}} \frac{\partial K_{z,i}}{\partial \psi_i}$$

$$\frac{\partial \beta_{z-,i}}{\partial \psi_{i-1}} = \frac{w\, A_0\, K_{z,i-1}^{w-1}}{\Delta z_i + \Delta z_{i-1}} \left[0.5(K_{z,i}^{w} + K_{z,i-1}^{w})\right]^{\frac{1-w}{w}} \frac{\partial K_{z,i-1}}{\partial \psi_{i-1}}$$

weighted harmonic mean

$$\frac{\partial \beta_{z+,i}}{\partial \psi_i} = \frac{2\, A_0\, \Delta z_i\, K_{z,i+1}^{2}}{(\Delta z_i K_{z,i+1} + \Delta z_{i+1}\, K_{z,i})^2} \frac{\partial K_{z,i}}{\partial \psi_i}$$

$$\frac{\partial \beta_{z+,i}}{\partial \psi_{i+1}} = \frac{2\, A_0\, \Delta z_{i+1}\, K_{z,i}^{2}}{(\Delta z_i K_{z,i+1} + \Delta z_{i+1}\, K_{z,i})^2} \frac{\partial K_{z,i+1}}{\partial \psi_{i+1}} \qquad \text{(B.5)}$$

$$\frac{\partial \beta_{z-,i}}{\partial \psi_i} = \frac{2\, A_0\, \Delta z_i\, K_{z,i-1}^{2}}{(\Delta z_i\, K_{z,i-1} + \Delta z_{i-1}\, K_{z,i})^2} \frac{\partial K_{z,i}}{\partial \psi_i}$$

$$\frac{\partial \beta_{z-,i}}{\partial \psi_{i-1}} = \frac{2\, A_0\, \Delta z_{i-1}\, K_{z,i}^{2}}{(\Delta z_i\, K_{z,i-1} + \Delta z_{i-1}\, K_{z,i})^2} \frac{\partial K_{z,i-1}}{\partial \psi_{i-1}}$$

Derivative of F_i w.r.t. ψ_i

$$\frac{\partial F_i}{\partial \psi_i} = \frac{\partial \beta_{z+,i}}{\partial \psi_i} + \frac{\partial \beta_{z-,i}}{\partial \psi_i} + \sum_{j=1}^{4} \left[\frac{\partial \gamma_{i,j}^{1}}{\partial \psi_i} + \frac{\partial \gamma_{i,j}^{2}}{\partial \psi_i} \right] \tag{B.6}$$

Derivative of F_i w.r.t. ψ_{i+1} and ψ_{i-1}

$$\frac{\partial F_i}{\partial \psi_{i+1}} = \frac{\partial \beta_{z+,i}}{\partial \psi_{i+1}}$$

$$\frac{\partial F_i}{\partial \psi_{i-1}} = \frac{\partial \beta_{z-,i}}{\partial \psi_{i-1}} \tag{B.7}$$

Derivative of G_i w.r.t. ψ_i

$$\frac{\partial G_i}{\partial \psi_i} = \frac{V_i}{\Delta t} \frac{\partial \eta_i}{\partial \psi_i} \tag{B.8}$$

Derivative of $\gamma^1_{i,j}$ and $\gamma^2_{i,j}$ w.r.t. ψ_i

$$\frac{\partial \gamma^1_{i,j}}{\partial \psi_i} = \frac{0.5\ w\ A'_{i,j}\ (K_{i,j}A'_{i,j})^{w-1}}{\Delta L_j + \Delta L'_j} \left[0.5((K_{i,j}A'_{i,j})^w + (K_{k,j}A'_{k,j})^w)\right]^{\frac{1-w}{w}} \frac{\partial K_{i,j}}{\partial \psi_i} \tag{B.9}$$

$$\frac{\partial \gamma^2_{i,j}}{\partial \psi_i} = \frac{0.5\ w\ A'_{i,j}\ (K_{i,j}A'_{i,j})^{w-1}}{\Delta L_j + \Delta L'_j} \left[0.5((K_{i,j}A'_{i,j})^w + (K_{k+\delta k,j}A'_{k+\delta k,j})^w)\right]^{\frac{1-w}{w}} \frac{\partial K_{i,j}}{\partial \psi_i}$$